

THE OXIDATION OF PEROXIREDOXINS IN ENVIRONMENTAL LUNG INJURY AND COPD

Claire Job



A Thesis Presented for the Degree of Doctor of Philosophy

Cardiff University

June 2011

Cardiff School of Biosciences

Cardiff University

Museum Avenue

CARDIFF

CF10 3AX

UMI Number: U585490

All rights reserved

INFORMATION TO ALL USERS

The quality of this reproduction is dependent upon the quality of the copy submitted.

In the unlikely event that the author did not send a complete manuscript and there are missing pages, these will be noted. Also, if material had to be removed, a note will indicate the deletion.



UMI U585490

Published by ProQuest LLC 2013. Copyright in the Dissertation held by the Author.
Microform Edition © ProQuest LLC.

All rights reserved. This work is protected against
unauthorized copying under Title 17, United States Code.



ProQuest LLC
789 East Eisenhower Parkway
P.O. Box 1346
Ann Arbor, MI 48106-1346

CONTENTS

CONTENTS	i
ACKNOWLEDGEMENTS	x
DECLARATION	xi
PUBLICATIONS	xii
ABBREVIATIONS	xiv
ABSTRACT	xix
1. INTRODUCTION	1
1.1 STUDY INTRODUCTION	2
1.2 THE HUMAN RESPIRATORY SYSTEM	2
1.2.1 STRUCTURE AND FUNCTION OF THE RESPIRATORY SYSTEM	2
1.2.2 ANATOMY OF THE LUNGS	4
1.3 THE PULMONARY EPITHELIUM	6
1.4 CELLS OF THE BRONCHIAL EPITHELIUM (BE)	7
1.4.1 CILIATED CELLS	7
1.4.2 GOBLET CELLS	9
1.4.3 BASAL CELLS	10
1.4.4 INTERMEDIATE CELLS	11
1.4.5 CLARA CELLS	11
1.5 DEFENCE MECHANISMS OF THE RESPIRATORY TRACT (RPT)	12
1.5.1 NON-IMMUNOLOGICAL DEFENCE MECHANISMS	12
1.5.1.1 MECHANICAL BARRIERS	12
1.5.1.2 CELL JUNCTIONS IN THE BE	13
1.5.1.3 MUCOCILIARY ESCALATOR	13

1.5.2 IMMUNOLOGICAL DEFENCE MECHANISMS	15
1.5.2.1 INNATE IMMUNITY	15
1.5.2.2 ADAPTIVE IMMUNITY	16
1.6 LUNG DISEASE	18
1.7 CHRONIC OBSTRUCTIVE PULMONARY DISEASE (COPD)	18
1.7.1 SYSTEMIC EFFECTS OF COPD	18
1.7.2 COPD RISK FACTORS	20
1.7.3 COPD DISEASES	20
1.7.3.1 CHRONIC BRONCHITIS	21
1.7.3.2 OBSTRUCTIVE BRONCHIOLITIS	22
1.7.3.3 EMPHYSEMA	22
1.7.4 INFLAMMATION IN COPD	24
1.7.5 COPD AND OXIDATIVE STRESS	27
1.8 REACTIVE OXYGEN SPECIES (ROS)	27
1.8.1 ENDOGENOUS ROS PRODUCTION	28
1.8.2 EXOGENOUS ROS PRODUCTION	29
1.8.3 OXIDATIVE STRESS	30
1.8.3.1 CELLULAR DAMAGE CAUSED BY OXIDATIVE STRESS	31
1.8.4 ROS SIGNALLING	32
1.8.4.1 H ₂ O ₂ : AN INTRACELLULAR MESSENGER	32
1.8.4.2 DETRIMENTAL ROS SIGNALLING	33
1.9 LUNG ANTIOXIDANT DEFENCE MECHANISMS	34
1.9.1 NON-ENZYMATIC ANTIOXIDANTS	34
1.10 PEROXIREDOXINS (PRX)	36
1.10.1 PRX DISCOVERY	37
1.10.2 PRX SUBGROUPS	37

1.10.2.1 TYPICAL 2-CYS PRXS	38
1.10.2.2 ATYPICAL 2-CYS PRXS	41
1.10.2.3 1-CYS PRXS	42
1.10.3 PRX ACTIVE SITES	43
1.10.4 PRX REGULATION	44
1.10.4.1 PHOSPHORYLATION	45
1.10.4.2 TRUNCATION	45
1.10.4.3 OLIGOMERISATION	46
1.10.4.4 HYPEROXIDATION	47
1.11 <i>IN VITRO</i> CELL CULTURE	47
1.11.1 NHBE CELL CULTURE MODEL	50
1.12 BIOMARKERS	51
1.12.1 BIOMARKERS IN COPD	51
1.12.2 THE PRXS AS BIOMARKERS	52
1.13 AIMS AND OBJECTIVES OF THE STUDY	52
1.13.1 THE HYPOTHESIS	52
1.13.2 PROJECT AIMS AND OBJECTIVES	53
2. PRX STATUS DURING NHBE CELL MODEL MORPHOGENESIS	57
2.1 INTRODUCTION	58
2.1.1 RESEARCH AIMS	59
2.2 MATERIALS AND STOCK SOLUTIONS	60
2.2.1 MATERIALS AND SUPPLIERS	60
2.2.2 STOCK SOLUTIONS	61
2.3 METHODS	63
2.3.1 CELL CULTURE	63
2.3.1.1 FIRST PASSAGE	63

2.3.1.2 SECOND PASSAGE	63
2.3.1.3 SEEDING INTO MILLIPORE [®] INSERTS	64
2.3.1.4 CONFLUENT INSERT CULTURES	64
2.3.2 TRANS-EPITHELIAL ELECTRICAL RESISTANCE (TEER)	65
2.3.3 BRADFORD ASSAY	65
2.3.4 WESTERN BLOT/ANTIBODY DETECTION	66
2.3.4.1 1D SDS PAGE (POLYACRYLAMIDE GEL ELECTROPHORESIS)	66
2.3.4.2 WESTERN BLOT (WB)	67
2.3.4.3 ANTIBODY INCUBATION AND DETECTION	67
2.3.5 STATISTICAL ANALYSIS	68
2.4 RESULTS	69
2.4.1 NHBE MORPHOGENESIS: CELL CULTURE	69
2.4.2 NHBE MORPHOGENESIS: TEER ANALYSIS	72
2.4.3 NHBE MORPHOGENESIS: WESTERN BLOT ANALYSIS	73
2.4.3.1 NHBE MORPHOGENESIS: WB (TOTAL PRX LEVELS)	73
2.4.3.2 NHBE MORPHOGENESIS: WB (PRX III ACTIVITY)	75
2.5 DISCUSSION	76
2.5.1 NHBE MORPHOGENESIS: CELL CULTURE AND TEER ANALYSIS	76
2.5.2 NHBE MORPHOGENESIS: WESTERN BLOT ANALYSIS	77
2.6 CONCLUSION	78
3. IHC ANALYSIS OF PRX STATUS DURING NHBE MODEL MORPHOGENESIS	80
3.1 INTRODUCTION	81
3.1.1 RESEARCH AIMS	81
3.2 MATERIALS AND STOCK SOLUTIONS	82
3.2.1 MATERIALS AND SUPPLIERS	82
3.2.2 STOCK SOLUTIONS	84

3.3 METHODS	85
3.3.1 HISTOLOGICAL ANALYSIS OF THE NHBE CELL CULTURES	85
3.3.1.1 TISSUE PROCESSING	85
3.3.1.2 PARAFFIN EMBEDDING	86
3.3.1.3 SECTIONING	86
3.3.1.4 DE-WAXING	86
3.3.1.5 HAEMATOXYLIN AND EOSIN (H+E) STAINING	87
3.3.1.6 DEHYDRATION AND MOUNTING	87
3.3.2 CHROMOGENIC IHC OF THE NHBE CELL CULTURES	87
3.3.2.1 ANTIBODY INCUBATION AND DETECTION	87
3.3.3 FLUORESCENT IHC OF THE NHBE CELL CULTURES	88
3.3.3.1 TISSUE PROCESSING	88
3.3.3.2 ANTIBODY INCUBATION AND DETECTION	89
3.3.4 IMMUNO EM OF THE NHBE CELL CULTURES	89
3.3.4.1 TISSUE PROCESSING	89
3.3.4.2 DEHYDRATION	90
3.3.4.3 RESIN INFILTRATION AND EMBEDDING	90
3.3.4.4 PREPARATION OF THE SUPPORTING FILM (PIOLOFORM)	90
3.3.4.5 PREPARATION OF GRIDS	90
3.3.4.6 SECTIONING	91
3.3.4.7 ANTIBODY INCUBATION AND DETECTION	91
3.3.4.8 COUNTER-STAINING	92
3.4 RESULTS	92
3.4.1 NHBE MORPHOGENESIS: HISTOLOGICAL ANALYSIS	92
3.4.2 NHBE MORPHOGENESIS: CHROMOGENIC IHC ANALYSIS	93
3.4.3 NHBE MORPHOGENESIS: FLUORESCENT IHC ANALYSIS	94
3.4.4 NHBE MORPHOGENESIS: IMMUNO EM ANALYSIS	95

3.5 DISCUSSION	97
3.5.1 NHBE MORPHOGENESIS: HISTOLOGICAL ANALYSIS	97
3.5.2 NHBE MORPHOGENESIS: CHROMOGENIC IHC ANALYSIS	97
3.5.3 NHBE MORPHOGENESIS: FLUORESCENT IHC ANALYSIS	98
3.5.4 NHBE MORPHOGENESIS: IMMUNO EM ANALYSIS	99
3.6 CONCLUSION	99
4. RESPONSE OF PRX STATUS TO HYDROGEN PEROXIDE EXPOSURE	101
4.1 INTRODUCTION	102
4.1.1 RESEARCH AIMS	103
4.2 MATERIALS AND STOCK SOLUTIONS	105
4.2.1 MATERIALS AND SUPPLIERS	105
4.2.2 STOCK SOLUTIONS	105
4.3 METHODS	106
4.3.1 H ₂ O ₂ EXPOSURE	106
4.3.2 ATP ASSAY	107
4.3.4 H ₂ O ₂ GENERATED BY GOX	108
4.3.5 GOX EXPOSURE	109
4.4 RESULTS	109
4.4.1 H ₂ O ₂ EXPOSURE	109
4.4.1.1 H ₂ O ₂ EXPOSURES: TEER AND ATP ANALYSIS	109
4.4.1.2 H ₂ O ₂ EXPOSURES: WB (TOTAL PRX LEVELS)	110
4.4.2 ANTIOXIDANT ADDITION	112
4.4.2.1 NAC EXPOSURES: TEER AND ATP ANALYSIS	112
4.4.2.3 GLUTATHIONE EXPOSURES: TEER AND ATP ANALYSIS	113
4.4.2.4 GLUTATHIONE EXPOSURES: WB (TOTAL PRX LEVELS)	114
4.4.3 GOX EXPOSURE	115

4.4.3.1 H ₂ O ₂ GENERATED BY GOX	115
4.4.3.2 GOX EXPOSURES: TEER AND ATP ANALYSIS	116
4.4.3.3 GOX EXPOSURES: WB (TOTAL PRX LEVELS)	117
4.4.3.4 GOX EXPOSURES: WB (ACTIVE PRX III)	119
4.5 DISCUSSION	121
4.5.1 H ₂ O ₂ EXPOSURE	121
4.5.2 ANTIOXIDANT ADDITION	123
4.5.3 GOX EXPOSURE	123
4.6 CONCLUSION	125
5. RESPONSE OF PRX STATUS TO CIGARETTE SMOKE EXPOSURE	126
5.1 INTRODUCTION	127
5.1.1 RESEARCH AIMS	127
5.2 MATERIALS AND STOCK SOLUTIONS	129
5.2.1 MATERIALS AND SUPPLIERS	129
5.3 METHODS	129
5.3.1 CS EXPOSURE	129
5.4 RESULTS	131
5.4.1 CS EXPOSURE: TEER AND ATP ANALYSIS	131
5.4.2 CS EXPOSURES: WB (TOTAL PRX LEVELS)	133
5.4.3 CS EXPOSURES: WB (ACTIVE PRX III)	137
5.4.4 CS EXPOSURE IHC ANALYSIS	140
5.5 DISCUSSION	142
5.5.1 CS EXPOSURE: TEER AND ATP ANALYSIS	142
5.5.2 CS EXPOSURE: WESTERN BLOT ANALYSIS	143
5.5.3 CS EXPOSURE: IHC ANALYSIS	144
5.6 CONCLUSION	145

6. <i>In Vivo</i> CORRELATION OF PEROXIREDOXIN STATUS	147
6.1 INTRODUCTION	148
6.1.1 RESEARCH AIMS	148
6.2 MATERIALS AND STOCK SOLUTIONS	150
6.2.1 MATERIALS AND SUPPLIERS	150
6.3 METHODS	150
6.3.1 HISTOLOGICAL ANALYSIS OF THE HUMAN TISSUE SAMPLES	150
6.3.1.1 SAMPLE ACQUISITION	151
6.3.1.2 SAMPLE PREPARATION	151
6.3.1.3 SECTIONING, DE-WAXING AND H+E STAINING	151
6.3.2 CHROMOGENIC IHC OF THE HUMAN TISSUE SAMPLES	152
6.4 RESULTS	153
6.4.1 GROSS PATHOLOGY	153
6.4.2 RE-EPITHELISATION (EARLY STAGE REPAIR)	154
6.4.3 HYPERPLASIA	156
6.4.4 INFLAMMATION	159
6.4.5 ENDOTHELIUM/ SMOOTH MUSCLE	161
6.5 DISCUSSION	162
6.5.1 BE REMODELLING	163
6.5.2 PRX AND CK 5/6 LEVELS IN THE BE OF THREE COPD PATIENTS	164
6.6 CONCLUSION	167
7. GENERAL DISCUSSION	168
7.1 RESEARCH OVERVIEW	169
7.1.1 RECAPITULATION OF HYPOTHESES	170
7.2 CONCLUSIONS	172
7.3 FUTURE WORK	175

7.3.1 <i>IN VITRO</i> NHBE MODEL	175
7.3.2 TOXICOLOGICAL EXPOSURE	178
7.3.3 EXPERIMENTAL DEVELOPMENT	178
7.4 FUTURE BENEFITS	179
7.5 FINAL CONCLUSION	181
REFERENCES	182
APPENDIX	223

ACKNOWLEDGEMENTS

Firstly, I would like to thank the Medical Research Council and AstraZeneca for funding my research project. In particular all those up in Loughborough who have been so generous with their time and knowledge throughout this project, a big thank you.

I would like to say a huge thank you to Dr. Kelly BéruBé and Dr. Victor Oreffo for giving me the opportunity to undertake this PhD project. Your continuous support and encouragement has no limits. Thank you both for all the time and energy you have spent on me. I'd also like to thank Dr. Nick Heintz for his input and expert knowledge, it has been extremely helpful and greatly appreciated, and finally Dr. Anthony Hann for all his expert guidance.

Thanks to everyone in W2.01 in both the KAB and DPR groups, I've really enjoyed all the big nights out, the sports debates and the banter (especially Wales v England!), you've all made the last three years really enjoyable (apart from the hangovers!). I would especially like to thank Keith (aka 'the oracle') your limitless knowledge and patience has been invaluable, without you it would have been impossible. Pat, we've made it through a degree and a PhD together (with a bit of help from YouTube and Facebook!), and I know we'll stay in touch for years to come. Zoe, thanks for teaching me everything I know about cell culture, and being there when I needed a chat and James, thanks for all the help you've given me, you're a great teacher.

Finally I would like to thank my family for all their love and support, my brother, grandparents, aunties, uncles and cousins; you've all been constantly there for me, whatever I needed. Most importantly I'd like to thank my Mam and Dad, I feel so lucky to have such amazing parents, you've always been there for me (even when I veered slightly off the straight and narrow!) and you've always believed in me, thank you so much, I hope I've made you proud. Lastly, and by no means least, my gorgeous kiwi (and hubby to-be!) Dan, thank you so much for all your support throughout my write-up, I couldn't have done it without you. This last year has been a mental whirlwind, I'm so happy I went to Ascot that day and I can't wait for us to get married and go on our epic adventure together! Caru ti am byth.

DECLARATION

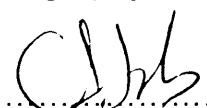
This work has not previously been accepted for any degree and is not concurrently submitted in candidature for any degree.

Signed  (Candidate)

Date 17-8-11

STATEMENT 1

This thesis is the result of my own investigations, except where otherwise stated. Other sources are acknowledged by footnotes giving explicit references. A bibliography is appended.

Signed  (Candidate)

Date 17-8-11

STATEMENT 2

I hereby give consent for my thesis, if accepted, to be made available for photocopying and for inter-library loan, and for the title and summary to be made available to outside organisations.

Signed  (Candidate)

Date 17-8-11

PUBLICATIONS

BéruBé, K.A., Prytherch, Z., Job, C., and Hughes, T. (2010). Human Primary Bronchial Lung Cell Constructs: The New Respiratory Models. *Toxicology* **278**: 311-318.

BéruBé, K.A., Pitt, A., Hayden, P., Prytherch, Z., and Job, C. (2010). Filter-Well Technology for Advanced Three-Dimensional Cell Culture: Perspectives for Respiratory Research. *Altern Lab Anim* **38 Suppl 1**: 49-65.

BéruBé, K.A., Gibson, C., Job, C., and Prytherch, Z. (2011). Human Lung Tissue Engineering: A Critical Tool for Safer Medicines. *Cell Tissue Bank* **12**: 11-13.

PUBLICATIONS (IN PREPARATION)

Job, C., Oreffo, V., Foster, M., Heintz, N., and BéruBé, K.A. (2011/12). Peroxiredoxin Status During NHBE Cell Model Morphogenesis.

Job, C., Oreffo, V., Foster, M., Heintz, N., and BéruBé, K.A. (2011/12). Peroxiredoxin as a Biomarker: Response to H₂O₂ and Cigarette Smoke.

Job, C., Oreffo, V., Foster, M., Heintz, N., and BéruBé, K.A. (2011/12). Using the Peroxiredoxins as Biomarkers of COPD.

COMMUNICATIONS

The Oxidation of Peroxiredoxins in Environmental Lung Injury and COPD. AstraZeneca Local Science Day, Alderly Edge, UK. **2011.** Platform Presentation.

Peroxiredoxins as Biomarkers: Response to H₂O₂ and Cigarette Smoke. AstraZeneca Local Science Day, Alderly Edge, UK. **2010.** Poster Presentation.

Using the Peroxiredoxins as Biomarkers of Oxidative Lung Injury. 8th CITER Annual Meeting, Cardiff University, UK. **2009.** 1st Prize Platform Presentation

Peroxiredoxins as Biomarkers of Intracellular Oxidative Stress. The Di-One Symposium: Moving Beyond reductionism in airways disease. Maastricht, Netherlands. **2009.** Poster Presentation.

Peroxiredoxin Status During NHBE Cell Model Morphogenesis. AstraZeneca Local Science Day, Alderly Edge, UK. **2009.** Poster Presentation.

ABBREVIATIONS

1°	Primary
2°	Secondary
α1-AT	α1 Antitrypsin
aa	Amino Acid
AB	Antibody
AFS	Automatic Freeze Substitution
AJ	Adherens Junctions
ALI	Air Liquid Interface
AO	Antioxidant
AOE 372	Antioxidant Enzyme 372
AoP1	Antioxidant Protein 1
APC	Antigen Presenting Cell
ARDS	Adult Respiratory Distress Syndrome
Arg	Arginine
ATF	Activating Transcription Factor
ATP	Adenosine Tri Phosphate
AU	Arbitrary Units
AZ	AstraZeneca
B	Catalytic Base
BAL	Bronchoalveolar Lavage
BALF	Bronchoalveolar Lavage Fluid
BC	Basal Cell
BCH	Basal Cell Hyperplasia
BDWG	Biomarkers Definitions Working Group
BE	Bronchial Epithelium
BEBM®	Bronchial Epithelium Basal Medium
BEGM®	Bronchial Epithelium Growth Medium
BSA	Bovine Serum Albumin
BT	Biotransformation
C	Acidic Base
CBE1	Ciliated Bronchial Epithelium 1
CC	Ciliated Cell

cDNA	Complimentary Deoxyribonucleic Acid
CDK	Cyclin Dependant Kinase
CK	Cytokeratin
CIC	Clara Cell
CO ₂	Carbon Dioxide
COPD	Chronic Obstructive Pulmonary Disease
CPD	Critical Point Drying
CS	Cigarette Smoke
Cu	Copper
CYP	Cytochrome
Cys	Cysteine
D	Desmosome
Da	Daltons
DAB	Diaminobenzidine
dH ₂ O	Deionised Water
ddH ₂ O	Double Distilled Water
DMEM	Dulbecco's Modified Eagle's Medium
DMSO	Dimethyl Sulfoxide
DNA	Deoxyribonucleic Acid
EC	Extra Cellular
ECM	Extra Cellular Matrix
EGF	Epidermal Growth Factor
EGFR	Epidermal Growth Factor Receptor
EM	Electron Microscopy
Erk1/2	Extracellular Signal-Related Kinase
EU	European Union
EVOM	Epithelial Voltmeter
FCS	Foetal Calf Serum
Fe ²⁺	Ferrous Ion
FEV ₁	Forced Expiratory Volume in 1 Second
FT	Full Thickness
FVC	Forced Vital Capacity
GA	Gluteraldehyde
GC	Goblet Cell

GCH	Goblet Cell Hyperplasia
GCM	Goblet Cell Metaplasia
GOLD	Global Initiative for Obstructive Lung Disease
GOx	Glucose Oxidase
GPx	Glutathione Peroxidase
GSH	Glutathione
H₂O₂	Hydrogen Peroxide
HBP23	Heme Binding Protein 23
HBSS	Hank's balanced Salt Solution
H+E	Haematoxylin and Eosin
His	Histidine
Hr	Hour(s)
HRP	Horseradish Peroxidase
HTP	High Throughput
IARC	International Agency for Research on Cancer
IC	Intermediate Cell
Ig	Immunoglobulin
IHC	Immunohistochemistry
IL	Interleukin
ISO	International Standardisation Organisation
IUPAC	International Union of Pure Applied Chemistry
JNK	c-Jun N Terminal Kinase
LC	Lead Citrate
LM	Light Microscopy
LPO	Lipid Peroxidation Products
LSD	Least Significant Difference
Lys	Lysine
MAPK	Mitogen Activated Protein Kinase
MEK	Mitogen Activated Protein Kinase Kinase
MER5	Murine Erythroleukemia Cells
MESNA	2-Mercaptoethanosulfonate
Min	Minute(s)
MMP	Matrix Metalloproteinase
Mn	Manganese

MRC	Medical Research Council
MSP23	Macrophage23KDa Stress-Induced Protein
n	Number of replicates
N	Nucleus
NAC	N-Acetyl Cysteine
NADPH	Nicotinamide Adenine Dinucleotide Phosphate
NBF	Neutral Buffered Formalin
NFkB	Nuclear Factor Kappa B
NHBE	Normal Human Bronchial Epithelium
NKEF-A	Natural Killer Cell Enhancing Factor A
NKEF-B	Natural Killer Cell Enhancing Factor B
NO	Nitric Oxide
NO₂	Nitrogen Dioxide
NOEL	No Observed Effect Level
O₂	Oxygen
O₂⁻	Superoxide Anion
OH[•]	Hydroxyl Radical
ONOO⁻	Peroxynitrite
OSF3	Osteoblast Specific Factor 3
OT	Osmium Tetroxide
PAG1	Proliferation-Associated Gene 1
PAGE	Polyacrylamide Gel Electrophoresis
PAS	Periodic-Acid Schiff
PBS	Phosphate Buffered Saline
P-Erk1/2	Phosphorylated Extracellular Signal-Related Kinase 1/2
PFA	Paraformaldehyde
PrP	Prion Protein
Pro	Proline
Prx	Peroxiredoxin
Prx-SO₃	Hydroxymethylated Peroxiredoxin
PVDF	Hybond-P Polyvinylidene difluoride
Q-PCR	Quantitative Polymerase Chain Reaction
RA	Retinoic Acid
RB	Respiratory Bronchioles

RNA	Ribonucleic Acid
ROS	Reactive Oxygen Species
RpT	Respiratory Tract
RT	Room Temperature
SD	Standard Deviation
SDS	Sodium Dodecyl Sulphate
Sec	Second(s)
SLPI	Secretory Leukocyte Protease Inhibitor
SMGC	Small Mucous Granule Cells
SOD	Superoxide Dismutase
S_P	Peroxidatic Cysteine
SP	Sodium Periodate
S_POH	Sulphenic Acid
S_R	Resolving Cysteine
S-S	Disulphide Bond
TBS/T	Tris Buffered Saline/ Tween-20
TCA	Trichloroacetic Acid
TD₂₀	Toxic Dose 20%
TEER	Trans-Epithelial Electrical Resistance
TEM	Transmission Electron Microscopy
Thr	Threonine
TJ	Tight Junctions
TNF	Tumour Necrosis Factor
TPx	Thioredoxin Peroxidase
Trx	Thioredoxin
TSA	Thiol Specific Antioxidant
UA	Uranyl Acetate
UV	Ultra Violet
WAG	Welsh Assembly Government
WB	Western Blot
WHO	World Health Organisation
Z	Generation
Zn	Zinc

ABSTRACT

Numerous chronic lung diseases are characterised by oxidative stress or more accurately, perturbations in redox cycling and signalling. Cellular redox alterations lead to phenotypic adaptations such as increased cell proliferation, altered differentiation and induction of apoptosis. Biomarkers that reflect changes in cellular oxidation states as a function of normal redox signalling as well as following environmental insults would be extremely useful for studying disease processes in the lung *in vitro* and *in vivo*. One current area of interest in this field is the Peroxiredoxins (Prxs), a family of ubiquitously expressed antioxidant (AO) enzymes. The aim of this project was to assess the utility of measuring the changes in Prx expression levels and oxidation states as a quantitative biomarker of oxidative lung injury.

Utilising normal human bronchial epithelial (NHBE) primary cells, which were cultured at an air-liquid interface (ALI), Prx status was analysed throughout culture morphogenesis, and following oxidative insult via glucose oxidase (GOx) and cigarette smoke (CS) exposures. Human *in vivo* correlation was also undertaken, using lung tissue from COPD (GOLD4) patients. Results were analysed using conventional toxicology, Western blotting (WB) and immunohistochemistry (IHC) techniques. Preliminary results revealed elevated basal levels of oxidative stress within the NHBE model, which was alleviated via the addition of AO to the media. Following GOx and CS exposures, there was increased Prx hyperoxidation in conjunction with variations in expression. A dose-dependant response to GOx and CS was observed in the NHBE cultures +AO. Variations in Prx expression levels and oxidation state were also detected throughout the *in vivo* correlation, with specific Prx responses observed in the different stages of airway remodelling.

The Prxs were determined to be sensitive and reliable biomarkers of intracellular oxidative stress, injury severity and epithelial remodelling, thus indicating a role for the Prxs as an 'early stage' biomarker, with disruptions in redox state occurring in advance of phenotypic or morphological adaptations. Additionally, by eliminating the issue of interspecies reactivity, there may be a potential role for the NHBE-Prx system as an *in vivo* pre-screening tool.

CHAPTER 1:

INTRODUCTION

1.1 STUDY INTRODUCTION

Numerous chronic lung diseases are characterised by oxidative stress or more accurately, perturbations in redox cycling and signalling (Jones, 2006). Cellular redox alterations lead to phenotypic adaptations such as increased cell proliferation, altered differentiation and induction of apoptosis (Thannickal and Fanburg, 2000; Halliwell, 2007a). Biomarkers that reflect changes in cellular oxidation states, as a function of normal redox signalling and following environmental insults would be extremely useful for studying disease processes in the human lung at both the *in vitro* and *in vivo* levels.

Peroxiredoxins (Prxs) are a family of ubiquitously expressed antioxidant (AO) enzymes that regulate oxidant-dependant signalling through a variety of redox dependant pathways (Hofmann *et al.*, 2002). The principal investigation site of this research project was the bronchial epithelium (BE), with the aim being to assess the utility of measuring the changes in Prx expression levels and oxidation states as a quantitative biomarker of oxidative lung injury, such as that observed in chronic obstructive pulmonary disease (COPD).

1.2 THE HUMAN RESPIRATORY SYSTEM

Respiration in humans can be defined as the exchange of gases between the cells of the body and the external environment; the mechanical aspect of respiration is the movement of air in and out of the lungs or ventilation. Respiration itself can be divided into two types, external and internal. External respiration involves gas exchange between the lungs and the blood, whereas internal respiration is the exchange of gas between the blood and the cells of the body (Shier *et al.*, 2004).

1.2.1 STRUCTURE AND FUNCTION OF THE RESPIRATORY SYSTEM

Anatomically, the human respiratory tract (RpT) can be divided into two regions: (1) the upper RpT; nose, nasal passages, sinuses and the pharynx, and (2) the lower RpT; larynx, trachea, bronchi, bronchioles, respiratory

bronchioles and the alveolar unit (Figure 1.1; Levitsky, 2003). The lower RpT can be further divided into the distal RpT, to denote the regions involved in gas exchange (i.e. respiratory bronchioles and alveoli). The function of the upper airways is mainly to warm and humidify the inspired air, but the nose is also a potent filter, using its vibrissae (nasal hairs) and mucous membrane to trap and then clear particles larger than $10\mu\text{m}$ in diameter (Berne *et al.*, 2004). Airway mucus protects the airways from any harmful inspired molecules and also prevents the desiccation of the airway surfaces (Chilvers and O'Callaghan, 2000). The lower RpT conducts the inspired air from the external environment to the site of gaseous exchange whilst ensuring that any harmful molecules are removed before they reach the alveoli (Hasleton, 1996). The distal RpT is the site of gaseous exchange, where the alveoli provide a large surface allowing O_2 to diffuse into the pulmonary capillaries and CO_2 to diffuse into the alveolus (Gardner, 2006).

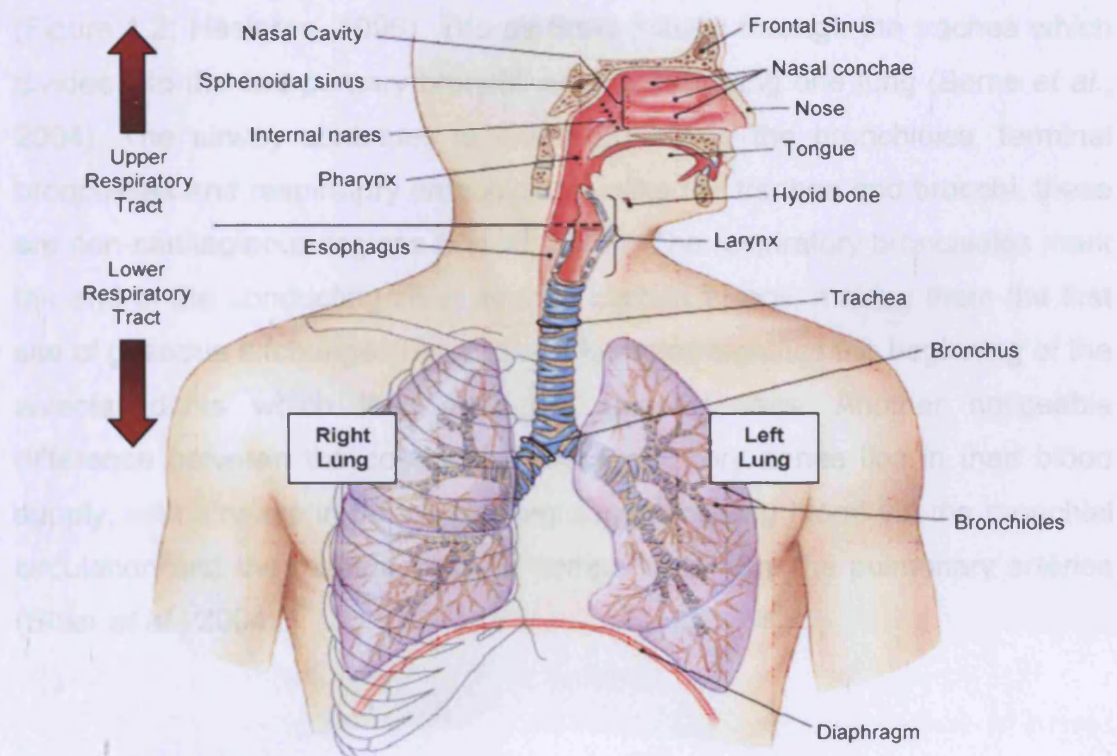


Figure 1.1: Depiction of the anatomy of the respiratory system.

The respiratory system can be divided into the upper and lower RpT. The lower respiratory tract can be further divided into the distal RpT, with the latter containing all regions involved in gas exchange (Adapted from Sexton, 2009).

bronchioles and the alveolar unit (Figure 1.1; Levitsky, 2003). The lower RpT can be further divided into the distal RpT, to denote the regions involved in gas exchange (i.e. respiratory bronchioles and alveoli). The function of the upper airways is mainly to warm and humidify the inspired air, but the nose is also a potent filter, using its vibrissae (nasal hairs) and mucous membrane to trap and then clear particles larger than $10\mu\text{m}$ in diameter (Berne *et al.*, 2004). Airway mucus protects the airways from any harmful inspired molecules and also prevents the desiccation of the airway surfaces (Chilvers and O'Callaghan, 2000). The lower RpT conducts the inspired air from the external environment to the site of gaseous exchange whilst ensuring that any harmful molecules are removed before they reach the alveoli (Hasleton, 1996). The distal RpT is the site of gaseous exchange, where the alveoli provide a large surface allowing O_2 to diffuse into the pulmonary capillaries and CO_2 to diffuse into the alveolus (Gardner, 2006).

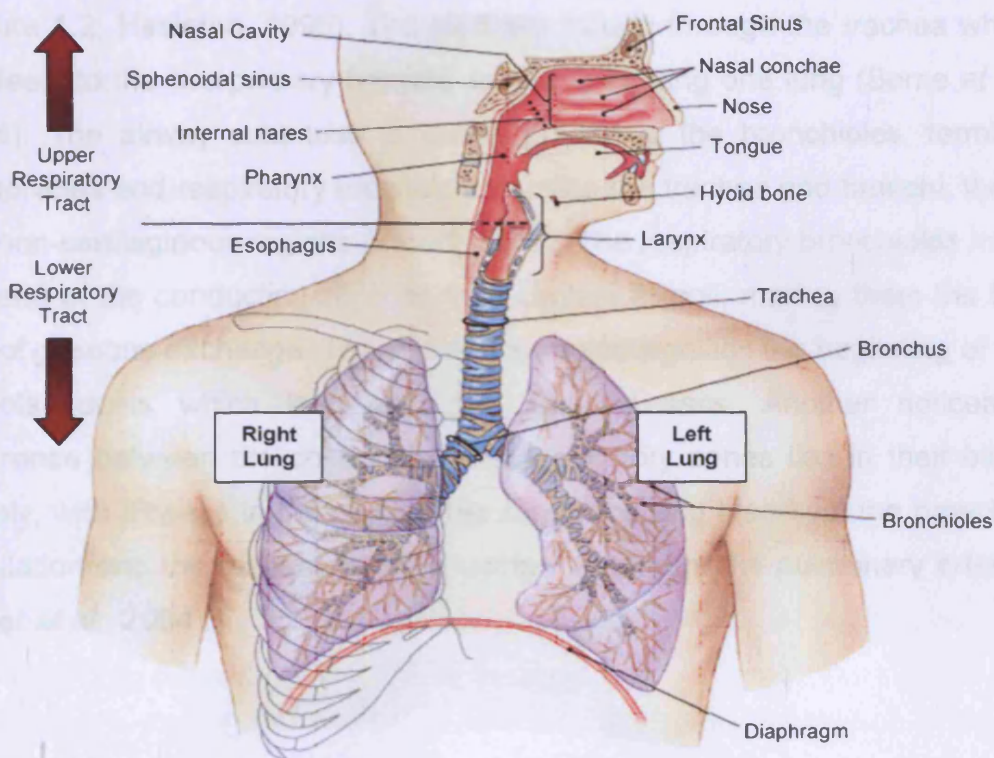


Figure 1.1: Depiction of the anatomy of the respiratory system.

The respiratory system can be divided into the upper and lower RpT. The lower respiratory tract can be further divided into the distal RpT, with the latter containing all regions involved in gas exchange (Adapted from Sexton, 2009).

Functionally, the respiratory system is divided into two zones: (1) the 'conducting' and (2) the 'respiratory' (Figure 1.2; Hasleton, 1996). The conducting zone consists of the trachea, bronchi, bronchioles and terminal bronchioles. It is named so as air merely passes through its structures (i.e. conducts air) and has no gas exchange with the blood; the volume of air within this zone is referred to as anatomic dead space (West, 1995). The respiratory zone is the region where gas exchange takes place between the lungs and the pulmonary capillaries (Gardner, 2006).

1.2.2 ANATOMY OF THE LUNGS

The lungs are divided into five lobes, where the right lung consists of upper, middle and lower lobes and the left lung has only an upper and lower lobe (Levitsky, 2003). Air enters the lungs via the tracheobronchial system, also known as the bronchial tree, which contains up to 23 airway generations (Figure 1.2; Hasleton, 1996). The air flows initially through the trachea which divides into the two primary bronchi, each penetrating one lung (Berne *et al.*, 2004). The airway continues to divide producing the bronchioles, terminal bronchioles and respiratory bronchioles, unlike the trachea and bronchi, these are non-cartilaginous regions (Proud, 2008). The respiratory bronchioles mark the end of the conducting zone as they contain alveoli, making them the first site of gaseous exchange. The end of this region signifies the beginning of the alveolar ducts which lead onto the alveolar sacs. Another noticeable difference between the conducting and respiratory zones lies in their blood supply, with airways in the conducting zone receiving blood via the bronchial circulation and the respiratory zone components from the pulmonary arteries (Shier *et al.*, 2004).



Zones	Anatomy	Structure	Generation (Z)	Cell Types
Conducting Zone		Larynx	N/A	<ul style="list-style-type: none">• Ciliated Cells• Goblet Cells• Basal Cells
		Trachea	0	<ul style="list-style-type: none">• Ciliated Cells• Goblet Cells• Basal Cells• Serous Cells• Serous Gland Cells• Mucous Gland Cell
		Primary Bronchi	1	
		Secondary Bronchi	2	<ul style="list-style-type: none">• Ciliated Cells• Goblet Cells• Basal Cells• Serous Cells
		Tertiary Bronchi	3	
		Small Bronchi	4	
		Bronchioles	5	
		Terminal Bronchioles	6-16	<ul style="list-style-type: none">• Ciliated Cells• Clara Cells• Basal Cells
Respiratory Zone				<ul style="list-style-type: none">• Ciliated Cells• Clara Cells• Basal Cells
		Respiratory Bronchioles	17-19	<ul style="list-style-type: none">• Alveolar Type I Cells• Alveolar Type II Cells
		Alveolar Sacs	23	<ul style="list-style-type: none">• Alveolar Type I Cells• Alveolar Type II Cells

Figure 1.2: Conducting and respiratory zones of the RpT.

The conducting zone consists of the trachea, bronchi and terminal bronchioles, air passes through these structures and no gaseous exchange takes place. The respiratory zone consists of respiratory bronchioles, the alveolar ducts and alveolar sacs; this is the site of gas exchange between the lung and pulmonary capillaries. The branching of the airways form up to 23 generations (Z), from the trachea $Z = 0$ to the alveolar sacs $Z = 23$ (not shown above are the alveolar ducts, $Z = 20-22$) (Adapted from Bérubé *et al*, 2010b).

1.3 THE PULMONARY EPITHELIUM

As the airway progresses from the conducting to the respiratory zones, the cell types alter to accommodate the function of each region (Figure 1.3). At the transition from the vestibule (conductive portion following the nostrils) to the respiratory region of the nasal cavity, the epithelium becomes first stratified squamous and then pseudo-stratified columnar and ciliated (Popp and Martin, 1984). This type of epithelium is characteristic for all conductive passages dedicated to the respiratory system, and therefore, it is also referred to as the 'respiratory epithelium'. Mucus producing goblet cells (GC) are present in the epithelium, along with ciliated and basal cells (BC), all of which are firmly attached to the basal membrane (Knight and Holgate, 2003). Submucosal glands also line the trachea and bronchi, and contain serous and mucous gland cells, that supplement the secretions of the GCs (Meyrick and Reid, 1970).

As the airway divides from the bronchioles into the terminal bronchioles, the numbers of ciliated cells (CC) decrease and eventually cease before the division into respiratory bronchioles (Hasleton, 1996). Clara cells are found in the terminal and respiratory bronchioles, whereby they replace the GCs of the more proximal airway tract, and secrete proteins used in xenobiotic metabolism (Reynolds and Malkinson, 2010).

The gaseous exchange region of the human lung is only 0.2-0.4 μ m in thickness; however, the barrier possesses great strength which is essential in order to avoid stress failure (Costello *et al.*, 1992; West and Mathieu-Costello, 1999). The alveolar unit contains Type I and II alveolar pneumocyte cells, which work in conjunction to ensure effective oxygen delivery to the blood stream (Hansel and Barnes, 2004). Type I pneumocytes act to provide a large thin surface area where gas exchange occurs, accounting for 95% of the alveolar lining but only 40% of pneumocytes. The most important role of the Type II pneumocyte is surfactant production; which acts to prevent the collapse of the alveoli; they account for only 5% of the alveolar lining but make up 60% of pneumocytes (Hasleton, 1996).

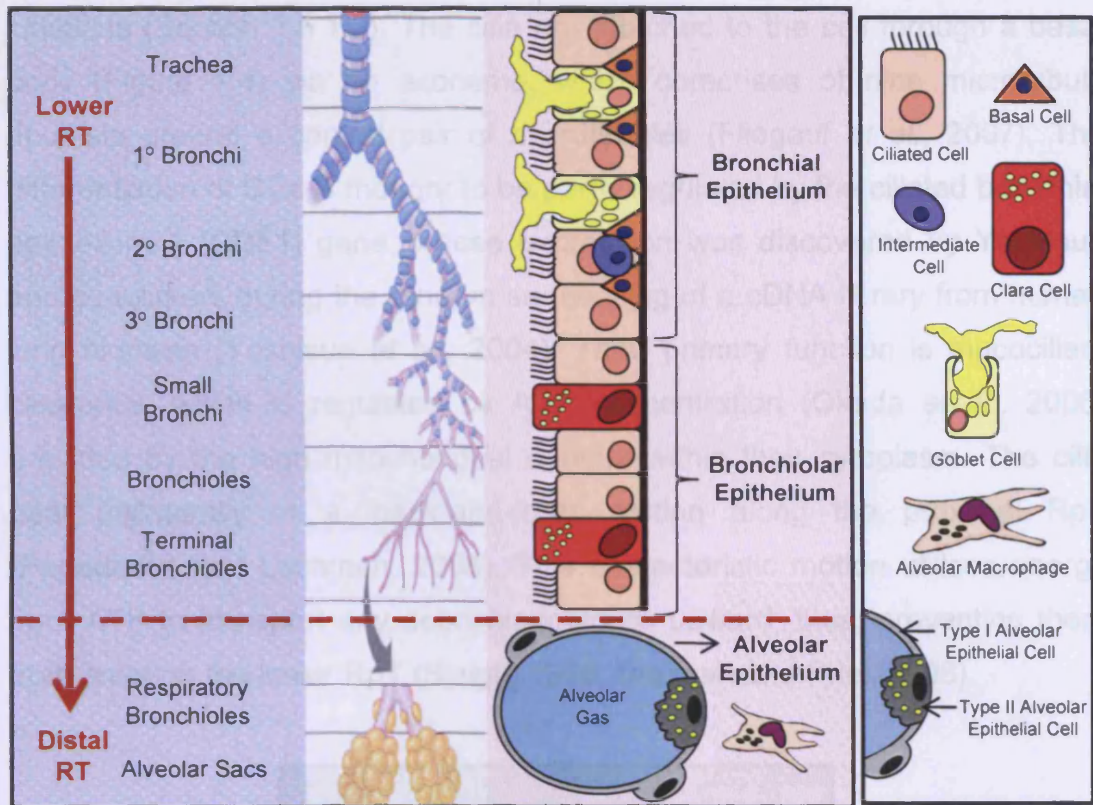


Figure 1.3 Cells of the pulmonary epithelium.

The more proximal region of the lower RpT consists of a BE, as the airways decrease in size the epithelium becomes more characteristically bronchiolar. The distal airways, also known as the region of gaseous exchange comprises of alveolar epithelium, which include type I and II alveolar epithelial cells and alveolar macrophages (Bérubé *et al.*, 2010b, Drawn by C.Job).

1.4 CELLS OF THE BRONCHIAL EPITHELIUM

The BE contained within the lower RpT consists of CCs, BCs, intermediate cells (IC) and GCs (Figure 1.3). The epithelium of this region represents the focal point of the PhD investigation, and as such, the constituent cells of the distal RpT will not be discussed.

1.4.1 CILIATED CELLS

CCs are roughly columnar in shape (20µm in length and 10µm in width), and are covered with ~250 cilia (3-6µm in length and 0.3µm in width). They outnumber GCs in the ratio of 5:1 in the BE (Knight and Holgate, 2003) and are attached to the basal lamina via desmosomes and interconnected via tight

junctions (Section 1.5.1.2). The cilia are attached to the cell through a basal body (Figure 1.4) via an axoneme, which comprises of nine microtubule doublets around a central pair of microtubules (Fliegeauf *et al.*, 2007). The differentiation of CCs is thought to be partly regulated by the ciliated bronchial epithelium 1 (CBE1) gene, whose expression was discovered by Yoshisue and co-workers during the random sequencing of a cDNA library from human lung biopsies (Yoshisue *et al.*, 2004). Their primary function is mucociliary clearance, which is regulated by ATP concentration (Okada *et al.*, 2006) provided by the high mitochondrial content within their cytoplasm. The cilia beat unilaterally in a 'back-and-forth' motion along the proximal RpT (Papadakos and Lachman, 2008). This characteristic motion utilises energy from ATP to transport any debris/xenobiotics upward, thus, preventing them from entering the lower RpT (Sleigh, 1990; Braiman and Priel, 2008).

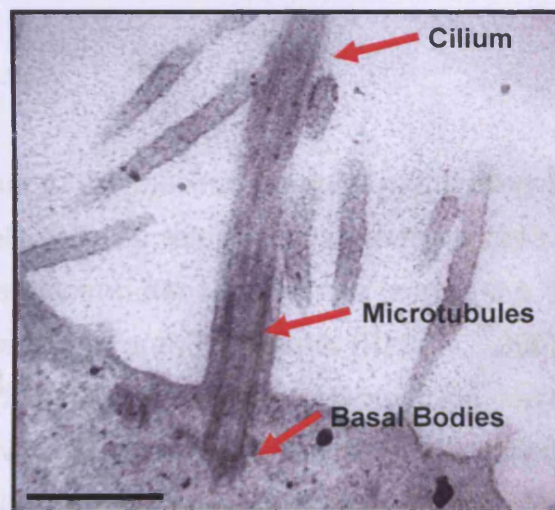


Figure 1.4: TEM image of cilia on the apical surface of the BE.

Transmission electron micrograph (TEM) image of the NHBE cells (*in vitro* cell culture) from Day 15. Cilia may be seen protruding from the apical surface of the BE. Basal bodies may be observed just under the apical surface and the internal microtubules were evident. Scale bar represents 500nm (Image courtesy Dr. K. Bérubé, Cardiff University).

Interspersed among the cilia are microvilli (2µm in height and 0.1µm in width). Microvilli are particularly abundant on the apical surface of the CCs and immature CCs (Figure 1.5; Breeze and Wheeldon, 1977). The microvilli are also associated with mucous cells; either small mucous granule cells (SMGC) or mucus filled GCs (McDowell *et al.*, 1978).

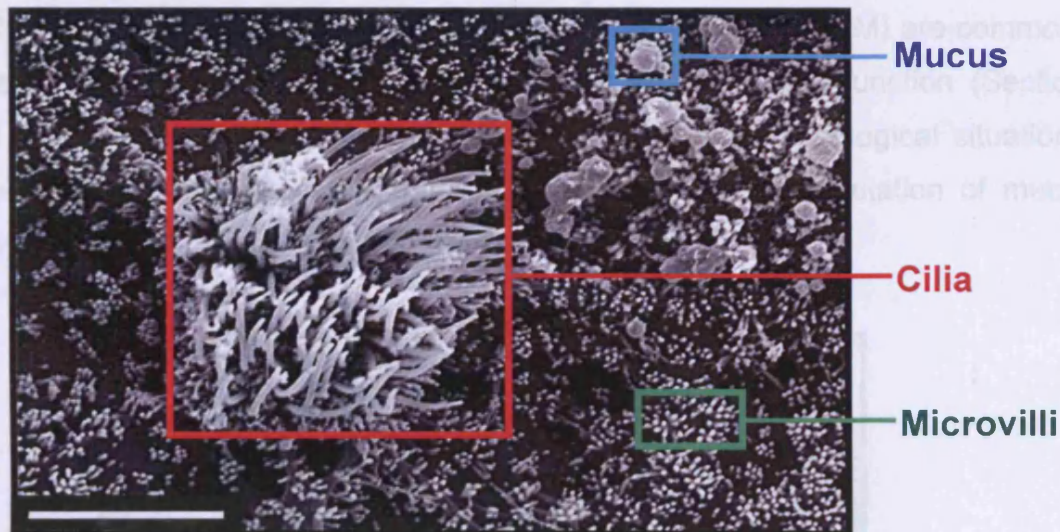


Figure 1.5: SEM image of the BE apical surface.

Scanning electron micrograph (SEM) image of the NHBE cells (*in vitro* cell culture) from Day 27, showing the cilia, microvilli and mucus droplets. Scale bar represents 5 μ m (Image courtesy of Dr. Z. Prytherch, Cardiff University).

1.4.2 GOBLET CELLS

GCs, named so due to the mucous granules within their cytoplasm creating a 'goblet' shaped cell, are also referred to as mucous cells (Proud, 2008). They often appear to be electron-dense in comparison to the other cells of the BE, due to their high secretory granule content (Rhodin, 1966). GCs are dispersed throughout the BE, primarily in the cartilaginous regions, becoming less frequent as the airway becomes smaller in the more distal regions, where they are replaced by Clara cells (Davis and Dickey, 2008). The GCs are secretory cells that release mucus by merocrine-type secretion (Figure 1.6). The mucus serves a protective function by trapping any unwanted particles and removing them from the airflow (Rogers, 2003) (Section 1.5.1.3). This protective mucus barrier is the primary function of GCs (Chilvers and O'Callaghan, 2000).

GCs are known to be capable of differentiating into CCs when required, primarily following injury to the epithelium (Ayers and Jeffery, 1988). Conversely, progenitor CCs that contain the CC marker FOXJ1 have been shown to differentiate into GCs under pathological conditions (i.e. asthma and COPD), leading to mucus overproduction within the airway (Turner *et al.*,

2011). In COPD, GC hyperplasia (GCH) and metaplasia (GCM) are common, leading to increased mucus secretion and impaired lung function (Section 1.7.3). The inflammatory conditions observed during pathological situations also induce mucous metaplasia, manifested by the up-regulation of mucin synthesis in Clara cells (Davis and Dickey, 2008).

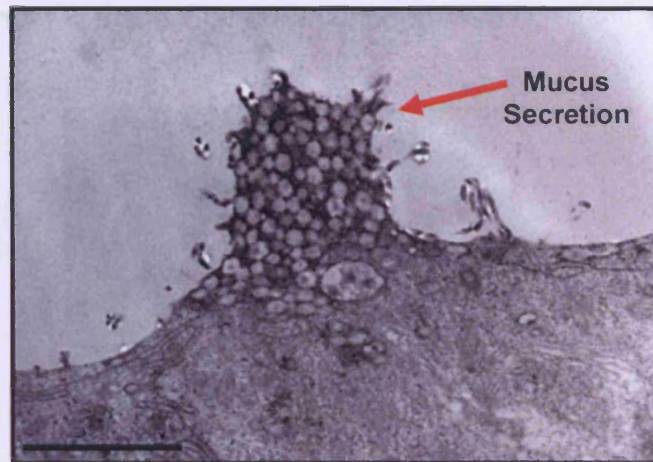


Figure 1.6: TEM image of mucus secretion.

TEM image of the NHBE cells (*in vitro* cell culture) from Day 30. This image reveals a mucus droplet being released from a goblet cell at the apical surface of the BE. Scale bar represents 2 μ M (Image courtesy of Dr. K. Bérubé, Cardiff University).

1.4.3 BASAL CELLS

BCs are relatively round and small (Figure 1.7) in comparison to CCs and GCs (Rhodin, 1966), and are firmly attached to the basement membrane via hemidesmosomes (Section 1.5.1.2) (Knight and Holgate, 2003). They cover a large surface area and provide desmosomal attachments (Section 1.5.1.2) for CCs and GCs to the basal lamina, creating the pseudo-stratified appearance (Baldwin, 1994). BC numbers decrease as the generations of the RpT increase, with BCs accounting for 31% in the airways with a diameter of 4mm or more, but only 6% in airways with a diameter of less than 0.5mm (Boers *et al.*, 1998). A unique feature of the BCs is their progenitor stem cell-like ability, allowing them to repopulate the BE by differentiating into BCs, ICs, CCs and GCs (Breeze and Wheeldon, 1977; Ayers and Jeffery, 1988; Engelhardt *et al.*, 1995; Hong *et al.*, 2004).

G

1.4.4 INTERMEDIATE CELLS

ICs can be seen throughout the pseudo-stratified BE positioned slightly above the BC layer but beneath the GCs and CCs (Figure 1.7). The term 'intermediate' is indicative of cells that are in the process of differentiating into surface epithelial cells (Hasleton, 1996), and therefore the ICs are capable of differentiating into GCs and CCs (Blenkinsopp, 1967).

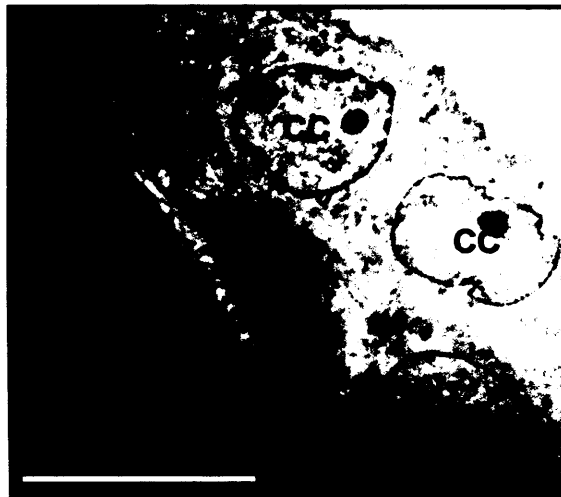


Figure 1.7: TEM image of the bronchial epithelium.

TEM image of the NHBE cells (*in vitro* cell culture) from Day 27. This image reveals the intermediate cells (IC) present throughout the pseudo-stratified BE, being positioned slightly above the basal cell (BC) layer but beneath the goblet and ciliated cells (CC). Scale bar represents 400 μ M (Image courtesy of Dr. K. Bérubé, Cardiff University).

1.4.5 CLARA CELLS

As the airway progresses throughout the conducting region toward the bronchioles, the GCs are replaced by Clara cells (CIC) (Widdicombe, 2002). CIC are non-ciliated, non-mucus, dome-shaped, secretory epithelial cells, that contain microvilli on their apical surface. They are renowned for being metabolically very active and contain numerous mitochondria for this purpose (Boers *et al.*, 1999). CICs are known to secrete a variety of proteins: 10kDa protein (CC10 or CCSP); 55kDa protein; tryptase, β -galactoside-binding lectin; surfactant proteins A, B and D (SpA, SpB and SpD); and phospholipase. CC10 is one of the most prevalent proteins in the airway lining

fluid (Berne *et al.*, 2004) with its main actions thought to be anti-inflammatory and immuno-suppressive (Singh and Katyal, 2000) CICs also possess a stem cell like ability, where they contribute to cell renewal in normal conducting airways (Reynolds and Malkinson, 2010).

1.5 DEFENCE MECHANISMS OF THE RPT

The RpT is a prime target for oxidative injury due to its direct exposure to harmful compounds. Consequently, it relies on a battery of defence mechanisms to remove any potential threat. Initial protection is non-specific and provided by ever-present mechanical barriers and components of the innate immune system (Medzhitov and Janeway, 1997). Failure of the innate system to eliminate any inhaled debris (e.g. solid and gaseous detritus) results in the activation of the adaptive immune system; a specific response induced by exposure to non-self substrates (Gardner, 2006). The two systems are not mutually exclusive; they operate in conjunction with one another to protect the lung. The components of the two systems can be divided into non-immunological and immunological defence mechanisms.

1.5.1 NON-IMMUNOLOGICAL DEFENCE MECHANISMS

Non-immunological processes are the first line of defence against inhaled xenobiotics. They include reflexive responses such as coughing or sneezing and mechanical barriers, including nasal hairs (i.e. vibrissae) and mucus (Korpas and Honda, 1996). Mucociliary clearance is considered to be non-immunological; however, many mucus components are, in fact, immunological (Section 1.5.1.3).

1.5.1.1 MECHANICAL BARRIERS

Inhaled particles are humidified as they enter the upper RpT, with their diameter determining their depth of penetration (Bittar, 2002). Nasal hairs act as the initial filter, trapping the majority of particles over 20µm in diameter. Mouth breathing also acts as a filter with the use of saliva and mucus lined

walls, dissolving toxic gases (Germann and Stanfield, 2004) and preventing most particles over 10µm proceeding to the trachea (Berne *et al.*, 2004). However, if particles do avoid capture by the nasal hairs and proceed to the nasal cavity, they can stimulate nerve endings, resulting in a cough or sneeze reflex. This either propels the particle from the body or allows them to be swallowed down the gastrointestinal tract (Hlastala and Berger, 2001).

1.5.1.2 CELL JUNCTIONS IN THE BE

Maintenance of the protective barrier between the cells of the BE and the airway lumen is essential for sustaining a healthy epithelial phenotype (Folkerts and Nijkamp, 1998). The cell-cell junctions present within the BE include the tight junctions (i.e. zonula occludens; closely associated areas of two cells), adherens junctions (i.e. zonula adherens; protein complexes that occur at cell-cell junctions in epithelial tissue), desmosomes (i.e. macula adherens; localised spot-like adhesions on lateral side of plasma membranes), and the gap junctions, whereby the cytoplasms of neighbouring cells are directly inter-connected, which allow ions to pass freely between cells. There are also cell-matrix junctions in the form of hemidesmosomes that anchor the cells to the basal lamina (Figure 1.8; Alberts *et al.*, 2002).

1.5.1.3 MUCOCILIARY ESCALATOR

Epithelial protection is provided by airway mucus, which is a viscoelastic gel that forms a thin film overlaying the internal surface of the airway (Chilvers and O'Callaghan, 2000). Mucus is a heterogeneous mixture of water, ions, proteins, lipids, glycoproteins and a myriad of primary defence mechanisms (i.e. inflammatory cells and immunoglobulins), with the major macromolecule constituent of mucus being the long, thread-like, high-molecular-weight glycoprotein mucin (Rose and Voynow, 2006). The secreted oligomeric mucin provides mucus with its rheological properties, by controlling its consistency and hence gel formation (Thornton and Sheehan, 2004). MUC5AC, MUC2 and MUC5B are the major mucins present in airway secretions (Davies *et al.*, 2002), and recent studies have shown that activation of the epidermal growth

factor receptor (EGFR) plays a pivotal role in the expression of the MUC genes (Takeyama *et al.*, 2001; Rogers, 2003). The mucus functions by trapping harmful particles, allowing them to be removed by the cilia towards the pharynx for degradation or 'mucociliary clearance' (Figure 1.9; Braiman and Priel, 2008). Although mucociliary clearance is seen as a non-immunological process, numerous mucus components are in fact immunological, including, immunoglobulin A, lysozyme, and defensins, lactoferrin and collectins (Nicod, 1999; Boyton and Openshaw, 2002).

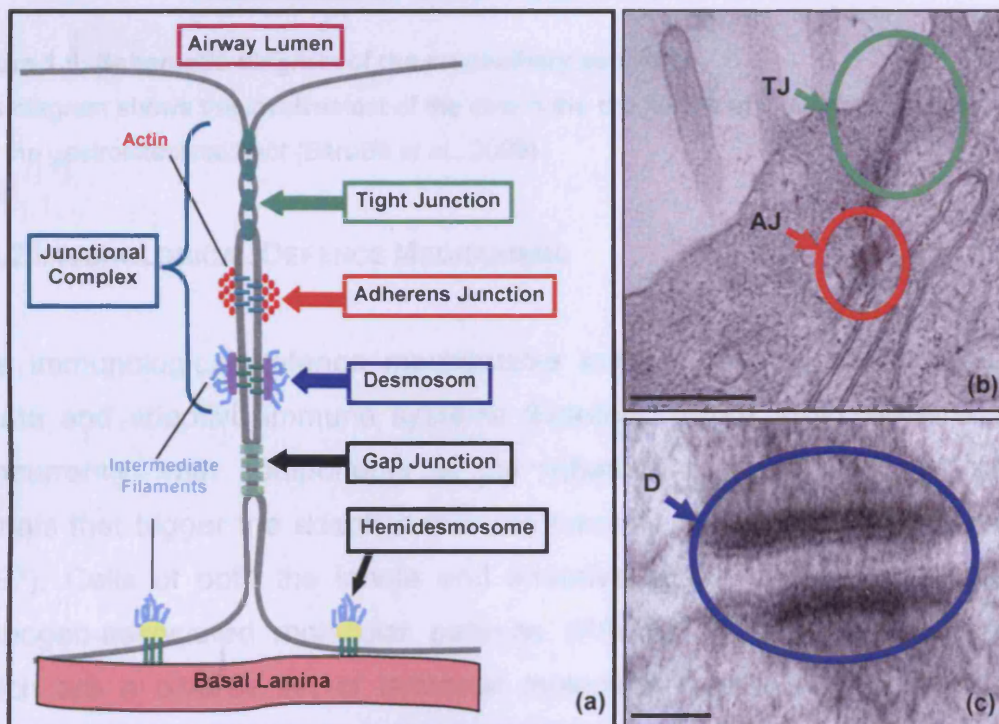


Figure 1.8: Schematic diagram of the various epithelial cell junctions.

(a) Tight junctions are essential in maintaining the barrier properties of epithelial sheets. Adherens junctions are associated with actin filaments, usually forming an adhesion belt around the cells. Desmosomes form cell-cell contacts and are associated with intermediate filaments. Gap junctions allow the passage of small water-soluble ions and molecules. Hemidesmosomes resemble half a desmosomes and form cell-extracellular matrix junctions. (b) TEM image of the NHBE cells (*in vitro* cell culture) from Day 9. This apical surface view shows microvilli, tight junctions (TJ) and adherent junctions (AJ). (c) TEM image of the NHBE cells (*in vitro* cell culture) from Day 9. This image shows a desmosome (D), which is found at the mid-basal surface of the BE. Scale bars represent (b) 500nm and (c) 100nm. (Adapted from Bérubé *et al.*, 2010b).

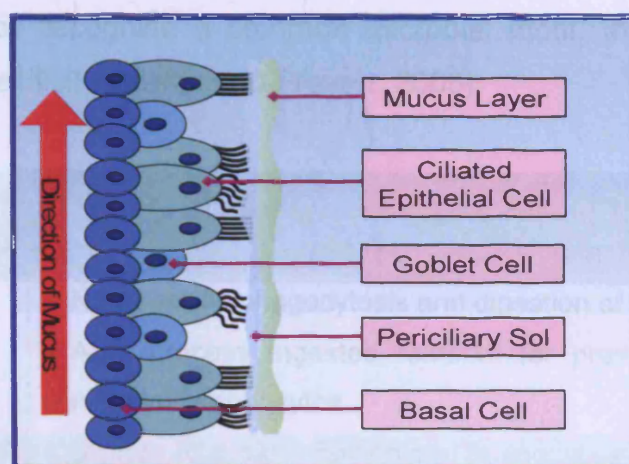


Figure 1.9: Schematic diagram of the mucociliary escalator.

This diagram shows the involvement of the cilia in the propulsion of mucus out of the airways into the gastrointestinal tract (Bérubé *et al.*, 2009).

1.5.2 IMMUNOLOGICAL DEFENCE MECHANISMS

The immunological defence mechanisms include constituents of both the innate and adaptive immune systems (Gardner, 2006). Both systems work concurrently, with components of the innate immune system generating signals that trigger the adaptive immune response (Medzhitov and Janeway, 1997). Cells of both the innate and adaptive immunity systems recognise pathogen-associated molecular patterns (PAMPs) on invading pathogens, which are a diverse set of microbial molecules (Janeway and Medzhitov, 2002). The PAMPs are recognised primarily through the toll-like receptors (TLRs) present on the cells of the innate and adaptive immunity systems; this activation goes on to activate signalling pathways including the NF- κ B pathway. The PAMPs are considered to be a subgroup of the larger damage associated molecular patterns (DAMPs) family (Bianchi, 2007).

1.5.2.1 INNATE IMMUNITY

Innate immunity refers to the non-specific and ever-present components of the immune system (Table 1.1). They include the cells and their products that act immediately to eliminate inhaled pathogens within minutes to hours (Travis *et al.*, 2001). Innate immune components include soluble proteins and

leukocytes. They recognise a common microbial motif, that provides them with a broad specificity (Martin and Frevert, 2005).

Innate immunity cell type	Function within the innate immune system of the RT
Macrophage	<ul style="list-style-type: none"> • Non-specific phagocytosis and digestion of antigenic substances • APC process ingested material for presentation to antigen-reactive lymphocytes
Neutrophil	<ul style="list-style-type: none"> • Migrate to site of infection and phagocytise invading particles • Contain enzymes within their secretory granules, aiding destruction of engulfed particles
Natural killer cell	<ul style="list-style-type: none"> • Kills infected cell not invading pathogens • Activation releases perforin and granzyme which causes destruction of the infected cell by apoptosis/necrosis
Dendritic cell	<ul style="list-style-type: none"> • Non-specific phagocytosis and digestion of antigenic substances • APC process ingested material for presentation to antigen-reactive lymphocytes • Induce T-lymphocyte proliferation • The main link between innate and adaptive immunity

Table 1.1: Components of the innate immune system within the RT.

Innate immunity refers to the non-specific and ever-present components of the immune system. Antigen presenting cell, APC; surfactant protein, SP; leukotriene, LT; interleukin, IL, prostaglandin, PG. (White *et al.*, 1995; Travis *et al.*, 2001; Bittar, 2002; Com *et al.*, 2003; Prussin and Metcalfe, 2003; Martin and Frevert, 2005; Gardner, 2006; Akuthota *et al.*, 2008).

1.5.2.2 ADAPTIVE IMMUNITY

The adaptive immune response is triggered following the failure of the innate system to eradicate pathogens (Medzhitov, 2007). The components of the innate system play a pivotal role in the activation of the adaptive system, via the antigen presenting cells (APC) (e.g. macrophages and dendritic cells) (Proud, 2008). Adaptive immunity is antigen specific and lymphocyte mediated (Table 1.2), accordingly, the system involves production of antibodies specific to sequences present on the invading pathogen in conjunction with activation of the T and B lymphocyte cells (Lederer *et al.*,

1999). The lymphocytes provide a specific response to pathogens, however, the onset is slow with a delay of days compared to minutes for the innate components (Travis *et al.*, 2001). The adaptive system involves production of antibodies specific to sequences present on the invading pathogen (Martin and Frevert, 2005).

Adaptive immunity cell type	Functions within the adaptive immune system of the RT
T-Cells	<ul style="list-style-type: none"> • T-cells are activated upon antigen encounter, they continually circulate between the blood, tissue and lymph • Cytotoxic T-cells (CD8⁺) adhere to cells and release their granule content (perforins, serine proteases and granzymes). They mediate cell lysis of cells displaying an antigen in conjunction with a class I MHC i.e. cells that have been infected • T helper (T_H) cells (CD4⁺) recognise cells displaying MHC class II in conjunction with an antigen • T_H1 cell differentiation is induced by cytokines, upon activation they themselves release specific cytokines including IL-2 and INF-γ, leading to macrophage activation • T_H2 cell differentiation is induced by cytokines, upon activation they are involved in humoral immunity, themselves releasing specific cytokines including IL-4 and IL-5, leading to, plasma cell differentiation/antibody synthesis,
B-Cells	<ul style="list-style-type: none"> • Activated by direct antigen-antibody contact or by T_H2 cell stimulation • B-cells initially produce IgM which undergoes isotype switch to IgG, IgA or memory B-cells • Ig release leads to neutralisation, opsonisation, complement activation and the formation of the 'membrane attack complex'

Table 1.2: Components of the adaptive immune system within the RT.

The adaptive immune response is triggered following the failure of the innate system to eradicate any pathogens. Adaptive immunity is a complex response consisting of B and T lymphocytes. Major histocompatibility complex, MHC; Interleukin, IL; interferon-gamma, INF- γ . (Moore *et al.*, 2001; Bittar, 2002; Gardner, 2006).

1.6 LUNG DISEASE

The human respiratory system is precariously balanced between healthy and diseased states (Rahman *et al.*, 2006). Its constant exposure to the external environment through inhalation of ambient air, containing a myriad of harmful compounds, biological components and detritus, puts the defence mechanisms under strain, and in the event of these defence mechanisms being overwhelmed, lung disease can occur (Decramer *et al.*, 2011).

1.7 CHRONIC OBSTRUCTIVE PULMONARY DISEASE (COPD)

COPD is a complex multifactorial lung disease that has been classified by the GOLD (Global Initiative for Chronic Obstructive Lung Disease) committee as “a preventable and treatable disease with some significant extrapulmonary effects that may contribute to the severity in individual patients. Its pulmonary component is characterised by airflow limitation that is not fully reversible. The airflow limitation is usually progressive and associated with an abnormal inflammatory response of the lungs to noxious particles or gases” (GOLD, 2006). According to the World Health Organisation, COPD is currently the fourth most common cause of death Worldwide and is estimated to rise to third by 2020 (Raherison and Girodet, 2009). COPD severity has been classified by the GOLD committee using a scale of I-IV (Table 1.1). The least severe being Stage I, which represents an individual that is often unaware of any abnormal lung function. As the disease severity increases an individual forced expiratory volume in one second (FEV₁) decreases significantly, restricting airflow and lung function (GOLD, 2006).

1.7.1 SYSTEMIC EFFECTS OF COPD

COPD is a systemic disease, with the pathological effects spreading far beyond the lungs (Agusti, 2006). The comorbidities associated with COPD include, cardiovascular disease, muscle wasting, diabetes, osteoporosis and kidney disease; all of which usually arise once an individual is in the latter stages of the disease (Langen *et al.*, 2003; Decramer *et al.*, 2005; Sin *et al.*,

2006; Mannino and Braman, 2007; Nussbaumer-Ochsner and Rabe, 2011). The widespread consequences of COPD arise due to 'systemic inflammation', which is caused primarily by the elevated levels of endogenous reactive oxygen species (ROS) within the pulmonary tissue leaking into the blood stream (Oudijk *et al.*, 2003). This was demonstrated by elevated levels of superoxide anion ($O_2^{\bullet-}$) in the peripheral blood neutrophils of COPD patients (Morrison *et al.*, 1999). In turn, the elevated levels of ROS within the blood go on to activate leukocytes, which themselves produce further ROS, all of which perpetuates the systemic inflammatory response (Rennard, 2007).

GOLD Stage	FEV ₁ /FVC	FEV ₁ (% Predicted)	Symptoms
I (Mild)	<0.70	≥ 80	<ul style="list-style-type: none"> • Chronic cough • Sputum production (not always)
II (Moderate)	<0.70	50-80	<ul style="list-style-type: none"> • Chronic cough • Sputum production • Shortness of breath
III (Severe)	<0.70	30-50	<ul style="list-style-type: none"> • Increased shortness of breath • Reduced exercise capacity • Fatigue • Repeated exacerbations • Impaired quality of life
IV (Very Severe)	<0.70	< 30	<ul style="list-style-type: none"> • Respiratory failure • <i>Cor pulmonale</i> (right heart failure) • Severely impaired quality of life

Table 1.1: Classification of COPD severity.

There are four stages of COPD severity (I-IV), as classified by the GOLD committee. Patients with Stage I COPD are often unaware of any abnormal lung function, experiencing only a persistent cough. Stage II patients also experience a persistent cough coupled with sputum production, by this point medical advice is usually sought. Stage III patients suffer impaired quality of life due to repeated exacerbations, fatigue and shortness of breath. By Stage IV patient develop respiratory failure, which often leads to *cor pulmonale* (right heart failure). Stage IV patients experience a severely impaired quality of like, with a total lung transplant often determined to be the only option for improved quality of life. FEV₁: forced expiratory volume in one second; FVC: forced vital capacity; *cor pulmonale*: elevation in the jugular venous pressure and pitting ankle oedema (Adapted from GOLD, 2006).

1.7.2 COPD Risk Factors

The main cause of COPD is cigarette smoke (CS), CS contains thousands of toxic compounds, (Section 1.8.2) including ROS, which are known to cause severe damage to the lung (MacNee and Rahman, 2001). The CS also enhances the damage caused by other environmental toxins, through the stimulation of neutrophils and macrophages, to release additional ROS (Taylor, 2010).

Smokers comprise of over 90% of all COPD sufferers (Boots *et al.*, 2003). However, only a small proportion, 15-20%, of smokers go onto develop the disease (Snider, 1989); the exact characteristics of a 'susceptible' smoker remains elusive (Siafakas and Tzortzaki, 2002; Tonello and Poli, 2011). The 'susceptibility' factor indicates that some individuals possess a greater resistance to oxidant imbalance than others, which is reinforced by the detection of up-regulated AO enzymes within smokers in comparison to non-smokers (Hackett *et al.*, 2003).

Other contributing factors include age, with natural lung function beginning to decline in healthy individuals after the age of thirty (Fletcher *et al.*, 1976). This is greatly accelerated in individuals with COPD, especially in patients who continue to smoke (Figure 1.10). Other risk factors include exposure to combustion derived particles from solid biomass fuels e.g. diesel exhaust, coal fly ash, coal, wood and straw (Lopez *et al.*, 2006). It has also been suggested that genetic variations between individuals play a role in disease progression (Mannino and Buist, 2007) including a deficiency in α_1 -antitrypsin (α_1 -AT), which is a serine protease inhibitor. This deficiency has been detected in up to 3% of COPD sufferers (Stoller and Aboussouan, 2005).

1.7.3 COPD Diseases

COPD can be divided into three sub-diseases, which include chronic bronchitis, obstructive bronchiolitis and emphysema (Szilasi *et al.*, 2006).

However increasing evidence suggests that COPD is a heterogeneous disease that cannot be compartmentalised; and that treatment should be unique to each patient in accordance with the breadth of the pathological modifications present (Cerveri and Brusasco, 2010). The typical phenotypic adaptations within the airways of COPD sufferers include inflammatory cell infiltration, smooth muscle hypertrophy, goblet cell hyperplasia (GCH) and metaplasia (GCM) and increased wall thickening (Repine *et al.*, 1997). These adaptations lead to mucus hypersecretion in chronic bronchitis, small airway obstruction in obstructive bronchiolitis and parenchymal lung damage in emphysema (Szilasi *et al.*, 2006).

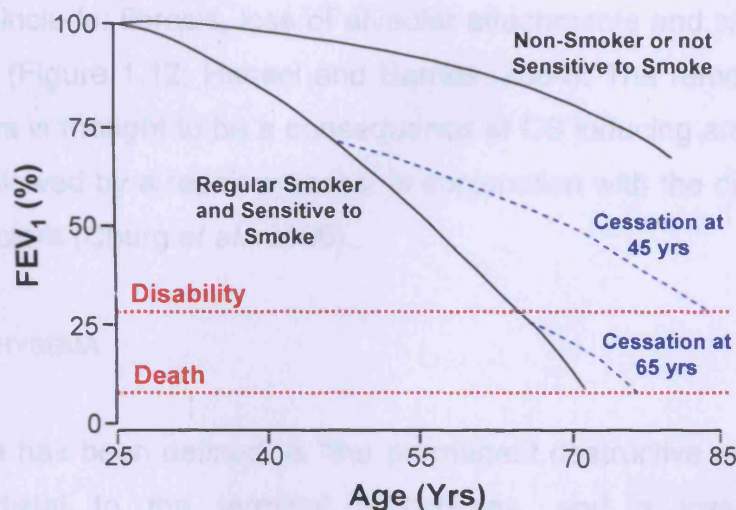


Figure 1.10: Decrease in FEV₁ over time in smokers and non-smokers.

After the age of thirty there is a natural decline in FEV₁ (forced expiratory volume in 1s) or 'lung function'. However, in individuals that regularly smoke the decline is rapidly accelerated, this decline can be slowed down by the cessation of smoking. A FEV₁ of below 30% will cause disability, whereas a FEV₁ of below 10% will lead to death (Adapted from Raheison and Girodet, 2009)

1.7.3.1 CHRONIC BRONCHITIS

Chronic bronchitis is manifested as a persistent recurrent exasperation and bronchial hypersecretion (Fletcher and Pride, 1984), caused by large airway mucus gland hyperplasia and inflammation (Figure 1.11; Repine *et al.*, 1997). It is clinically defined as a mucus producing cough that lasts 3 months and recurred for at least 2 consecutive years (MRC, 1965; Hansel and Barnes,

2004). Recent work has defined chronic bronchitis as an inflammatory subtype of COPD, with an elevated distribution of eosinophils toward the airway lumen (Snoeck-Stroband *et al.*, 2008).

1.7.3.2 OBSTRUCTIVE BRONCHIOLITIS

The inflammation in COPD causes obstruction of the small and peripheral airways, predominantly as a result of smoking. Pathological features of obstructive bronchiolitis include: mucus hypersecretion, as a result of GCH (Ebert and Hanks, 1981) and collapsing of the lumen, which is due to high surface tension produced by the excessive mucus (Szilasi *et al.*, 2006). Other pathologies include: fibrosis, loss of alveolar attachments and smooth muscle hypertrophy (Figure 1.12; Hansel and Barnes, 2004). The remodelling of the small airways is thought to be a consequence of CS inducing an inflammatory response followed by a repair process, in conjunction with the direct induction of growth factors (Churg *et al.*, 2006).

1.7.3.3 EMPHYSEMA

Emphysema has been defined as “the permanent destructive enlargement of airspaces distal to the terminal bronchioles, and a loss of alveolar attachments due to apoptosis and necrosis of alveolar epithelial cells” (Fletcher and Pride, 1984). There are two forms of emphysema, i.e. centrilobular and panlobular/panacinar (Kim *et al.*, 1991), both of which are associated with a decreased diffusing capacity and appear as reduced lung parenchymal density on a chest radiograph (Repine *et al.*, 1997). Centrilobular emphysema is most common in smokers, with the respiratory bronchioles (RB) being the main site of inflammation; particularly the 3rd order RBs. Panacinar emphysema is most common in patients with a α 1-AT deficiency, and is localised in the lower lung lobes, effecting the RB, alveolar ducts and sacs equally (Szilasi *et al.*, 2006).

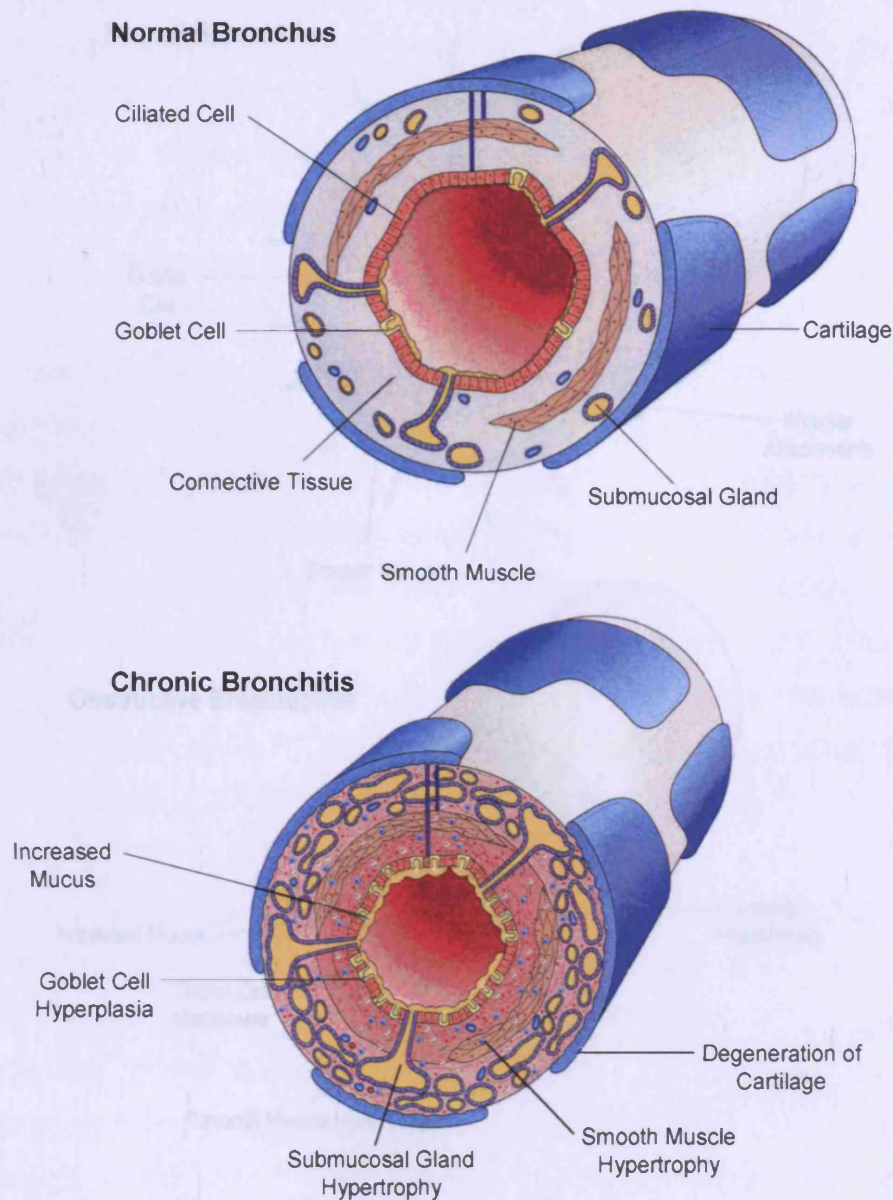


Figure 1.11: Normal bronchus and chronic bronchitis.

The normal bronchus has a pseudo-stratified appearance with bands of smooth muscle that do not form a complete layer. During chronic bronchitis there is smooth muscle and submucosal gland hypertrophy, GCH and increased mucus production and cartilage degeneration (Adapted from Hansel and Barnes, 2004).

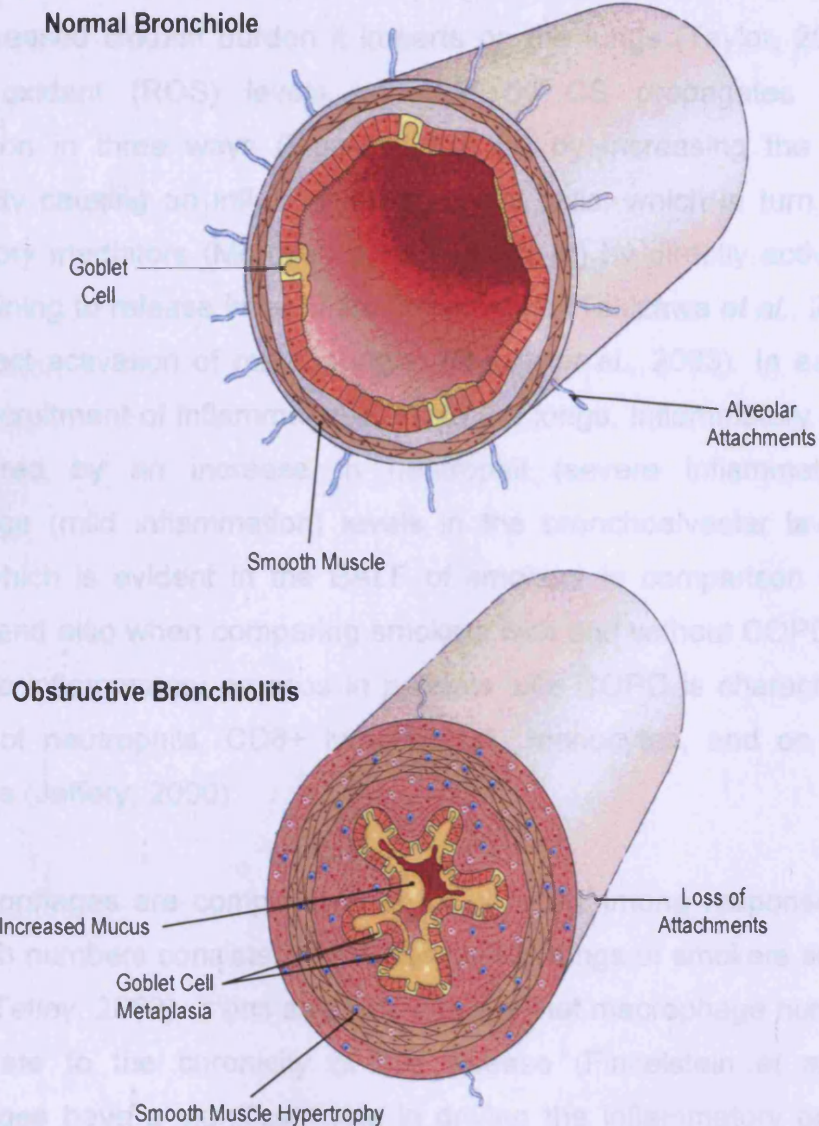


Figure 1.12: Normal bronchiole and obstructive bronchiolitis.

The normal bronchiole has a simple cuboidal appearance, with a continuous layer of smooth muscle. During obstructive bronchiolitis there is smooth muscle hypertrophy, loss of alveolar attachments, GCM leading to increased mucus production (Adapted from Hansel and Barnes, 2004).

1.7.4 INFLAMMATION IN COPD

The current working definition of COPD (Section 1.3.1) was only recently amended to acknowledge inflammation as a key process, this sparked significant interest into the inflammatory responses, which consist of neutrophils, macrophages and T lymphocytes (Barnes *et al.*, 2003).

CS is considered to be the major cause of COPD (Section 1.7.2), mainly due to the increased oxidant burden it imparts on the lungs (Taylor, 2010). The elevated oxidant (ROS) levels imparted by CS propagates abnormal inflammation in three ways (Figure 1.13): (1) by increasing the epithelial permeability causing an influx of inflammatory cells, which in turn activates inflammatory mediators (Morrison *et al.*, 1999); (2) by directly activating the epithelial lining to release inflammatory mediators (Takizawa *et al.*, 2000) and (3) by direct activation of macrophages (Oudijk *et al.*, 2003). In each case, there is recruitment of inflammatory cells to the lungs. Inflammatory cell influx is measured by an increase in neutrophil (severe inflammation) and macrophage (mild inflammation) levels in the bronchoalveolar lavage fluid (BALF), which is evident in the BALF of smokers in comparison with non-smokers, and also when comparing smokers with and without COPD (Saetta, 1999). The inflammatory process in patients with COPD is characterised by an influx of neutrophils, CD8⁺ lymphocytes, monocytes, and on occasion eosinophils (Jeffery, 2000).

The macrophages are components of the innate immune response (Taylor, 2010), with numbers consistently elevated in the lungs of smokers and COPD patients (Tetley, 2002). It has also been stated that macrophage numbers are proportionate to the chronicity of the disease (Finkelstein *et al.*, 1995). Macrophages have a significant role in driving the inflammatory process by generating ROS and inflammatory mediators such as leukocyte chemoattractants, e.g. TNF- α and IL-8, which attract a variety of leukocytes, such as neutrophils, causing further inflammation (Figure 1.13; Szilasi *et al.*, 2006).

Neutrophils, like macrophages, form part of the innate immune response. They are responsible for producing ROS, and chemoattractants, e.g. IL-8. IL-8 recruits further neutrophils to the site of inflammation, perpetuating the inflammatory response (Szilasi *et al.*, 2006). Neutrophilia is a prominent feature of COPD (Figure 1.13; Ryttilä *et al.*, 2006) with elevated levels of neutrophils observed in the induced sputum of COPD sufferers (Keatings *et al.*, 1996). A unique way in which neutrophils drive COPD is through the

production of serine proteases known to stimulate mucus production and cause alveolar destruction which contribute to chronic bronchitis and emphysema (Ilumets *et al.*, 2008).

The cytokine TNF- α is secreted by cigarette smoke activated macrophages; it can mediate epithelial cell apoptosis, as well as being able to induce both the expression of itself and IL-8 (Szilasi *et al.*, 2006). Both TNF- α and IL-8 are also regulated by the transcription factor nuclear factor kappa B (NF- κ B), which itself is known to be activated by oxidants. Thus illustrating that this key inflammatory response is redox sensitive (Rahman and MacNee, 1998; MacNee, 2001).

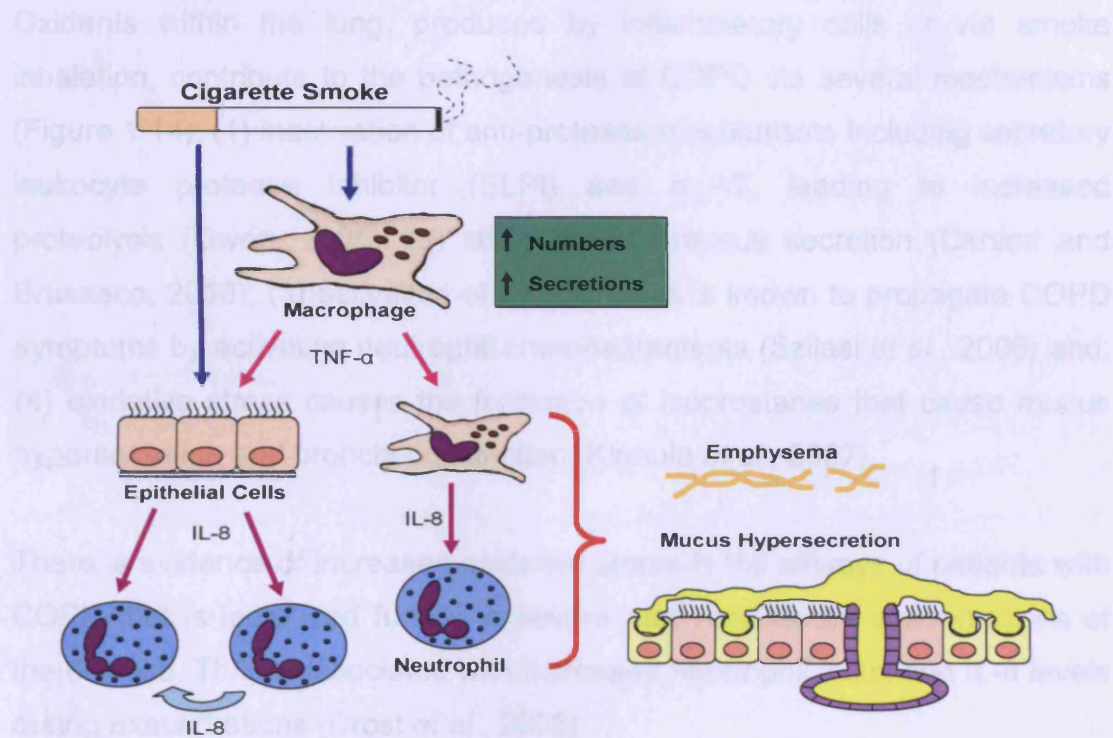


Figure 1.13: Inflammation in COPD.

CS imparts elevated levels of ROS onto the pulmonary tissue which in turn propagates abnormal inflammation in three ways: (1) increases epithelial permeability, to allow inflammatory cell influx; (2) directly activates macrophages to release inflammatory mediators and; (3) directly activates epithelial cells to release inflammatory mediators. The activated macrophages release TNF- α , which in turn causes the release of IL-8. IL-8 attracts neutrophils, which themselves secrete IL-8 to perpetuate the response. The activated macrophages and neutrophils elicit the pathological responses, which include mucus hypersecretion and parenchymal destruction (emphysema). The effects of ROS are discussed in more detail below (Adapted from Hansel and Barnes, 2004).

1.7.5 COPD AND OXIDATIVE STRESS

Progression of COPD within an individual coincides with an increase in oxidant burden, coupled with insufficient AO capabilities (Rahman, 2006). This imbalance was demonstrated by elevated levels of oxidative stress indicators within the COPD patients (Boots *et al.*, 2003). The stress indicators included: lung inflammation (MacNee, 2001), exhaled hydrogen peroxide (H_2O_2) (Nowak *et al.*, 1996) and 8-isoprostane (Kinnula *et al.*, 2007), lipid peroxidation products (LPO) (Nowak *et al.*, 1999), and protein damage (Janoff *et al.*, 1983).

Oxidants within the lung, produced by inflammatory cells or via smoke inhalation, contribute to the pathogenesis of COPD via several mechanisms (Figure 1.14): (1) inactivation of anti-protease mechanisms including secretory leukocyte protease inhibitor (SLPI) and α_1 -AT, leading to increased proteolysis (Owen, 2005); (2) stimulation of mucus secretion (Cerveri and Brusasco, 2010); (3) activation of NF- κ B which is known to propagate COPD symptoms by activating neutrophil chemoattractants (Szilasi *et al.*, 2006) and; (4) oxidative stress causes the formation of isoprostanes that cause mucus hypersecretion and bronchoconstriction (Kinnula *et al.*, 2007).

There is evidence of increased oxidative stress in the airways of patients with COPD that is increased further in severe and very severe exacerbations of the disease. This is associated with increased neutrophil influx and IL-8 levels during exacerbations (Drost *et al.*, 2005).

1.8 REACTIVE OXYGEN SPECIES

ROS including $\text{O}_2^{\bullet-}$, hydroxyl radical (OH^{\bullet}) and hydrogen peroxide (H_2O_2), are named so as they possess a higher reactivity in comparison to molecular oxygen (O_2) (Thannickal and Fanburg, 2000). There are endogenous and exogenous sources of ROS within the lungs (Figure 1.15). Both the inflammatory response and metabolic by-products are endogenous sources of

ROS (Halliwell and Gutteridge, 1999), whereas an example of a primary exogenous source is CS (Taylor, 2010).

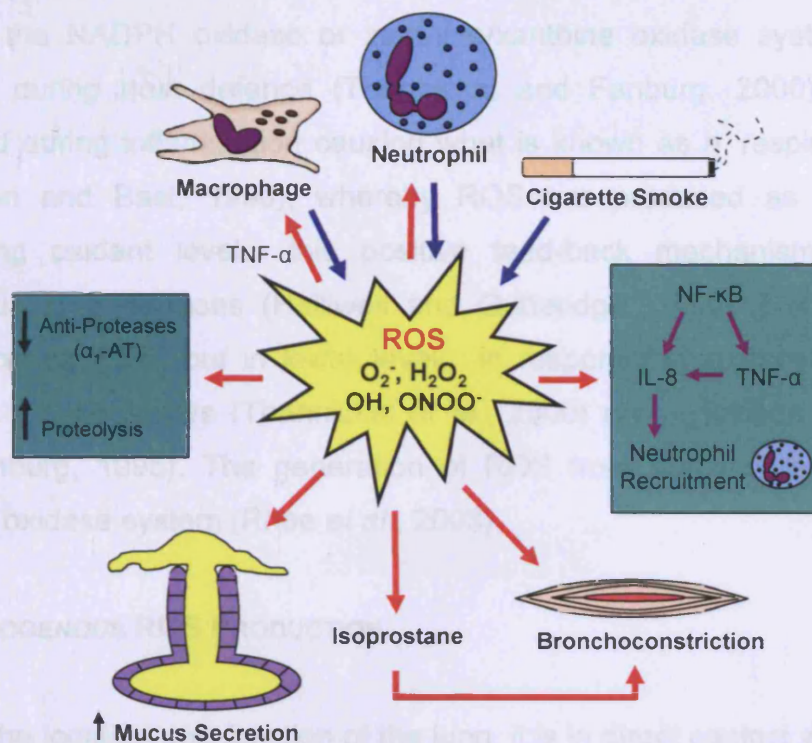


Figure 1.14: The effect of ROS on COPD pathology.

The ROS, superoxide anion ($O_2^{\bullet-}$), hydroxyl radical (OH^{\bullet}), peroxynitrite ($ONOO^{\bullet}$) and hydrogen peroxide (H_2O_2) are released from cigarette smoke and inflammatory cells. All of which mediate several damaging phenotypic adaptations manifested in COPD sufferers e.g. increased mucus secretion, bronchoconstriction, increased isoprostane levels, neutrophil recruitment and increased proteolysis (Adapted from Hansel and Barnes, 2004).

1.8.1 ENDOGENOUS ROS PRODUCTION

The incomplete reduction of O_2 to $O_2^{\bullet-}$ during cellular respiration is the primary source of ROS within the lung (Halliwell and Gutteridge, 1999). Superoxide anion is enzymatically or spontaneously dismutated to produce H_2O_2 ($O_2^{\bullet-} + O_2^{\bullet-} + 2H^+ \rightarrow H_2O_2 + O_2$) (McCord and Fridovich, 1969), which in the presence of a transition metal ion forms the extremely reactive and toxic OH^{\bullet} via the Fenton reaction ($H_2O_2 + Fe^{2+} \rightarrow Fe^{3+} + OH^- + OH^{\bullet}$). It can also react with nitric oxide (NO) to produce peroxynitrite ($ONOO^{\bullet}$) that can go on to form the highly reactive OH^{\bullet} via decomposition (Figure 1.15; Halliwell, 1991).

Other endogenous ROS producers within the lung include eosinophils, alveolar macrophages, monocytes and neutrophils (Ciencewicki *et al.*, 2008). These phagocytic cells have $O_2^{\bullet -}$ generating plasma membranes (PM), utilizing the NADPH oxidase or xanthine/xanthine oxidase systems, which function during host defence (Thannickal and Fanburg, 2000). They are activated during inflammation causing what is known as a 'respiratory burst' (Doelman and Bast, 1990), whereby ROS are produced as a result of increasing oxidant levels; this positive feed-back mechanism results in numerous lung diseases (Halliwell and Gutteridge, 1999). Non-phagocytic cells produce ROS, but in lower levels, in response to extracellular stimuli such as growth factors (Thannickal *et al.*, 2000) and cytokines (Thannickal and Fanburg, 1995). The generation of ROS from these cells utilises the NADPH oxidase system (Rhee *et al.*, 2003).

1.8.2 EXOGENOUS ROS PRODUCTION

Due to the location and function of the lung, it is in direct contact with airborne oxidants e.g. nitrogen dioxide, ozone, radiation (Janssen *et al.*, 1993) and CS (Taylor, 2010), all of which generate ROS, that cause lung damage via inflammatory responses. CS, in particular is highly toxic, containing a mixture of over 4,700 components (Sexton *et al.*, 2008), including semiquinone radicals, $O_2^{\bullet -}$, NO and numerous carcinogenic organic compounds; all capable of reacting further to produce highly reactive species leading to serious injury (Nakayama *et al.*, 1989). The inhalation of air pollutants causes a localised inflammatory response, recruiting inflammatory cells (Section 1.7.4) that release more ROS, thus enhancing the pathological effects (Ciencewicki *et al.*, 2008). Exogenous ROS can also go on to trigger endogenous ROS production by inflammatory cells, e.g. neutrophils and macrophages (Rahman and Adcock, 2006).

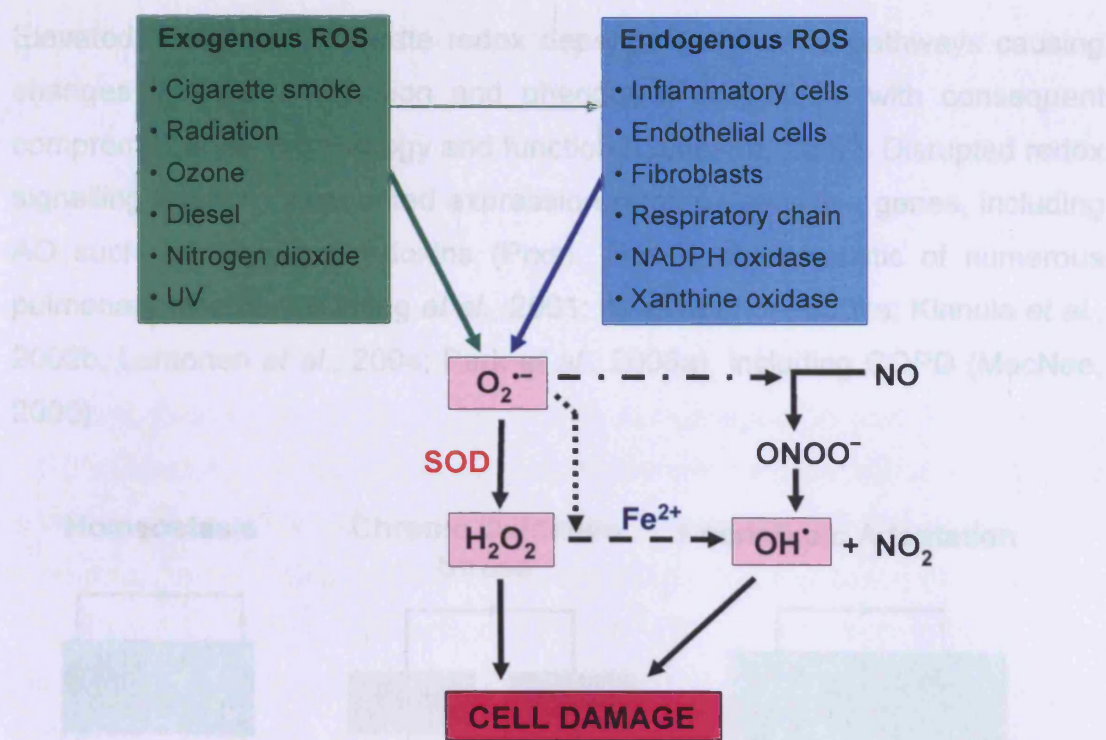


Figure 1.15: Cellular generation of ROS.

There are numerous exogenous and endogenous sources of ROS, reactions occur endogenously that lead to the production of yet more toxic species. Superoxide anion ($O_2^{\bullet-}$), hydroxyl radical (OH^{\bullet}), hydrogen peroxide (H_2O_2), nitric oxide (NO), peroxynitrite ($ONOO^-$), nitrogen dioxide (NO_2), ferrous ion (Fe^{2+}), superoxide dismutase (SOD) (Adapted from Rahman *et al.*, 2006).

1.8.3 OXIDATIVE STRESS

Oxidative stress refers to an increased generation of ROS within cells and tissues, however, it has recently been argued that the term oxidative stress should be redefined as “disruption of redox signalling and cycling”, as this is the exact consequence of excessive amounts of ROS, resulting in pulmonary damage (Jones, 2006). All the major lung inflammatory diseases share a common feature of oxidant/AO imbalance (Rahman *et al.*, 2006), leading to ‘disrupted redox signalling’, ‘phenotypic adaptation’ and eventual ‘tissue remodelling’ (Figure 1.16; Heintz, 2008).

Increased oxidant burden leads to cycles of injury and repair causing perturbations that result in increased ROS production (Valko *et al.*, 2007).

Elevated ROS levels activate redox dependant signalling pathways causing changes in gene expression and phenotypic adaptation, with consequent compromised cell morphology and function (Genestra, 2007). Disrupted redox signalling leads to augmented expression of redox sensitive genes, including AO such as the peroxiredoxins (Prxs). This is characteristic of numerous pulmonary disorders (Chang *et al.*, 2001; Kinnula *et al.*, 2002a; Kinnula *et al.*, 2002b; Lehtonen *et al.*, 2004; Park *et al.*, 2006a), including COPD (MacNee, 2000).

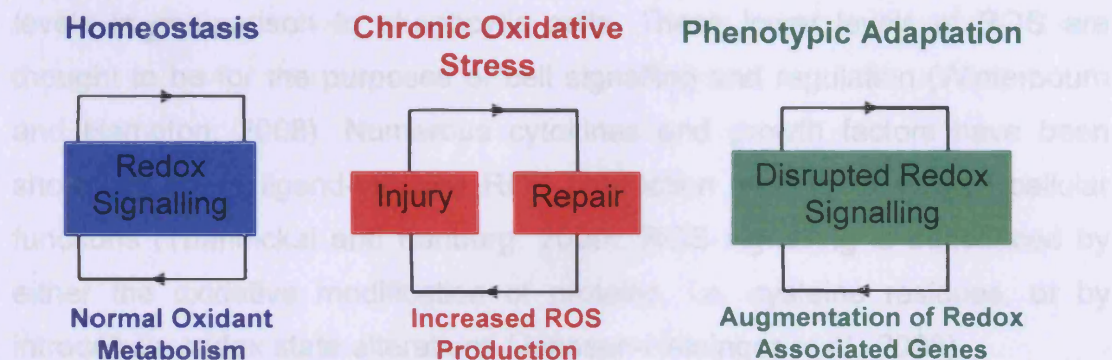


Figure 1.16: A model for the role of ROS in the pathogenesis of lung disease.

Optimal redox signalling occurs to maintain homeostasis within the lung of a healthy individual. Following chronic oxidative stress there is increased ROS production, leading to cycles of injury and repair. Over-time the redox signalling within the lung is permanently disrupted, leading to phenotypic adaptation through the augmented expression of redox associated genes such as antioxidants (Adapted from Heintz, 2008).

1.8.3.1 CELLULAR DAMAGE CAUSED BY OXIDATIVE STRESS

Chronic oxidative stress causes significant damage to all aspects of the lungs' tissue, structure and function including: (1) lipid peroxidation, which is a direct result of oxidative stress, causing cell membrane damage and ultimately cell death (Chen *et al.*, 2007); (2) oxidation of the polypeptide backbone within proteins, yielding peptide bond cleavage and amino acid side chain modification (Kelly and Mudway, 2003); (3) formation of the reactive OH^\bullet following radiation exposure, which damages DNA and alters gene and protein expression (Evans *et al.*, 2004) and; (4) DNA base oxidation, often found in malignant tumours. However, the role of ROS in cancer is thought to

be more complex than this, with it exhibiting additional effects on p53 and cell proliferation (Halliwell, 2007b).

1.8.4 ROS SIGNALLING

Although ROS on the whole are viewed as unwanted and harmful metabolic by-products, there is growing evidence of their roles as mediators in cell signalling processes (Valko *et al.*, 2007). Non-phagocytic cells can produce ROS in response to cytokines and growth factors (Section 1.8.1) but at lower levels in comparison to phagocytic cells. These lower levels of ROS are thought to be for the purposes of cell signalling and regulation (Winterbourn and Hampton, 2008). Numerous cytokines and growth factors have been shown to act in ligand-induced ROS production leading to diverse cellular functions (Thannickal and Fanburg, 2000). ROS signalling is transduced by either the oxidative modification of proteins, i.e. cysteine residues, or by intracellular redox state alterations (Janssen-Heininger *et al.*, 2008).

1.8.4.1 H₂O₂: AN INTRACELLULAR MESSENGER

The toxic effects of H₂O₂ have been well characterised, therefore, the suggestion of cells producing seemingly harmful molecules, to act as signal transducers, was met with cynicism (Forman *et al.*, 2004; Rhee, 2006). Nevertheless, the role of NO, itself a reactive species (Sections 1.8.1 and 1.8.2), in signal transduction is unanimously accepted, whereby high levels are produced by phagocytic cells during host defence and low levels generated by non-phagocytic cells for use in signal transduction; it is in the same manner that H₂O₂ is thought to function (Finkel, 1998). It is now accepted that low levels of H₂O₂, produced by non-phagocytic cells, act as intracellular messengers mediating cell proliferation, differentiation and migration (Rhee *et al.*, 2000). Until recently, the mechanism by which H₂O₂ functioned in signal transduction remained elusive. It has since been revealed that H₂O₂ modifies its target molecules through the oxidation of essential cysteine residues, which include protein tyrosine phosphatases and the lipid phosphatase PTEN (Rhee *et al.*, 2005b).

1.8.4.2 DETRIMENTAL ROS SIGNALLING MECHANISMS

Not all oxidant-mediated signalling is required for normal cellular function, the redox-sensitive activation of transcription factors by ROS initiates inflammatory responses throughout the lung (Poli *et al.*, 2004; Waris and Ahsan, 2006). An example of this is the release of the pro-inflammatory cytokine IL-8 in lung epithelial cells following the oxidant-mediated NF- κ B DNA binding (Antonicelli *et al.*, 2002). Another example is the activation of the MAP Kinase and/or redox-sensitive signalling cascades in lung epithelial cells, following oxidant inhalation. This leads to the activation of several target genes, initiating cell proliferation, differentiation, inflammation and death (Figure 1.17; Mossman *et al.*, 2006; Waris and Ahsan, 2006).

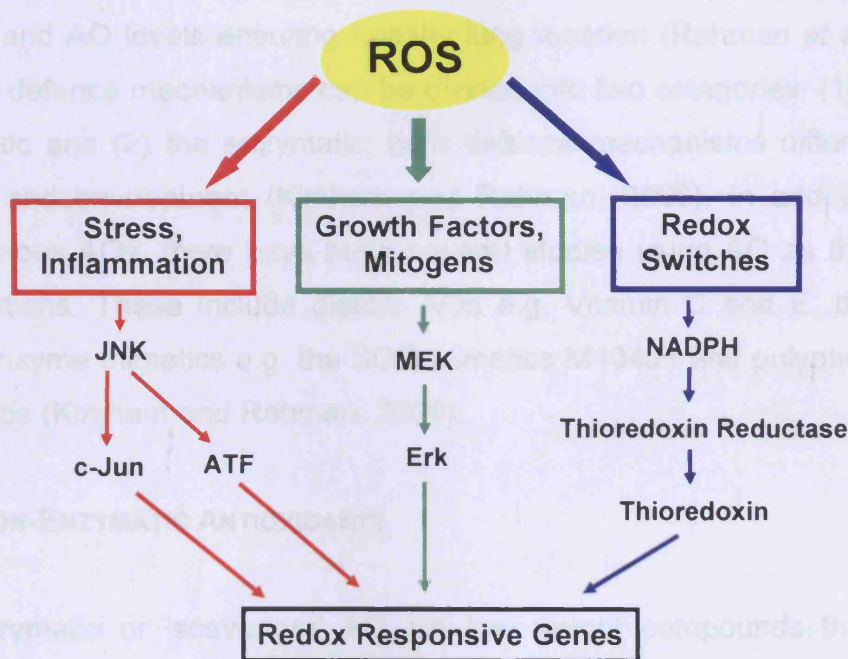


Figure 1.17: Signalling cascades triggered by ROS.

The two mitogen activated protein kinases (MAPK) pathways (i.e. JNK and MEK), and the redox sensitive kinase pathway are three pathways through which ROS exert an effect, leading to the augmentation of redox sensitive genes and ultimately phenotypic adaptations, including, cell proliferation, differentiation and death. JNK: c-Jun N-terminal kinase; MEK: mitogen-activated protein kinase kinase; ATF: activating transcription factor; Erk: extracellular signal-regulated kinase; NADPH: nicotinamide adenine dinucleotide phosphate (Adapted from Waris and Ahsan, 2006).

1.9 LUNG ANTIOXIDANT DEFENCE MECHANISMS

In broad terms, an AO can be defined as “a substance that when present at low concentrations, compared with that of an oxidisable substrate, significantly delays or prevents oxidation of that substrate” (Halliwell and Gutteridge, 1999). Oxidative stress is detrimental to numerous macromolecules (Section 1.8.3.1), therefore the term ‘oxidisable substrate’ encompasses the vast majority of intracellular molecules (Halliwell, 1991). ROS are produced as by-products of cellular metabolism, in addition to their intake via exogenous sources (Section 1.8). Consequently, AO mechanisms have evolved to protect the organs most at risk from oxidative damage, namely, the lungs (Fridovich and Freeman, 1986; Halliwell, 2006). The purpose of these mechanisms is to maintain the precarious balance between oxidant and AO levels ensuring healthy lung function (Rahman *et al.*, 2006). The AO defence mechanisms can be divided into two categories: (1) the non-enzymatic and (2) the enzymatic; both defence mechanisms differ between tissues and environment (Kirkham and Rahman, 2006). In addition to the endogenous AOs, there have been several studies using AO as therapeutic interventions. These include dietary AOs e.g. Vitamin C and E, thiols, e.g. GSH, enzyme mimetics e.g. the SOD mimetics M40401 and polyphenols e.g. flavenoids (Kirkham and Rahman, 2006).

1.9.1 NON-ENZYMATIC ANTIOXIDANTS

Non-enzymatic or ‘scavenger’ AO are low weight compounds that act as scavengers, reacting directly with oxidising agents (Rahman *et al.*, 2006). They include: β -carotene, uric acid (UA), albumin, vitamin E, vitamin C and glutathione. β -carotene and UA both react with peroxyl radicals and $O_2^{\cdot-}$. Albumin functions by binding to transition metals and preventing Fenton chemistry reactions (Comhair and Erzurum, 2002). Vitamin E reacts with lipid peroxyl radicals (Bast *et al.*, 1991) and vitamin C reacts with $O_2^{\cdot-}$ and HO^{\cdot} , forming a free radical that is reduced by reduced glutathione (McCay, 1985). GSH reacts non-enzymatically by binding to radicals via its reactive sulphide bond (Kelly, 1999).

1.9.2 ENZYMATIC ANTIOXIDANTS

There are a host of enzymatic AO that protect the lungs by reacting with oxidants to produce less toxic species (Kinnula, 2005). These include superoxide dismutases (SODs), catalase, glutathione peroxidase, peroxiredoxins (Prx), thioredoxins, glutaredoxins, and heme oxygenase-1 (Table 1.2). They all act to maintain a healthy oxidant/AO balance. However, incorrect functioning and in many cases, AO overexpression has been found in a variety of pulmonary diseases (Rahman *et al.*, 2006).

Enzyme	M _R (KDa)	Lung Localisation	Function	Diseases
Catalase	240	Macrophages, fibroblasts, pneumocytes	H ₂ O ₂ to water	Lung parenchymal disease, asthma
Cu,Zn SOD	17-28	Bronchial, alveolar epithelium, macrophages, fibroblasts, pneumocytes	Scavenges O ₂ ^{-•}	Sarcoidosis, COPD, inflammation, hypoxia
EC-SOD	135	Bronchial epithelium, macrophages, neutrophils, vascular walls, pneumocytes	Scavenges O ₂ ^{-•}	COPD, sarcoidosis, alveolitis, lung cancer
Glutathione Peroxidase	85	Lavage cells, epithelium, macrophages, other lung cells	Organic hydroperoxides to organic hydroxides	COPD, asthma, CF
Heme Oxygenase-1	30-33	Alveolar, bronchial epithelium, macrophages, inflammatory cells of lungs	Heme to carbon monoxide, biliverdin	Fibrosis, interstitial pneumonias, interstitial lung disease, COPD, CF
Mn ₂ SOD	88	Bronchial epithelium, macrophages, neutrophils, vascular walls, pneumocytes	Scavenges O ₂ ^{-•}	Asthma, sarcoidosis, interstitial lung disease
Thioredoxin	10-12	Bronchial epithelium, macrophages	Prot-S-S-Prot to Prot-SH	Idiopathic pulmonary fibrosis, CF, COPD
Peroxiredoxin	17-28	Alveolar, bronchial epithelium, macrophages	Antioxidant, signalling, H ₂ O ₂ breakdown	Alveolitis, COPD, hyperoxia, lung cancer

Table 1.2: Antioxidant enzymes of the lung.

The function, location and involvement in pulmonary diseases of the enzymatic antioxidants. **Blue** represents a decrease in expression within a given lung disease, **green** represents both an increase and decrease in expression. COPD: chronic obstructive pulmonary disorder;; CF: cystic fibrosis; O₂^{-•}: superoxide anion; H₂O₂: hydrogen peroxide; Cu: copper; Zn: zinc; Mn: manganese; EC: extracellular; Prot: protein; S-S: disulphide bond (Adapted from Rahman *et al.*, 2006). The peroxiredoxins (**red**) are the main focus of this research project.

1.10 PEROXIREDOXINS

Peroxiredoxins (Prxs) are a family of ubiquitously expressed AO enzymes, that exhibit peroxidase activity by reducing harmful organic peroxides ($\text{ROOH} + 2\text{e}^- \rightarrow \text{ROH} + \text{H}_2\text{O}$), produced both endogenously and exogenously (Hofmann *et al.*, 2002). In addition to reducing oxidants, the Prxs are capable of removing amino acid, peptide and protein hydroperoxides formed as a result of oxidative damage (Peskin *et al.*, 2010). Prx family members exist in all kingdoms (Chae *et al.*, 1994b) with sizes ranging from 20-30kDa. There are currently 6 Prx (Prx I-VI) mammalian isoforms with varied cellular location and expression patterns (Seo *et al.*, 2000). There are very few residues that are conserved throughout the peroxiredoxin family, with the conserved sites located in the catalytic regions (Hofmann *et al.*, 2002).

Prx Subtype	Polypeptide Length	Human Chromosomal Location	Cellular Location
Prx I (Typical 2-Cys)	199aa	1q34.1	Cytosol, Nucleus
Prx II (Typical 2-Cys)	198aa	13q12	Cytosol, Membrane
Prx III (Typical 2-Cys)	198aa	10q25-q26	Mitochondria
Prx IV (Typical 2-Cys)	271aa (Cleaved at 36-37) ^a	10p22.13	Cytosol, Golgi, Secreted
Prx V (Atypical 2-Cys)	214aa (Cleaved at 52-53) ^a	11q13	Mitochondria, Peroxisome, Cytosol
Prx VI (1-Cys)	224aa	1q23.3	Cytosol

Table 1.3: Six mammalian Prx isoforms.

The 6 Mammalian Prx isoforms can be further divided into three subgroups regarding their catalytic mechanisms; typical and atypical 2-Cys and 1-Cys. Each isoforms varies in size and sub-cellular location, allowing diverse functions in addition to their peroxidase activity. aa: amino acid; ^a: these proteins are modified post-translation (Adapted from Wood *et al.*, 2003b).

The 6 mammalian Prx isoforms are divided into three subgroups (Section 1.10.2), in accordance with their catalytic reaction intermediates (Rhee *et al.*,

2005a). It is important to note that the roles of Prxs are not restricted to peroxide reduction, with evidence of them participating in cellular functions as diverse as basal metabolism, cell cycle progression, cell signalling, proliferation, chaperone activity, differentiation and apoptosis (Prosperi *et al.*, 1993; Kang *et al.*, 1998b; Leyens *et al.*, 2003; Forman *et al.*, 2004; Phalen *et al.*, 2006; Kim *et al.*, 2008). In a review by Hoffman and co-workers it was stated that 'Prxs should not be underestimated and thought of only as a back-up system in the defence against peroxides, but that their discrete regulatory roles should be further investigated' (Hofmann *et al.*, 2002).

1.10.1 PRX DISCOVERY

Peroxiredoxins were initially discovered in yeast via an observation that yeast glutamine synthase was degraded in a purified but not a crude extract. This discovery led to the determination that a mechanism was present within the crude extract that provided protection against reactive chemical species (Kim *et al.*, 1985). Further investigation by the group led to the isolation of a 25KDa protein, thiol-specific antioxidant (TSA), named due to its ability to protect cellular components from oxidation systems in which thiols function as the reducing equivalent (Kim *et al.*, 1988). Later work deemed thioredoxin peroxidase (TPx) to be a more appropriate name than TSA. This was due to the thiol-containing donor molecule, thioredoxin (Trx) being identified as the electron donor within the catalytic cycle (Chae *et al.*, 1994a). However, following the isolation and cloning of the cDNA corresponding to TSA from rat brain, TPx was regarded as misleading, with some TPx homologs reducing peroxides without Trx. The name Prx was therefore more suitable to encompass the entire family (Chae *et al.*, 1994b).

1.10.2 PRX SUBGROUPS

Unlike other peroxidases, such as catalase and glutathione peroxidase (GPx), Prxs do not contain any redox cofactors (Chae *et al.*, 1994c). Their ability to reduce peroxides stems entirely from conserved redox-active cysteine residues, i.e. the N-terminal (N-term) peroxidatic cysteine (S_P) and the C-

terminal (C-term) resolving cysteine (S_R) (Wood *et al.*, 2003b). Prxs were initially divided into two subgroups, based on the number of cysteine residues required for their catalytic function, 2-Cys Prx (S_P and S_R required) and 1-Cys Prx (S_P only required) (Chae *et al.*, 1994b). The conserved cysteines were identified at amino acid positions 47 and 170 in yeast, and mutagenesis investigations to replace the conserved cysteines with serine revealed that Cys-47 was the primary site of oxidation. This determined that Cys-47 (S_P) was essential to AO function, with cysteines corresponding to Cys-47 identified as the conserved residues in both 2-Cys and 1-Cys subgroups. The presence of the second conserved cysteine (Cys-170) seemed to be dependent on the sequence conservation surrounding the N-term cysteine (Chae *et al.*, 1994c). More recent evidence shows a further divide in the 2-Cys subgroup, known as the typical and atypical 2-Cys Prxs, with the atypical type having only one conserved cysteine but requiring another for its catalytic function (Seo *et al.*, 2000; Rhee *et al.*, 2001).

The three Prx subgroups undergo a 2-step catalytic cycle, where step one involves the reduction of the peroxide leading to the oxidation of the Prx, and the second step sees the reduction of the oxidised Prx returning it to its original state. The first step in this cycle is common to all three subgroups (Choi *et al.*, 1998), in which the peroxide is reduced following a nucleophilic attack by the S_P , leading to the formation of cysteine sulphenic acid (S_POH) (Figure 1.18; Ellis and Poole, 1997). The mechanism by which Prxs are recycled distinguish the three subgroups (Wood *et al.*, 2003b).

1.10.2.1 TYPICAL 2-CYS PRXS

The typical 2-Cys Prxs (Prx I-IV) are C-term swapping (Hirotsu *et al.*, 1999) head-to-tail homodimers (Chae *et al.*, 1994c). They contain conserved S_P and S_R that form an inter-subunit disulphide bond following S_P oxidation (Ellis and Poole, 1997). The oxidation of the S_P causes a conformational rearrangement bringing the S_P and S_R into close enough proximity to form a disulphide bond (Hofmann *et al.*, 2002); Trx was identified as the reducing agent (Chae *et al.*, 1994a). Following the purification of a mammalian Prx (Chae *et al.*, 1994b), a

database search revealed homologs that were initially characterized without reference to their peroxidase activity, and these were later classified as Prx I-IV (Table 1.4).

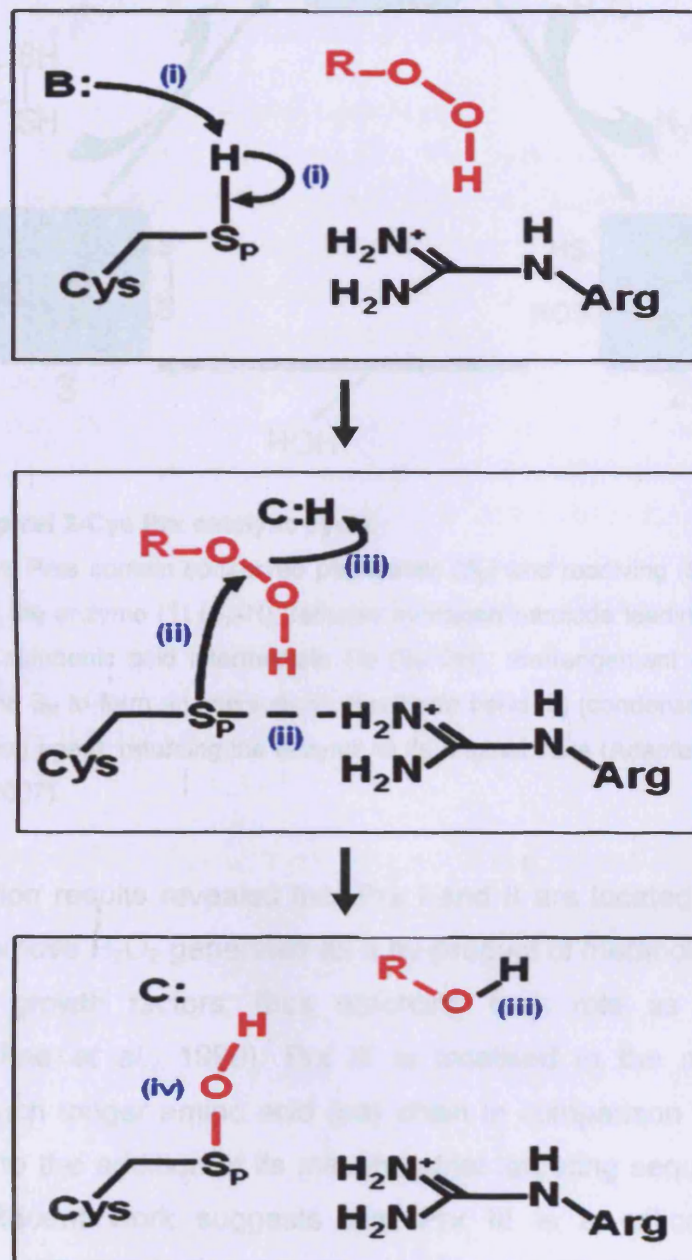


Figure 1.18: Peroxide reduction, the first step in the Prx catalytic cycle.

The first step in the Prx mechanism is common to all subgroups; (i) the initial deprotonation of the peroxidatic cysteine (S_P) by a catalytic base (B). (ii) The S_P reduces the peroxide through a nucleophilic attack; a conserved arginine residue stabilizes the thiolate anion. (iii) The RO⁻ leaving group is protonated by a catalytic acid (C). (iv) Finally there is formation of a sulphenic acid (S_POH) (An intermediate for the 2-Cys Prx subgroups, but more stable in the 1-Cys Prxs) (Adapted from Wood *et al.*, 2003b).

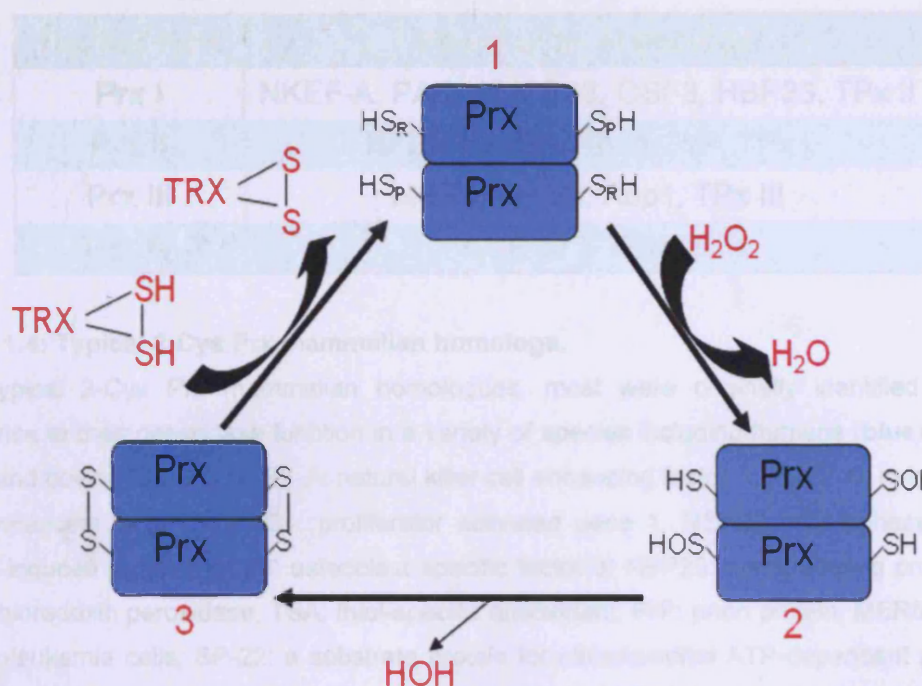


Figure 1.19: Typical 2-Cys Prx catalytic cycle.

The typical 2-Cys Prxs contain conserved peroxidatic (S_P) and resolving (S_R) cysteines. The reduced form of the enzyme (**1**) (S_P -H), reduces hydrogen peroxide leading to the formation of the cysteine sulphenic acid intermediate (**2**) (S_P -OH), rearrangement of the homodimer allows the S_P and S_R to form an intersubunit disulphide bond (**3**) (condensation). Thioredoxin acts as a reducing agent, returning the enzyme to its original state (Adapted from D'Autreaux and Toledano, 2007).

Characterisation results revealed that Prx I and II are located in the cytosol, where they remove H_2O_2 generated as a by-product of metabolism and also in response to growth factors; thus enforcing their role as cell signalling mediators (Chae *et al.*, 1999). Prx III is localised in the mitochondria, it contains a much longer amino acid (aa) chain in comparison to Prx I and II, which is due to the addition of its mitochondrial targeting sequence (Rhee *et al.*, 2001). Recent work suggests that Prx III is a critical regulator of mitochondrial H_2O_2 levels, and hence, a key regulator of apoptotic signalling (Chang *et al.*, 2004). Prx IV is a secretory protein initially identified through its interaction with Prx I (Jin *et al.*, 1997). It contains an N-term hydrophobic sequence, consistent with other secretory proteins and was located in the endoplasmic reticulum of COS-1 cells (Matsumoto *et al.*, 1999).

Prx Subtype	Mammalian Homologs
Prx I	NKEF-A, PAG1, MSP23, OSF3, HBP23, TPx II
Prx II	NKEF-B, TSA, Torin, PrP, TPx I
Prx III	MER5, SP-22, Aop1, TPx III
Prx IV	AOE 372, TRANK

Table 1.4: Typical 2-Cys Prx mammalian homologs.

The typical 2-Cys Prx mammalian homologues, most were originally identified without reference to their peroxidase function in a variety of species including humans (**blue**), murine (**red**) and bovine (**green**) NKEF-A: natural killer cell enhancing factor A; NKEF-B: natural killer cell enhancing factor B; PAG1: proliferator activated gene 1; MSP23: macrophage 23kDa stress-induced protein; OSF3: osteoblast specific factor 3; HBP23: heme binding protein 23; TPx: thioredoxin peroxidase; TSA: thiol-specific antioxidant; PrP: prion protein; MER5: murine erythroleukemia cells; SP-22: a substrate protein for mitochondrial ATP-dependant protease in bovine adrenal cortex; Aop1: antioxidant protein 1; AOE 372: antioxidant enzyme 372; TRANK: Tx peroxidase-related activator of natural killer κ B and c-Jun N-terminal kinase (Harris, 1968; Yamamoto *et al.*, 1989; Ishii *et al.*, 1993; Lim *et al.*, 1993; Prosperi *et al.*, 1993; Chae *et al.*, 1994b; Kawai *et al.*, 1994; Shau and Kim, 1994; Watabe *et al.*, 1994; Iwahara *et al.*, 1995; Tsuji *et al.*, 1995; Haridas *et al.*, 1998; Mitsumoto *et al.*, 2001).

1.10.2.2 ATYPICAL 2-CYS PRXS

The atypical 2-cys Prxs (Prx V) were located in the cytosol, peroxisomes and mitochondria (Knoops *et al.*, 1999). They are the most recently discovered members of the Prx family (Seo *et al.*, 2000) and unlike the typical 2-Cys Prx, they are functionally monomeric (Declercq *et al.*, 2001). They have only one conserved N-term cysteine (Cys-48), however, like the typical 2-Cys Prx, a further cysteine is required for catalytic function. Following oxidation to cysteine sulphenic acid (S_POH), Prx V forms an intra-molecular disulphide bond (Seo *et al.*, 2000), where, like the typical 2-Cys Prxs, Trx is used as a reducing agent (Rhee *et al.*, 2001). Prx V has also been shown to possess peroxynitrite reductase activity, allowing it to reduce harmful peroxynitrite to nitrite, and reducing the damage to cellular components (Dubuisson *et al.*, 2004).

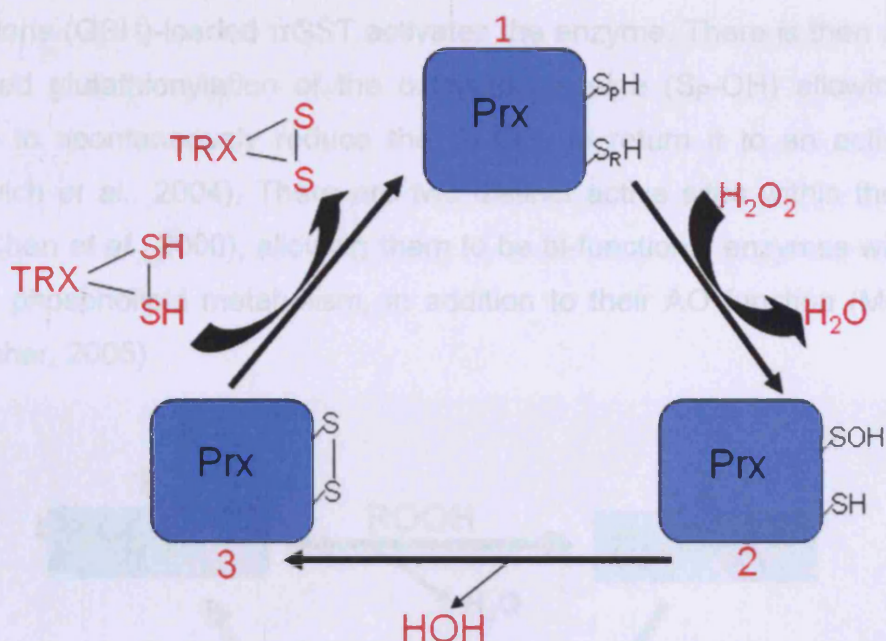


Figure 1.20: Atypical 2-Cys Prx catalytic cycle.

The atypical 2-Cys Prxs are functionally monomeric, they contain one conserved peroxidatic (S_P) cysteine, but require a further non-conserved cysteine (shown here as S_R) for their catalytic function. The reduced form of the enzyme (**1**) (S_P -H), reduces hydrogen peroxide leading to the formation of the cysteine sulphenic acid intermediate (**2**) (S_P -OH), this is followed by the formation of an intrasubunit disulphide bond (**3**) (condensation). Thioredoxin acts as a reducing agent, returning the enzyme to its original state (Adapted from D'Autreaux and Toledano, 2007).

Figure 1.21: 1-Cys Prx catalytic cycle.

1.10.2.3 1-Cys PRXS

The Mammalian 1-Cys Prxs were termed Prx VI (Rhee *et al.*, 2001), and like the typical 2-Cys Prxs, they formed head to tail homodimers during catalysis. This subgroup was identified as a member of the Prx family following random cloning and sequence deduction (Nagase *et al.*, 1995). Their subsequent characterisation revealed the ability to reduce peroxides but unlike the 2-Cys Prx subgroups, the 1-Cys Prxs utilizes only one conserved N-term cysteine for catalytic function (Cys-47), and hence, an inter- or intra-molecular disulphide bond is not formed during catalysis (Kang *et al.*, 1998a). They are induced by oxidative stress, demonstrating their AO function (Kim *et al.*, 2003). However, unlike the 2-Cys Prxs, they do not use Trx as a reducing agent and until recently, their recycling mechanism remained elusive. Subsequent work by Manevich *et al.* revealed that heterodimerisation between 1-Cys Prx and

glutathione (GSH)-loaded π GST activates the enzyme. There is then a π GST catalysed glutathionylation of the oxidised cysteine (S_P -OH) allowing GSH access to spontaneously reduce the S_P -OH, to return it to an active form (Manevich *et al.*, 2004). There are two distinct active sites within the 1-Cys Prxs (Chen *et al.*, 2000), allowing them to be bi-functional enzymes with roles in lung phospholipid metabolism, in addition to their AO function (Manevich and Fisher, 2005).

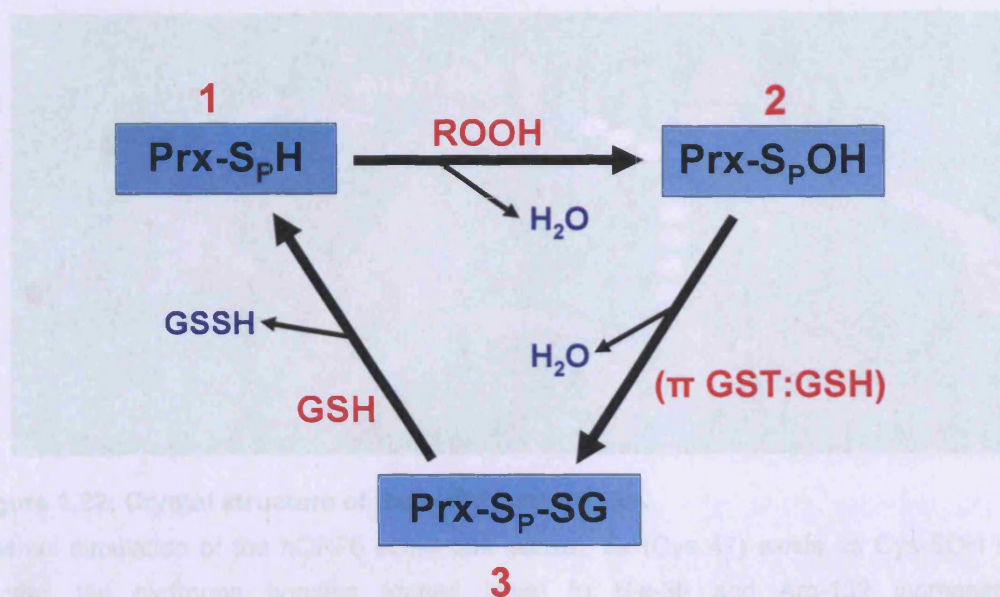


Figure 1.21: 1-Cys Prx catalytic cycle.

The 1-Cys Prxs (Prx VI) contain and require only one conserved Peroxidatic (S_P) cysteine, for their catalytic function. The reduced form of the enzyme (1) ($Prx-S_PH$) reduces the peroxide and forms cysteine sulphenic acid (2) ($Prx-S_POH$) in the process. This is followed by heterodimerisation of S_P and GSH loaded π GST (3), allowing the glutathiolation of S_P ($Prx-S_P-SG$), the GSH is now in a position to act as the reducing agent, returning Prx to its original state (Adapted from Manevich and Fisher, 2005).

1.10.3 PRX ACTIVE SITES

The first crystal structure of human Prxs was the 1-Cys Prx hORF6, which provided an insight into the active site arrangement and would serve as a basis for understanding the biological activities of Prxs (Choi *et al.*, 1998). Examples from all Prx subgroups have now been crystallised and they reveal great similarities regarding Prx active sites (Choi *et al.*, 1998; Hirotsu *et al.*, 1999; Declercq *et al.*, 2001). The unusually high efficiency of Prx, when

considering its catalytically active components suggested that the S_P was activated. This was confirmed by crystallisation images of hORF6 (Figure 1.22), revealing that the S_P (Cys-47) is in close proximity to the positively charged guanidine group of Arg-132 and hydrogen bonded to His-39; both of which act to increase its nucleophilicity by stabilizing the thiolate anion (Choi *et al.*, 1998).

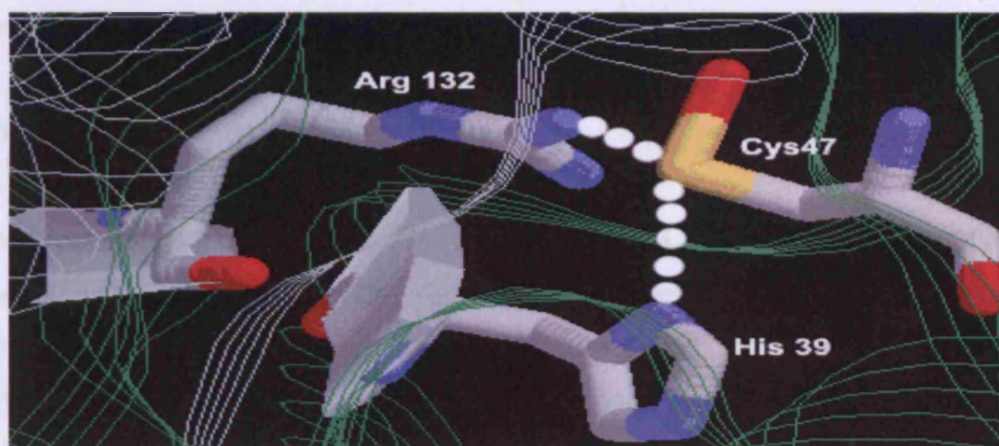


Figure 1.22: Crystal structure of the hORF6 active site.

Rasmol simulation of the hORF6 active site pocket, S_P (Cys 47) exists as Cys-SOH in the crystal, the hydrogen bonding (dotted lines) to His-39 and Arg-132 increases the nucleophilicity of Cys-47 by stabilising the thiolate anion (Adapted from Choi *et al.*, 1998).

The active site of Prx like many other redox active proteins, is located within a thioredoxin-like fold (Choi *et al.*, 1998). Further sequence analysis revealed that the S_P of Prx and the selenocysteine of GPx are structurally equivalent (Schroder and Ponting, 1998). It has since become apparent that this loop-helix motif, which is largely hydrophobic, places the reduced S_P in a solvent accessible narrow pocket. This is a feature of all Prx subgroups, as are the highly conserved residues Pro, Thr and Arg surrounding the S_P (Hall *et al.*, 2010), with the exception of Thr being substituted for His in 1-Cys Prxs (Wood *et al.*, 2003b).

1.10.4 REGULATION

1.10.4 PRX REGULATION

Peroxide accumulation, in particular that of the intracellular messenger hydrogen peroxide (Thannickal and Fanburg, 2000), is often required for

various cellular functions. Regulatory mechanisms are therefore present to reversibly inhibit Prxs. There is evidence of Prx regulation, through various post-translational modifications including, phosphorylation, truncation, oligomerisation and hyperoxidation (Chang *et al.*, 2002; Koo *et al.*, 2002; Wood *et al.*, 2002; Yang *et al.*, 2002). The Prx are known to be implicated in several signalling pathways, primarily through their ability to regulate intracellular concentrations of H_2O_2 (Rhee *et al.*, 2005b). Accordingly, they have been linked to lung diseases including COPD (Chen *et al.*, 2010).

1.10.4.1 PHOSPHORYLATION

Prx I contains a consensus site (Thr⁹⁰-Pro-Lys-Lys) that is phosphorylated specifically on Thr⁹⁰ by cyclin dependant kinases (CDKs) and in particular Cdc2. Phosphorylation was shown to reduce peroxidase activity by 80% but only during mitosis (Chang *et al.*, 2002), because Prx I is a cytosolic protein and its only contact with Cdc2 is following the breakdown of the nuclear envelope (Rhee *et al.*, 2005a). This suggests that H_2O_2 accumulation is needed for cell cycle progression (Chang *et al.*, 2002). Further work revealed that Prx II was also phosphorylated by Cdc2, with its inactivation speculated to occur in the same way (Rhee *et al.*, 2005c). One possible target of the accumulated H_2O_2 is Cdc25C, a dual-specificity phosphatase that is inactivated by the increased levels of H_2O_2 . This action is thought to be part of a wider mechanism involving the initial activation of Cdc2 at the onset of mitosis (Figure 1.23). Whereby Cdc25C activates the cyclin B bound Cdc2 by dephosphorylating its Thr¹⁴ and Tyr¹⁵ residues (Morgan, 1995), Cdc2 then goes on to phosphorylate Prx I and II rendering its peroxidase function inactive. However, once H_2O_2 levels rise, Cdc25C is inactivated which may be important to promote exit from mitosis (Rhee *et al.*, 2005c).

1.10.4.2 TRUNCATION

Studies in *Schizosaccharomyces pombe* revealed that TPx, which is a member of the Prx family, displayed C-terminal truncations that affected its peroxidase activity and also rendered it less sensitive to peroxide

overoxidation and subsequent inactivation. The inhibition of peroxidase activity resulted from the removal of a positive charge within Lys¹⁹¹, causing a loss of affinity to H₂O₂, while the corresponding Lys residues are conserved in all Prx isoforms except Prx V (Koo *et al.*, 2002). Isolated erythrocyte enzymes corresponding to Prx II were also shown to possess a truncated C-term (Cha *et al.*, 2000).

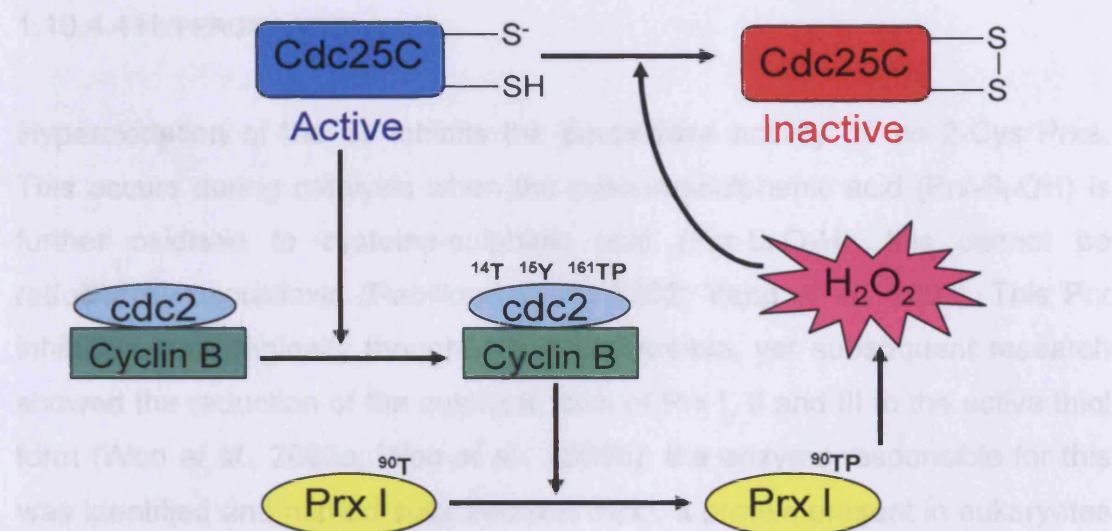


Figure 1.23: Inactivation of Prx I by Cdc2-dependant Phosphorylation.

The dual-specificity phosphatase Cdc25C activates cyclin B bound Cdc2 through the dephosphorylation of Thr¹⁴ and Tyr¹⁵, the activated Cdc2 goes on to phosphorylate Prx I on Thr⁹⁰, rendering it inactive, allowing H₂O₂ accumulation which in turn inactivates Cdc25C by oxidising its catalytic cysteine residue (Adapted from Rhee *et al.*, 2005c).

1.10.4.3 OLIGOMERISATION

TEM work on torin, a human erythrocyte protein, which is now known as Prx II (Harris *et al.*, 2001), revealed complexes resembling decamers (Harris, 1969). The typical 2-Cys Prxs are known homodimers (α_2), but they are capable of existing in two different oligomeric states, dimers α_2 and doughnut shaped decamers (α_2)₅ (Wood *et al.*, 2002), with the dimeric form exhibiting less peroxidase activity in comparison to the decameric form (Kitano *et al.*, 1999). The transition between the dimeric and decameric form is thought to be regulated by the redox states of the enzyme (Barranco-Medina *et al.*, 2009; Rinalducci *et al.*, 2011), with the reduced S_P favouring the decameric form

and the disulphide bonded S_P preferring the dimeric form (Wood *et al.*, 2002). Continued overoxidation causes the decamers to aggregate into high molecular weight (HMW) species with chaperone activity (Barranco-Medina *et al.*, 2009; Kim *et al.*, 2009). However, it has recently been established that glutathionylation of Prx I leads to the dissociation of the HMW complex, and hence the loss of chaperone activity (Park *et al.*, 2011).

1.10.4.4 HYPEROXIDATION

Hyperoxidation of the S_P inhibits the peroxidase activity of the 2-Cys Prxs. This occurs during catalysis when the cysteine-sulphenic acid ($\text{Prx-S}_P\text{OH}$) is further oxidised to cysteine-sulphinic acid ($\text{Prx-S}_P\text{O}_2\text{H}$), this cannot be reduced by thioredoxin (Rabilloud *et al.*, 2002; Yang *et al.*, 2002). This Prx inhibition was originally thought to be irreversible, yet subsequent research showed the reduction of the sulphinic form of Prx I, II and III to the active thiol form (Woo *et al.*, 2003a; Woo *et al.*, 2003b), the enzyme responsible for this was identified and named sulphiredoxin (Srx), a protein present in eukaryotes only (Biteau *et al.*, 2003). The fact that Srx is present in eukaryotes only reinforces the findings that eukaryotic 2-Cys Prxs have evolved to become much more sensitive to oxidative inactivation in comparison to bacterial 2-Cys Prxs. The floodgate hypothesis has therefore been proposed, whereby basal levels of H_2O_2 are kept low, but higher levels are permitted during signal transduction (Wood *et al.*, 2003a). Not only does hyperoxidation regulate intracellular signalling pathways, it has also been shown to affect cell cycle progression, with the hyperoxidation causing structural transitions leading to cell cycle arrest by alerting cells to perturbations in peroxide homeostasis (Phalen *et al.*, 2006). Often the hyperoxidation caused *in vitro* is not as pertinent *in vivo* (Lehtonen *et al.*, 2008).

1.11 *IN VITRO* CELL CULTURE

Traditionally, animal *in vivo* studies have been widely used in the field of respiratory toxicology; however, seeking viable human *in vitro* alternatives to accurately mimic the *in vivo* environment, has become increasingly important

(BéruBé *et al.*, 2009). In addition to the obvious advantages of human end-point data, provided by the *in vitro* systems, there is also a need to reduce the number of animals used in scientific research (EU Directive 76/68/EEC, 2003). In light of this, an increasing number of scientists are working towards the Three R's principles, which refers to the "reduction, refinement and replacement" of animal experiments (Russell and Burch, 1959).

Whole animal *in vivo* inhalation studies provide systemic data on a given compound (BéruBé, 2011); however, the task of extrapolating the data to predict human responses is complex (Miller *et al.*, 1983). There are significant interspecies issues that impact on the reliability of the data, including, anatomical variations (Brody, 1984), disparities in cellular composition (Thomassen and Nettesheim, 1990) and differences in biotransformation (Castell *et al.*, 2005).

To overcome the interspecies discrepancies often encountered with *in vivo* studies (Travis, 1991; Lin, 1998), human cell line cultures have been increasingly utilised (Table 1.5). There are two main types of human monolayers, carcinoma-derived and virus-transformed cell lines; both of which have their limitations (Forbes, 2000). The carcinoma-derived cell lines are sourced from human cells that have become carcinogenic, they are immortalised and can be passaged indefinitely, which is a great advantage in cell culture (Freshney, 2005). One example of a carcinoma-derived cell line is the popular Calu-3 cells that are sourced from a human bronchial adenocarcinoma. These cells have the ability to form tight junctions, develop cilia and produce mucin (Grainger *et al.*, 2006), however due to their neoplastic nature they may present an abnormal phenotype and lack metabolic activity (Foster *et al.*, 2000). The virally-transformed cell lines have been immortalised through the use of viral genes or vectors, examples of these commercially available cells lines include the BEAS-2B and 16HBE14o-cells (Steimer *et al.*, 2005). The BEAS-2B cells have been transformed using the 12-SV40 adenovirus, these cells are able to express AOs (Veranth *et al.*, 2007) and secrete cytokines (Veranth *et al.*, 2004), but lack the ability to secrete mucin and form tight junctions (Steimer *et al.*, 2005). The 16HBE14o-

cells have been transformed using the SV40 adenovirus (Westmoreland *et al.*, 1999), form tight junctions and develop cilia (Cozens *et al.*, 1994), but fail to secrete mucus (Steimer *et al.*, 2005). Consequently, the reliability of cell line data has been scrutinised, with some cell lines reported as containing the wrong cell type entirely (Drexler *et al.*, 2003).

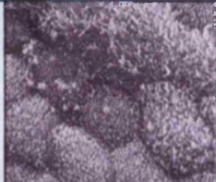
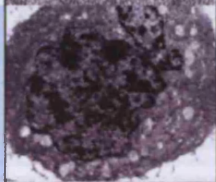
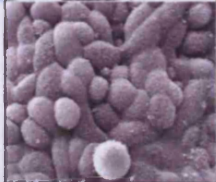
Cell Model	Derivation	Pros	Cons	Micrographs
Calu-3	Carcinoma of the Bronchus	<ul style="list-style-type: none"> • Immortalised • Form Confluent Monolayers • Develop Cilia • Express Mucin Genes 	<ul style="list-style-type: none"> • Variation in Tight Junction Formation 	
BEAS-2B	Transformed Bronchial Epithelium	<ul style="list-style-type: none"> • Immortalised • Form Confluent Monolayers • Secrete Cytokines • Express Antioxidants 	<ul style="list-style-type: none"> • No Mucin Secretion • Lack Tight Junctions 	
16HBE14o-	Transformed Bronchial Epithelium	<ul style="list-style-type: none"> • Immortalised • Differentiated & Multilayered • Develop Cilia & Microvilli • Secrete Cytokines 	<ul style="list-style-type: none"> • No Mucin Secretion 	

Table 1.5: Proximal lung cell lines.

The Calu-3 cell line is a carcinoma derived cell line, whereas the BEAS-2B and 16HBE14o- cell lines are both virally transformed (Adapted from Bérubé *et al.*, 2010b).

An alternative to cell lines are primary cells, which originate from human donors, either during surgery or immediately after death. Both alveolar (Elbert *et al.*, 1999) and tracheobronchial epithelial (Hill *et al.*, 1998) primary cell cultures have been utilised as investigating models. However, monolayers in general have their disadvantages, with a wide body of evidence supporting the need for three-dimensional (3D) tissue physiology (Griffith and Swartz, 2006; Pampaloni *et al.*, 2007; Bérubé *et al.*, 2010a; Scotton, 2011). The normal human bronchial epithelial (NHBE) cell culture model is derived from primary cells that differentiate into a fully-functioning pseudo-stratified BE containing ciliated, goblet, Clara, intermediate and basal cells. The model is cultured at an air-liquid interface (ALI), thus providing an *in vivo* like

environment for chemical exposure (Figure 1.24; Bérubé *et al.*, 2010b; Prytherch, 2010).

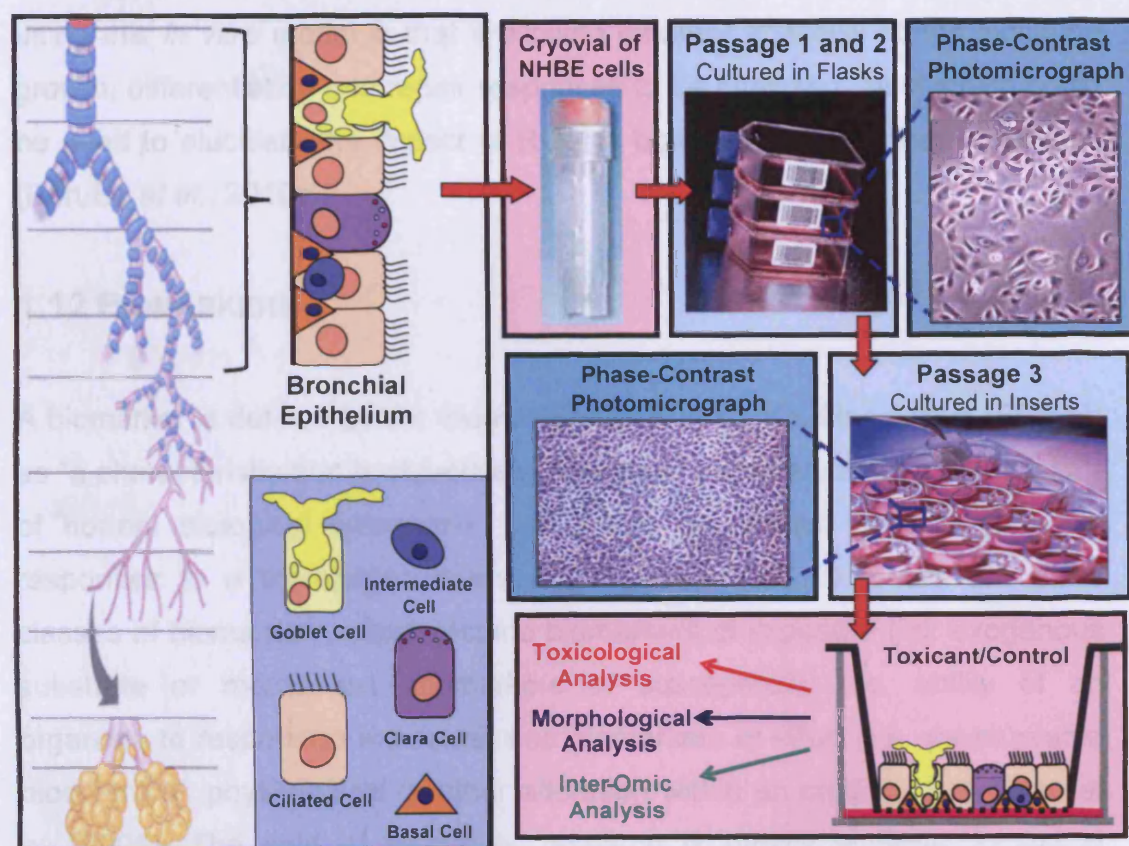


Figure 1.24: NHBE cells cultured at Air-Liquid Interface.

The Lonza (Basel, Switzerland) NHBE cells were taken from a *post-mortem* donors. Excision of the NHBE cells from donors was followed by maceration and enzyme digestion that returned the cells to their undifferentiated progenitor (basal) forms. The NHBE cells then underwent two Passages in flasks (T75 and T175), where they remained in their undifferentiated form. The cells were then transferred to individual Millipore inserts® to be cultured at an ALI. The differentiated NHBE cell model then consisted of ciliated, goblet, Clara, intermediate and basal cells. Once the culture was fully formed and stable (Days 27-33) toxicological exposures took place (Bérubé *et al.*, 2010b, Drawn by C. Job).

1.11.1 NHBE CELL CULTURE MODEL

The natural history of the NHBE cell model during normal growth and development, as well as during toxicant challenge has been fully-characterised (Prytherch, 2010). The cells were purchased from Lonza (Basel, Switzerland) as cryopreserved primary cells (≥500,000 cells/cryovial)

and underwent two Passages in flasks, where they remained as undifferentiated basal cells, until transferred to individual Millipore inserts, creating an ALI, permitting cells to differentiate (Figure 1.24). An advantage of using this *in vitro* model is that it allowed different epithelial states including growth, differentiation and repair responses to be analysed, all of which could be used to elucidate the impact of ROS in both normal and diseased states (BéruBé *et al.*, 2010a).

1.12 BIOMARKERS

A biomarker is defined by the Biomarkers Definitions Working Group (BDWG) as “a characteristic that is objectively measured and evaluated as an indicator of normal biological processes, pathogenic processes, or pharmacologic responses to a therapeutic intervention” (BDWG, 2001). There are three classes of biomarkers, which include biomarkers of exposure (i.e. exogenous substrate or metabolite), biomarkers of susceptibility (i.e. ability of an organism to respond to exposure) and biomarkers of effect (i.e. measureable biochemical, physiological or other alteration within an organism) (Garban *et al.*, 2005). The field of biomarker research is rapidly evolving, providing measurable end-points that are invaluable for diagnosis, disease management and drug approval (Puntmann, 2009).

1.12.1 BIOMARKERS IN COPD

Biomarkers of COPD are generally taken from four main pulmonary sources, which include, sputum, bronchial biopsies, bronchoalveolar lavage (BAL) and exhaled breath (Barnes *et al.*, 2006). Exhaled breath is the simplest form of analysis (Montuschi *et al.*, 2010), producing markers such as 8-Isoprostane (Makris *et al.*, 2008) and H₂O₂ (Dekhuijzen *et al.*, 1996). Other common markers of COPD include inflammatory markers such as IL-8, increased proteases such as the matrix metalloproteinases (MMPs) (Barnes *et al.*, 2006) and the acute phase protein, C -reactive protein, which is found in blood (Anderson, 2006).

Oxidative stress has become widely accepted as the earliest pathological event, which leads to lung disease (Doelman and Bast, 1990; Valko *et al.*, 2007). Therefore, biomarkers that reflect changes in cellular oxidation states as a function of normal redox signalling and environmental insults would be extremely useful for studying human disease processes *in vitro* and *in vivo*.

1.12.2 THE PRXS AS BIOMARKERS

The Prxs become reversibly inactivated (Woo *et al.*, 2003a; Woo *et al.*, 2003b; Wood *et al.*, 2003b; Cox *et al.*, 2010a) and demonstrate altered expression levels (Rhee *et al.*, 2001; Immenschuh and Baumgart-Vogt, 2005) during times of oxidative stress. They have also been shown to undergo structural transitions during the catalytic cycle and as such, may be utilised as candidates for biomarkers of oxidative lung injury (Phalen *et al.*, 2006).

To assess the utility of using Prx as biomarkers, their expression levels, locations and oxidation states must be determined. These Prx parameters would need to be measured during both normal growth conditions and following insults, including H₂O₂ and CS, to allow the significance of any changes related to oxidative stress to be fully appreciated.

1.13 AIMS AND OBJECTIVES OF THE STUDY

1.13.1 THE HYPOTHESIS

The hypothesis for this research project was three-fold:

1. Prx status can be used in conjunction with the *in vitro* NHBE cell model, as a biomarker of intracellular oxidative stress.
2. Exposure of the NHBE cell cultures to H₂O₂ and CS will alter Prx status, providing a parameter directly linking the level of oxidative stress to the injury severity and repair competency of the cell system.

3. *In vivo* correlation analysis, with human lung tissue from COPD transplant patients, will substantiate the NHBE *in vitro* findings by confirming that Prx status is a sensitive biomarker of oxidative stress and epithelial remodelling.

1.13.2 PROJECT AIMS AND OBJECTIVES

The overall aim of this project was to determine whether the 2-Cys typical Prx isoforms I, II and III could be used as biomarkers of intracellular oxidative stress, and hence the level of oxidative damage caused as a result of external insults i.e. H₂O₂ and CS. Furthermore, to determine whether the *in vitro* NHBE cell culture model could provide a system to evaluate the effect of the impact of ROS in normal as well as disease pathology phenotypes, using Prx status as dosimeters for redox dependant signalling events. Prx I, II and III were chosen as they were the three 2-Cys Prx isoforms expressed the strongest within the BE, which was the focus of this project.

The clinical application would be to establish whether the NHBE-Prx system could be utilised to assess the extent of oxidative damage caused as a result of inhaled or systemic drug exposure. The system could inform on the ability of pre-clinical compounds to increase intracellular oxidative stress resulting in formation of ROS and disruption in redox cycling and signalling. These events lead to a perturbation of oxidative metabolism that eventually results in pulmonary damage.

The specific aims and objectives for this project were three-fold:

1. To define the expression levels and oxidation states of Prx I, II and III during NHBE cell model morphogenesis (Figure 1.25):
 - Primary NHBE cells will be cultured to produce a fully differentiated and stable bronchial epithelium (BE) phenotype. Trans-epithelial electrical resistance (TEER) will be measured

throughout the 42 day time-course of the *in vitro* model to inform on junction integrity and culture development.

- Reducing and non-reducing gel electrophoresis followed by Western blotting and chemiluminescence detection will be used to determine the expression levels and oxidation states of Prx I, II and III over a 42 day time-course in the *in vitro* NHBE model.
- Immunohistochemistry (IHC) at the light microscope (LM) and electron microscope (EM) levels will be used to establish the levels and specific location of the Prx isoforms and hyperoxidised Prx in the *in vitro* NHBE cell model.

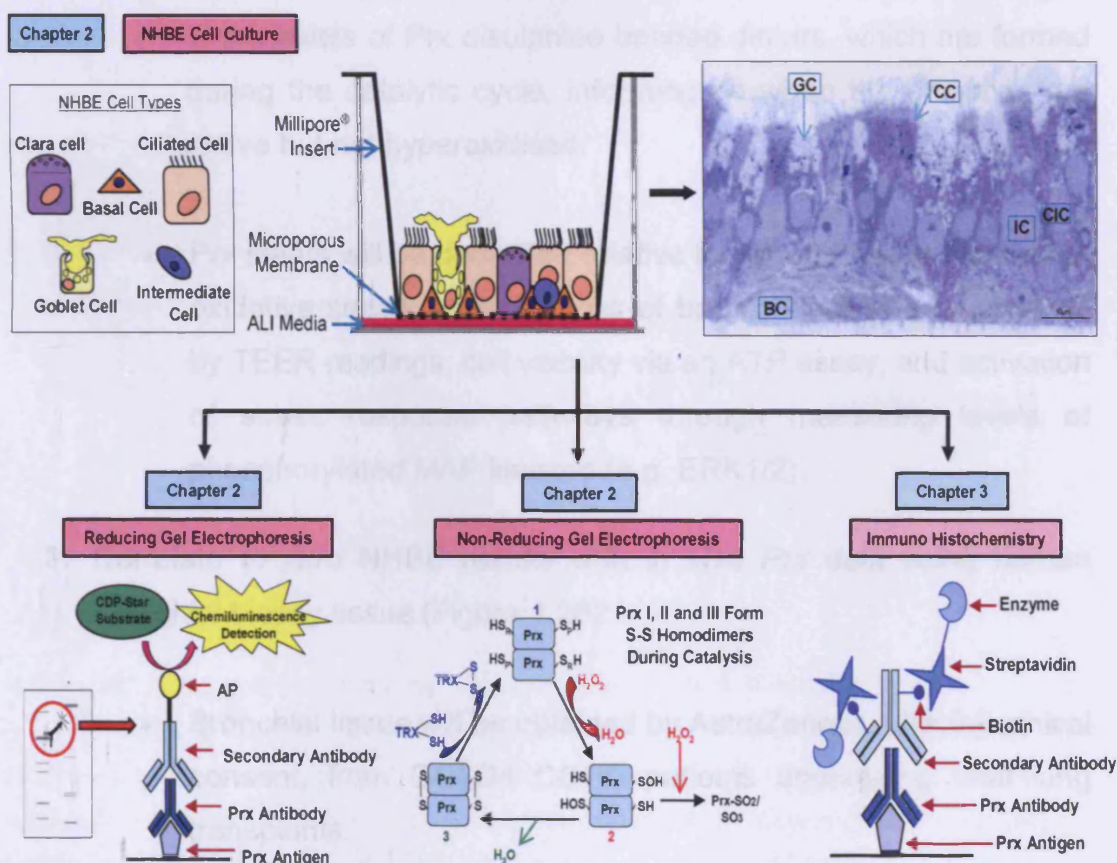


Figure 1.25: Flow chart of experimental work in Chapters 2 and 3.

Experimental work in Chapters 2 and 3 focused on primary NHBE cell culture and Prx status elucidation throughout the morphogenesis of the *in vitro* model. Reducing and non-reducing gel electrophoresis conditions were used to determine Prx expression levels and oxidation states, alongside IHC techniques at the LM and EM level.

2. Define changes in Prx status following exposure to fluxes of H₂O₂, either directly or via the glucose/glucose oxidase (GOx) system, and CS (Figure 1.26):

- The cell cultures will be apically exposed to direct H₂O₂, GOx or CS.
- Reducing gel electrophoresis will be used to inform on the total level of Prx expression and also levels of total hyperoxidation within the exposed cultures. IHC at the LM level will also be used to inform on Prx levels.
- Non-reducing gel electrophoresis will be used to reveal changes in the levels of Prx disulphide bonded dimers, which are formed during the catalytic cycle, informing on when the enzymes are active but not hyperoxidised.
- Prx status will be quantified relative to cell and tissue markers of oxidative stress, including loss of barrier function as measured by TEER readings, cell viability via an ATP assay, and activation of stress response pathways through measuring levels of phosphorylated MAP kinases (e.g. ERK1/2).

3. Correlate *in vitro* NHBE results with *in vivo* Prx data using human bronchial biopsy tissue (Figure 1.26):

- Bronchial tissue will be obtained by AstraZeneca, with full ethical consent, from GOLD4 COPD patients undergoing total lung transplants.
- IHC at the LM level will utilise DAB as a chromagen for Prx antigen visualisation. This will establish the levels and specific cellular locations of the Prx isoforms and hyperoxidised Prx within the human tissue samples.

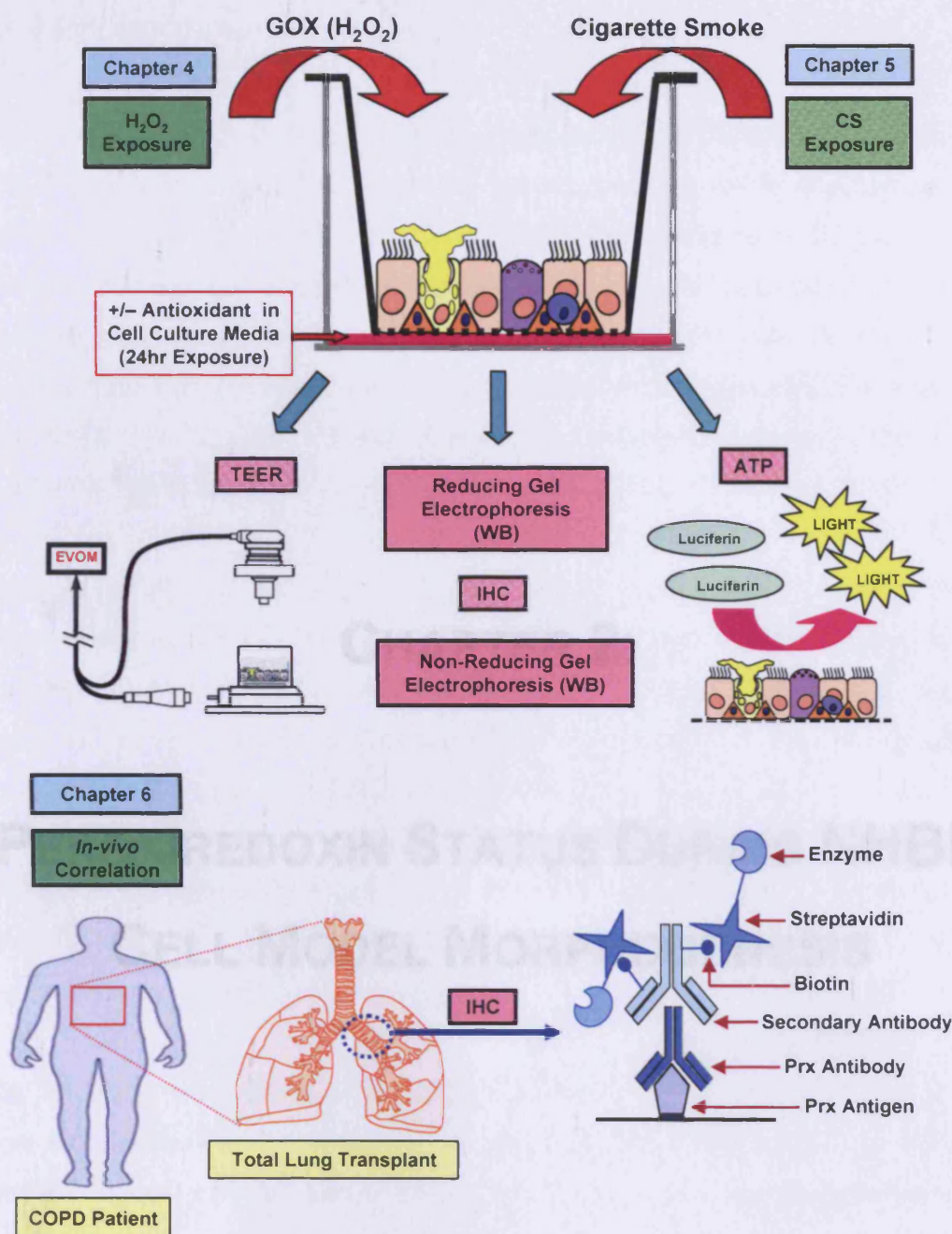


Figure 1.26: Flow chart of experimental work in Chapters 4, 5 and 6.

The main focus of experimental work in Chapters 4 and 5 involved exposing the NHBE cell cultures to toxicants, including H₂O₂ (directly and utilising the GOX system) and CS. Prx expression levels and oxidation states were determined using reducing and non-reducing gel electrophoresis conditions, alongside IHC techniques at the LM level. Cell viability and junction integrity following exposure was also determined via ATP assays and TEER measurements respectively. Chapter 6 focused on *in vivo* correlation analysis, whereby bronchial biopsy samples were taken from COPD patients undergoing double lung transplants. IHC techniques at the LM level were utilised to determine Prx levels.

CHAPTER 2:

PEROXIREDOXIN STATUS DURING NHBE CELL MODEL MORPHOGENESIS

2.1 INTRODUCTION

With the advent of European Union legislation (EU; Directive 76/768/EEC, 2003) calling for a reduction in animal testing, seeking viable alternatives has become increasingly necessary. The NHBE cell model is a 3D cell culture platform that aims to alleviate the quantities of animals required for inhalation toxicological testing, whilst providing human end-point data. Morphological and biochemical characterisation have established that the NHBE model is a high throughput system capable of mimicking important aspects of the *in situ* human BE (BéruBé *et al.*, 2009; BéruBé *et al.*, 2010b; Prytherch, 2010).

By 2020 COPD is set to rise to the third most common cause of death Worldwide (Raheison and Girodet, 2009). In light of this, there is an increasing need for early stage biomarkers of injury and repair, and in particular, biomarkers identifying perturbations in redox cycling and signalling, i.e. oxidative stress (Halliwell and Gutteridge, 1999; Jones, 2006). The Peroxiredoxins (Prxs) are a family of ubiquitously expressed AO enzymes that are directly affected by levels of intracellular oxidative stress (Wood *et al.*, 2003b), rendering them as strong candidates for use as redox sensitive biomarkers.

The following work utilised the NHBE cell model in the determination of the Prxs as biomarkers of oxidative stress. The basal expression levels and oxidation states of Prx I and III during NHBE cell model morphogenesis were established. The isoforms had similar properties, formed the same catalytic intermediate and underwent the same catalytic cycle (Wood *et al.*, 2003b). Previous research showed that Prx I and III were present within the BE (Kinnula *et al.*, 2002a). Therefore, a confirmation of the presence of Prxs would substantiate the validity of the NHBE model as an *in vitro* BE alternative. In order to assess Prx expression levels and oxidation states, reducing and non-reducing gel electrophoresis conditions were used (Cox *et al.*, 2010a), followed by Western blotting and chemiluminescent detection. Basal levels of hyperoxidised Prx (Prx-SO₃) were determined, with increased levels indicating elevated intracellular oxidative stress (Phalen *et al.*, 2006)

2.1.1 RESEARCH AIMS

The research aims for experimental work in Chapter 2 (Figure 2.1) were as follows:

- Culture the NHBE cell model into a system containing a fully differentiated and functioning BE phenotype. Assess the viability of the epithelial barrier by measuring the Trans-Epithelial Electrical Resistance (TEER) values to determine the integrity of the intercellular junctions.
- Quantify the expression levels and oxidation states of each Prx isoform, within the NHBE model during morphogenesis, through utilising reducing and non-reducing gel electrophoresis conditions followed by Western blotting and chemiluminescence.

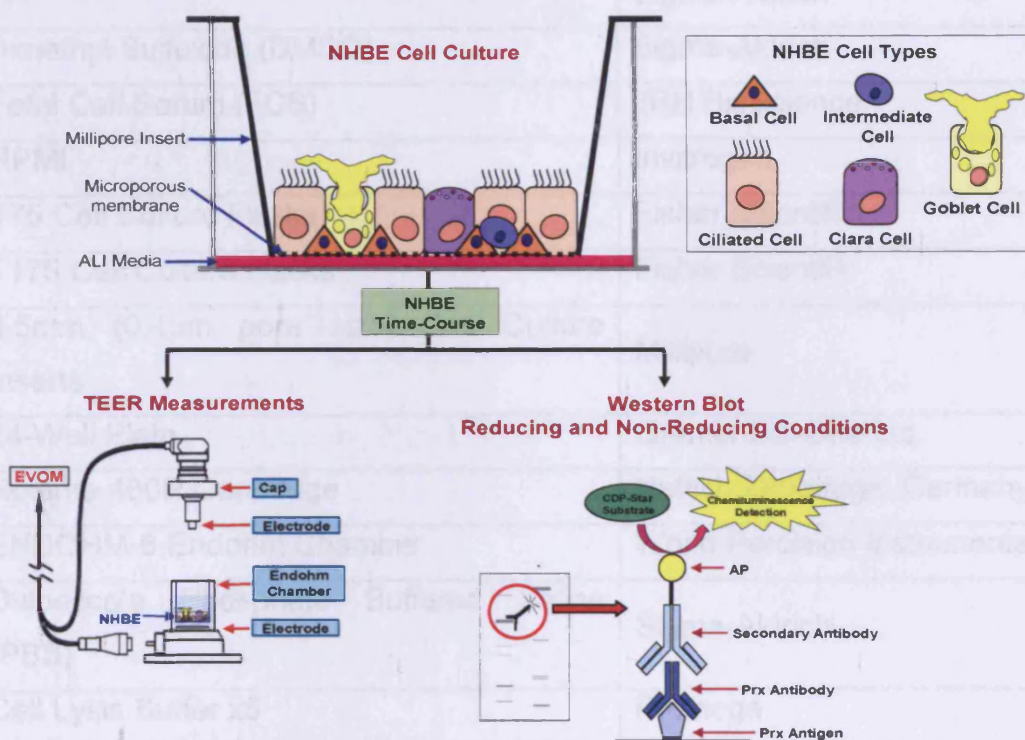


Figure 2.1: Flowchart of experimental work in Chapter 2.

Experimental aims included NHBE cell culture followed by Prx status elucidation throughout morphogenesis. TEER readings indicated junction integrity and culture differentiation. Reducing and non-reducing gel electrophoresis followed by Western blotting and chemiluminescent detection determined Prx expression levels and oxidation states. ALI (air liquid interface).

2.2 MATERIALS AND STOCK SOLUTIONS

2.2.1 MATERIALS AND SUPPLIERS

MATERIALS:	SUPPLIER:
NHBE Cells, with Retinoic Acid (RA)	Lonza Group Ltd, Switzerland
Bronchial Epithelial Basal Medium (BEBM)	Lonza Group Ltd, Switzerland
Bronchial Epithelium Growth Medium [®] (BEGM) SingleQuots [®]	Lonza Group Ltd, Switzerland
Dulbecco's Modified Eagles Medium (DMEM), w/4.5g/L Glucose, L-Glutamine, w/out Pyruvate	Lonza Group Ltd, Switzerland
Trypsin-EDTA	Lonza Group Ltd, Switzerland
Hank's Balanced Salt Solution (HBSS)	Lonza Group Ltd, Switzerland
RA	Sigma-Aldrich
Dimethyl Sulfoxide (DMSO)	Sigma-Aldrich
Fetal Calf Serum (FCS)	JRH BioScience
RPMI	Invitrogen
T75 Cell Culture Flasks	Fisher Scientific
T175 Cell Culture Flasks	Fisher Scientific
6.5mm (0.4µm pore size) Cell Culture Inserts	Millipore
24-Well Plate	Grenier Bio-One Ltd.
Rotanta 460R Centrifuge	Hettich Zentrifuga, Germany
ENDOHRM-6 Endohm Chamber	World Percision Instruments
Dulbecco's Phosphate Buffered Saline (PBS)	Sigma-Aldrich
Cell Lysis Buffer x5	Promega
XCell SureLock [®] Mini-Cell and XCell II [™] Blot Module Kit CE Mark	Invitrogen
NuPAGE [®] Novex 4-12% Bis-Tris Gel 1.0mm, 10 Well	Invitrogen
20x NuPAGE [®] MOPS SDS Running Buffer	Invitrogen

Pre-stained SeeBlue Plus 2 [®] Molecular Weight Marker	Invitrogen
Glycerol	Melford
Bromophenol Blue	Sigma-Aldrich
β -Mercaptoethanol	Sigma-Aldrich
10x Tris-Glycine Transfer buffer	Sigma-Aldrich
Methanol	Fisher Scientific
Sodium Dodecyl Sulphate (SDS)	Sigma-Aldrich
Tris Base	Sigma-Aldrich
Hybond-P Polvinylidenedifluoride (PVDF) Membrane	GE Healthcare
Tris-Buffered Saline-Tween (TBS/T)	Sigma-Aldrich
I-Block	Applied Biosystems
Sodium Azide	Sigma-Aldrich
Bradford Reagent and BSA Standards	Sigma-Aldrich
Prx-I Primary Antibody	Lab Frontier, Korea
Prx-II Primary Antibody	Lab Frontier, Korea
Prx-III Primary Antibody	Lab Frontier, Korea
Prx-SO ₃ Primary Antibody	Lab Frontier, Korea
β -Actin Primary Antibody	Sigma-Aldrich
Goat-Anti-Rabbit IgG AP Conjugate	Bio-Rad
CDP-Star Substrate	Applied Biosystems
Whatman Chromatography Paper 3MM	Jencons
P200 Gel Loading Tips	Alpha Laboratories
Biospectrum-AC Imaging System	Ultra Violet Products
2-Mercaptoethanosulfonate (MESNA)	Sigma-Aldrich
Phase Contrast light Microscope (DM2500)	Leica Ltd.

Table 2.1: Materials used and their suppliers. All suppliers were UK based unless stated.

2.2.2 STOCK SOLUTIONS

All stock solutions were prepared and stored at room temperature (RT) unless stated otherwise.

RA was prepared as a 5×10^{-5} working solution from a 1×10^{-2} M stock solution, by diluting in DMSO. This working solution was stored in 25 μ l aliquots at -20°C in a light tight container.

FCS was prepared as a 10% working solution by diluting the stock solution in RPMI.

Running Buffer was prepared as a 1x working solution from a 20x NuPAGE® MOPS SDS Running Buffer stock.

Transfer Buffer was prepared as a 1x working solution from a 10x stock 0.25M Tris-base, 192M glycine and 10% (v/v) analysis grade methanol.

Sample Buffer (Reducing) was prepared as a 2x working solution containing glycerol, double distilled (dd) H₂O, SDS, 1M Tris-HCl pH 6.8, 0.2% bromophenol blue and β -mercaptoethanol to 10%.

Sample Buffer (Non-Reducing) was prepared as a 4x working solution containing glycerol, ddH₂O, SDS, 1M Tris-HCl pH 6.8 and 0.2% Bromophenol Blue.

TBS/T was prepared as a 1x working solution by dissolving 1 packet of powdered stock in 1L of deionised water, yielding 0.05M Tris, 0.138M NaCl, 0.0027M KCL, pH 8 at 25°C, 0.05% Tween 20.

Blocking Buffer was prepared as a 1x working solution containing 0.2% I-block and 0.02% (v/v) sodium azide (NaN₃) supplemented in TBS/T. The blocking buffer was stored for up to 1 month at 4°C.

MESNA Stripping Buffer was prepared as a 1x working solution containing 62.5mM Tris-HCl pH 6.8, 2% w/v SDS and 50mM MESNA. MESNA stripping buffer was kept for no longer than two weeks and was stored at 4°C.

2.3 METHODS

2.3.1 CELL CULTURE

2.3.1.1 FIRST PASSAGE

In accordance to the manufacturer's recommended methods (Lonza Group Ltd, Switzerland), a 1ml cryovial of NHBE cells (~500,000 cells) was thawed at 37°C and re-hydrated in 60ml of BEGM at 37°C. BEGM was prepared using BEBM and growth supplements (Appendix i). The hydrated NHBE cells (30ml) were transferred to T75 flasks and incubated at 37°C; cells adhered to the flasks during the initial incubation. Twenty four hours post-seeding the BEGM (30ml) was replaced with 30ml of fresh BEGM medium; this was repeated (two out of three Days) until the cells reached 70% confluency (~2-3 Days).

2.3.1.2 SECOND PASSAGE

Cell cultures were transferred from two T75 flasks and re-seeded into six T175 flasks, maximising the cell numbers. Initially, 5ml of HBSS at 37°C was added to each T75 flask to wash the cells, 3ml of Trypsin-EDTA solution at 37°C was then added for 2-3min, until all cells detached. Following this, 30ml of 10% FCS with RPMI (30ml) was added to stop the trypsinisation of the cells, and cell suspensions were centrifuged at 72 (x g) for 4min, the supernatant was removed. The BEGM (180ml) was prepared, and each cell pellet re-suspended in 2ml BEGM at 37°C, the BEGM-cell suspension was then added to remaining BEGM. The BEGM-cell suspension (30ml) was transferred into a T175 flask and incubated at 37°C; cells adhered to the flasks during the initial incubation. Twenty four hours post-seeding the BEGM was replaced with 30ml fresh BEGM medium; this was repeated (two out of three Days) until the cells reached 70% confluency (~2-3 Days).

2.3.1.3 SEEDING INTO MILLIPORE® INSERTS

Cell cultures were transferred from T175 flasks into Millipore® inserts, allowing the progenitor cells to differentiate. Initially, 5ml of HBSS at 37°C was added to each T175 flask to wash the cells, 3ml of Trypsin-EDTA solution at 37°C was then added for 2-3min, until all cells detached. The 10% FCS with RPMI (30ml) was added to cease the trypsinisation of the cells and cell suspensions were then centrifuged at 72 (x g) for 4min, the supernatant was removed and three cell pellets were re-suspended in 2ml BEGM at 37°C. A haemocytometer with a 5x5 grid was used to determine the cell concentration of the cell suspension. For seeding into inserts, the density required was 0.5 million cells/ml; the cell suspension was added to the required volume of BEGM. The BEGM-cell suspension (150µl) was added apically into each insert and 500µl BEGM was added basally; cells adhered to the insert membrane during the initial incubation.

2.3.1.4 CONFLUENT INSERT CULTURES

The apical media was removed 24hr post-seeding, creating an air-liquid interface (ALI) culture (Day 1) (Figure 2.2). The basal media was replaced with 300µl of ALI media (Appendix ii). Basal ALI media was changed daily, adding 300µl of fresh ALI medium into each well. Once mucin secretion began to appear on the apical surface (~Day 15), it was removed by aspiration every second Day, preventing mucin accumulation (mimicking *in vivo* conditions).

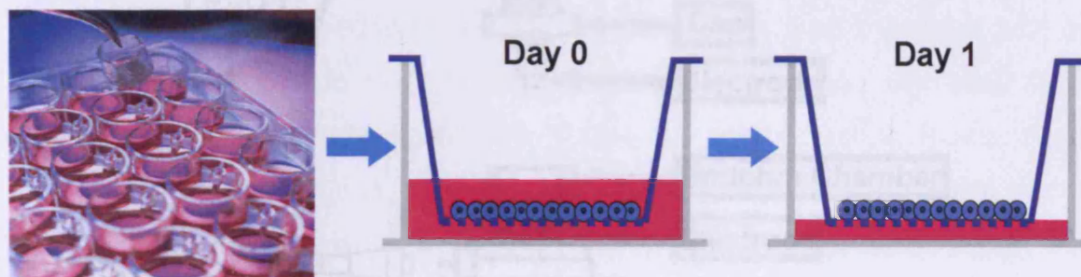


Figure 2.2: Schematic diagram depicting the inserts within a 24-well plate.

Illustration of the cultures at Day 0 (seeding of cells) and Day 1 (removal of apical media). Only the progenitor basal cells were present following seeding (Diagram courtesy of Dr. Z. Prytherch, Cardiff University).

2.3.2 TRANS-EPITHELIAL ELECTRICAL RESISTANCE (TEER)

The Endohm chamber (Figure 2.3) was filled with 1ml of PBS and a cell insert was placed inside. PBS (150 μ l) was placed on the apical region of the cultures and the top electrode was placed on top of the insert, the reading was then taken by releasing the current. The TEER value (recorded on ohms; Ω) displayed was indicative of the junctional formation within the culture (Figure 2.4). A TEER reading using an insert without cells was taken to use as a 'blank' measurement, and the TEER results from cultures were normalised against this. NHBE samples were taken off for analysis every three Days throughout the life span of the NHBE model (n=3).

2.3.3 BRADFORD ASSAY

The Bradford assay (Bradford, 1976) was undertaken to accurately measure protein concentration. A BSA protein standard of 2mg/ml was diluted into the following concentrations with PBS: 2 μ g/ml, 4 μ g/ml, 6 μ g/ml, 8 μ g/ml, 10 μ g/ml, 12 μ g/ml and 14 μ g/ml, these were used to establish a concentration curve. Fifty microlitres of Bradford reagent (colorimetric chemical agent) along with 150 μ l of the standard was placed in a plate reader (x3) and read at 570nm wavelength. A standard curve was established from which unknown sample protein concentrations could be determined.

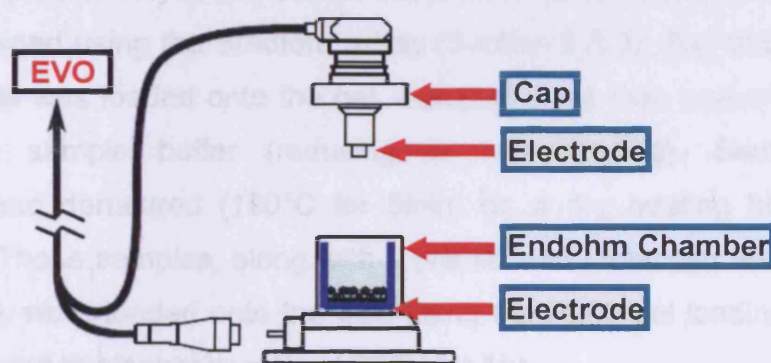


Figure 2.3: Apparatus used to record TEER readings.

The culture was placed inside the Endohm chamber and filled with PBS; the cap was then placed onto the chamber, thus creating a closed circuit. The current was then released from the EVOM and the reading taken (Diagram courtesy of Dr. D. Balharry, Cardiff University).

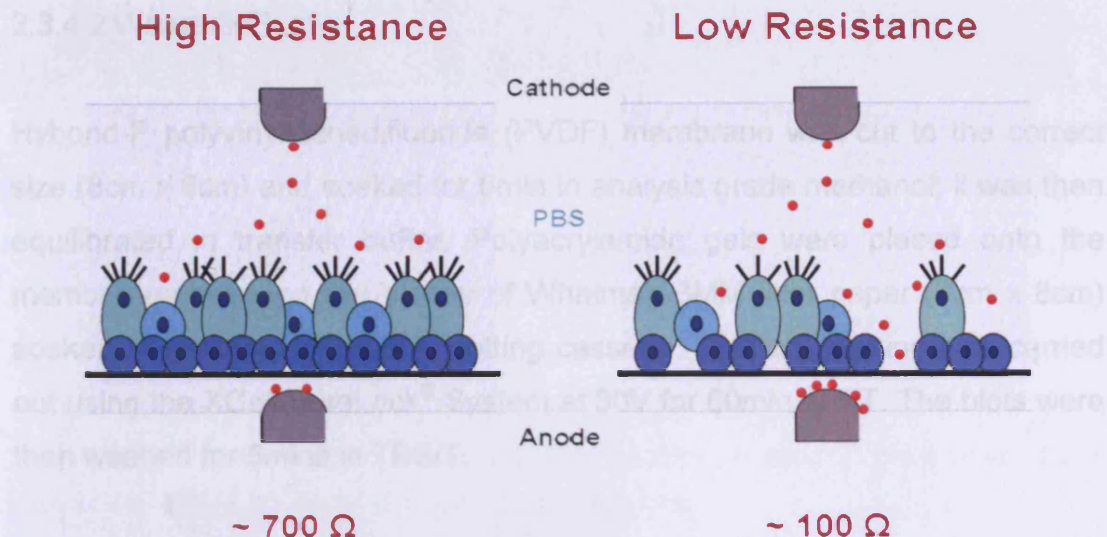


Figure 2.4: Variation in TEER values.

Schematic diagram depicting the differences in TEER readings between a healthy ($\sim 700\Omega$) confluent epithelial culture and a culture with a disrupted epithelial barrier (i.e. compromise tight junction formation) ($\sim 100\Omega$) (Diagram courtesy of Dr. D. Balharry, Cardiff University).

2.3.4 WESTERN BLOT/ANTIBODY DETECTION

2.3.4.1 1D SDS PAGE (POLYACRYLAMIDE GEL ELECTROPHORESIS)

The gel electrophoresis apparatus was assembled according to the manufacturer's instructions. The comb was removed from the pre-cast 4-12% gel and the wells flushed with 1x MOPS running buffer, the gel was then placed into the main tank and the system was filled with 1x running buffer. Cells were lysed with lysis buffer and the protein concentration of each lysate was determined using the Bradford assay (Section 2.3.3); $2\mu\text{g}$ of protein from each sample was loaded onto the gel. Samples were then prepared with the appropriate sample buffer (reducing or non-reducing). Samples were sonicated and denatured (100°C for 5min) on a dry heating block (Stuart Scientific). These samples, along with a pre-stained molecular weight marker (Figure 2.5), were loaded onto the gels using the P200 gel loading tips. Gels were subjected to electrophoresis at 200V for 1hr.

2.3.4.2 WESTERN BLOT

Hybond-P polyvinylidenedifluoride (PVDF) membrane was cut to the correct size (8cm x 8cm) and soaked for 5min in analysis grade methanol; it was then equilibrated in transfer buffer. Polyacrylamide gels were placed onto the membranes between two pieces of Whatman 3MM filter paper (8cm x 8cm) soaked in transfer buffer in a blotting cassette. Western blotting was carried out using the XCell SureLock® System at 30V for 60min at RT. The blots were then washed for 5mins in TBS/T.

2.3.4.3 ANTIBODY INCUBATION AND DETECTION

Western blots were incubated in a sealed polyethylene bag with 20ml of blocking buffer for 1hr at RT on an orbital shaker (Stuart-Scientific). The blocking buffer was then replaced with 10ml of primary antibody diluted to the required concentration in blocking buffer (Table 2.2). Blots were then incubated with primary antibody overnight at 4°C on an orbital shaker. For reduced blots, the membrane was cut (Figure 2.5) to run the Prx and actin antibodies simultaneously. However this was not possible for non-reduced blots, as Prx dimers were too close in size, and therefore, the blot was incubated with each primary antibody in succession. Post-incubation, blots were washed for 5min in TBS/T (4x). Subsequently, the blots were incubated for 1hr with 12ml of alkaline phosphatase (AP)-conjugated secondary antibody diluted with blocking buffer (Table 2.2). Blots were then washed for 5min in TBS/T (4x).

Blots were then incubated with 1ml CDP-Star Chemiluminescent Substrate for 5min in a section of a polyethylene film, excess reagent was removed and blots placed in a new polyethylene bag. Blots were then transferred to the Biospectrum-AC imaging system for chemiluminescent detection. Following exposure, the blots were stripped by incubating in a sealed polyethylene bag with approximately 20ml of MESNA stripping buffer for 30min at 50°C. Blots were then washed for at 10min in TBS/T (3x) and blocked for 1hr; this allowed the blots to be re-probed for additional primary antibodies (Figure 2.5).

1° Antibody	MW (KDa)	Dilution	Final Concentration	2° Antibody	Dilution
α -Actin	45	1:5000	200ng/ml	Anti-Rabbit	1:3000
Prx I	22	1:1000	1 μ g/ml	Anti-Rabbit	1:3000
Prx II	22	1:100	10 μ g/ml	Anti-Rabbit	1:3000
Prx III	28	1:2000	500ng/ml	Anti-Rabbit	1:3000
Prx-SO ₃	22/28	1:1000	1 μ g/ml	Anti-Rabbit	1:3000

Table 2.2: Primary and secondary antibodies for Westerns.

Overview of the primary (1°) and secondary (2°) antibodies with their optimised dilution factor used in the antibody detection of a Western blot technique.

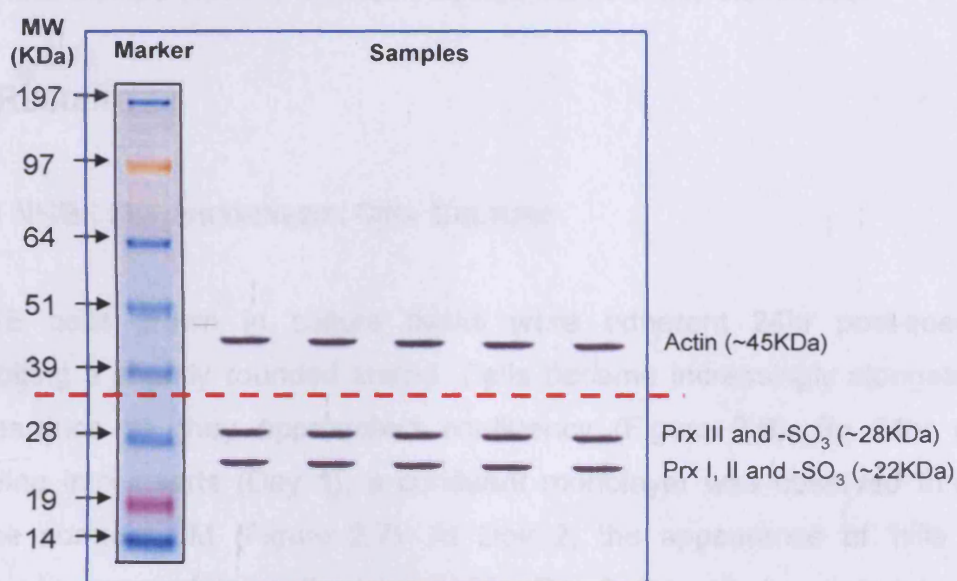


Figure 2.5: Schematic overview of Western blot (reducing gel electrophoresis).

The membrane was cut where indicated (red dotted line). The pre-stained marker values shown were for MOPS buffer (protein bands have different motilities in different buffer systems) (Invitrogen, 2011).

2.3.5 STATISTICAL ANALYSIS

All descriptive statistics (e.g. mean and standard deviation [SD]) were calculated using the Minitab software package (Version 16). The regression equation of the Minitab software was used to determine the standard curves for protein concentration in the Bradford assay and for H₂O₂ determination in the GOx assay (Dytham, 2003). A one-way ANOVA was performed in

conjunction with a Levene test (Dytham, 2003) for equal variance, if the data was of equal variance the least significant difference (LSD) test (Dytham, 2003) was performed to indicate significance, if the data was not of equal variance significance was determined via the Games-Howell test (Dytham, 2003). Both the LSD and Games-Howell tests were performed when the ANOVA result was significant ($P < 0.05$) (Dytham, 2003). Conventionally a one-way ANOVA would not be performed if data was not normally distributed, however, recent studies (Gillard, 2011) have suggested it is a more powerful test to use when the sample number is limited (i.e. $n=3$ in this study). Therefore, the same tests were performed (i.e. one-way ANOVA, Levene, LSD and Games-Howell) for data that was not normally distributed.

2.4 RESULTS

2.4.1 NHBE MORPHOGENESIS: CELL CULTURE

NHBE cells grown in culture flasks were adherent 24hr post-seeding, exhibiting a slightly rounded shape. Cells became increasingly elongated in appearance as they approached confluency (Figure 2.6). By 24hr post-seeding into inserts (Day 1), a confluent monolayer was observed through phase contrast LM (Figure 2.7). At Day 2, the appearance of 'hills' and 'valleys' were predominantly seen, and by Day 3, the cells began to take on a regular pavement or 'cobblestone' style appearance, which remained as such until culture demise (Day 42). Real-time observations using the LM revealed ciliary action at Day 15, which was manifested as tiny 'flickers' and observed until culture demise.

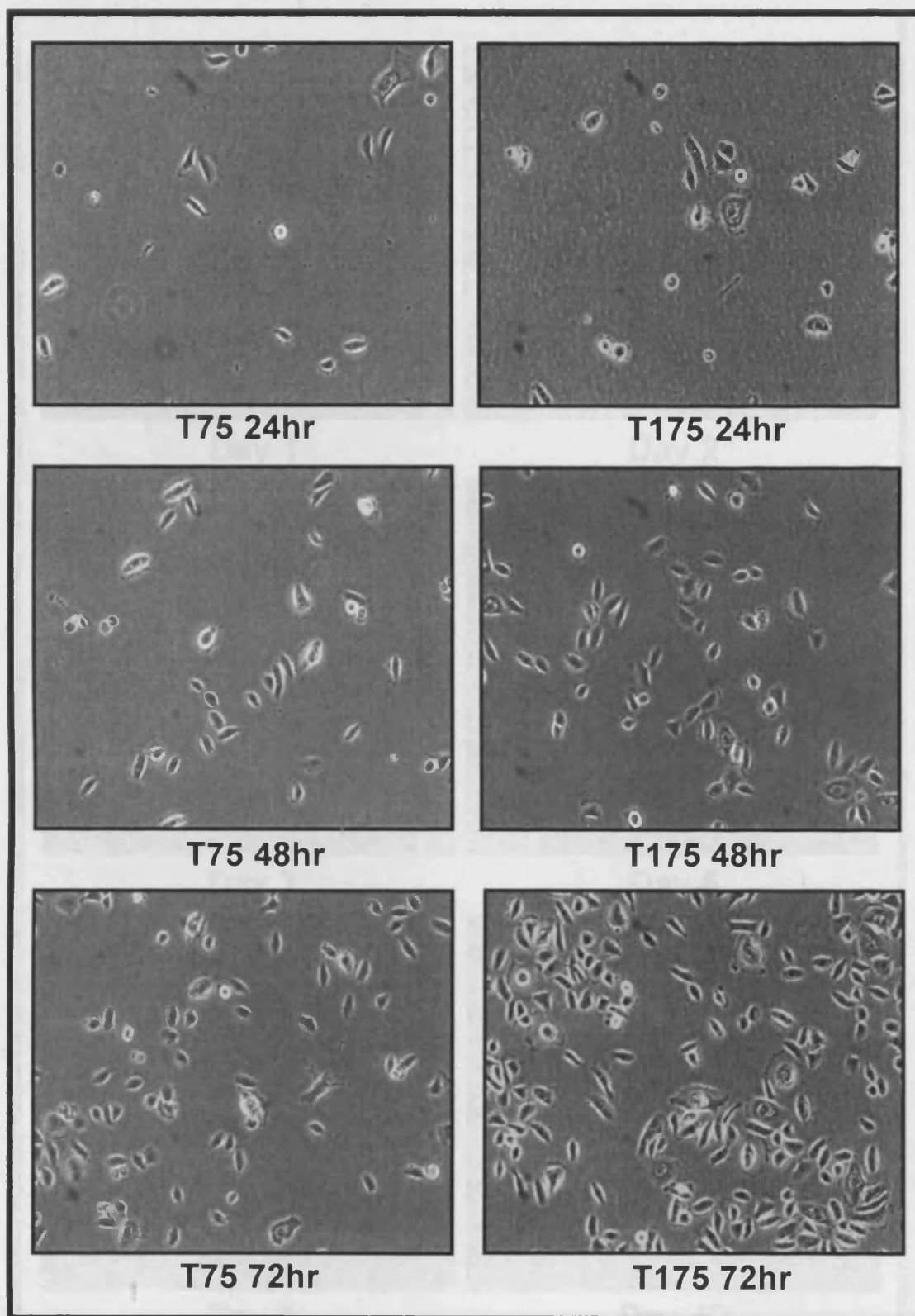


Figure 2.6: Phase contrast LM images of NHBE cells in flasks.

Cells were initially cultured in T75 flasks until they reached ~70% confluency; they were then seeded into T175 flasks, and again cultured until they reached ~70% confluency. Cells appeared oblong in shape, indicating good viability, confluency increased at a steady rate from 24hr to 72hr in both flasks. Hours (hr) were post-seeding into the corresponding flasks.

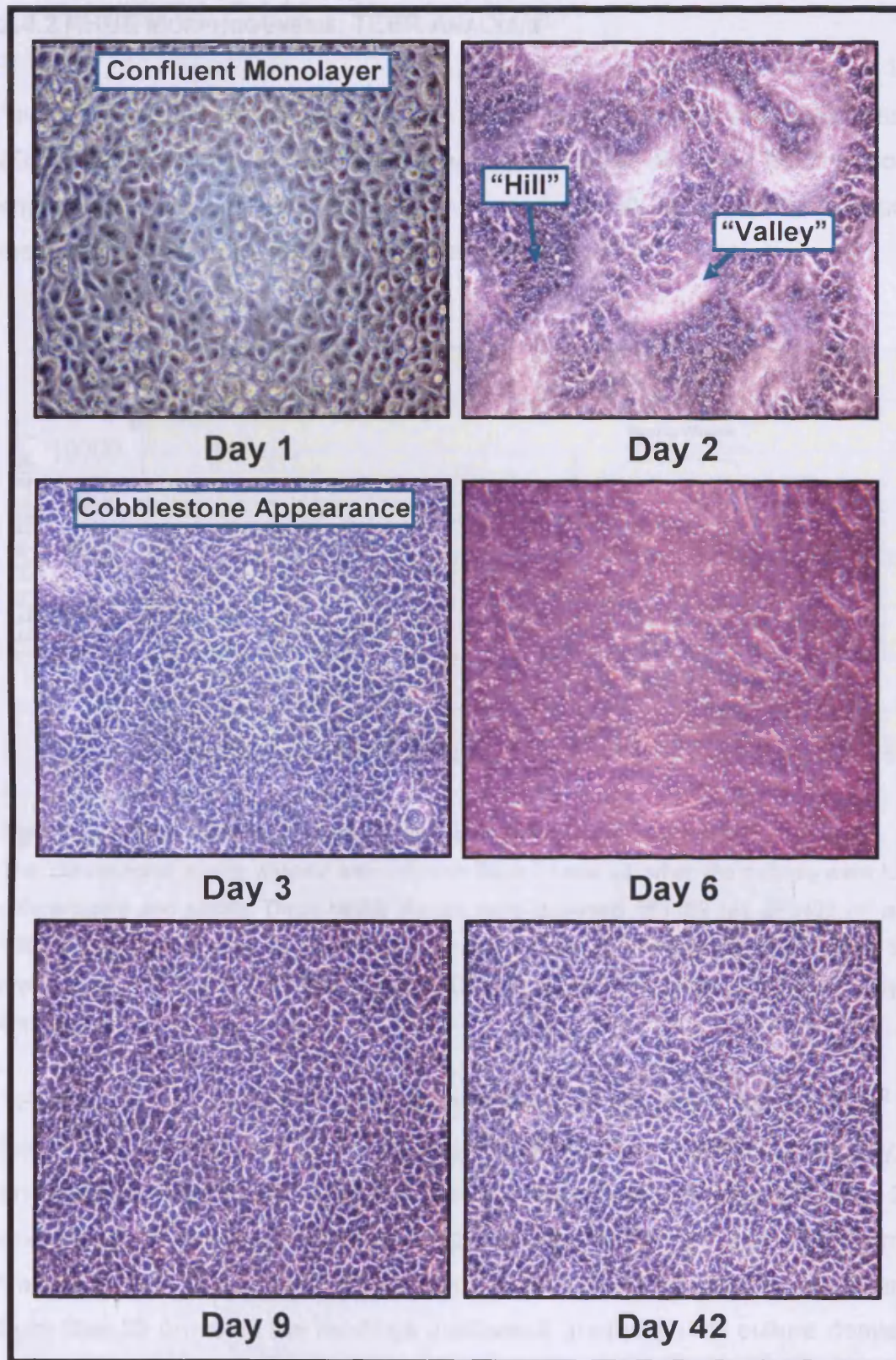


Figure 2.7: Phase contrast LM images of NHBE cells in Transwell® inserts.

At Day 1 the cells formed a confluent monolayer, by Day 2 'hills' and 'valleys' appeared which indicated bilayer formation. The 'cobblestone' appearance was maintained from Day 3 until culture demise at Day 42. Days were post-seeding into inserts.

2.4.2 NHBE MORPHOGENESIS: TEER ANALYSIS

The TEER values were measured every third Day (n=3), over a 42 Day period (Figure 2.8). Three NHBE donors were analysed, all were healthy non-smoking Caucasian men ranging in age from 30 to 50. TEER values increased significantly ($P \leq 0.05$) between Day 9 and 12.

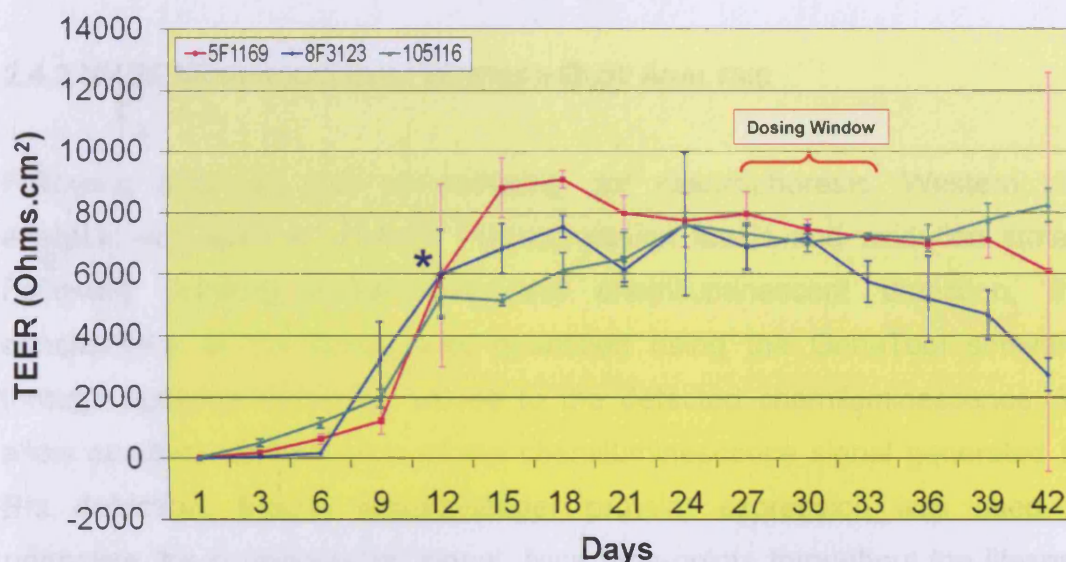


Figure 2.8: TEER values throughout NHBE cell culture morphogenesis.

The 'conventional dosing window' was between Days 27 and 33, when the cultures were fully differentiated and stable. Three NHBE donors were analysed 5F1169 (■), 8F3123 (◆) and 105116 (▲). The asterisk (*) denoted a significant ($P \leq 0.05$) increase in TEERs from the previous day. I Signified \pm SD for n=3. TEER values significantly increased between Day 9 and 12.

TEER readings from the 8F3121 donor increased gradually from $16\Omega\text{.cm}^2$ at Day 1 to $174\Omega\text{.cm}^2$ at Day 6, with a steep increase to $3229\Omega\text{.cm}^2$ at Day 9 and again to $6831\Omega\text{.cm}^2$ at Day 15. The readings plateaued between Days 24 and 30 with average values remaining between $6900\Omega\text{.cm}^2$ and $7600\Omega\text{.cm}^2$. Values at Day 33 were $5751\Omega\text{.cm}^2$, which was outside the plateau range, and from Day 33 onwards the readings decreased gradually until culture demise. TEER readings from donor 105116 increased steadily from $22\Omega\text{.cm}^2$ at Day 1 to $1945\Omega\text{.cm}^2$ at Day 9, this was followed by a steep increase to $5256\Omega\text{.cm}^2$ at Day 12. The readings plateaued between Days 24 and 33 with average values remaining between $7000\Omega\text{.cm}^2$ and $7600\Omega\text{.cm}^2$, and from Day 39

onwards, the TEER values increased. Donor 5F1169 displayed the same pattern as the previous two donors, in that there was a gradual increase from $29\Omega\cdot\text{cm}^2$ at Day 1 to $1223\Omega\cdot\text{cm}^2$ at Day 9, which was followed by a steep increase to $5956\Omega\cdot\text{cm}^2$ at Day 12, and again to $9087\Omega\cdot\text{cm}^2$ at Day 18. There was a plateau phase from Day 21 to 33 where the TEER values remained between $7100\Omega\cdot\text{cm}^2$ and $8000\Omega\cdot\text{cm}^2$. This preceded a decline in readings which went from $6966\Omega\cdot\text{cm}^2$ at Day 36 to $6077\Omega\cdot\text{cm}^2$ at Day 42.

2.4.3 NHBE MORPHOGENESIS: WESTERN BLOT ANALYSIS

Following reducing and non-reducing gel electrophoresis, Western blot analysis was used to quantify Prx expression levels and oxidation states. Following antibody incubations and chemiluminescent detection, the densitometry of the bands was quantified using the GeneTool software, through applying numerical values to the detected chemiluminescence. To allow accurate interpretation of the chemiluminescence signal generated by Prx detection, β -actin (house-keeper protein) expression was used to normalise the corresponding signal. Nine time-points throughout the lifespan of the model were chosen for Western blot analysis. Each Day represented a significant stage in the models development. At Days 1 and 3 cells remained as undifferentiated basal cells, at Day 9 the intercellular junctions had begun to form, by Day 15 there was mucus production and cilia beating, by Day 21 the cells were fully differentiated. Days 27, 30 and 33 represented the 'dosing window' and Day 39 marked the beginning of culture demise.

2.4.3.1 NHBE MORPHOGENESIS: WESTERN BLOT ANALYSIS (TOTAL PRX LEVELS)

NHBE cultures from the nine key time-points throughout morphogenesis were subjected to reducing gel electrophoresis conditions and analysed via Western blotting (Figure 2.9). During initial morphogenesis, i.e. Days 1 and 3, Prx I levels were negligible at 0.28 and 0.35, respectively, with levels of total Prx III from comparable Days nearly four times greater at 0.84 and 1.1, respectively. There were significant ($P\leq 0.05$) increases in Prx I expression between Days 3 and 9, 15 and 21. Prx III levels were consistently high, with

significant ($P \leq 0.05$) increases in expression between Days 3 and 9, 9 and 15, 27 and 30, 33 and 39. There were peaks of Prx III expression reached at Days 33 and 39 measuring 2.65 and 3.0, respectively. Levels of Prx-SO₃ were elevated throughout morphogenesis, consistently remaining above 1.0. Levels remained steady and under 2 from Days 1 to 30, however, by Day 33 they had risen to 3.8 and continued to rise to 3.88 at Day 39. Prx II was not sufficiently detected.

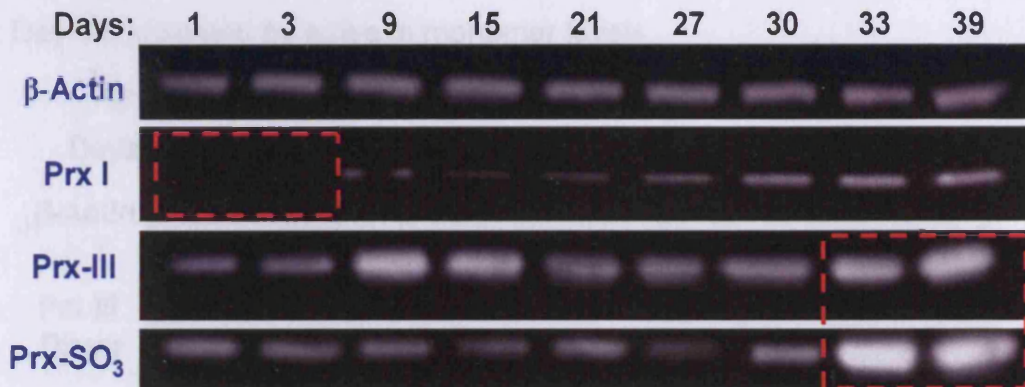


Figure 2.9: Western blot analysis of total Prx levels during NHBE morphogenesis.

Whole cells extracts were generated from NHBE cells during morphogenesis, Days were post-seeding into inserts. Lysates were resolved by reducing 1D SDS-PAGE electrophoresis followed by Western blotting and chemiluminescent detection. Proteins were analysed using 1° ABs specific to Prx I, III, -SO₃ and β-actin. Red denoted bands of interest with minimal Prx I expression at Days 1 and 3, and elevated Prx III and Prx-SO₃ at Days 33 and 39.

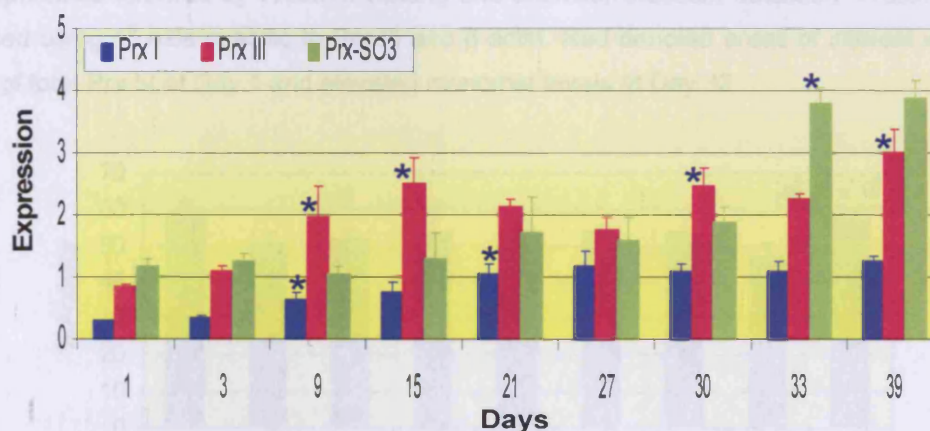


Figure 2.10 Densitometry analysis of total Prx levels during NHBE morphogenesis.

The GeneTool software calculated Prx I (■), Prx III (■) and Prx-SO₃ (■) band densitometry for Western blot (reducing conditions) results of NHBE cell cultures during morphogenesis. Results were normalised using the corresponding β-actin expression. The asterisk (*) denoted a significant ($P \leq 0.05$) increase in TEERs from the previous day. I Signified \pm SD for $n=3$.

2.4.3.2 NHBE MORPHOGENESIS WESTERN BLOT ANALYSIS (PRX III ACTIVITY)

NHBE cultures from the nine key time-points throughout morphogenesis were subjected to non-reducing gel electrophoresis conditions and analysed via Western blotting (Figure 2.11). The dimer levels (active Prx III) were strong throughout morphogenesis, however monomer (inactive Prx III) were also consistently elevated, leading to Prx III activity levels of ~50% throughout the entire time-course. There was a noteworthy reduction in Prx III activity to 47% at Day 33, indicated by a rise in monomer levels.

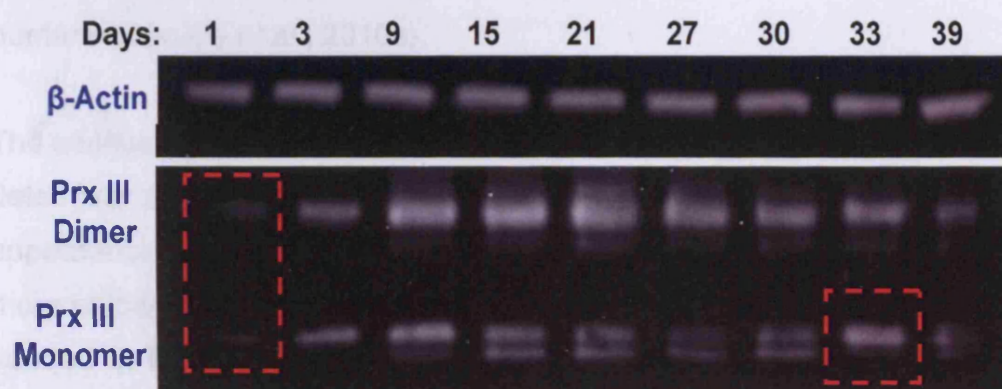


Figure 2.11: Western blot analysis of Prx III activity during NHBE morphogenesis.

Whole cells extracts were generated from NHBE cells during morphogenesis, Days were post-seeding into inserts. Lysates were resolved by non-reducing 1D SDS-PAGE electrophoresis followed by Western blotting and chemiluminescent detection. Proteins were analysed using 1° ABs specific to Prx III and β -actin. Red denoted areas of interest with low levels of total Prx III at Day 1 and elevated monomer levels at Day 33.

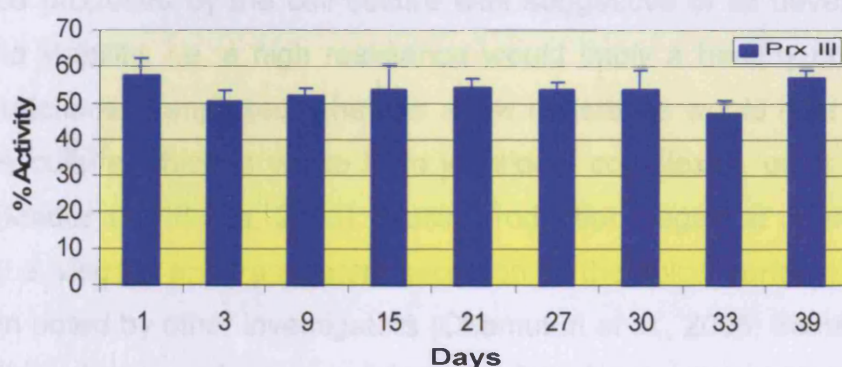


Table 2.12: Densitometry analysis of Prx III activity during NHBE morphogenesis.

The GeneTool software calculated Prx III (■) monomer and dimer band densitometry from Western blots (non-reducing conditions) of NHBE cell cultures during morphogenesis. Results were normalised using the corresponding β -actin expression. I signified \pm SD for $n=3$.

2.5 DISCUSSION

2.5.1 NHBE MORPHOGENESIS: CELL CULTURE AND TEER ANALYSIS

The NHBE model was derived from healthy human primary explant tissue, consequently, the cells were genotypically and phenotypically more representative of normal epithelia; in comparison to other classical respiratory models (e.g. A549, BEAS-2B, Calu-3 and 16HBE14o; (BéruBé *et al.*, 2010b). The cultures were able to form a 3D, pseudo-stratified state that exhibited a functional mucociliary phenotype with tight junctions as observed *in vivo* in humans (BéruBé *et al.*, 2010a).

The confluency of the dividing cells was monitored using phase contrast LM to determine the rate at which the cells divided post-seeding. The morphological appearance of the cells was also a determining factor in their viability, with a more oblong shape denoting increased viability (Prytherch, 2010). NHBE cells seeded in flasks, retained an undifferentiated basal (progenitor) phenotype, cells adopted a differentiated phenotype when transferred to the individual Millipore® inserts. Twenty four hours post-seeding into inserts, cultures took on a 'cobblestone' appearance; by 48hr post-seeding there was a characteristic 'hills' and 'valleys' phenotype, indicating bilayer formation. Early stage differentiation began at Day 9 with the formation of junctional complexes, denoted by an increase in TEER values (Noske *et al.*, 1994). The resistance produced by the cell culture was suggestive of its developmental stage and viability, i.e. a high resistance would imply a healthy culture with formed junctional complexes, whereas a low resistance would infer either an immature culture which is yet to form junctional complexes, or, a damaged culture (Matter and Balda, 2003). Mucin production began at approximately Day 15 (i.e. viscous and transparent secretion on the apical surface). This has also been noted by other investigators (Chemuturi *et al.*, 2005; Balharry *et al.*, 2008). The presence of mucin, and hence, fully functioning goblet cells has been verified by periodic acid Schiff (PAS) analysis (Prytherch, 2010). Day 15 also marked the appearance of beating cilia, observed as tiny flickers using real-time LM, and the hallmark of fully differentiated ciliated cells. By Day 27,

cultures were fully differentiated and remained stable until Day 36. After this point, TEER values dropped marking the beginning of culture demise. A reduction in the colour change (dark pink to pale pink) of the media confirmed that nutrients were no longer being taken up by the cultures.

2.5.2 NHBE MORPHOGENESIS: WESTERN BLOT ANALYSIS

In order to understand the significance of using Prxs as biomarkers of intracellular oxidative stress, their status within the NHBE model during morphogenesis was warranted. The aim of using reducing and non-reducing conditions, in conjunction with Western blotting, was to determine the expression levels and oxidation states of each Prx isoform. For oxidation state elucidation, levels of hyperoxidised Prx (Prx-SO₃) were analysed.

Western blot analysis of the reduced protein samples revealed a significant difference in expression levels between Prx I and III throughout the nine key day time-course. The low levels of Prx I, which is situated in the cytosol (Chae *et al.*, 1999), were detected during the earliest stage of development (Days 1 to 3) suggested that Prx I was not a feature of basal cell antioxidant defence, with only a basal population present in the cultures at this stage. Expression of Prx II, which is situated in the cytosol (Chae *et al.*, 1999), were not sufficiently detected to warrant further analysis within this project. Prx III, which is situated in the mitochondria (Rhee *et al.*, 2001), was expressed at comparatively high levels throughout morphogenesis; this was consistent with *in vivo* research (Kinnula *et al.*, 2002a). Expression levels rose consistently until Day 9, whereby they remained constant until Day 15. This coincided with the formation of the cilia, and hence, an increase in the mitochondria levels due to the increasing requirement for ATP to drive cilia beating (Bittar, 2002). Following the increase in expression there was a plateau phase that remained constant until Day 33, suggesting that by Day 33, biochemically, the cultures were not stable. This needed to be addressed with regard to the selection of an appropriate 'dosing window', which had been previously established by Prytherch and co-workers.

Analysis of reduced and non-reduced protein samples revealed elevated levels of hyperoxidised Prxs throughout model morphogenesis and inferred that significant basal levels of oxidative stress were occurring. This may be due to the nature of the NHBE cell model environment, as it corresponded to a repairing airway, having previously undergone maceration and de-differentiation upon removal from *post-mortem* donors (BéruBé *et al.*, 2010b). An increased level of oxidative stress is a recognised limitation of *in vitro* cell culture (Halliwell, 2011), and a parameter that should be taken into consideration during data analysis. *In vitro* conditions impose oxidative stress upon the cells leading to a phenomenon known as 'culture shock' (Halliwell, 2003). The NHBE cultures were 'static' and did not allow the cyclic change of nutrients and removal of waste-products; factors that elicit elevated oxidative stress levels. Days 33 and 39 exhibited a significant increase in hyperoxidised Prx, suggesting that by this stage the cells could no longer suppress the elevated stress levels imposed by the static culture conditions. These collective results supported the need to modify the dosing window, given that NHBE cell cultures exhibited loss in both phenotypic and biochemical stability by Day 33.

2.6 CONCLUSION

The detection of two out of the three Prx isoforms within the NHBE cell model was a result that further validated this system as a viable *in vitro* model. Secondly, the expression levels observed for each isoform corresponded to existing BE *in vivo* data. The stable expression patterns of Prx I and III within the period of toxicological analysis (i.e. dosing window) was a positive indicator of their potential role as biomarkers. Predictable expression under normal conditions would further highlight fluctuations observed as a direct result of increased oxidative stress, either following lung injury or via the addition of toxicants.

There was a need to modify the existing 'dosing window', to a period where the model was fully differentiated and the cultures were stable. Previous work by Prytherch and co-workers had established this stable period to be between

Days 27 and 33; yet, current results suggested that the Prxs oxidation state and hence, levels of oxidative stress were not stable at Day 33. A more suitable dosing window would be between Days 21 and 30. However, when taking into account previous morphological analysis (Prytherch, 2010), it was finally concluded that Days 25 to 30 would be a more suitable time-frame to employ for the remaining experimental work (i.e. Chapters 3 to 5).

Western blot analysis identified heightened basal levels of Prx hyperoxidation within the model. Therefore, it would be necessary to confirm the Western blot morphogenesis data and the cellular locations of the Prx isoforms I and III, in conjunction with the levels of Prx-SO₃, within the NHBE cell culture model (Chapter 3).

CHAPTER 3:

IMMUNOHISTOCHEMISTRY ANALYSIS OF PEROXIREDOXIN STATUS DURING NHBE CELL MODEL MORPHOGENESIS

3.1 INTRODUCTION

Immunohistochemistry (IHC) analysis, at both the LM and electron microscopy (EM) levels, was required to corroborate the Western blot morphogenesis data (Chapter 2), and to provide a more comprehensive representation of Prx status at basal levels in the NHBE model. The primary objective here was to determine the cellular locations of the Prx isoforms I and III and the levels of hyperoxidised Prx (Prx-SO₃) within the NHBE cell model. Secondary to the immunological analysis, conventional histological assessments with haematoxylin and eosin (H+E) were also undertaken. These involved examinations of the NHBE cell culture during morphogenesis (42 Days) to provide complementary data for the TEER and phase contrast LM results (Chapter 2).

All IHC assessments utilised polyclonal Prx antibodies for antigenic detection within the NHBE cultures. Results were visualised using chromogenic and fluorescent detection at the LM level, and colloidal gold conjugates at the EM level. IHC was not a quantitative method since antigenic activity was greatly reduced by the process of tissue fixation (Newman and Hobot, 2001). It did however, inform on the cellular location of the isoforms, thus augmenting the overall understanding of Prx status. Of the nine key developmental time-points investigated by Western blotting (Chapter 2), only four days were chosen for morphological analysis (i.e. Days 1, 3, 9 and 30). These four key days represented the widest breadth of morphological and biochemical modification within the BE architecture.

3.1.1 RESEARCH AIMS

The research aims for experimental work in Chapter 3 (Figure 3.1) were as follows:

- Employ conventional histology (H+E) to characterise the morphological development of the NHBE cell model throughout the 42 day time-course.

- Determine the cellular locations of the Prx isoforms within the fully differentiated NHBE model, utilising IHC chromogenic and fluorescent detection (LM level) and the conjugated colloidal gold (TEM level) systems.

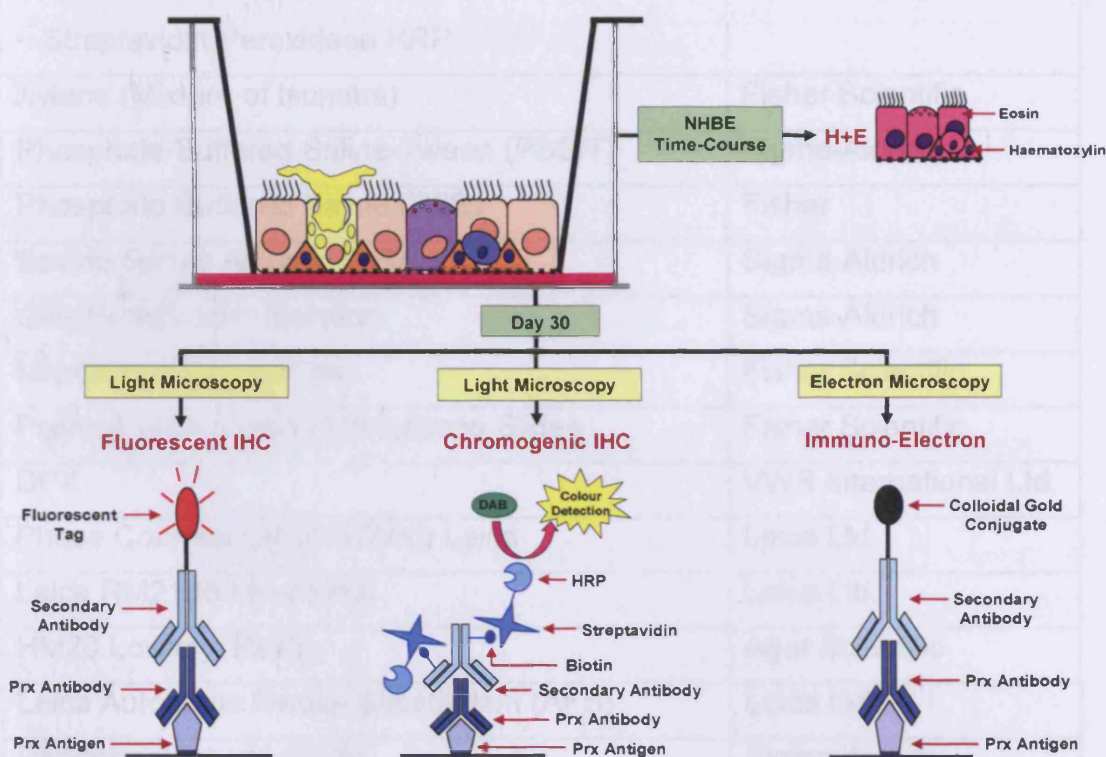


Figure 3.1: Flowchart of experimental work in Chapter 3.

Experimental aims included histological H+E analysis of the NHBE model throughout morphogenesis and immunological analysis utilising Prx primary antibodies to visualise Prx location at the LM and TEM levels in fully differentiated NHBE cultures.

3.2 MATERIALS AND STOCK SOLUTIONS

3.2.1 MATERIALS AND SUPPLIERS

MATERIALS:	SUPPLIER:
10% Neutral Buffered Formalin (NBF)	Sigma-Aldrich
Ethanol	Fisher Scientific
Anti-Rabbit IgG	Vector Labs
3,3'-Diaminobenzidine (DAB) Chromogen Kit	Dako

Histostain Plus Bulk Kit (Rabbit): <ul style="list-style-type: none"> • Blocking Serum Solution 10% Goat Non-Immune System • Biotinylated Secondary Antibody, Goat-Anti-Rabbit • Streptavidin-Peroxidase HRP 	Zymed Laboratories (Invitrogen)
Xylene (Mixture of Isomers)	Fisher Scientific
Phosphate Buffered Saline-Tween (PBS/T)	Sigma-Aldrich
Phosphate Buffered Saline (PBS)	Fisher
Bovine Serum Albumin (BSA)	Sigma-Aldrich
Gills Hematoxylin Solution	Sigma-Aldrich
Microscope Cover Slips	Fisher Scientific
Poly-L-Lysine Coated Microscope Slides	Fisher Scientific
DPX	VWR International Ltd.
Phase Contrast LM (DM2500) Leica	Leica Ltd.
Leica RM2135 Microtome	Leica Ltd.
HM20 Lowicryl Resin	Agar Scientific
Leica Automatic Freeze Substitution (AFS)	Leica Ltd.
Paraformaldehyde (PFA)	Sigma-Aldrich
Gluteraldehyde (GA)	Agar Scientific
Sucrose	Sigma-Aldrich
Osmium Tetroxide (OT)	Agar Scientific
Uranyl Acetate (UA)	Agar Scientific
Nickel Mesh Grids 3.05mm	Agar Scientific
Pioloform Film	Agar Scientific
Chloroform	Fisher Scientific
Parafilm	Pechiney, USA
Sodium Periodate (SP)	Agar Scientific
Reynold's Lead Citrate (LC)	Agar Scientific
Normal Goat Serum	Dako
Ultra Microtome	Leica Ltd.
Petri Dishes	Fisher Scientific
Diamond Knife, 2.5mm Edge, 45° Blade Angle	Agar Scientific

2° Antibody 10nm Colloidal Gold Conjugate	British BioCell
Transmission Electron Microscope (TEM) 208	Phillips
Tween 20	Invitrogen
2° Fluorescent Antibody Goat-Anti-Rabbit	Dako
Vectashield with DAPI	Vector Lab, USA
Leica TCS SP2 AOBS Laser Scanning Confocal Microscope	Leica Ltd
Eosin Y (High Purity)	Acros Organics, USA

Table 3.1: Materials used and their suppliers. All suppliers were UK based unless stated.

3.2.2 STOCK SOLUTIONS

All stock solutions were prepared and stored at RT unless stated otherwise.

PBS/T was prepared as a 1x working solution by dissolving 1 packet of powdered stock in 1L of deionised water, yielding 0.01M PBS (NaCl- 0.138M, KCl- 0.027M) pH 7.4 at 25°C. Tween 20 was added to 0.05%.

PBS was prepared as a working solution by dissolving 100 PBS tablets in 10L of deionised water, yielding (g/L): NaCl, 8.0; KCl, 0.2; Na₂HPO₄, 1.15; KH₂PO₄, 0.2; pH 7.3 at 25°C.

BSA/PBS/T was prepared as a 1% BSA/PBS + 0.05% Tween working solution using BSA, PBS and Tween-20. This working solution was stored at 4°C.

DAB Chromogen was prepared as a working solution containing 1 drop of DAB chromogen for every 1ml of DAB substrate buffer. This working solution was used following preparation and not stored.

Fixation Solution was prepared using 2% PFA and 0.4% GA. This solution was stored at 4°C.

Cryoprotectant was prepared using 25g sucrose, 30ml glycerol and 70ml Sørensen buffer. This buffer was stored at 4°C.

OT was prepared as a 0.2% working solution from a 2% stock solution using cryoprotectant.

Sørensen Buffer was prepared using solution A ($\text{Na}_2\text{HPO}_4 \cdot 2\text{H}_2\text{O}$ 5.938g/500ml) and solution B (KH_2PO_4 0.908g/100ml), both were dissolved in ddH₂O. Solution A and B were then combined (81.8ml + 18.2ml, respectively) with a final pH of 7.4.

3.3 METHODS

3.3.1 HISTOLOGICAL ANALYSIS OF THE NHBE CELL CULTURES

3.3.1.1 TISSUE PROCESSING

Cell culture inserts were fixed in 10% NBF at 4°C for 24hr prior to paraffin embedding and sectioning. Embedding and subsequent sectioning of the tissue was carried out by a histotechnologist, Mr Derek Scarborough, at the School of Biosciences, Cardiff University.

The formalin fixed tissue was embedded in paraffin which allowed sections 3µm to 10µm in thickness to be cut. Embedding involved tissue dehydration, clearing and paraffin infiltration. The dehydration process was necessary to remove the remaining water in the tissue and involved a series of alcohol treatments in incremental stages (i.e. 70%, 95% and 100%). Clearing removed any alcohol from the tissue. Xylene was used through several changes, as it was miscible with paraffin. Finally, the tissue was infiltrated with molten paraffin wax at 60°C, whereby several treatments of paraffin were used. Samples were then placed in plastic cassettes before being loaded for automatic processing, using a fully enclosed vacuum tissue processor.

3.3.1.2 PARAFFIN EMBEDDING

Air pockets that remained within the tissue were removed by placing the 'cleared' sample into a vacuum. This allowed the tissue to be fully supported by the paraffin wax and prevented any shredding of the tissue during sectioning. NHBE cell cultures were placed into embedding moulds and a Leica EG1140 Embedding Centre was used to embed the tissue in warm paraffin wax. The samples were set for 30min using a cold plate and when removed from the moulds, were ready for sectioning.

3.3.1.3 SECTIONING

Paraffin embedded NHBE cell cultures were cut into 5µm sections, allowing visualisation of the tissue by LM. Sectioning was carried out using a Leica RM2135 microtome. Prior to sectioning, embedded samples were placed on ice to ensure uniform sections were obtained. Placing the samples on ice hardened the wax and softened the tissue, providing the sections with consistent thickness. Cut sections were immediately floated on a warm water bath at 40-50°C to facilitate the removal of any wrinkles and air bubbles formed during sectioning. Sections were then collected on a poly-L-lysine coated microscope slide, improving the adhesion between sections and slide. The section coated slide was left on a hot plate for 15-30min and then left in an oven at 37-45°C for 24hr (minimum) to ensure binding of the sections to the slide.

3.3.1.4 DE WAXING

The paraffin wax was removed from the tissue, allowing water soluble dyes to penetrate the sections. Sections were de-waxed using xylene and decreasing alcohol concentrations (i.e. 100%, 95% and 70%). Slides were then submerged in tap water to prevent the samples drying out. A wax contour was drawn around the sections to keep solutions in place.

3.3.1.5 HAEMATOXYLIN AND EOSIN STAINING

De-waxed tissue sections were stained with Gills Haematoxylin for 8sec, followed by washing in running tap water for 10min; giving the 'blue' haematoxylin colour. The sections were then submerged in eosin Y (high purity) for 2min and washed in running tap water for 2min (Bancroft and Gamble, 2001).

3.3.1.6 DEHYDRATION AND MOUNTING

Stained sections were dehydrated using increasing alcohol concentrations (i.e. 70%, 95%, and 100%) and then submerged in xylene. DPX mountant (10µl) was placed on a coverslip; slides were taken from the xylene and carefully lowered onto the coverslip and DPX. The slides were left overnight at RT. The stained sections were then ready to be viewed by LM (Bancroft and Gamble, 2001). Sections were viewed using a Leica Phase Contrast LM (DM2500) attached to a digital camera (Leica DFC 320).

3.3.2 CHROMOGENIC IMMUNOHISTOCHEMISTRY OF THE NHBE CELL CULTURES

Sample preparation and de waxing procedures were carried out as described in Sections 3.3.1.1 to 3.3.1.4.

3.3.2.1 ANTIBODY INCUBATION AND DETECTION

Following de waxing, sections were incubated with serum blocking solution for 10min; this was blotted off prior to antibody (AB) incubation. Sections were incubated with the 1^o ABs overnight in a moist chamber at 4°C (Table 3.2) or with the serum control (a negative control was performed for every dilution of the Prx antibodies used). ABs were diluted in 1% BSA/PBS + 0.05% tween-20.

Following 1^o AB incubation the sections were submerged in PBS for 5min (3x), excess PBS was blotted off and sections incubated with the biotinylated

secondary (2°) AB for 10min. Sections were then submerged once more in PBS for 5min (3x), excess PBS was blotted off and sections incubated with streptavidin peroxidase-HRP for 10min, sections were again washed in PBS for 5min (3x).

To allow AB visualisation, the slides were incubated with DAB chromogen solution for 2min (an optimised time). The chromogen was removed by placing the slides under running tap water for 2min; slides were then counter-stained by immersing in Gills haematoxylin for 8sec. Any excess staining was removed by washing the slides in running tap water for 10min. Dehydration and Mounting was carried out as described in Section 3.3.1.6

1° Antibody	Dilution	Final Concentration	Incubation Period	DAB Incubation Period
Prx I Prx II Prx III Prx-SO ₃	1:200	5µg/ml	24h (4°C)	2min
	1:400	2.5µg/ml	24h (4°C)	2min
	1:1000	1µg/ml	24h (4°C)	2min
	1:2000	500ng/ml	24h (4°C)	2min
	1:4000	250ng/ml	24h (4°C)	2min

Table 3.2: Chromogen immunohistochemistry: Optimisation of 1° AB concentrations.

Each of the 1° Prx ABs (Prx I, II, III and -SO₃) were prepared in a range of concentrations from 5µg/ml to 250ng/ml. Every optimisation experiment was performed on paraffin Day 30 - wax embedded NHBE cell cultures.

3.3.3 FLUORESCENT IMMUNOHISTOCHEMISTRY OF THE NHBE CELL CULTURES

3.3.3.1 TISSUE PROCESSING

Cell culture inserts were fixed in 4% PFA at 4°C for 20min. PFA was then removed and replaced with PBS and stored at 4°C prior to paraffin embedding and sectioning. Embedding and sectioning of the tissue was carried out by Mr Derek Scarborough at the School of Biosciences, Cardiff University (Sections 3.3.1.1 to 3.3.1.4).

3.3.3.2 ANTIBODY INCUBATION AND DETECTION

Sections were submerged in tap water for 2min and then washed in PBS for 2min (3x); they were then incubated with serum blocking solution for 10min which was blotted off prior to AB incubation. The prepared sections were incubated with the 1° ABs overnight in a humidifying chamber at 4°C (Table 3.3) or with the serum control (a negative control was performed for every dilution of the Prx ABs used). ABs were diluted in 1% BSA/PBS + 0.05% Tween. Following 1° AB incubation the sections were submerged in PBS for 5min (3x), excess PBS was blotted off and sections incubated with the fluorescent goat-anti-rabbit 2° AB (1:400) for 1hr at RT in the dark. Sections were then submerged once more in PBS for 5min (3x) (in the dark). Vectashield (w/DAPI) mountant (10µl) was placed on coverslips and slides taken from PBS carefully lowered onto them. Clear nail varnish was used to surround the coverslip and ensure no detachments. Slides were left overnight at 4°C in the dark. The sections were viewed with a Leica laser scanning confocal microscope and the images were produced via photomultiplier tubes.

1° Antibody	Dilution	Final Concentration	Incubation Period
Prx III	1:500	2µg/ml	24h (4°C)
	1:1000	1µg/ml	24h (4°C)
	1:2000	500ng/ml	24h (4°C)

Table 3.3: Fluorescent immunohistochemistry: Optimisation of 1° AB concentrations.

Prx III was prepared in a range of concentrations from 2µg/ml to 500ng/ml. Every optimisation experiment was performed on Day 30 paraffin-wax embedded NHBE cell cultures. Prx III stock concentration was 1mg/ml.

3.3.4 IMMUNO ELECTRON MICROSCOPY OF THE NHBE CELL CULTURES

3.3.4.1 TISSUE PROCESSING

Cell culture inserts were immersed in fixation solution for 45min at 4°C; allowing time for sufficient protein cross-linking. The samples were then

removed from the fixation solution and washed in Sørensen buffer for 5min. Culture inserts were immersed in cryoprotectant for 15min and then post-fixed in 0.2% OT for 30min. Post-fixation reduced damage to granulocytes and goblet cells during the subsequent dehydration process (Newman and Hobot, 2001).

3.3.4.2 DEHYDRATION

Cultures were dehydrated in increasing alcohol concentrations (i.e. 30%, 55%, 70%, 80%, 90% and 100%) and initial dehydrations (30% and 55%) were at 4°C, whereas all the subsequent dehydrations were carried out at -25°C in the AFS.

3.3.4.3 RESIN INFILTRATION AND EMBEDDING

Cultures were infiltrated in increments with lowicryl HM20 resin. Firstly, cultures were incubated in 1:1 (HM20:ETOH) for 60min and then in 2:1 for 60min, followed by 3:1 for 60min; all at -25°C. Cultures were then embedded in pure HM20 at -25°C for 60min (2x) the resin was changed for a third time and a UV light used to polymerise the resin for 24hr at -25°C.

3.3.4.4 PREPARATION OF THE SUPPORTING FILM (PIOLOFORM)

Pioloform was prepared as a 0.8% working concentration using chloroform. A clear microscope slide was covered in pioloform and left for 5min. The slide was then scored on both sides and placed into a water bath at 90° until both sections of the pioloform floated to the surface of the water bath.

3.3.4.5 PREPARATION OF GRIDS

Nickel mesh grids were placed dull side down onto a Pioloform film floating in a water bath. Once the film was covered in grids, parafilm was superimposed (sterile side) to enable removal of the grid/parafilm from the water bath. Grids were left to air dry for 1hr before use and stored inside a sterile Petri dish.

3.3.4.6 SECTIONING

Ultra-thin (60-90nm) sections were cut on a Leica ultra-microtome using a diamond knife. Sections were floated on a water trough and collected onto Pioloform coated nickel mesh grids. Sections were allowed to air dry inside a Petri dish for 1hr prior to use.

3.3.4.7 ANTIBODY INCUBATION AND DETECTION

Aliquots (100µl) of each solution required for AB detection were placed in rows on the sterile side of parafilm; the grids were floated section side down on a given droplet in sequence. Firstly, sections were incubated with saturated SP for 2hr to remove the OT and unmask the antigens. They were then washed in filtered ddH₂O for 2min (3x) and submerged in 20% normal goat serum overnight at 4°C to prevent unspecific antigen binding. NHBE sections were then incubated overnight at RT with various concentrations of Prx III 1° AB (Table 3.4) or the rabbit IgG negative control. ABs were diluted in 1% BSA/PBS + 0.05% Tween. Following 1° AB incubation, sections were taken through 1% BSA/PBS for 5min (2x). Sections were then incubated in 10nm colloidal gold conjugates (1:40) for 2hr; colloidal gold conjugates were diluted in Tris-buffered BSA, pH 8.5. NHBE sections were then washed using 1% BSA/PBS for 5min (2x), before being submerged in ddH₂O for 5min (2x).

1° Antibody	Dilution	Final Concentration	Incubation Period
Prx III	1:200	5µg/ml	1h (RT)
	1:400	2.5µg/ml	1h (RT)
	1:800	1.25µg/ml	1h (RT)
	1:1600	750ng/ml	1h (RT)
	1:3200	375ng/ml	1h (RT)

Table 3.4: Immuno electron microscopy: Optimisation of 1° AB concentrations.

Prx III was prepared in a range of concentrations from 5µg/ml to 375ng/ml. Every optimisation experiment was performed on Day 30 lowicryl embedded NHBE cell cultures. Prx III stock concentration was 1mg/ml.

3.3.4.8 COUNTER-STAINING

NHBE cell culture sections underwent heavy metal staining (counter-staining) to resolve their ultrastructure. Reynold's LC and 2% aqueous UA were used to counter-stain. UA stained membranous structures and nucleic acids. The lead in LC bound to RNA-containing structures and hydroxyl groups of carbohydrates (Newman and Hobot, 2001). Droplets of UA and LC were placed in rows on sterile parafilm and the grids counter-stained. Sections were stained for 10min with UA, followed by staining for 5min with LC. They were then washed by transferring over 3 drops of ddH₂O for 5min and air dried at RT inside sterile Petri dishes prior to visualisation. The sections were imaged using a Phillips TEM 208 at an acceleration voltage of 80KeV.

3.4 RESULTS

3.4.1 NHBE MORPHOGENESIS: HISTOLOGICAL ANALYSIS

Key time-points in the development of the NHBE cell model, corresponding to TEER and Western blot analysis (Chapter 2), were analysed using H+E staining (Figure 3.2). Day 1 was the earliest point in the models development, whereby cells remained as undifferentiated basal (progenitor) cells. There were large gaps between the cells that had successfully adhered to the membrane. By Day 3 the cells had proliferated into a bilayer, however, no visible junctional complexes were observed. By Day 9 the cultures took on a more pseudo-stratified appearance and some intercellular junctions could be identified. The columnar cells had begun to differentiate, but no cilia were distinct. By Day 30 the cultures were fully differentiated, cilia could be visualised and a defined pseudo-stratified BE phenotype was achieved. Junctional complexes were fully formed and no intercellular gaps were visible.

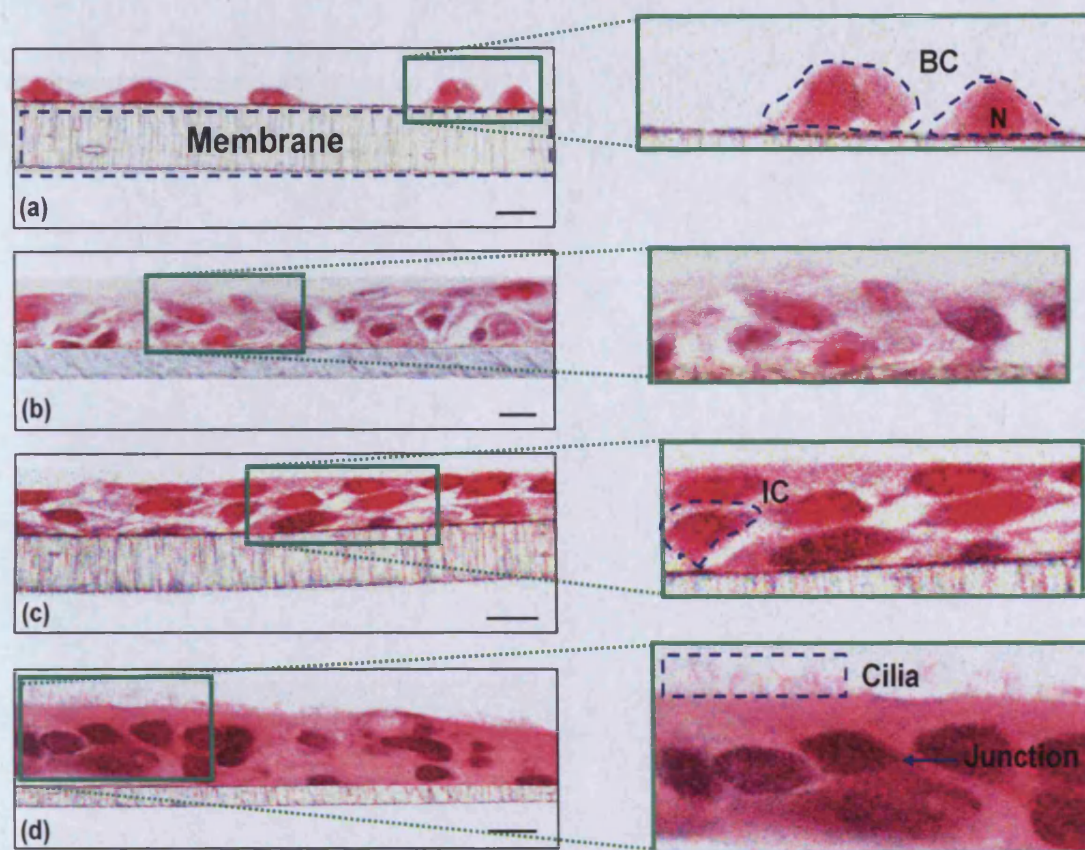


Figure 3.2: Histological H+E analysis of the NHBE cell model during morphogenesis.

Paraffin-fixed 5µm sections, from four key time-points in the morphogenesis of the NHBE cell model, were visualised using H+E. Green denoted areas of interest: (a) Day 1, only progenitor basal cells (BC) present, no intercellular junctions formed. Nucleus (N); (b) Day 3, bilayer formation, no junctional complexes formed; (c) Day 9, pseudo-stratified epithelium observed, intermediate cells (IC) present, the beginning of junctional formation; (d) Day 30, fully differentiated BE, cilia present and intercellular junctions formed. Scale bars represented 10µm.

3.4.2 NHBE MORPHOGENESIS: CHROMOGENIC IHC ANALYSIS

Paraffin sections (5µm) of Day 30 NHBE cultures were used to optimise Prx 1^o AB concentrations (Table 3.2). Results from the Western blots (Chapter 2) suggested the Prx isoforms were expressed at varying levels within the cultures. This was verified by the IHC optimisation results (Figure 3.3). Prx I was expressed throughout the columnar cells, but not in the basal cells. Prx III and -SO₃ were optimised at a 1:2000 dilution with Prx III in particular, exhibiting strong immuno positivity towards the apical region within the columnar cells. Prx-SO₃ was also expressed within the columnar cells,

although it wasn't restricted to the apical regions. The negative control demonstrated that there was no non-specific binding. Prx II was not detected at the highest AB concentration (images not shown).

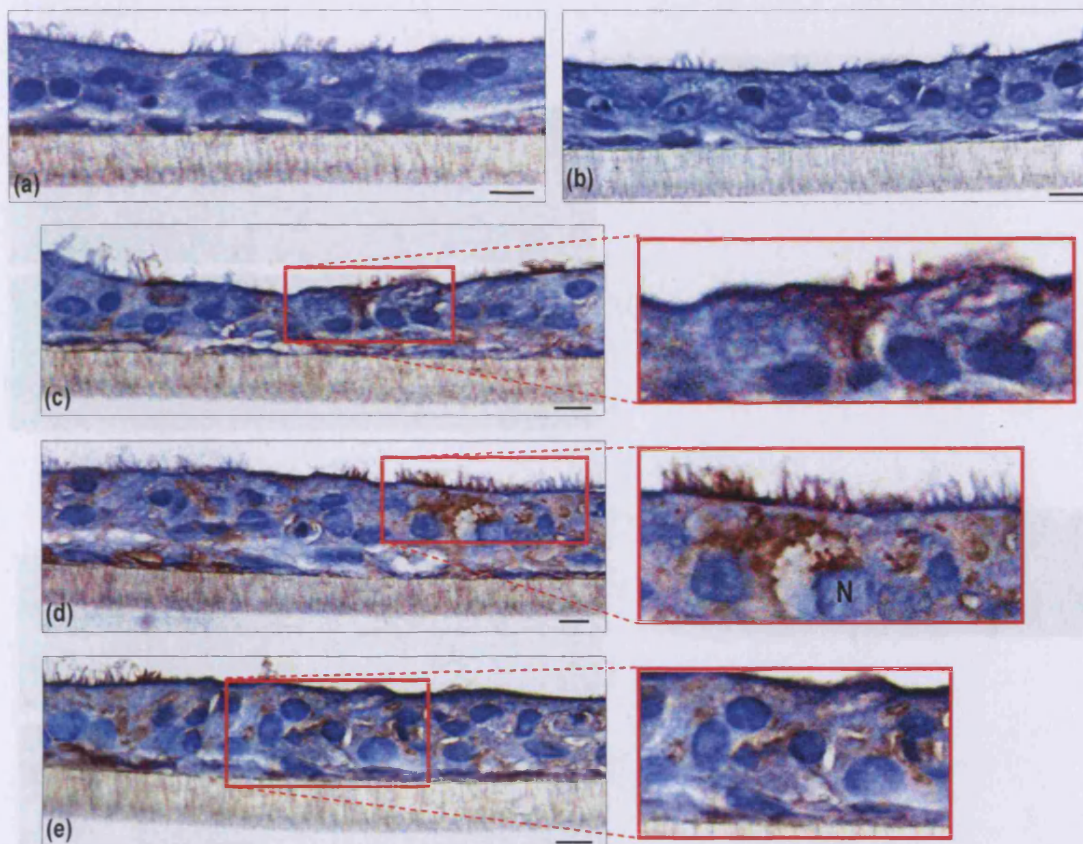


Figure 3.3: Chromogenic IHC analysis of the NHBE cell model.

Paraffin-fixed 5μm sections, from the NHBE Day 30 cultures, were incubated overnight with Prx 1° ABs and corresponding negative controls. DAB was used as a chromogen for immuno positivity. Red denoted areas of interest: (a) rabbit IgG 1:200; (b) rabbit IgG 1:2000, demonstrating no non-specific binding; (c) Prx I (1:200) expression confined to the columnar cells; (d) Prx III (1:2000) expression principally in the apical region of the ciliated cells. Nucleus (N); (e) Prx-SO₃ (1:2000) was dispersed throughout the epithelium. Scale bars represented 10μm.

3.4.3 NHBE MORPHOGENESIS: FLUORESCENT IHC ANALYSIS

The Prx III isoform was expressed the strongest within the NHBE cultures (Chapter 2), and was therefore used in confocal studies to corroborate the chromogenic IHC data. Fluorescent IHC results (Figure 3.4) confirmed that there was no non-specific binding in the negative controls. Both Prx III (1:1000

and 1:2000) incubations displayed antigenic detection throughout the apical region of the columnar cells, with Prx III at the 1:2000 dilution displaying gaps in detection at the apical surface. The 1:500 dilutions caused severe overstaining (images not shown).

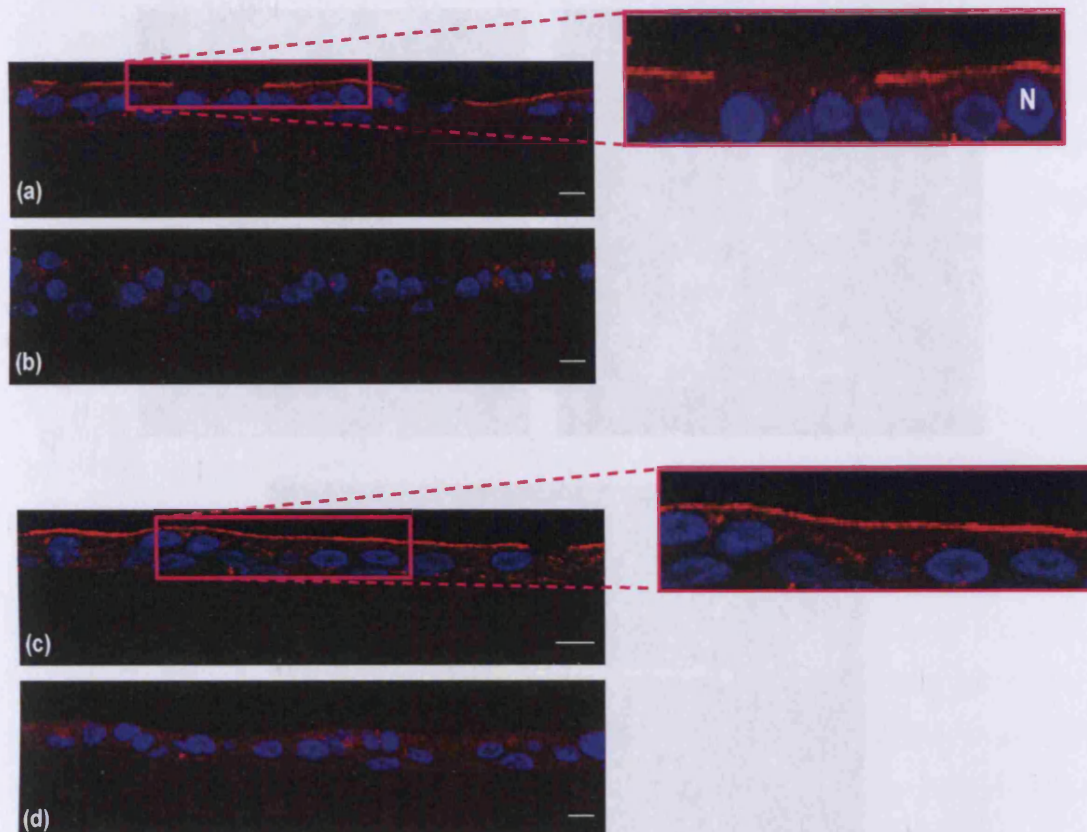


Figure 3.4: Fluorescent IHC analysis of the NHBE cell model.

Paraffin-fixed 5µm sections, from the NHBE Day 30 cultures, were incubated overnight with a Prx III 1° AB and corresponding negative controls. A fluorescent 2° AB was used to detect immuno positivity. Pink denoted areas of interest: (a) Prx III (1:2000) expression predominantly at the apical regions of the columnar cells, gaps present possibly where goblet cells appear. Nucleus (N); (b) rabbit IgG 1:2000, no non-specific binding; (c) Prx III (1:1000), expression at the apical regions of the columnar cells, possibly over-stained as no gaps in expression visible; (d) rabbit IgG 1:1000, no non-specific binding. Scale bars represented 10µm.

3.4.4 NHBE MORPHOGENESIS: IMMUNO ELECTRON MICROSCOPY ANALYSIS

Ultra-thin sections (80-90nm) were used to optimise Prx III concentration for antigenic detection. Prx III was located in the mitochondria of the ciliated cells (Figure 3.5). The gold conjugates localised to this area, which reinforced

previous LM results (fluorescent [Section 3.4.3] and chromogenic [Section 3.4.2]). The optimum dilution factor was 1:400, which minimised non-specific binding while maintaining sufficient antigenic detection. The negative control displayed no non-specific binding.

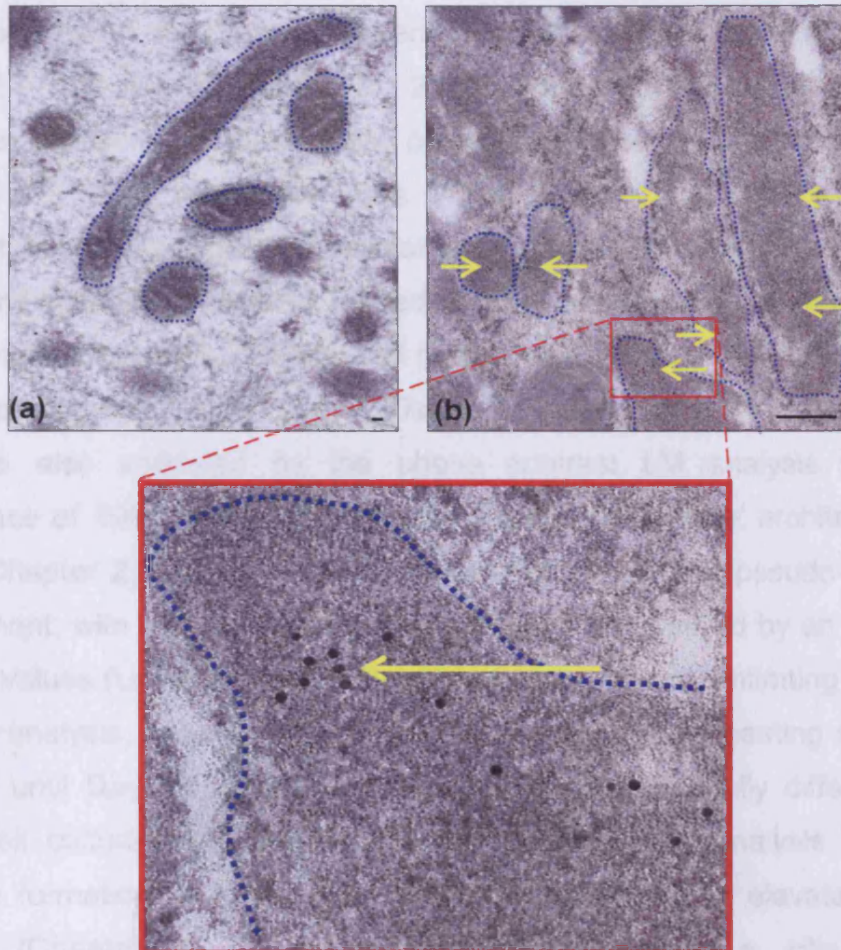


Figure 3.5: Immuno electron analysis of the NHBE cell model.

Ultra-thin lowicryl sections from the NHBE Day 30 cultures were incubated overnight with a Prx III primary antibody and the corresponding negative controls. A colloidal gold conjugate 2^o AB was used to detect immuno positivity. Yellow arrows indicated areas of Prx III expression: (a) rabbit IgG 1:400, no non-specific binding; (b) Prx III (1:400) expression was located primarily in the mitochondria (dotted dark blue outline) of the ciliated cells. Scale bars represented (a) 100nm and (b) 300nm.

3.5 DISCUSSION

3.5.1 NHBE MORPHOGENESIS: HISTOLOGICAL ANALYSIS

The four days chosen for morphological analysis (1, 3, 9 and 30) represented the widest breadth of morphological and biochemical modification with regard to the BE architecture (BéruBé *et al.*, 2010b; Prytherch, 2010). The formation of cellular junctions at these days corroborated the previous TEER data (Chapter 2). TEER values for Days 1 and 3 were negligible, which was representative of the large intercellular gaps observed in the cultures on the corresponding days. This also related to previous research confirming that cultures consisted solely of basal cell types on these days (Prytherch, 2010). The morphology of the cultures by Day 3 had taken on a bilayer formation. This was also validated by the phase contrast LM analysis with the appearance of 'hills' and 'valleys' at Day 2 and 'cobblestone' architecture by Day 3 (Chapter 2). At Day 9, the cultures took on a more pseudo-stratified arrangement, with the development of tight junctions signified by an increase in TEER values (Lin *et al.*, 2007). No cilia were observed, confirming the real-time LM analysis, whereby tiny flickers representing cilia beating were not detected until Day 15. Day 30 marked the presence of fully differentiated NHBE cell cultures and the subsequent morphological analysis revealed complete formation of intercellular junctions; confirmed by elevated TEER readings (Chapter 2). The different NHBE cell types (i.e. cilia, goblet, intermediate and basal) were clearly distinguished, indicative of a healthy BE phenotype; providing confidence in subsequent toxicological analysis (BéruBé *et al.*, 2010a).

3.5.2 NHBE MORPHOGENESIS: CHROMOGENIC IHC ANALYSIS

The chromogenic IHC results (Figure 3.3) supported earlier Western blot analysis (Chapter 2), with Prx I expression detected at much lower levels than Prx III within the NHBE cell cultures. Prx I was optimised at ten times the concentration of Prx III and -SO₃, which also corresponded to previous findings of expression variations between such isoforms within the BE

(Kinnula *et al.*, 2002a). The relatively weak Prx I expression was detected throughout the columnar cells but not in the basal cells; supporting Western blot data, whereby no Prx I expression was detected at Days 1 and 3 (i.e. when only basal cells were present). Prx III expression was primarily confined to the apical regions of the columnar cells, where the cilia could be clearly distinguished. It was expected that Prx III expression corresponded to the ciliated cell location, due to their high mitochondrial content (Bittar, 2002). Unlike Prx I, Prx III was also detected in the basal layer of the epithelium, which correlated to Western blot data (Chapter 2), where its expression was detected from Day 1. Prx-SO₃ was visible throughout the BE, indicating elevated basal levels of oxidative stress; the detected levels of Prx-SO₃ correlated to earlier results (Chapter 2), and previous research into cell culture induced oxidative stress (Halliwell, 2003, 2011). The levels of hyperoxidation visualised through IHC were lower than expected, in comparison to Western blot analyses. This confirmed the non-quantitative status of IHC, due to the destruction of antigens by the tissue processing procedure (Newman and Hobot, 2001). Prx II was not sufficiently detected at the highest concentration (results not shown), and due to this result, no further analysis with Prx II was conducted.

3.5.3 NHBE MORPHOGENESIS: FLUORESCENT IHC ANALYSIS

Fluorescent IHC was undertaken in order to validate the chromogenic IHC findings. Prx III was chosen for further IHC analysis due to its highly specific location within the NHBE cultures. Significant Prx III expression at the apical region of the columnar cells, in particular the ciliated cells, was demonstrated (Figure 3.4). This was due to the extensive number of mitochondria required in this area to provide sufficient ATP for adequate cilia beating (Braiman and Priel, 2008). The optimal Prx III dilution was determined to be 1:2000, which was the same dilution optimised during chromogenic IHC. The consistency between both LM level IHC techniques further validated the NHBE model. Future work could include dual immunofluorescence to localize the various Prx staining to specific cell types e.g using p63 as a BC marker, Muc5A as a stain for GCs and acetylated-tubulin markers for cilia staining.

3.5.4 NHBE MORPHOGENESIS: IMMUNO ELECTRON MICROSCOPY ANALYSIS

The antigenic detection at the EM level established the presence of Prx III in the mitochondria of the NHBE columnar cells (Figure 3.5), which was consistent with *in vivo* analysis (Kinnula *et al.*, 2002a), as well as IHC results at the LM level. The embedding technique employed allowed for a compromise between structural preservation and the conservation of the Prx antigens (Newman and Hobot, 2001). Conventional embedding at high temperatures destroys the antigenic activity but preserved the mitochondrial ultrastructure more effectively (data not shown). However, with the aim being to detect Prx III presence, low temperature embedding was a far more viable option. A higher concentration of 1° AB was needed for Prx III detection at the TEM level in comparison with the LM level, due to the nature of the embedding technique (Newman and Hobot, 2001); further reinforcing the notion that IHC was not a quantitative technique. The immuno EM data substantiated those at the LM level and supported the use of the NHBE cell model as a viable *in vitro* alternative.

3.6 CONCLUSION

Prx detection via IHC analysis of the NHBE cultures, using chromogenic and fluorescent techniques at the LM level, along with colloidal gold IHC at the EM level, correlated accurately with documented *in vivo* findings and previous NHBE work by Prytherch and co-workers. Prx III was expressed in the mitochondria, and hence, there was significant antigenic detection (at LM and EM levels) along the apical region of the culture, due to high mitochondrial concentration in this area. Chromogenic IHC analysis revealed Prx I expression to be dispersed throughout the columnar cells, but not the basal cells, which corresponded accurately to Western blot data from the previous experimental work (Chapter 2). The hyperoxidised Prx results indicated relatively high basal levels, and as such, prominent oxidative stress within the cultures, that correlated directly with the Western blot analysis utilising the Prx-SO₃ primary antibody. The lower levels of Prx detection via IHC techniques, in comparison with other proteomic methods, supported the use

of IHC as a non-quantitative technique used to corroborate the quantitative Western blot data. Due to the difficulty in detecting Prx II, which was known to be expressed at much lower levels in the BE (in comparison to Prx I and III) and also shown to be problematic to detect in previous work (Chapter 2), it was concluded that it would not feature in any future experimental analysis. Prx I, which along with Prx II was expressed in the cytosol, would continue to be investigated, and hence, by dismissing Prx II from this study, the diversity of investigation into the 2-Cys Prxs within the NHBE cell model would not be critically affected. The experimental outcomes from Chapters 2 and 3 outlined Prx status during NHBE cell culture morphogenesis. Further investigations were required into the changes in Prx (I and III) status following toxicological exposures with H₂O₂ (Chapter 4) and cigarette smoke (CS) (Chapter 5). With regard to the elevated levels of Prx hyperoxidation within the NHBE cultures, measures were considered to alleviate this stress. The option chosen was AO addition to the ALI media (Chapter 4), mimicking more closely the *in vivo* lung environment.

CHAPTER 4:

RESPONSE OF PEROXIREDOXIN STATUS TO HYDROGEN PEROXIDE EXPOSURE

4.1 INTRODUCTION

An increasing need for sensitive biomarkers of oxidative stress have been well documented in the literature, and recently several AO, including thioredoxin and Prx, have become prominent contenders in this role (Jikimoto *et al.*, 2002; Yoshida *et al.*, 2009). However, with a focus on developments in the field of COPD, which is constantly seeking more effective biomarkers (Barnes *et al.*, 2006; Jones and Agusti, 2006), the Prxs may be an ideal respiratory biomarker candidate, informing on disrupted redox cycling and signalling; the earliest form of oxidative cell damage (Repine *et al.*, 1997; Rahman *et al.*, 2006).

The experimental work in this Chapter was aimed at assessing the changes in Prx expression levels and oxidation state following oxidative insult to the NHBE cell model. Continuing on from work in Chapter 2, the fully differentiated NHBE cultures were apically exposed to H₂O₂, as previous related studies have shown H₂O₂ was able to induce structural and oxidation state changes in the Prxs (Phalen *et al.*, 2006; Peskin *et al.*, 2007). H₂O₂ was applied both directly to the cultures and indirectly via the glucose-glucose oxidase (GOx) system. GOx catalyses the oxidation of glucose to H₂O₂ and gluconic acid in the presence of oxygen (Wilson and Turner, 1992), releasing linear fluxes of H₂O₂ over time; this is a more physiologically relevant exposure in comparison to the direct apical addition of H₂O₂ (van der Vliet *et al.*, 1997). The conventional toxicology (i.e. TEER and ATP) was monitored post-exposure to H₂O₂, and Prx status was determined using Western blotting for reducing and non-reducing gel electrophoresis conditions.

Work in previous Chapters revealed elevated basal levels of oxidative stress, which is often a limitation of cell culture conditions (Halliwell, 2003). The under appreciated problem of oxidative stress has lead many to question data obtained through *in vitro* studies (Halliwell, 2011). In light of this, precautions were needed to limit artefactual data within this study; and AO supplementation was chosen as the appropriate course of action. Several studies had previously supplemented cell cultures with AOs in order to

minimise the basal levels of oxidative stress, in particular glutathione (GSH) (Teramoto *et al.*, 1999; Chen *et al.*, 2009). Work in this Chapter aimed to evaluate the benefits of supplementing the NHBE model with AO prior to toxicological exposures.

Prx status was used as a dosimeter of intracellular oxidative stress, with increased hyperoxidation indicative of oxidative stress levels (Chapter 2). In conjunction with Prx status, the levels of the phosphorylated MAPK (mitogen activated protein kinase) Erk1/2 (extracellular signal-related kinases) were also analysed. Erk1/2 functions within the stress response pathway following activation by elevated levels of oxidative stress (Torres and Forman, 2003; Mossman *et al.*, 2006), and supplementation of cell cultures with AO has been shown to reduce its activation (Kim *et al.*, 2005). This provided an additional parameter that could be used to inform on intracellular levels of oxidative stress within the NHBE cell cultures post-exposure to H₂O₂.

4.1.1 RESEARCH AIMS

The research aims for experimental work in Chapter 4 (Figure 4.1), were as follows:

- Expose the fully differentiated NHBE cell cultures to a concentration range of H₂O₂, and evaluate the cell viability and epithelial barrier integrity by monitoring ATP and TEER activities, respectively.
- Investigating further, key H₂O₂ concentrations highlighted by the concentration range study. Prx status in NHBE culture, post-exposure to H₂O₂, will be analysed via reducing gel electrophoresis, Western blotting and chemiluminescence detection.
- Quench the basal levels of oxidative stress within the NHBE cultures through the addition of AO to the culture media.

- Instigate the glucose-glucose oxidase (GOx) system to produce linear fluxes of H_2O_2 over time. Assess the exposed cell cultures (-/+AO) using ATP and TEER measurements, in conjunction with reducing and non-reducing gel electrophoresis, Western blotting and chemiluminescence detection.

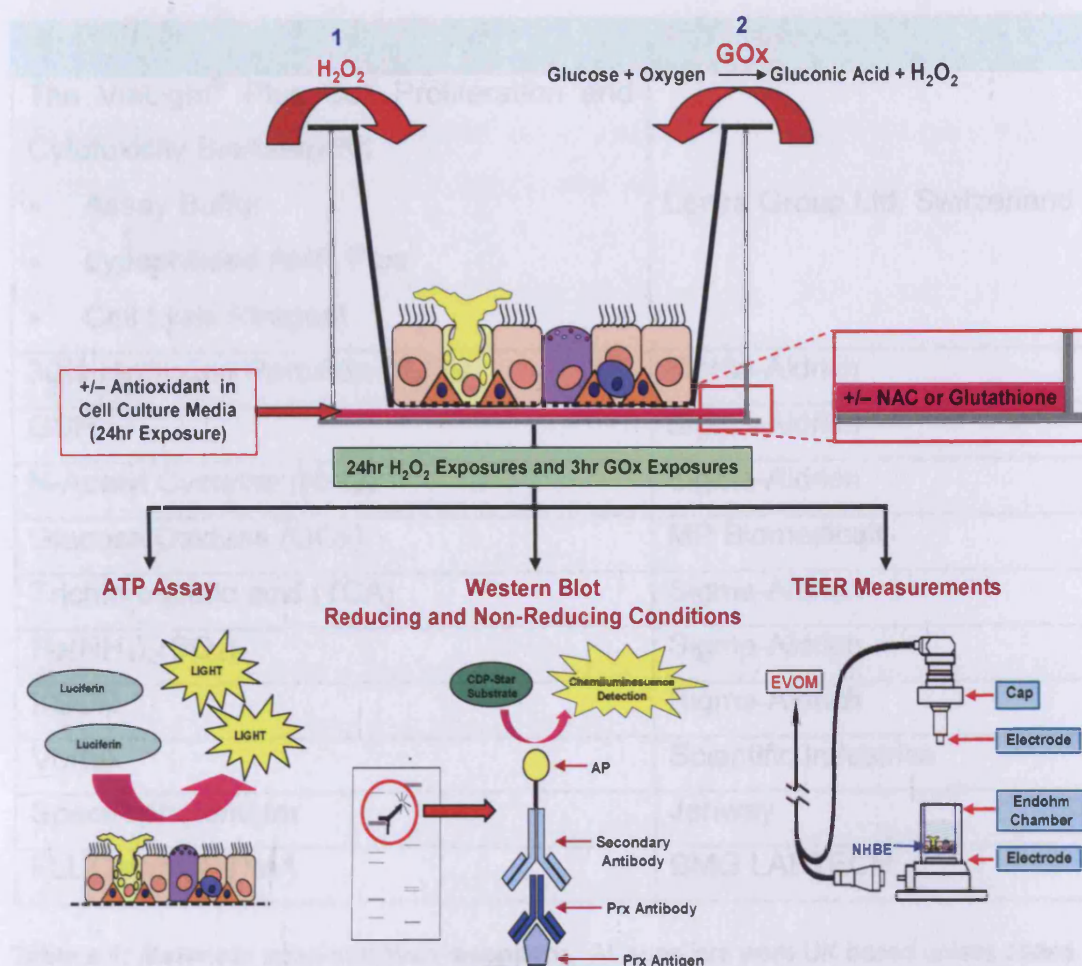


Figure 4.1: Flowchart of experimental work in Chapter 4.

Experimental aims included apical exposure of the NHBE cell cultures to H_2O_2 , either directly (1) or by means of the glucose-glucose oxidase (GOx) system (2). Investigations were undertaken to establish the optimum antioxidant concentration to minimise basal levels of oxidative stress, therefore the NHBE model was supplemented with a concentration gradient of either NAC or GSH. Culture viability and junction integrity were established via ATP and TEER analysis, respectively. Prx status (expression levels and oxidation state) were determined through reducing and non-reducing gel electrophoresis conditions followed by Western blotting and chemiluminescence detection.

4.2 MATERIALS AND STOCK SOLUTIONS

Materials and stock solutions from previous Chapters have not been included.

4.2.1 MATERIALS AND SUPPLIERS

MATERIALS:	SUPPLIER:
The ViaLight [®] Plus Cell Proliferation and Cytotoxicity BioAssay Kit <ul style="list-style-type: none"> Assay Buffer Lypophilised AMR Plus Cell Lysis Reagent 	Lonza Group Ltd, Switzerland
30% Hydrogen Peroxide (H ₂ O ₂)	Sigma-Aldrich
GSH	Sigma-Aldrich
N-Acetyl Cysteine (NAC)	Sigma-Aldrich
Glucose Oxidase (GOx)	MP Biomedicals
Trichloroacetic acid (TCA)	Sigma-Aldrich
Fe(NH ₄) ₂ (SO ₄) ₂	Sigma-Aldrich
KSCN	Sigma-Aldrich
Vortex	Scientific Industries
Spectrophotometer	Jenway
FLUOstar OPTIMA	BMG LABTECH

Table 4.1: Materials used and their suppliers. All suppliers were UK based unless stated.

4.2.2 STOCK SOLUTIONS

All stock solutions were prepared and stored at RT unless stated otherwise.

H₂O₂ was prepared as a 1M stock by diluting 30% H₂O₂ in PBS. The 1M stock was further diluted by 1:1000 to provide a working concentration of 1mM, stored at 4°C.

NAC was prepared as a 100mM working concentration by dissolving NAC powder in HBSS, the pH was adjusted to 7.4 and the solution filter sterilised and stored at 4°C.

GSH was prepared as a 10mM working concentration by dissolving GSH powder in ddH₂O, the pH was adjusted to 7.4 and the solution filter sterilised and stored at 4°C.

Phosphate Buffer was prepared as a working concentration of 10mM by diluting a 1M stock with ddH₂O; the pH was adjusted to 7.4.

GOx was prepared as a 10U/ml stock by dissolving GOx powder in 10mM phosphate buffer (pH 7.4). The 10U/ml stock was further diluted in 10mM phosphate buffer to a working concentration of 1U/ml and stored at -20°C.

TCA was prepared as a 100% stock by dissolving 100g in 100ml ddH₂O. 100% TCA was stored at 4°C.

BSA was prepared as a 10mg/ml working concentration by dissolving 100mg BSA in 10ml ddH₂O, this was stored at 4°C.

Fe(NH₄)₂(SO₄)₂ was prepared as a 250mM working concentration by dissolving 9.8035g in 100ml ddH₂O, this was made up fresh before use.

KSCN was prepared as a 250mM working concentration by dissolving 2.4295g in 100ml ddH₂O, this was made up fresh before use.

4.3 METHODS

4.3.1 H₂O₂ EXPOSURE

NHBE cell cultures (Section 2.2.1) were apically exposed to a concentration range of H₂O₂ (50µl), between Days 25 and 30, post-seeding into Millipore inserts. The 1mM H₂O₂ stock was further diluted to produce the concentration

range of 50 μ M, 100 μ M, 200 μ M, 400 μ M, 800 μ M and 1mM; PBS was used as a control solution. Inserts were apically exposed to H₂O₂ and incubated for 24hr at 37°C and 5% CO₂; TEER readings were taken before dosing (Section 2.3.2). Subsequent to H₂O₂ exposure, TEER values were recorded and the same insert was used to assess culture viability (Section 4.3.4). The concentration that elicited a 20% decrease in culture viability (TD₂₀: toxic dose 20%), when compared to controls, was used for further analysis. A H₂O₂ concentration of ten-fold less than the TD₂₀ H₂O₂ concentration was also used to further investigate the correlation between Prx status change and oxidative stress levels. The TD₂₀ concentration was chosen as it was sub-toxic, since the research objective was to identify Prx as a biomarker of oxidative stress, rather than studying dead or dying cells.

Additional exposure experiments were undertaken over a range of times (i.e. 1hr, 3hr and 6hr). Four inserts were apically exposed to H₂O₂ at 1mM (TD₂₀), 100 μ M or 0 μ M (control). Following exposure, excess apical solution was removed by aspiration, and the cells lysed with lysis buffer in preparation for Western blot analysis to determine Prx status (Section 2.3.4).

4.3.2 ATP Assay

The ViaLight[®] Plus cell Proliferation and Cytotoxicity BioAssay Kit was used to assess cellular ATP activity. ATP Monitoring Agent Plus (AMR Plus) was prepared by reconstituting the lypophilised AMR Plus with the supplied Assay Buffer. The AMR Plus was allowed to equilibrate for 15min at RT. Cell lysis solution was brought up to RT before use. The proliferation and cytotoxicity of mammalian cells in culture was measured by determination of their ATP levels.

Following apical exposures TEER measurements were taken (Section 2.3.2); inserts were then placed into an empty well in preparation for the ATP assay. Cell lysis reagent (100 μ l) was applied apically to each insert and incubated for 10min. The cell lysates (100 μ l) were then placed into the wells of a 96-well plate and AMR Plus reagent (100 μ l) added to each well and incubated for

2min (in the dark). The luminescence was read using the FLUOstar OPTIMA and analysed using the OPTIMA Control System software (BMG LABTECH).

4.3.3 ANTIOXIDANT ADDITION

Preliminary AO addition was undertaken as a continuous exposure throughout the morphogenesis of the NHBE cultures, whereby 1mM of NAC was added to the ALI media. Following the continuous exposure a more refined AO analysis took place between Days 25 and 30, post-seeding into Millipore inserts. NHBE cell cultures (Section 2.2.1) were basally exposed to a concentration range of NAC or GSH. NAC (100mM) or GSH (10mM) were diluted in the NHBE cell culture medium to create a concentration gradient (0mM to 10mM and 0mM to 5mM, respectively). TEER readings were taken before dosing (Section 2.3.2), cultures were then analysed 24hr post-addition via ATP (Section 4.3.4) and TEER readings. Prx status was elucidated via Western blotting (Section 2.3.4). Following the pilot optimisations, 800µM GSH was chosen as the optimum antioxidant concentration to supplement the NHBE cultures 24hr prior to toxicant exposure.

4.3.4 H₂O₂ GENERATED BY GOX

To accurately measure the H₂O₂ concentrations produced by the GOx system, a H₂O₂ determination method was utilised (van der Vliet *et al.*, 1997). A H₂O₂ stock of 1mM was diluted with DMEM to produce a concentration curve as follows: 0µM, 6.25µM, 12.5µM, 25µM, 50µM and 100 µM these were used to establish a concentration curve. Each H₂O₂ sample (800µl) was added to 100µl of 10mg/ml BSA and 100µl TCA (100%). This was then vortexed briefly and centrifuged in a microfuge for 2min at 14000rpm, the supernatant removed and added to 200µl Fe(NH₄)₂(SO₄)₂ and 100µl KSCN. The mixture was then vortexed briefly and the absorbance read at 450nm within 10min. A standard curve was established from which the H₂O₂ concentration in the GOx samples could be determined using the same method.

4.3.5 GOx EXPOSURE

NHBE cell cultures (Section 2.2.1) were apically exposed to a concentration range of GOx (50µl), between Days 25 and 30, post-seeding into Millipore inserts. The 1U/ml GOx stock was further diluted to produce the concentration range of 5mU/ml, 15mU/ml and 25mU/ml; DMEM was used as a control solution. Inserts were apically exposed to GOx and incubated for 3hr at 37°C and 5% CO₂, TEER readings were taken before dosing (Section 2.3.2). Subsequent to GOx exposure, TEER values were recorded and the same insert was used to assess culture viability (Section 4.3.4), followed Western blot analysis (Section 2.3.4) to establish Prx status following toxicant (GOx) exposure.

4.4 RESULTS

4.4.1 H₂O₂ EXPOSURE

4.4.1.1 H₂O₂ EXPOSURES: TEER AND ATP ANALYSIS

TEER values post-exposure (Figure 4.2) revealed that epithelial barrier integrities were not significantly ($P \leq 0.05$) compromised following all H₂O₂ exposures. There were significant ($P \leq 0.05$) increases in TEER readings at the 400uM and 800uM exposures, peaking at 162%. This was a direct result of the toxicant addition, leading to a survival response by the cells which involved tightening their intercellular junctions. There was a decrease in viability (TD₂₀) at the 1mM concentration. Consequently, the 100uM and 1mM H₂O₂ concentrations were selected for further analysis (Section 4.4.2).

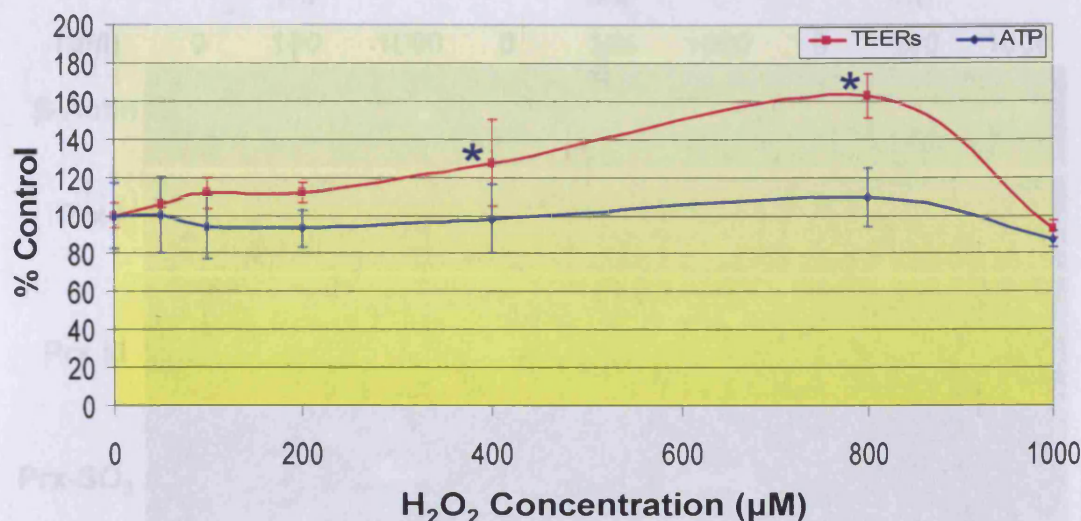


Figure 4.2: H₂O₂ dose range responses.

TEER (■) and ATP (◆) analysis of the NHBE cultures 24hr post-exposure to H₂O₂. Cultures were apically exposed to a concentration range of H₂O₂ (0mM to 1mM). The asterisk (*) denoted significance ($P \leq 0.05$) and I signified \pm SD for $n=3$. TEER values increased significantly post-exposure to 400µM and 800µM H₂O₂, while ATP levels displayed a biphasic response.

4.4.1.2 H₂O₂ EXPOSURES: WESTERN BLOT ANALYSIS (TOTAL PRX LEVELS)

NHBE cultures exposed to 100µM and 1mM H₂O₂ were subjected to reducing gel electrophoresis conditions and analysed via Western blotting (Figure 4.10). Expression of the house-keeping protein β -actin remained strong throughout, which confirmed the ATP and TEER data following the sub-toxic H₂O₂ concentrations. Total Prx I expression remained low throughout all H₂O₂ exposures, and decreased significantly ($P \leq 0.05$) (Figure 4.4) following the 1hr and 3hr 100µM exposures and the 1hr 1mM exposure. Total Prx III expression significantly ($P \leq 0.05$) decreased following the 3hr 100µM and 1mM exposures. Elevated levels of Prx-SO₃, at the 1mM exposures, were evident from the raw data blots. This was confirmed via densitometry analysis which revealed significant ($P \leq 0.05$) increases of 62% at the 1hr exposure and 54% following the 3hr exposure.



Figure 4.3: Western blot analysis of reduced Prxs post-exposure to H₂O₂.

NHBE cell cultures were apically exposed to 0μM, 100μM or 1mM H₂O₂ for 1hr, 3hr or 6hr, PBS was used as a control. Whole cells extracts were lysed following exposure. Lysates were resolved by reducing 1D SDS-PAGE electrophoresis followed by Western blotting and chemiluminescence detection. Proteins were analysed using primary antibodies specific to Prx I, III, -SO₃ and β-actin. Red denoted areas of interest, with increased Prx-SO₃ levels post-exposure to 1mM H₂O₂ for 1hr and 3hr.

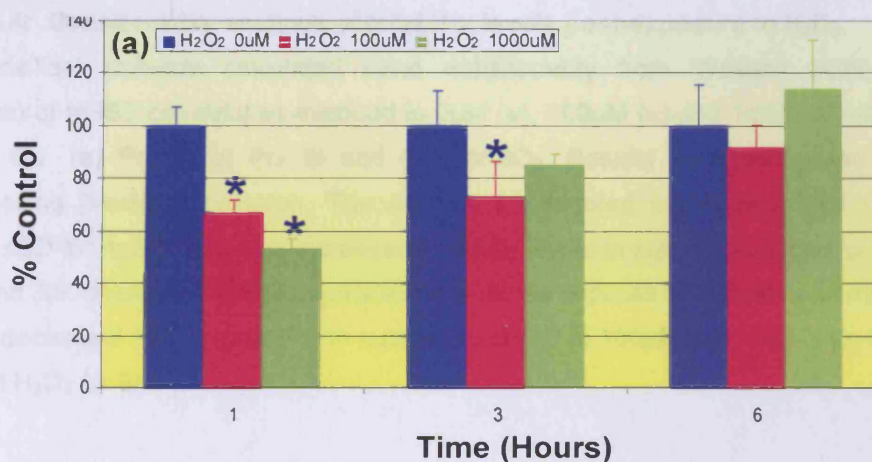


Figure 4.4: Densitometry analysis of total Prx levels post-exposure to H₂O₂.

Figure continued below.

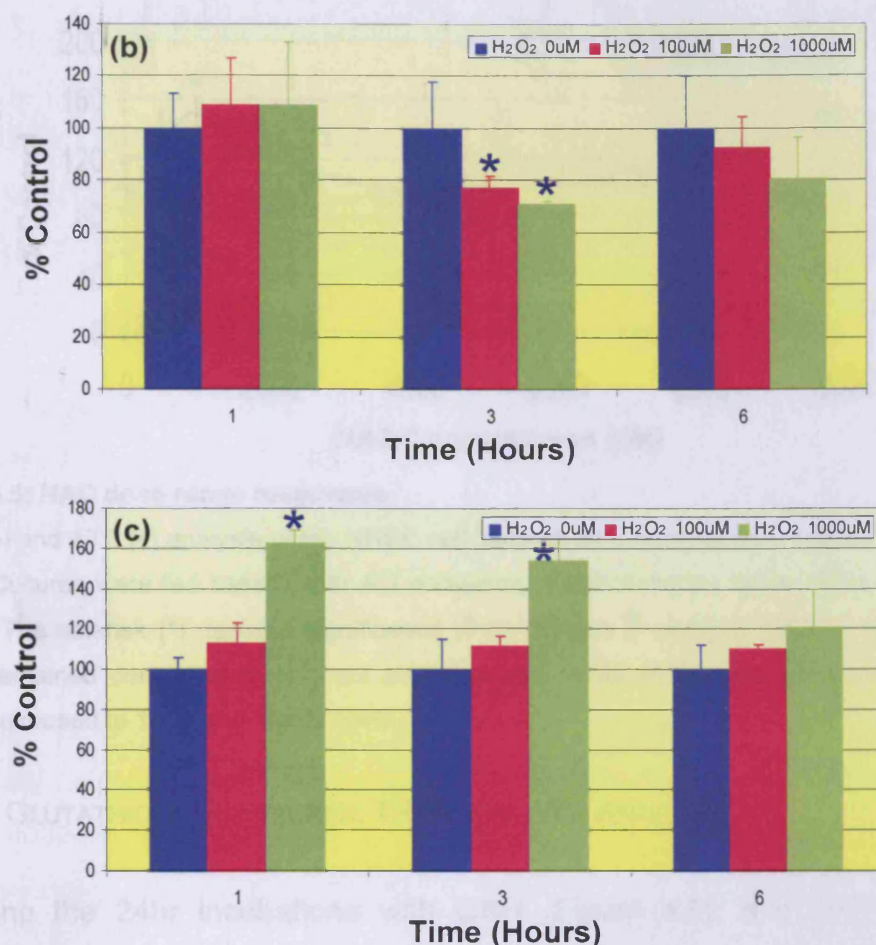


Figure 4.4: Densitometry analysis of total Prx levels post-exposure to H₂O₂.

The GeneTool software calculated band densitometry from Western blots (reducing conditions) of NHBE cell cultures exposed to 0μM (■), 100μM (■) and 1mM (■) H₂O₂, for 1hr, 3hr and 6hr. (a) Prx I, (b) Prx III and (c) Prx-SO₃. Results were normalised using the corresponding β-actin expression. The asterisk (*) denoted significance (P≤0.05) and I signified ±SD for n=3. There was increased Prx-SO₃ levels in cultures exposed to 1mM H₂O₂ for 1hr and 3hr, decreased Prx III expression in cultures exposes to 100μM and 1mM H₂O₂ for 3hr, and decreased Prx I expression in cultures exposed to 100μM and 1mM H₂O₂ for 1hr and to 100μM H₂O₂ for 3hr.

4.4.2 ANTIOXIDANT ADDITION

4.4.2.1 NAC EXPOSURES: TEER AND ATP ANALYSIS

Following the 24hr incubation with NAC (Figure 4.5), the TEER values remained consistent throughout all NAC concentrations. The ATP results demonstrated significant (P≤0.05) increases of 52% at the 1mM concentration, and 40% at the 10mM concentration.

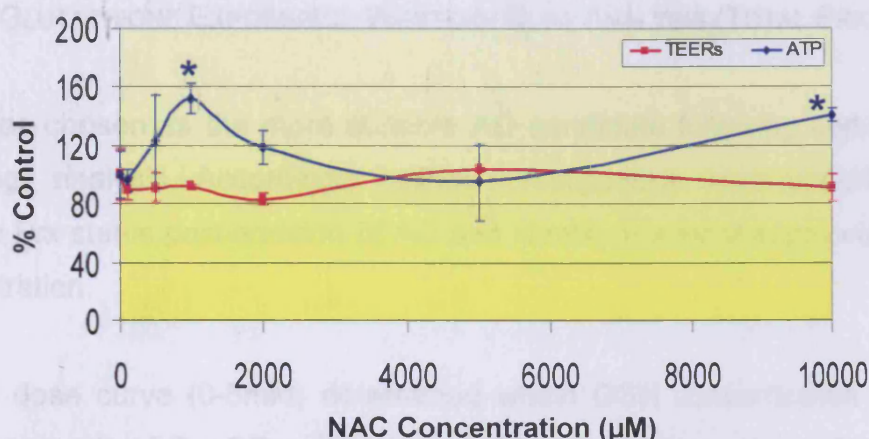


Figure 4.5: NAC dose range responses.

TEER (■) and ATP (◆) analysis of the NHBE cell cultures 24hr post-addition of NAC to the ALI media. Cultures were fed basally with ALI containing a concentration range of NAC (0µM to 10mM). The asterisk (*) denoted significance ($P \leq 0.05$) and \bar{I} signified \pm SD for $n=3$. TEER values remained consistent throughout all exposures, while ATP increased significantly in cultures exposed to 1mM and 10mM NAC.

4.4.2.3 GLUTATHIONE EXPOSURES: TEER AND ATP ANALYSIS

Following the 24hr incubations with GSH (Figure 4.6), the TEER values decreased significantly ($P \leq 0.05$) at the 5mM concentration. The ATP assay displayed values that did not veer significantly ($P \leq 0.05$) from the control levels throughout all exposures.

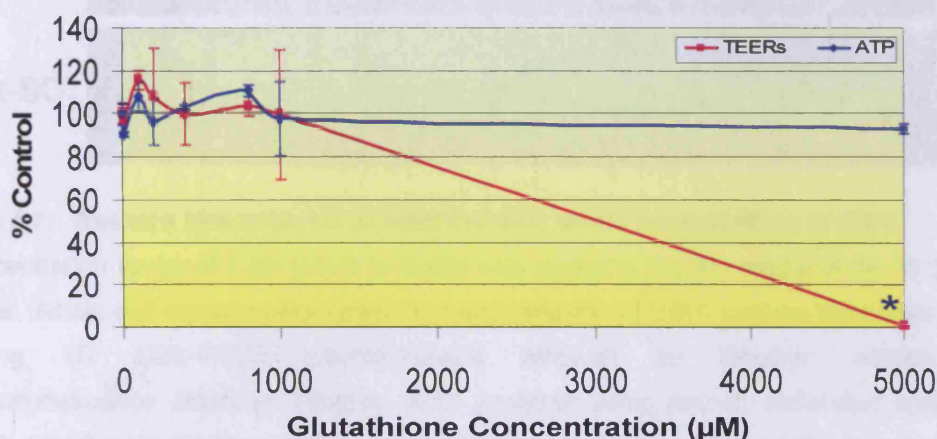


Figure 4.6: GSH dose range responses.

TEER (■) and ATP (◆) analysis of the NHBE cell cultures 24hr post-addition of GSH to the ALI media. Cultures were fed basally with ALI containing a concentration range of GSH (0mM to 5mM). The asterisk (*) denoted significance ($P \leq 0.05$) and \bar{I} signified \pm SD for $n=3$. TEER values decreased significantly in cultures exposed to 5mM GSH, ATP remained consistent.

4.4.2.4 GLUTATHIONE EXPOSURES: WESTERN BLOT ANALYSIS (TOTAL PRX LEVELS)

GSH was chosen as the more suitable AO candidate following conventional toxicology analysis. Accordingly further investigations were undertaken to analyse Prx status post-addition of AO and identify the most appropriate GSH concentration.

A GSH dose curve (0-5mM) determined which GSH concentration reduced the basal levels of Prx-SO₃ within the NHBE cell cultures. The cultures were exposed to GSH, subjected to reducing gel electrophoresis conditions and analysed via Western blotting (Figure 4.7). The levels of hyperoxidation were significantly ($P \leq 0.05$) increased (Figure 4.8) by 37% at the 400 μ M concentration and by 53% at the 800 μ M concentration. The only concentration to cause a reduction in Prx-SO₃ levels was the 800 μ M concentration, which elicited a decrease of 6%. The 800 μ M concentration was therefore chosen for future use in alleviating basal levels of intracellular oxidative stress within the NHBE cell cultures.

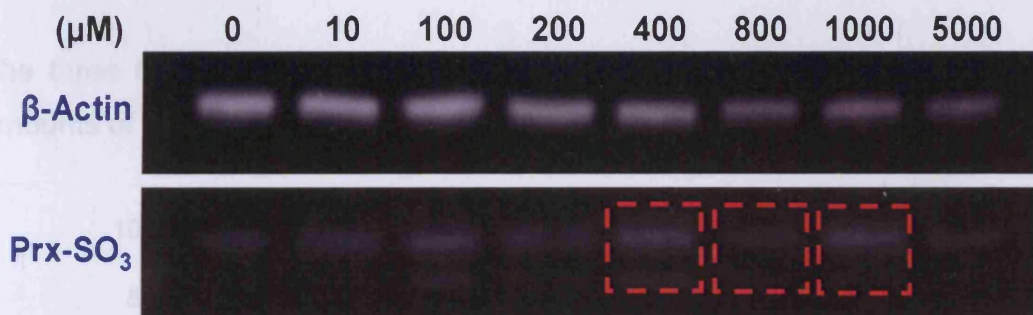


Figure 4.7: Western blot analysis of total Prx-SO₃ levels post-addition of GSH.

A concentration range of GSH (0mM to 5mM) was added to the ALI media of the NHBE cell cultures. Whole cell extracts were lysed 24hr post-addition of GSH. Lysates were resolved by reducing 1D SDS-PAGE electrophoresis followed by Western blotting and chemiluminescence detection. Proteins were analysed using primary antibodies specific to Prx-SO₃ and β -actin. Red denoted areas of interest with elevated levels of Prx-SO₃ in cultures exposed to 400 μ M and 1mM GSH, and decreased Prx-SO₃ levels in cultures exposed to 800 μ M GSH.

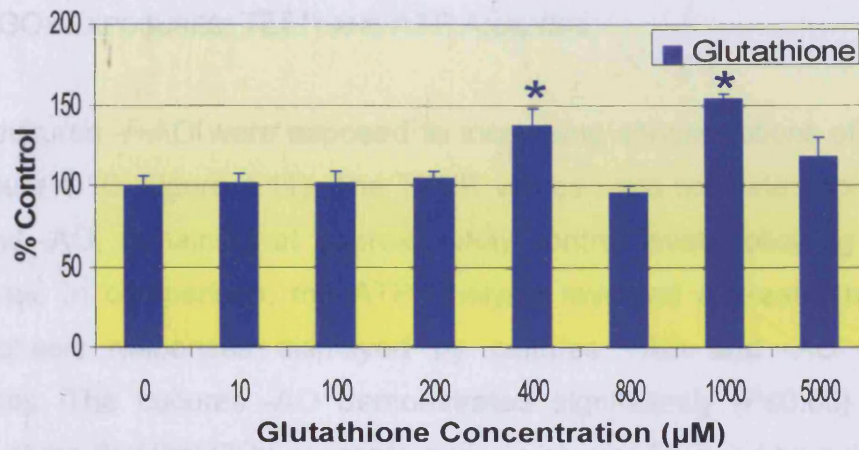


Figure 4.8: Densitometry analysis of total Prx-SO₃ levels post-addition of GSH.

The GeneTool software calculated band densitometry for Western blot (reducing conditions) results of NHBE cell cultures basally exposed to a concentration range of GSH (■) (0µM to 5mM). Results were normalised using the corresponding β-actin expression. The asterisk (*) denoted significance ($P \leq 0.05$) and I signified \pm SD for $n=3$. There were increased Prx-SO₃ levels in cultures exposed to 400µM and 1mM GSH.

4.4.3 GOx EXPOSURE

4.4.3.1 H₂O₂ GENERATED BY GOx

The three GOx concentrations, 5, 15 and 25mU/ml, released proportionate amounts of H₂O₂ (Figure 4.9), increasing over time in a linear manner.

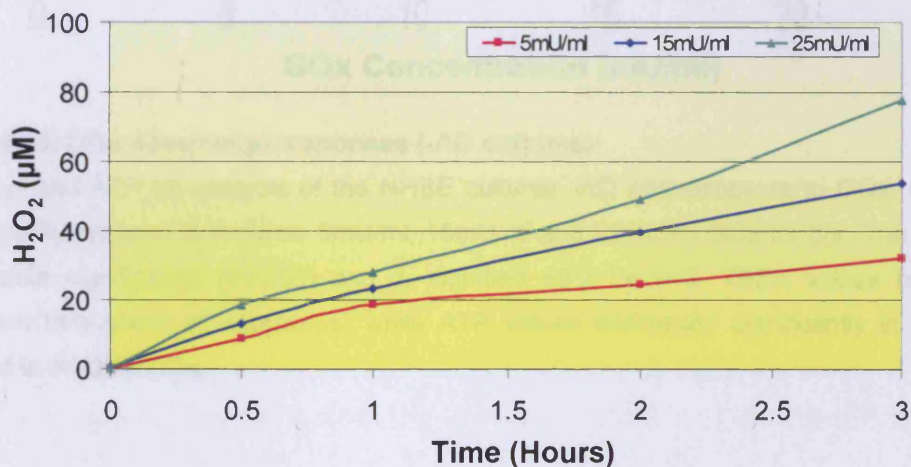


Figure 4.9: H₂O₂ generated by GOx in media over time.

The H₂O₂ concentration released over time by GOx: 5mU/ml (■), 15mU/ml (◆) and 25mU/ml (▲). GOx was diluted in DMEM. GOx analysis revealed linear increases in H₂O₂ concentration over time.

4.4.3.2 GOx EXPOSURES: TEER AND ATP ANALYSIS

NHBE cultures $-/+AO$ were exposed to increasing concentrations of GOx for 3hr (Figure 4.10, Figure 4.11). The TEER values were consistent for cultures $+AO$ and $-AO$, remaining at approximately control levels following all GOx exposures. In comparison, the ATP analysis revealed a greater response, with biphasic responses displayed by cultures $+AO$ and $-AO$ following exposures. The cultures $-AO$ demonstrated significantly ($P \leq 0.05$) reduced viability at the 5mU/ml GOx concentration, which was followed by a rise in cell viability at the 15mU/ml and 25mU/ml concentrations. The cultures $+AO$ responded with significant decreases at the 15mU/ml and 25mU/ml GOx concentrations.

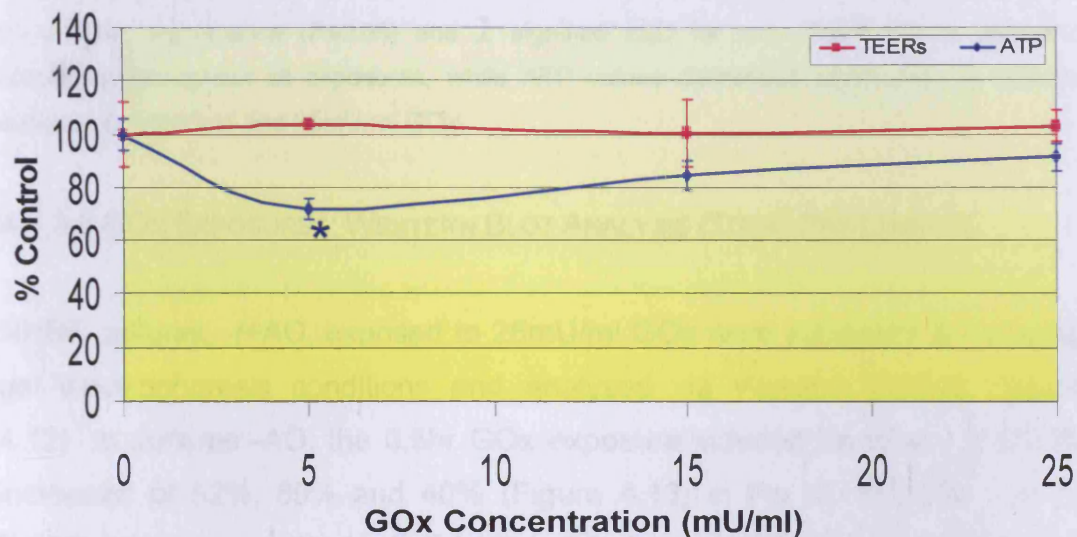


Figure 4.10: GOx dose range responses ($-AO$ cultures).

TEER (■) and ATP (♦) analysis of the NHBE cultures $-AO$ post-exposure to GOx. Cultures were apically exposed to 0mU/ml, 5mU/ml, 15mU/ml and 25mU/ml GOx for 3hr. The asterisk (*) denoted significance ($P \leq 0.05$) and \bar{I} signified $\pm SD$ for $n=3$. TEER values remained consistent throughout all exposures, while ATP values decreased significantly in cultures exposed to 5mU/ml GOx.

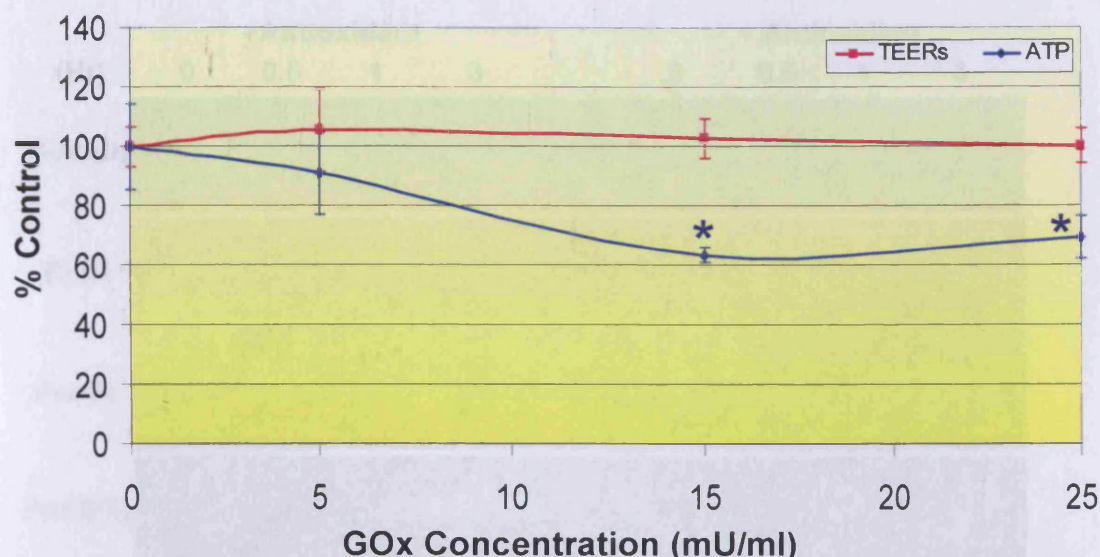


Figure 4.11: GOx dose range responses (+AO cultures).

TEER (■) and ATP (◆) analysis of the NHBE cultures +AO post-exposure to GOx. Cultures were apically exposed to 0mU/ml, 5mU/ml, 15mU/ml and 25mU/ml GOx for 3hr. The asterisk (*) denoted significance ($P \leq 0.05$) and I signified \pm SD for $n=3$. TEER values remained consistent throughout all exposures, while ATP values decreased significantly in cultures exposed to 15mU/ml and 25mU/ml GOx.

4.4.3.3 GOx EXPOSURES: WESTERN BLOT ANALYSIS (TOTAL PRX LEVELS)

NHBE cultures, -/+AO, exposed to 25mU/ml GOx were subjected to reducing gel electrophoresis conditions and analysed via Western blotting (Figure 4.12). In cultures -AO, the 0.5hr GOx exposure induced significant ($P \leq 0.05$) increases of 52%, 89% and 40% (Figure 4.13) in Prx III, Prx-SO₃ and P-Erk1/2 levels, respectively. P-Erk1/2 levels increased further to 52% by the 1hr exposure and by the 3hr exposure Prx III expression had decreased significantly ($P \leq 0.05$) by 25%. In cultures +AO the 3hr GOx exposure elicited a significant ($P \leq 0.05$) decrease of 30% in Prx I expression and significant increases of 25% in both Prx-SO₃ and P-Erk1/2 levels. In cultures +AO, the increase in Prx-SO₃ was proportionate to the H₂O₂ concentration, with the longer exposures eliciting higher H₂O₂ concentrations and elevated Prx-SO₃.



Figure 4.12: Western blot analysis of total Prx levels post-exposure to GOx.

NHBE cell cultures \pm AO were apically exposed to 25mU/ml GOx for 0hr, 0.5hr, 1hr and 3hr. Whole cells extracts were lysed following exposure. Lysates were resolved by reducing 1D SDS-PAGE electrophoresis followed by Western blotting and chemiluminescence detection. Proteins were analysed using primary antibodies specific to Prx I, Prx III, Prx-SO₃, P-Erk1/2 and β -actin. Red denoted areas of interest, with elevated Prx III, Prx-SO₃ and P-Erk1/2 in cultures -AO exposed to 25mU/ml GOx for 0.5hr, and elevated Prx III and Prx-SO₃ in cultures +AO exposed to 25mU/ml GOx for 3hr.

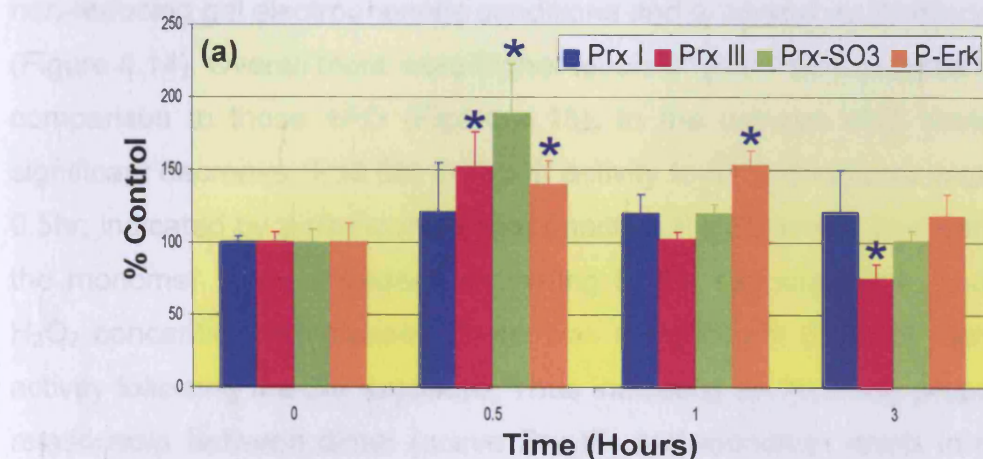


Figure 4.13: Densitometry analysis of total Prx levels post-exposure to GOx.

Figure continued below.

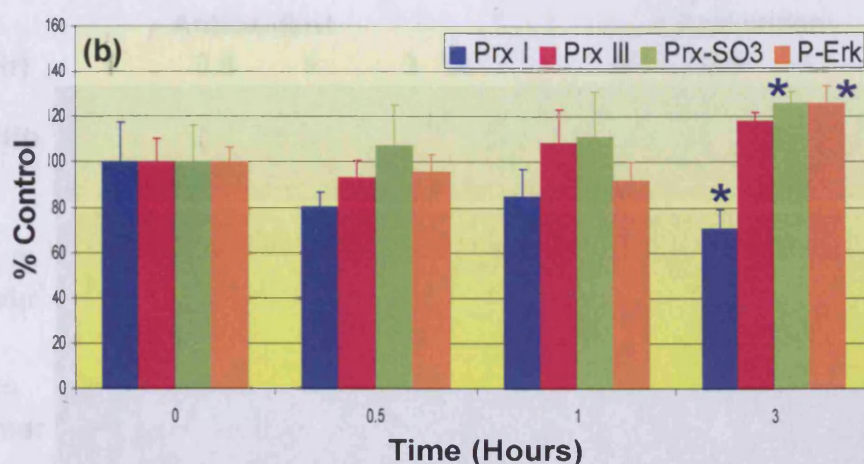


Figure 4.13: Densitometry analysis of total Prx levels post-exposure to GOx.

The GeneTool software calculated Prx I (■), Prx III (■), Prx-SO₃ (■) and P-Erk1/2 (■) band densitometry from Western blots (reducing conditions) of NHBE cell cultures (a) -AO and (b) +AO exposed to 25mU/ml GOx for 0hr, 0.5hr, 1hr and 3hr. Results were normalised using the corresponding β -actin expression. The asterisk (*) denoted significance ($P \leq 0.05$) and \bar{x} signified \pm SD for $n=3$. There were elevated Prx III, Prx-SO₃ and P-Erk1/2 levels in cultures -AO exposed to 25mU/ml GOx for 0.5hr, elevated P-Erk1/2 in cultures -AO exposed to 25mU/ml GOx for 1hr, and elevated Prx III and Prx-SO₃ and decreased Prx I in cultures +AO exposed to 25mU/ml GOx for 3hr.

4.4.3.4 GOX EXPOSURES: WESTERN BLOT ANALYSIS (ACTIVE PRX III)

NHBE cultures, -/+AO, exposed to 25mU/ml GOx for 3hr, were subjected to non-reducing gel electrophoresis conditions and analysed via Western blotting (Figure 4.14). Overall there were higher levels of total Prx III cultures in -AO in comparison to those +AO (Figure 4.15). In the cultures -AO, there was a significant decrease ($P \leq 0.05$) in Prx III activity to 51% in cultures exposed for 0.5hr; indicated by a rise in monomer (inactive Prx III) levels. In cultures +AO, the monomer levels increased according to the exposure time, and hence, H₂O₂ concentration increased, there was a significant ($P \leq 0.05$) decrease in activity following the 3hr exposure. Thus indicating an inversely proportionate relationship between dimer (active Prx III) and monomer levels in the +AO cultures exposed to GOx. In general, the cultures +AO had much more Prx III activity in comparison to the corresponding -AO cultures, in particular the two control samples (+AO: 92%; -AO: 78%).



Figure 4.14: Western blot analysis of Prx III activity post-exposure to GOx.

NHBE cell cultures $-/+AO$ were apically exposed to 25mU/ml GOx for 0hr, 0.5hr, 1hr and 3hr. Whole cells extracts were lysed following exposure. Lysates were resolved by non-reducing 1D SDS-PAGE electrophoresis followed by Western blotting and chemiluminescence detection. Proteins were analysed using primary antibodies specific to Prx III and β -actin. Dimers corresponded to active Prx III, whereas monomers represent hyperoxidised (inactive) Prx III. Red denoted areas of interest, with elevated monomer levels in cultures $-AO$ exposed to 25mU/ml GOx for 0.5hr, and monomer levels elevated in proportion to H_2O_2 concentration in cultures $+AO$.

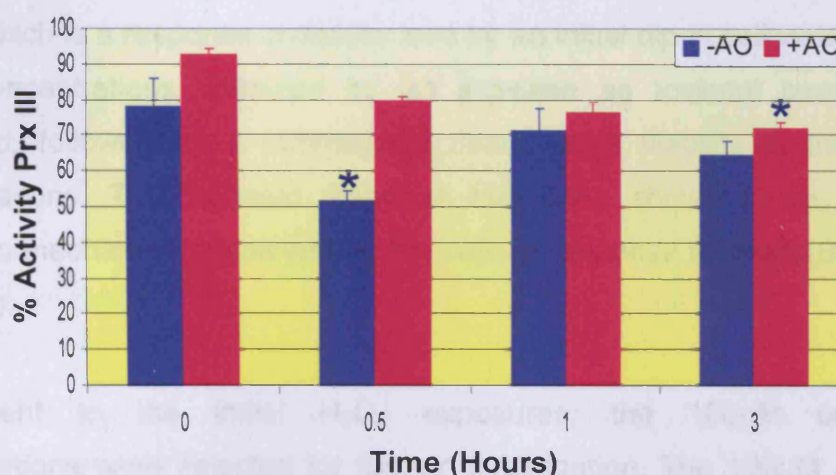


Figure 4.15: Densitometry analysis of Prx III activity post-exposure to GOx.

The GeneTool software calculated Prx III monomer and dimer band densitometry from Western blots (non-reducing conditions) of NHBE cell cultures $-AO$ (■) and $+AO$ (■) exposed to 25mU/ml GOx for 0hr, 0.5hr, 1hr and 3hr. Results were normalised using the corresponding β -actin expression. The asterisk (*) denoted significance ($P \leq 0.05$) and \bar{I} signified $\pm SD$ for $n=3$. There was decreased activity in cultures $-AO$ exposed to 25mU/ml GOx for 0.5hr, and decreased Prx III activity in cultures $+AO$ exposed to 25mU/ml GOx for 3hr.

4.5 DISCUSSION

4.5.1 H₂O₂ EXPOSURE

The previous experimental work (Chapters 2 and 3) established a modified toxicological exposure window, in accordance with Prx status at the biochemical level. This required moving away from the traditional dosing window of Days 27-33 (Prytherch, 2010), which was primarily based on morphological analysis, in favour of Days 25-30 (Chapters 2 and 3). The revised dosing window was utilised for toxicological analysis, where cultures were exposed to a concentration range of H₂O₂ and incubated for 24hr. The conventional toxicology revealed that even at the higher H₂O₂ concentrations, the NHBE cells remained intact and cell-cell junctions had not been overly compromised. There was a significant ($P \leq 0.05$) increase in the TEER values following the 800 μ M H₂O₂ exposure; this increase was attributed to a survival attempt, whereby the cultures constricted their intercellular tight junctions to prevent toxicant absorption (Schneeberger and Lynch, 1992). The ATP analysis revealed a biphasic response known as 'hormesis' (Calabrese, 2004), which is a response characterised by an initial dip in cell viability at the lower concentrations, followed by an increase as toxicant concentration increased, followed by a subsequent decrease in viability at the highest concentrations. The biphasic response has been shown to be an acute protection mechanism employed by the cells in response to insult (Balharry *et al.*, 2008).

Subsequent to the initial H₂O₂ exposures, the 100 μ M and 1mM concentrations were selected for further investigation. The 100 μ M and 1mM H₂O₂ concentrations were elevated in comparison to other studies utilising H₂O₂ (Phalen *et al.*, 2006; Cox *et al.*, 2009a), however, in comparison to monolayers of pulmonary cells, the NHBE system has been shown to be more resilient (Prytherch, 2010). Balharry and co-workers demonstrated that up to 10 times the concentration of a given classical pulmonary toxin (e.g. tobacco smoke components) was required to produce the same effect observed in comparable monolayer cultures (Balharry *et al.*, 2008).

The Western blot results demonstrated significant ($P \leq 0.05$) increases in the levels of Prx-SO₃ at the highest H₂O₂ concentrations (1mM). This was physiologically relevant; as cultures were not significantly ($P \leq 0.05$) compromised with regard TEER and ATP analysis. These findings corresponded to the current understanding of how oxidative stress effects redox signalling within the cell (Thannickal and Fanburg, 2000; Halliwell, 2007a). In the first instance, there would be no definable phenotypic adaptations, however, on the biochemical level, cycles of injury and repair would be occurring, as the cells struggled to maintain homeostasis (Heintz, 2008). Early stage oxidant damage would therefore be more likely to affect the Prx status, whereas the NHBE culture morphology would appear phenotypically normal (Rabilloud *et al.*, 2002). The Western blot observations demonstrated increased Prx hyperoxidation following H₂O₂ exposure, suggesting that Prx oxidation state may be used as an early predictor of elevated oxidative stress within the cells, before phenotypic adaptation occurred.

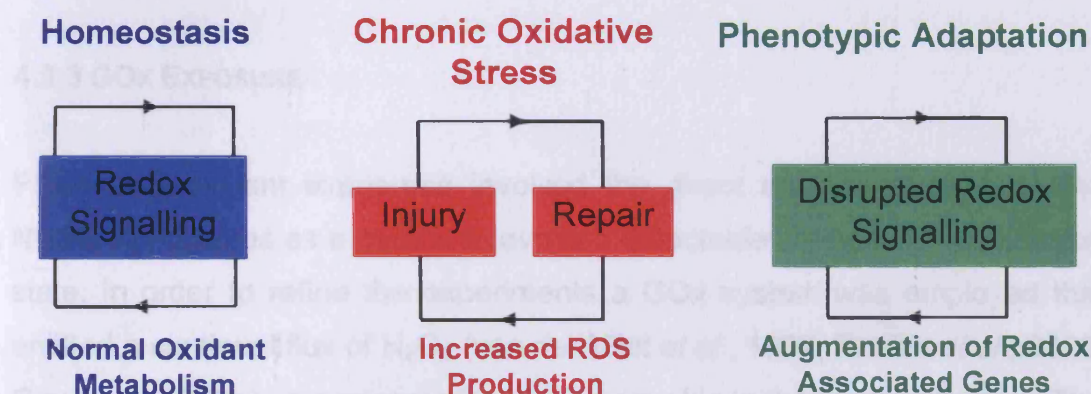


Figure 4.11: The effect of ROS on homeostasis within the bronchial epithelium.

Optimal redox signalling maintained homeostasis within the lung of a healthy individual. Following chronic oxidative stress, there would be increased ROS production, leading to cycles of injury and repair. Over-time the redox signalling within the lung would be permanently disrupted, leading to phenotypic adaptations through the augmentation of antioxidant expression (Adapted from Heintz, 2008).

4.5.2 ANTIOXIDANT ADDITION

The elevated levels of Prx-SO₃ within the control NHBE cultures (Sections 2.4.3 and 4.4.1) revealed a need to minimise the basal levels of oxidative stress. The continuous AO addition, whereby 1mM NAC was added to the ALI media for every media change, was unsuccessful as the cultures did not differentiate and died at around Day 9. Following the continuous AO experiments a concentration range of NAC and GSH was added to the ALI culture media, and the cultures analysed by conventional toxicology (ATP and TEER) 24hr post-addition. This was undertaken to determine the most effective AO supplementation for reducing oxidative stress levels within the NHBE cultures. ATP and TEER analysis suggested that 800µM GSH was the concentration of AO that had no significant detrimental effect in terms of ATP, TEERs and Prx-SO₃. Further analysis utilised Western blotting by probing for Prx-SO₃; this substantiated the ATP and TEER data, with 800µM GSH the only concentration to reduce the basal levels of Prx-SO₃. Additional work would involve assessing the baseline GSH status of the NHBE cultures.

4.5.3 GOx EXPOSURE

Preliminary oxidant exposures involved the direct addition of H₂O₂ to the NHBE cell cultures as a means to evoke a detectable change in Prx oxidation state. In order to refine the experiments a GOx system was employed that emitted a continual flux of H₂O₂ (van der Vliet *et al.*, 1997; Phalen *et al.*, 2006; Cox *et al.*, 2009a), in a manner that was more akin to the *in vivo* situation. The lower levels of H₂O₂ released by the GOx system permitted more robust characterisation of the changes in Prx status, as a result of more subtle increases in oxidant burden. The ability to detect and quantify subtle changes improved the capacity of the Prxs to be used as an early stage biomarker of oxidative stress.

The concentration range of GOx generated comparable TEER responses in cultures -/+AO, which remained constant at control levels for all concentrations. The ATP results were biphasic in cultures -/+AO, however,

the +AO cultures required a higher GOx concentration, in comparison to -AO cultures, in order to achieve the same initial stimulation (Rozman and Doull, 2003). This suggested that AO supplementation had buffered the effect of the increased oxidant, as observed *in vivo*.

Cox and co-workers discovered that the addition of cell extract to cell lysis buffer caused reduced Prxs to form dimers, therefore both reduced and oxidised Prx would appear on Western blots as a dimers following non-reducing gel electrophoresis conditions (Cox *et al.*, 2010a). This technique was therefore exploited to determine the levels of Prx hyperoxidation, with the monomer bands representative of Prx hyperoxidation. Western blot analysis of reduced and non-reduced NHBE samples revealed elevated levels of Prx III expression in GOx exposed cultures -AO, in comparison to corresponding +AO cultures; as a mode of compensating for the absence of a basal level AO protection (Lehtonen *et al.*, 2005). In cultures -AO exposed to GOx there were significantly ($P \leq 0.05$) increased levels of Prx III and Prx-SO₃ following the 0.5hr exposures. These elevated levels were not maintained following the 1hr and 3hr (highest H₂O₂ concentration) exposures. The rationale for these observations was linked to cell cycle arrest, whereby the 0.5hr exposures initiated arrest in response to a significant increase in Prx hyperoxidation levels (Phalen *et al.*, 2006). By the 1hr and 3hr exposures the overall levels of Prx had begun to reduce, and consequently, the levels of hyperoxidation did not increase further. In cultures +AO, the levels of Prx-SO₃ increased in proportion to H₂O₂ concentration; with a significant ($P \leq 0.05$) increase following the 3hr exposure. Prx III activity was consistently higher in cultures +AO in comparison to those -AO, with 92% activity in control samples. This was an indicator of the stability brought to the NHBE model through antioxidant supplementation (Leist *et al.*, 1996).

The levels of P-Erk1/2 were also analysed in order to fully relate Prx status change to levels of oxidative stress, since increased levels of phosphorylated MAP kinase represented activation of the stress response pathways (Waskiewicz and Cooper, 1995). The response patterns of Prx III and Prx-SO₃ was also seen for P-Erk1/2, whereby in cultures -AO there were significantly

($P \leq 0.05$) increased levels following the 0.5hr exposure, and in cultures +AO there were a significant ($P \leq 0.05$) increases following the 3hr exposure. Again, this demonstrated the enhanced stability of the +AO cultures in comparison to cultures -AO, with higher H_2O_2 concentrations needed to activate Erk1/2 (Kim *et al.*, 2005). Future work would involve total Erk1/2 levels to be analysed.

The collective Western blot results from GOx exposed cultures reinforced the need for AO addition in order to stabilise the cultures at the biochemical level, with analysis of cultures supplemented with GSH strengthening the use of Prx oxidation state as a marker of intracellular oxidant burden.

4.6 CONCLUSION

Exposing the NHBE cultures to H_2O_2 (directly and via the GOx system) revealed several key features with regard to the model and the potential biomarker role of the Prxs. Directly exposing the NHBE cultures to 1mM H_2O_2 for 24hr caused only a TD₂₀ (Toxic Dose 20%) response, but induced a significant increase in Prx hyperoxidation, demonstrating the models' resilience in comparison to less physiologically relevant monolayer cell systems. Cultures exposed to H_2O_2 via the GOx system also elicited significant increases in Prx hyperoxidation at the higher concentrations, with +AO cultures following a more expected trend, in terms of Prx status following exposure. It could be concluded that incorporating AO into the cell culture media, to alleviate the oxidant burden caused by culture conditions (Halliwell, 2003), enhanced the NHBE cell culture viability (i.e. increasing its potential as an *in vitro* alternative).

The GOx system created a more physiologically relevant H_2O_2 exposure system that increased Prx hyperoxidation levels, inferring that Prxs were sensitive to minor changes in oxidative stress. Therefore, Prx oxidation state may be exploited to elucidate intracellular oxidative stress levels. This, coupled with the stable NHBE phenotype at the higher H_2O_2 concentrations, recommended that Prx could act as an 'early stage biomarker' for events reflecting elevated levels of intracellular oxidative stress.

CHAPTER 5:

RESPONSE OF PEROXIREDOXIN STATUS TO CIGARETTE SMOKE EXPOSURE

5.1 INTRODUCTION

Cigarette smoke (CS) is the most common inhaled human toxicant (IARC, 2004), with smoking the most common cause of COPD Worldwide, accounting for over 90% of cases (Boots *et al.*, 2003). Each cigarette contains over 4000 compounds, including oxidants, mutagens and carcinogens, along with antigenic and cytotoxic components (Hansel and Barnes, 2004). In terms of oxidative stress, there is an estimated 10^{17} reactive oxygen species (ROS) per standard inhalation (MacNee and Rahman, 2001; IARC, 2004), imparting a substantial oxidant burden on the cells of the pulmonary epithelium.

Work in this Chapter involved exposing the fully differentiated NHBE cultures, both -/+AO, to a concentration range of CS. Conventional toxicology was utilised for culture analysis 3hr and 24hr post-exposure. Changes in junction integrity (TEER) and cell viability (ATP) were monitored over the CS concentration range, and Prx status was determined using Western blotting for reducing and non-reducing gel electrophoresis conditions. IHC analysis was undertaken to investigate further Prx expression levels and oxidation following CS exposure.

The aim was to analyse Prx status as a 'biomarker of oxidative damage' caused by the CS exposures. Analysis at 3hr and 24hr post-exposure was undertaken to gauge the repair competency of the NHBE model, potentially enhancing the models credentials as a viable *in vitro* alternative, through providing an *in vivo* like response.

5.1.1 RESEARCH AIMS

The research aims for experimental work in Chapter 5 (Figure 5.1), were as follows:

- Culture the NHBE cells until the point of full differentiation and expose to a concentration range of CS and assess conventional toxicology through TEER and ATP analysis.

- Quench the basal levels of oxidative stress within the NHBE cultures through the addition of AO to the culture media.
- Quantify the expression levels and oxidation state of the Prxs by employing reducing and non-reducing gel electrophoresis conditions, followed by Western blotting and chemiluminescence detection.
- Investigate further Prx oxidation state and region specific expression levels, following CS exposure, by utilising the IHC chromogenic detection system.

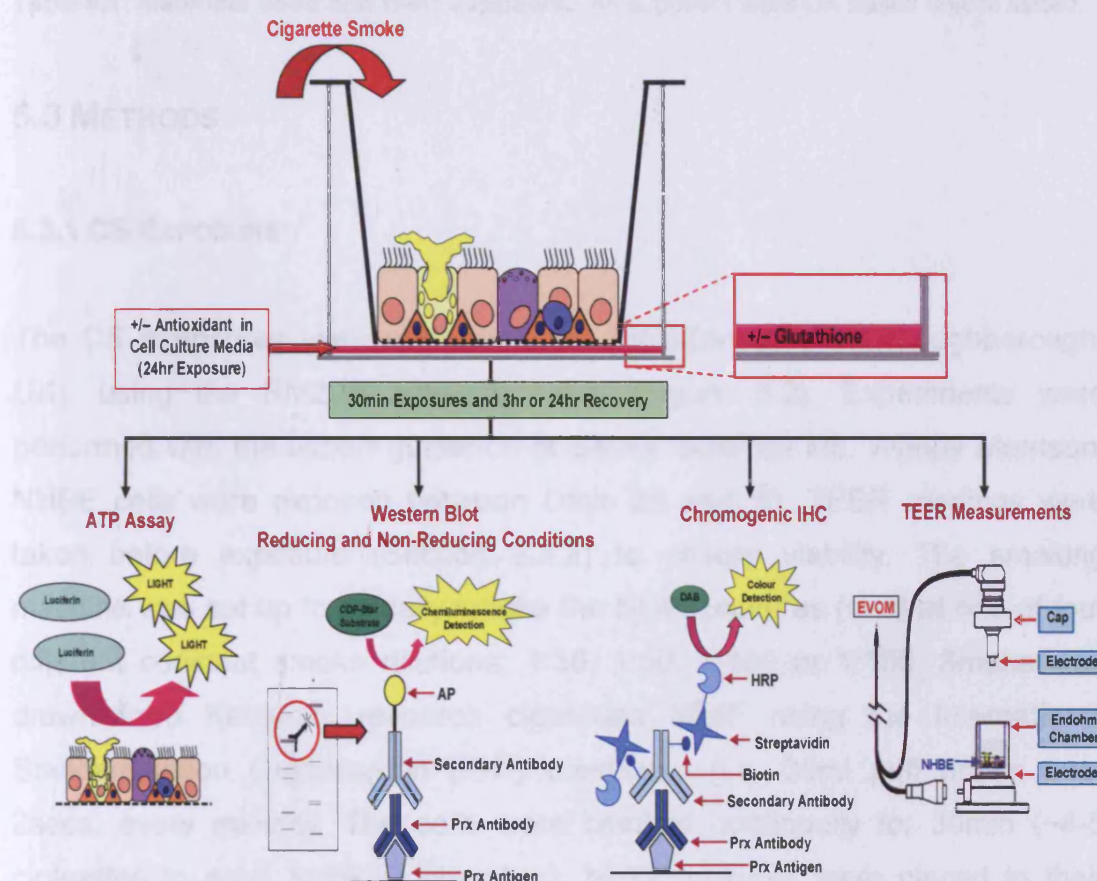


Figure 5.1: Flowchart of experimental work in Chapter 5.

Experimental aims included apical exposure of the NHBE cell cultures to CS, followed by analysis 3hr and 24hr post-exposure. Culture viability (ATP) and junction integrity (TEER) were established. Prx status (expression levels and oxidation state) was determined through reducing and non-reducing gel electrophoresis conditions followed by Western blotting and chemiluminescence detection. Chromogenic IHC was also undertaken.

5.2 MATERIALS AND STOCK SOLUTIONS

Materials and stock solutions from previous Chapters have not been included.

5.2.1 MATERIALS AND SUPPLIERS

MATERIALS:	SUPPLIER:
Kentucky Research Cigarettes, 3R4F	Tobacco-Health Research, University of Kentucky, USA
Smoking Robot RM20S	Borgwaldt-kc Teknik, Hamburg, Germany

Table 5.1: Materials used and their suppliers. All suppliers were UK based unless stated.

5.3 METHODS

5.3.1 CS EXPOSURE

The CS exposures were undertaken at AstraZeneca R&D (Loughborough, UK), using the RM20S smoking robot (Figure 5.2). Experiments were performed with the expert guidance of Senior Scientist Ms. Wendy Merrison. NHBE cells were exposed between Days 25 and 30. TEER readings were taken before exposure (Section 2.3.2) to ensure viability. The smoking machine was set up to apically smoke the NHBE cultures (n=3) at one of four different constant smoke dilutions; 1:30, 1:50, 1:100 or 1:150. Smoke was drawn from Kentucky research cigarettes 3R4F using the International Standardisation Organisation (ISO) conditions (i.e. 35ml puff drawn over 2secs, every minute). The cells were smoked continually for 30min (~4-5 cigarettes to each smoking chamber). NHBE cultures were placed in their smoking chambers (Figure 5.5) containing 38ml ALI media \pm 800 μ M glutathione. NHBE cells in the smoking chambers were kept in a cell culture laminar flow hood for the smoke exposure. Control cells were left in a cell culture laminar flow hood with ALI media for the duration of the experiment so that equivalent temperatures were maintained. Post-exposure the cultures recovered for 3hr or 24hr in fresh ALI media (\pm AO) at 37°C and 5% CO₂.

TEER analysis, ATP assays (Section 4.3.4) and Western blotting of the reduced and non-reduced samples (Section 2.3.4) were all utilised to analyse junction integrity, cell viability and Prx expression levels and oxidation state, respectively.

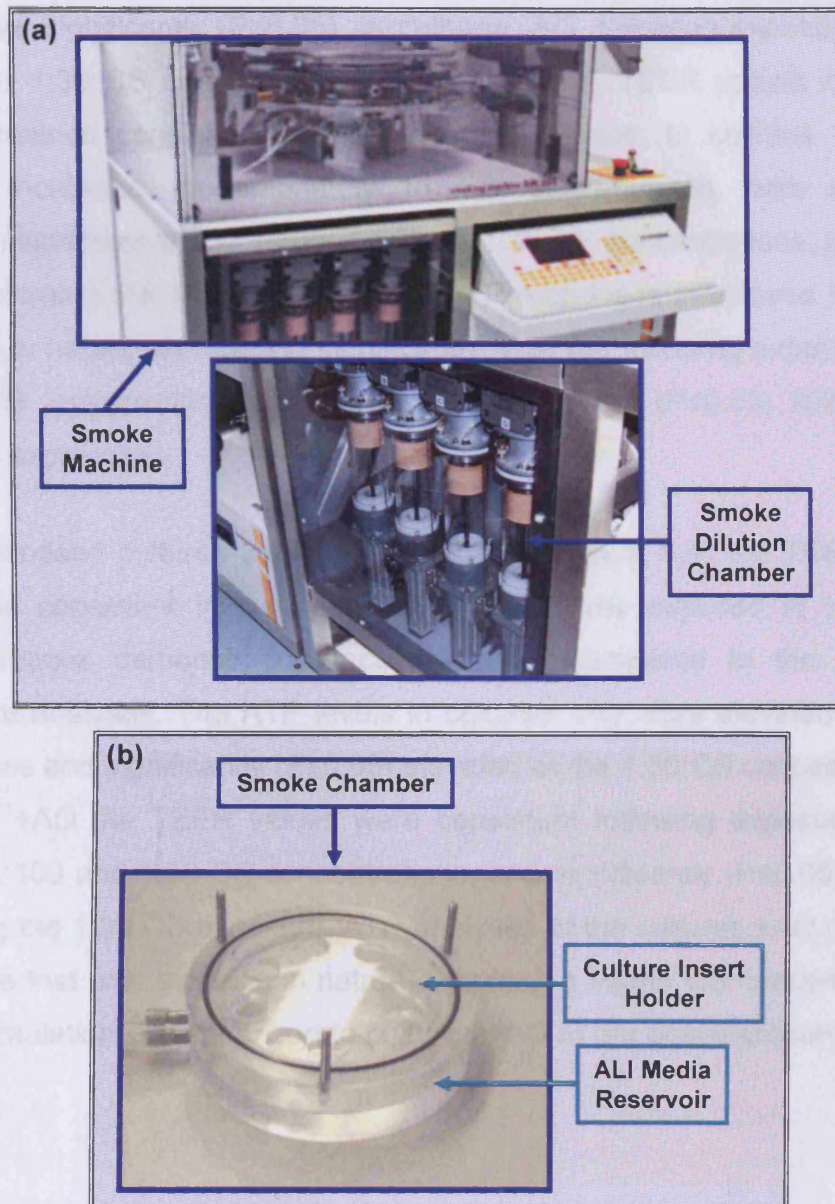


Figure 5.2: Smoking robot and Smoke chamber.

The smoking robot (a) used to smoke the NHBE cells along with a closer view of the smoke dilution chambers used to dilute the CS to the required concentrations. Eight individual NHBE culture inserts were held in the smoking chamber (b). The ALI media resided in the large well at the base of the smoking chamber and the NHBE culture inserts were placed into the appropriate holders. The large chamber lid was placed on top, and the pipes to the smoke machine were attached (not shown).

5.4 RESULTS

5.4.1 CS EXPOSURE: TEER AND ATP ANALYSIS

In CS exposed cultures 3hr post-exposure (Figure 5.3) the TEER values decreased significantly ($P \leq 0.05$), in cultures -AO, following exposures to the 1:50 and 1:30 CS concentrations. In comparison, TEER values in cultures +AO remained consistent throughout all exposures. In cultures -AO ATP activity increased proportionately to CS concentration, with significant ($P \leq 0.05$) increases at the 1:100, 1:50 and 1:30 CS concentrations, peaking at 183% following the 1:30 CS exposure. ATP responses in cultures +AO were biphasic in nature, decreasing significantly ($P \leq 0.05$) following exposure to the 1:150 CS concentration and increasing significantly ($P \leq 0.05$) following the 1:50 CS exposures.

In CS exposed cultures 24hrs post-exposure (Figure 5.4) the TEER values remained consistent in cultures -AO, with cultures exposed to higher CS concentrations demonstrating recovery when compared to the 3hr post-exposure analyses. The ATP levels in cultures -AO were elevated at all CS exposures and significantly ($P \leq 0.05$) elevated at the 1:30 CS concentration. In cultures +AO the TEER values were consistent following exposures to the 1:150, 1:100 and 1:50 CS concentrations, and significantly ($P \leq 0.05$) elevated following the 1:30 CS exposure. ATP analyses of the cultures +AO revealed a response that was biphasic in nature, requiring a higher CS concentration for initial stimulation in comparison to cultures +AO at 3hr post-exposure.

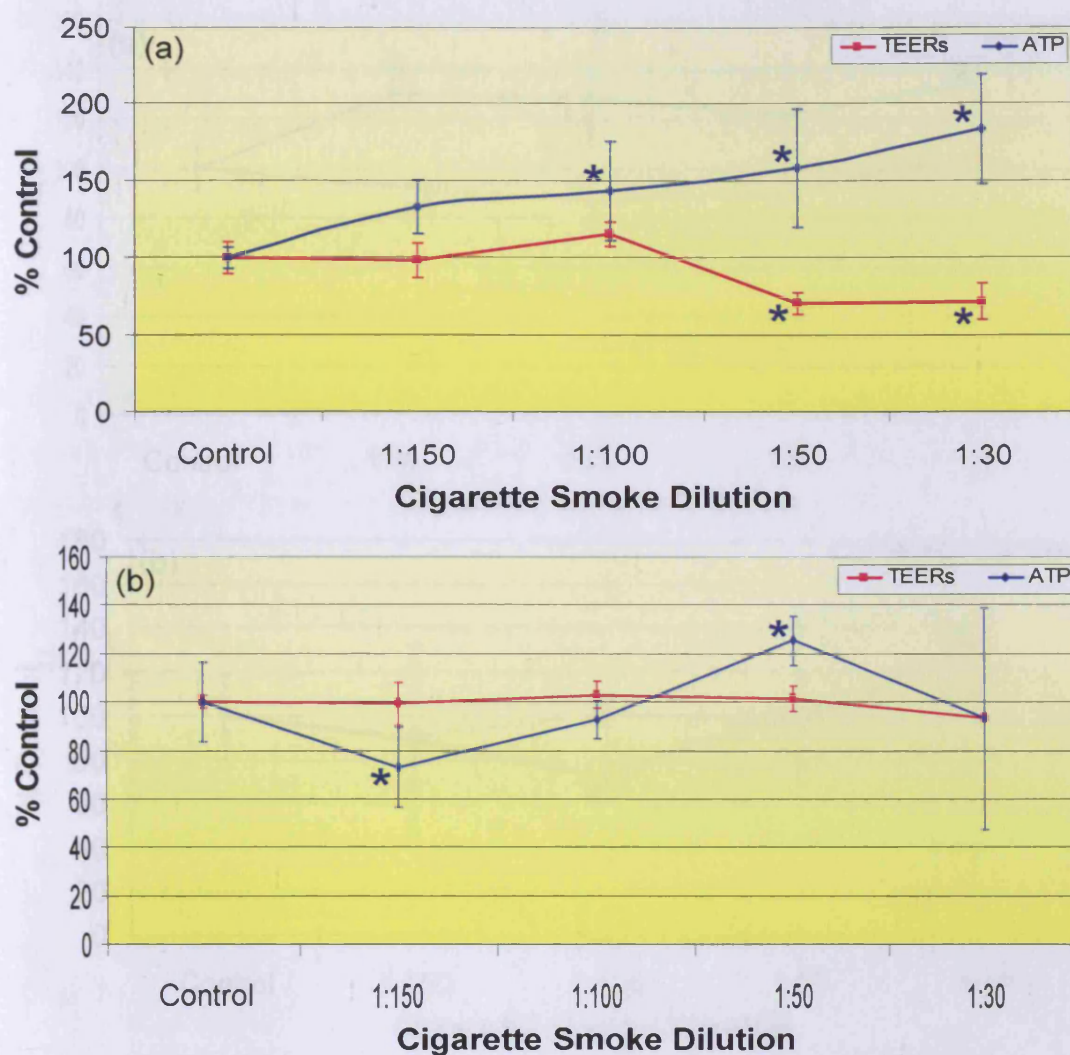


Figure 5.3: CS dose range response on TEER and ATP readings.

TEER (■) and ATP (◆) analysis of the NHBE cultures (a) -AO and (b) +AO 3hr post-exposure to CS. Cultures were apically exposed to 1:150, 1:100, 1:50 and 1:30 CS dilutions for 30min; air exposure was used as a control. The asterisk (*) denoted significance ($P \leq 0.05$) and I signified \pm SD for $n=3$. (a) TEER values decreased significantly at the 1:50 and 1:30 CS concentrations, while ATP values increased significantly at the 1:100, 1:50 and 1:30 concentrations; (b) TEER values remained consistent throughout all exposures, while ATP values decreased significantly following exposure to the 1:150 concentrations and increased significantly at the 1:50 concentration.

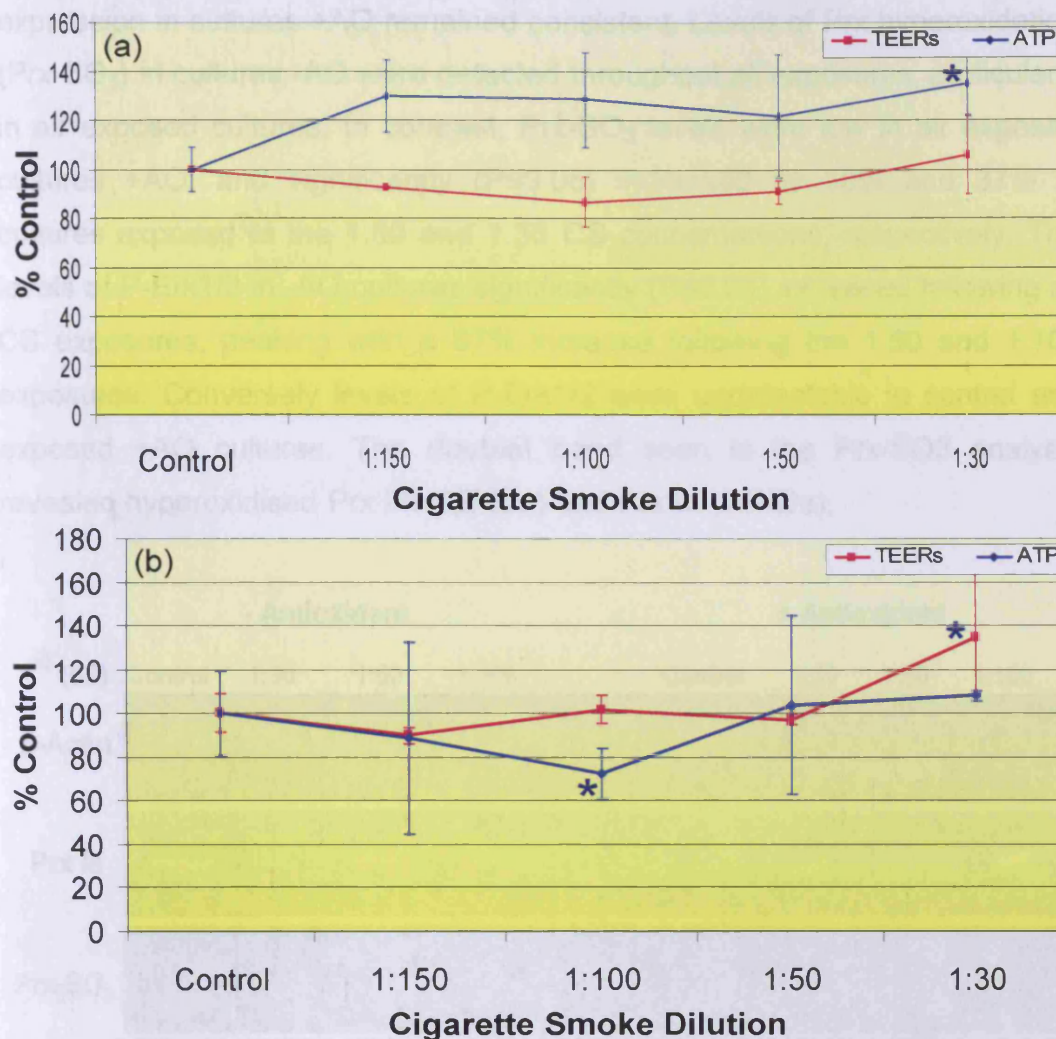


Figure 5.4: CS dose range response on TEER and ATP readings.

TEER (■) and ATP (♦) analysis of the NHBE cultures (a) -AO and (b) +AO 24hr post-exposure to CS. Cultures were apically exposed to 1:150, 1:100, 1:50 and 1:30 CS for 30min, air exposure was used as a control. The asterisk (*) denoted significance ($P \leq 0.05$) and I signified \pm SD for n=3. (a) TEER values were consistent throughout all exposures, while ATP values increased significantly at the 1:30 concentration; (b) TEER increased significantly at the 1:30 concentration, while ATP values decreased significantly at the 1:100 concentrations and increased significantly at the 1:50 concentration.

5.4.2 CS EXPOSURES: WESTERN BLOT ANALYSIS (TOTAL PRX LEVELS)

At 3hr post-exposure to CS the NHBE cultures -/+AO were subjected to reducing gel electrophoresis conditions and analysed via Western blotting (Figure 5.5). In cultures -AO the 1:50 CS concentration elicited a significant ($P \leq 0.05$) increase of 41% (Figure 5.6) in Prx III expression, whereas

expression in cultures +AO remained consistent. Levels of Prx hyperoxidation (Prx-SO₃) in cultures -AO were detected throughout all exposures, particularly in air exposed cultures. In contrast, Prx-SO₃ levels were low in air exposed cultures +AO, and significantly ($P \leq 0.05$) increased by 30% and 37% in cultures exposed to the 1:50 and 1:30 CS concentrations, respectively. The levels of P-Erk1/2 in -AO cultures significantly ($P \leq 0.05$) increased following all CS exposures, peaking with a 67% increase following the 1:50 and 1:100 exposures. Conversely levels of P-Erk1/2 were undetectable in control and exposed +AO cultures. The doublet band seen in the Prx-SO₃ analysis revealed hyperoxidised Prx I/II (22KDa) and Prx III (21KDa).

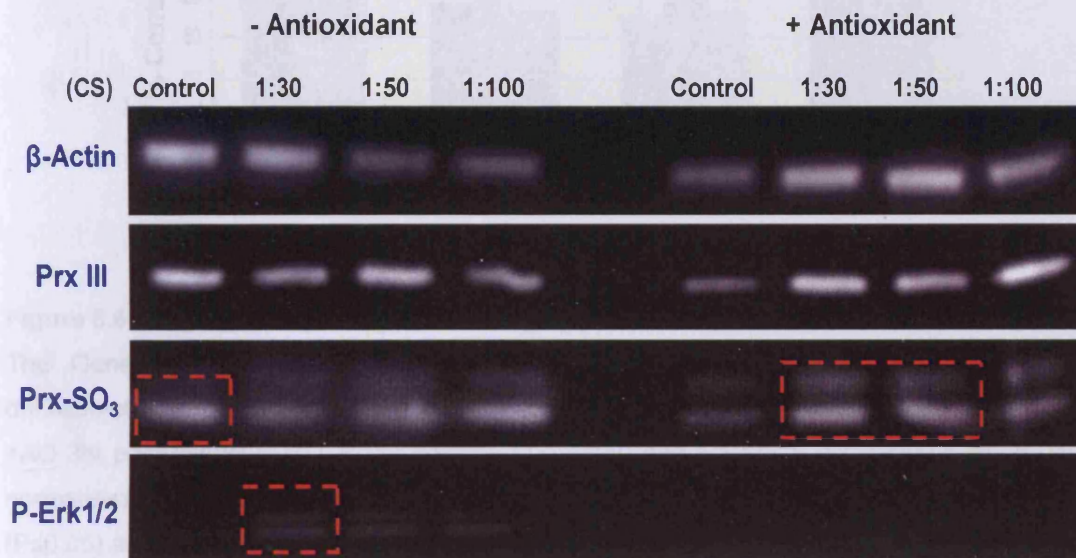


Figure 5.5: Western blot analysis of total Prx levels 3hr post-exposure to CS.

NHBE cell cultures -/+AO were apically exposed to 1:100, 1:50 and 1:30 CS for 30min, air exposure was used as a control. Cultures were analysed 3hr post-exposure. Whole cells extracts were lysed following exposure. Lysates were resolved by reducing 1D SDS-PAGE electrophoresis followed by Western blotting and chemiluminescence detection. Proteins were analysed using primary antibodies specific to Prx III, Prx-SO₃, P-Erk1/2 and β-actin. Red denoted areas of interest, with elevated Prx-SO₃ in control cultures -AO, elevated P-Erk1/2 in cultures -AO exposed to 1:30 CS, and elevated Prx-SO₃ in cultures +AO exposed 1:50 and 1:30 CS.



Figure 5.6: Densitometry analysis of total Prx levels 3hr post-exposure to CS.

The GeneTool software calculated Prx III (■), Prx-SO₃ (■) and P-Erk1/2 (■) band densitometry from Western blots (reducing conditions) of NHBE cell cultures (a) -AO and (b) +AO 3hr post-exposure to CS (air control, 1:30, 1:50 and 1:100 CS for 30min). Results were normalised using the corresponding β -actin expression. The asterisk (*) denoted significance ($P \leq 0.05$) and \bar{I} signified \pm SD for $n=3$. There was elevated Prx III in cultures -AO exposed to 1:50 CS, elevated P-Erk1/2 in cultures -AO exposed 1:100, 1:50 and 1:30 CS, and elevated Prx-SO₃ cultures +AO exposed 1:50 and 1:30 CS.

At 24hr post-exposure to CS the NHBE cultures -/+AO were subjected to reducing gel electrophoresis conditions and analysed via Western blotting (Figure 5.7). In cultures -AO, Prx III showed no significant ($P \leq 0.05$) changes in expression following exposure to all CS concentrations (Figure 5.8), which represented a decrease in expression when compared to the corresponding cultures at 3hr post-exposure (Figure 5.6). There were elevated levels of Prx-SO₃ in cultures -AO following all exposures, however, subsequent densitometry analysis revealed no significant ($P \leq 0.05$) changes. In contrast, the Western blots for cultures +AO revealed that levels of Prx-SO₃ decreased in proportion to CS concentration, which was substantiated by densitometry

analysis; this confirmed a recovery response in +AO cultures 24hr post-exposure when compared to the corresponding 3hr post-exposure cultures. Levels of P-Erk1/2 in cultures -AO were significantly ($P \leq 0.05$) increased by 38% following the 1:30 CS exposure, with more modest increases of 24% and 19% following the 1:50 and 1:100 CS exposures respectively, however, in comparison to the corresponding cultures at 3hr post-exposure, the P-Erk1/2 levels were decreased. The doublet band seen in the Prx-SO₃ analysis revealed hyperoxidised Prx I/II (22KDa) and Prx III (21KDa).

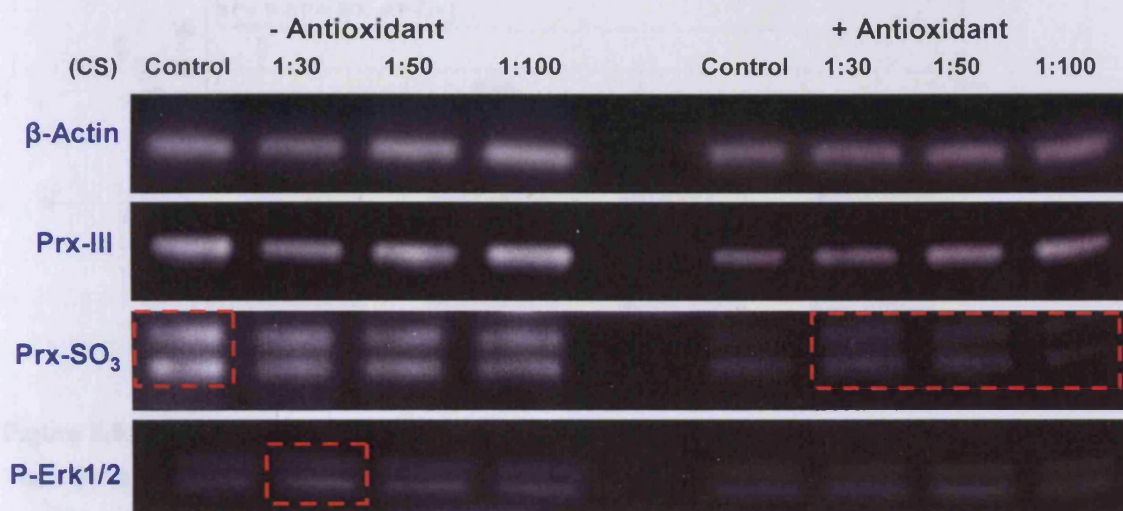


Figure 5.7 Western blot analysis of total Prx levels 24hr post-exposure to CS.

NHBE cell cultures +/-AO were apically exposed to 1:100, 1:50 and 1:30 CS for 30min, air exposure was used as a control. Cultures were analysed 24hr post-exposure. Whole cells extracts were lysed following exposure. Lysates were resolved by reducing 1D SDS-PAGE electrophoresis followed by Western blotting and chemiluminescence detection. Proteins were analysed using primary antibodies specific to Prx III, Prx-SO₃, P-Erk1/2 and β-actin. Red denoted areas of interest, with elevated Prx-SO₃ in control cultures -AO, elevated P-Erk1/2 in cultures -AO exposed to 1:30 CS and reduced Prx-SO₃ in cultures +AO in comparison to cultures +AO at 3hr post-exposure.

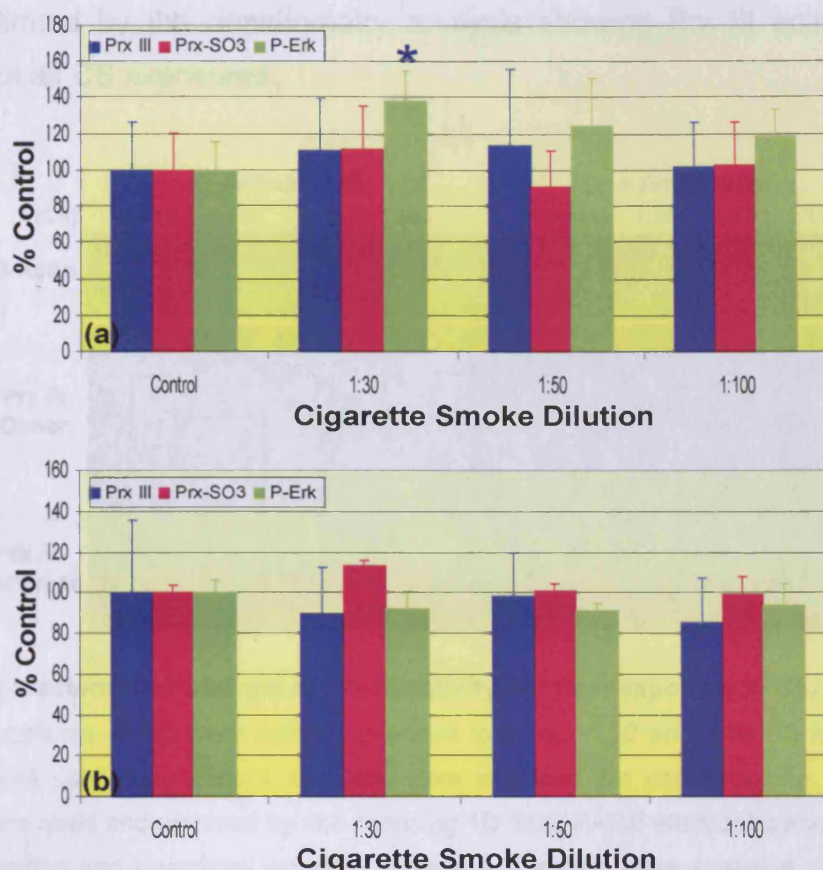


Figure 5.8: Densitometry analysis of total Prx levels 24hr post-exposure to CS.

The GeneTool software calculated Prx III (■), Prx-SO₃ (■) and P-Erk1/2 (■) band densitometry from Western blots (reducing conditions) of NHBE cell cultures (a) -AO and (b) +AO 24hr post-exposure to CS (air control, 1:30, 1:50 and 1:100 CS for 30min). Results were normalised using the corresponding β -actin expression. The asterisk (*) denoted significance ($P \leq 0.05$) and I signified \pm SD for $n=3$. There was elevated P-Erk1/2 in cultures -AO exposed 1:30 CS.

5.4.3 CS EXPOSURES: WESTERN BLOT ANALYSIS (ACTIVE PRX III)

At 3hr post-exposure to CS the NHBE cultures -/+AO were subjected to non-reducing gel electrophoresis conditions and analysed via Western blotting (Figure 5.9). In cultures -AO levels of monomeric Prx III (inactive Prx III) were elevated in cultures exposed to air controls and the 1:30 CS concentration. Subsequent densitometry evaluation revealed that only 55% of Prx III was active following the air exposure (Figure 5.10), which reduced to 53% following the 1:30 CS exposures. Conversely, in cultures +AO, the levels of dimeric Prx III (active Prx III) remained elevated throughout all exposures; this

was confirmed by the densitometry analysis showing Prx III activity ~80% throughout all CS exposures.

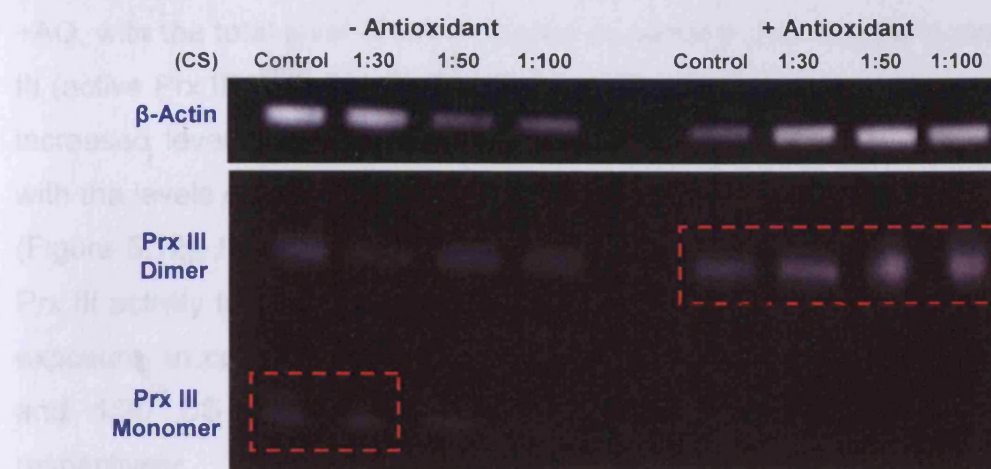


Figure 5.9: Western blot analysis of Prx III activity 3hr post-exposure to CS.

NHBE cell cultures \pm AO were apically exposed to 1:100, 1:50 and 1:30 CS for 30min, air exposure was used as a control. Cultures were analysed 3hr post-exposure. Whole cells extracts were lysed and resolved by non-reducing 1D SDS-PAGE electrophoresis followed by Western blotting and chemiluminescence detection. Proteins were analysed using primary antibodies specific to Prx III and β -actin. Dimers corresponded to active Prx III, whereas monomers represent hyperoxidised (inactive) Prx III. Red denoted areas of interest with elevated monomer levels in cultures -AO following the air control and 1:30 CS exposures, and consistently elevated dimer levels in cultures +AO following all exposures.

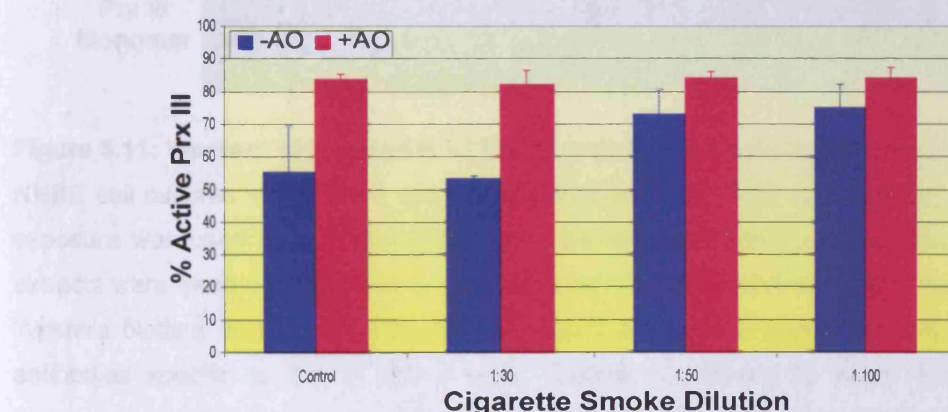


Figure 5.10: Densitometry analysis of Prx III activity 3hr post-exposure to CS.

The GeneTool software calculated band densitometry from Western blots (non-reducing conditions) of NHBE cell cultures -AO (■) and +AO (■) 3hr post-exposure to CS (air control, 1:30, 1:50 and 1:100 CS for 30min). Results were normalised using the corresponding β -actin expression. There was no significant ($P \leq 0.05$) increases/decreases in Prx III activity, I signified \pm SD for $n=3$.

At 24hr post-exposure to CS the NHBE cultures -/+AO were subjected to non-reducing gel electrophoresis conditions and analysed via Western blotting (Figure 5.11). The results revealed a contrast between cultures -AO and those +AO, with the total level of Prx III higher in cultures -AO. Levels of dimeric Prx III (active Prx III) in cultures -AO decreased at CS concentrations that elicited increased levels of monomeric Prx III (inactive Prx III); this was consistent with the levels of total Prx III, which remained stable throughout all exposures (Figure 5.12). In cultures -AO the air control exposure elicited a reduction in Prx III activity to 53%; this was further reduced to 46% following the 1:50 CS exposure. In cultures +AO the monomer levels increased following the 1:50 and 1:30 CS exposures, reducing Prx III activity to 69% and 55%, respectively.

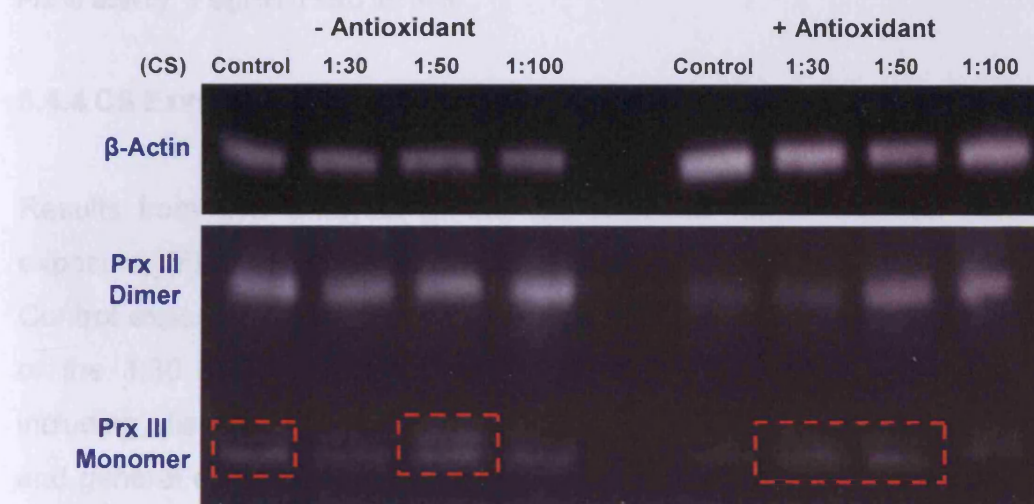


Figure 5.11: Western blot analysis of Prx III activity 24hr post-exposure to CS.

NHBE cell cultures -/+AO were apically exposed to 1:100, 1:50 and 1:30 CS for 30min, air exposure was used as a control. Cultures were analysed 24hr post-exposure. Whole cells extracts were lysed and resolved by non-reducing 1D SDS-PAGE electrophoresis followed by Western blotting and chemiluminescence detection. Proteins were analysed using primary antibodies specific to Prx III and β -actin. Dimers correspond to active Prx III, whereas monomers represent hyperoxidised (inactive) Prx III. Red denoted areas of interest with elevated monomer levels in cultures -AO following the air control and 1:50 CS exposures, and elevated monomer levels in cultures +AO following 1:50 and 1:30 CS exposures.

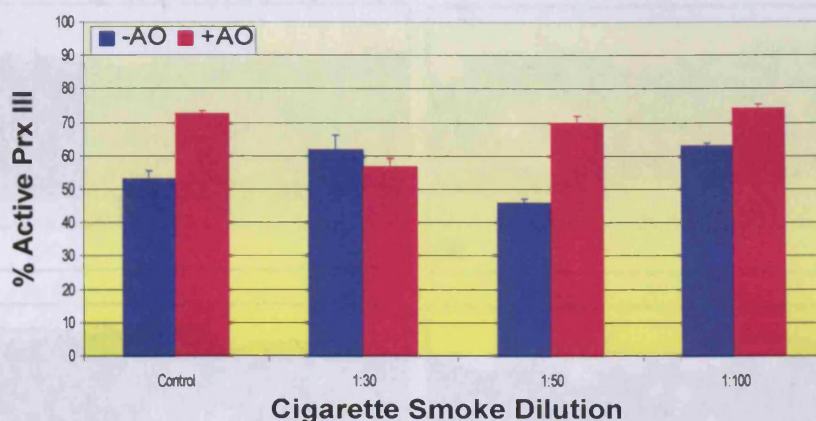


Figure 5.12: Densitometry analysis of Prx III activity 24hr post-exposure to CS.

The GeneTool software calculated -AO (■) and +AO (■) band densitometry from Western blots (non-reducing conditions) of NHBE cell cultures -/+AO 24hr post-exposure to CS (air control, 1:30, 1:50 and 1:100 CS for 30min). Results were normalised using the corresponding β -actin expression. There was no significant ($P \leq 0.05$) increases/decreases in Prx III activity, \bar{x} signified \pm SD for $n=3$.

5.4.4 CS EXPOSURE IHC ANALYSIS

Results from IHC analysis of the CS exposed NHBE cultures 24hr post-exposure (Figure 5.13) reinforced the corresponding Western blot data. Control exposures established negligible morphological damage, whereas all of the 1:30 CS exposed cultures contained varying degrees of damage, including, disruption of intercellular junctions, enlarged vacuoles, squamation and general epithelial degradation. The Prx III stained sections demonstrated no significant variation in expression between the control and the 1:30 CS exposed cultures. This correlated to Western blot data where levels of total Prx III did not increase or decrease significantly ($P \leq 0.05$), in cultures -/+AO, following CS exposures. In Prx-SO₃ stained sections there was a marked difference between cultures +AO and -AO, with elevated levels of Prx-SO₃ observed in control cultures -AO, which increased following 1:30 CS exposures. In contrast, control cultures +AO contained minimal levels of Prx-SO₃, with a detectable increase in levels following exposures at the 1:30 CS concentration.

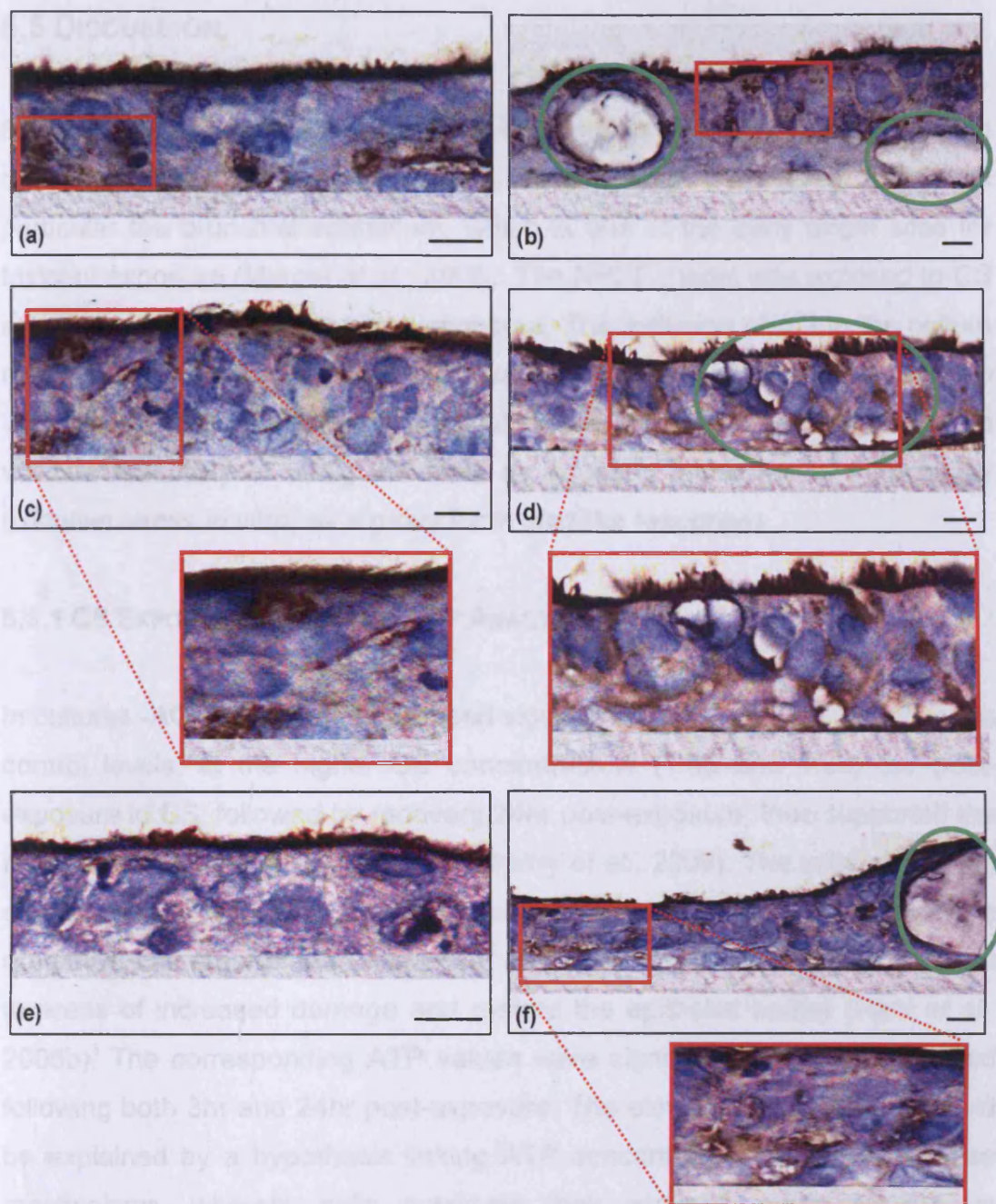


Figure 5.13: Chromogenic IHC analysis of the CS exposed NHBE cell cultures.

Paraffin-fixed 5µm sections from 30min CS exposed NHBE cultures were incubated overnight with Prx 1° ABs. Green denoted areas of damage as a result of CS exposures; red denoted areas of expression: (a) air exposed (control) cultures +AO 24hr post-exposure, moderate Prx III (1:2000) expression; (b) 1:30 CS +AO 24hr post-exposure, moderate Prx III (1:2000) expression; (c) air exposed cultures -AO 24hr post-exposure, elevated Prx-SO₃ (1:2000) expression; (d) 1:30 CS -AO 24hr post-exposure, elevated Prx-SO₃ levels; (e) Air exposed cultures +AO 24hr post-exposure, low Prx-SO₃ levels; (f) 1:30 CS +AO 24hr post-exposure, elevated Prx-SO₃ levels. DAB was used as a chromagen for immuno-positivity. Scale bars represented 10µm. Corresponding negative controls were clean (not shown).

5.5 DISCUSSION

Each CS inhalation has been shown to impart a significant oxidant burden onto the pulmonary epithelial cells (Foronjy and D'Armiento, 2006), in particular the bronchial epithelium, which is one of the early target sites for toxicant exposure (Mercer *et al.*, 2006). The NHBE model was exposed to CS and analysed 3hr and 24hr post-exposure. The inclusion of AO to the culture media was undertaken to resolve the oxidant/AO imbalance, and create an *in vitro* system to mimic the *in vivo* situation. CS exposures were employed to validate the utility of using the Prxs as an early biomarker of intracellular oxidative stress *in vitro*, as a proxy for *in vivo* like responses.

5.5.1 CS EXPOSURE: TEER AND ATP ANALYSIS

In cultures -AO, TEER values dropped significantly ($P \leq 0.05$), in comparison to control levels, at the higher CS concentrations (1:50 and 1:30) 3hr post-exposure to CS, followed by recovery 24hr post-exposure; thus supported the robust nature of the NHBE model (Balharry *et al.*, 2008). The initial disruption of epithelial cell junctions (i.e. 3hr post-exposure) may have been part of a protective and regeneration response, with cells detaching in order to migrate to areas of increased damage and restore the epithelial barrier (Park *et al.*, 2006b). The corresponding ATP values were significantly ($P \leq 0.05$) elevated following both 3hr and 24hr post-exposure. The elevation in ATP levels could be explained by a hypothesis linking ATP concentration to stress response mechanisms, whereby cells maximise their available adenylate pool in response to the increased oxidant burden (Ataullakhanov and Vitvitsky, 2002). This would account for the ATP increase observed as a result of CS exposure and furthermore the proportionate response recorded to increasing CS concentration.

In cultures +AO, there were no significant ($P \leq 0.05$) changes in TEER values for all CS exposures, both 3hr and 24hr post-exposure. This may have indicated enhanced culture resistance as a consequence of AO supplementation (Leist *et al.*, 1996). The ATP response was biphasic

(Calabrese, 2004) in nature, characterised by a low dose stimulation that was followed by a high dose inhibition (Rozman and Doull, 2003; Balharry *et al.*, 2008). When comparing the ATP results 3hr and 24hr post-exposure, there was a definite repair response evident, with the higher concentration needed to elicit the same initial stimulation with regard to the biphasic effect. A biphasic response was also elicited in +AO cultures exposed to GOx (Chapter 4). This reproducibility further strengthened the use of the AO supplemented NHBE model in toxicological screening, in addition to Prx as a biomarker of oxidant injury severity and repair competency.

5.5.2 CS EXPOSURE: WESTERN BLOT ANALYSIS

The Western blot analysis was used to determine the sensitivity of Prx as a potential biomarker of oxidative stress. CS contained several thousand compounds (Hansel and Barnes, 2004), including H₂O₂ (Pryor and Stone, 1993). Therefore, CS exposure would be expected to initiate a more complex and synergistic response, in comparison to the H₂O₂ exposure (Cantin, 2010). Cell cultures -/+AO when exposed to CS and analysed under reducing conditions elicited elevated Prx hyperoxidation 3hr and 24hr post-exposure. This inferred that a substantial oxidant burden was imparted onto the cultures by the CS, and that Prx oxidation state was a reliable measure of this. As with the ATP results, it was apparent that cultures -AO were not viable when analysing intracellular stress via the Prx system, with results 24hr post-exposure not indicating recovery, with regard to Prx hyperoxidation or P-Erk1/2 levels. This corroborated with data from several previous studies whereby cells supplemented before toxicant exposure were able to withstand greater insults (Leist *et al.*, 1996; Greer *et al.*, 2005). In contrast, the cultures +AO displayed Prx hyperoxidation proportionate to CS concentration, and hence, oxidative stress levels. The Western blot (Figure 5.5) revealed significantly ($P \leq 0.05$) increased levels of Prx-SO₃, in the +AO cultures, 3hr post-exposure that had decreased by 24hr post-exposure. The ability of the cells to demonstrate recovery post-exposure, at biochemical and morphological levels, enhanced not only the cultures *in vivo* comparability, but

also the Prxs responsiveness and sensitivity as a biomarker of intracellular oxidative stress.

The results from non-reduced CS exposed cultures -/+AO contradicted those obtained from the reduced blots, with levels of hyperoxidised Prx III (monomers) elevated at 24hr post-exposure in comparison to 3hr post-exposure -/+AO cultures. The reason for the discrepancy between the reduced and non-reduced data may have been due to the reduced results recording the total levels of Prx hyperoxidation (including Prx I, II, III and IV), whereas the non-reduced only reported the active (dimer) or hyperoxidised (monomer) Prx III (Cox *et al.*, 2010a). However, one aspect remained consistent, with hyperoxidised levels in -AO cultures continually surpassing those in the corresponding +AO cultures (Phalen *et al.*, 2006).

5.5.3 CS EXPOSURE: IHC ANALYSIS

The histological analysis was undertaken to establish morphological changes to the BE as a result of CS. The preliminary effect of CS was a reduction in cilia beat frequency (Simet *et al.*, 2010), preceding a total loss of cilia attachments (Sisson *et al.*, 1994). Previous work by Prytherch and co-workers identified loss of cilia and microvillus as a consequence of CS exposure, in conjunction with squamation and de-differentiation (Prytherch, 2010), accordingly, there was a distinct reduction in cilia number following the 1:30 CS exposures within cultures -/+ AO. In addition to the cilia damage the 1:30 CS exposed cultures -/+AO also sustained, disruption to intercellular junctions, enlarged vacuoles and squamation, which corroborated work by Sexton and co-workers, whereby the NHBE cultures were exposed to individual tobacco smoke components (Sexton *et al.*, 2008). The IHC analysis substantiated the Western blot data by displaying elevated levels of Prx hyperoxidation in control cultures -AO, in contrast to the minimal levels in +AO cultures, denoting reduced levels of oxidative stress due to AO supplementation (Leist *et al.*, 1996). The results obtained from the IHC analysis further strengthened the ability of Prx oxidation state to act as a reliable marker of intracellular oxidative stress, with levels of Prx-SO₃ visibly

increased following CS exposure. The IHC analysis confirmed Western blot results of lower levels of Prx-SO₃ within the NHBE cultures +AO in comparison to cultures -AO.

5.6 CONCLUSION

The CS exposure findings were consistent with the GOx data (Chapter 4) and upheld the ability of the Prxs to act as biomarkers of increased oxidant burden. The collective results verified the significant ($P \leq 0.05$) benefits brought through AO supplementation, showing that CS imparted a greater oxidant burden on cultures -AO, in comparison to cultures +AO. The Prx-SO₃, P-Erk1/2 and ATP levels did not recover by 24hr post-exposure, which suggested that the -AO cultures were unable to maintain the stable phenotype maintained in +AO cultures following CS exposures. Consequently, in cultures -AO, increased levels of Prx-SO₃ would exhibit biochemical instability, for which Prx oxidation state would act as a consistent biomarker. In +AO cultures, the biphasic ATP response further confirmed the use of the NHBE model in conjunction with the Prx system, with repair responses at the biochemical and morphological levels being observed. With regard to Prx as a biomarker of intracellular oxidative stress, its oxidation state has been shown to be sensitive enough to detect recovery responses; which will be further examined in Chapter 6.

The CS exposure findings were consistent with the GOx data (Chapter 4) and upheld the ability of the Prxs to act as biomarkers of increased oxidant burden. The collective results verified the significant ($P \leq 0.05$) benefits brought through AO supplementation, showing that CS imparted a greater oxidant burden on cultures -AO, in comparison to cultures +AO. The Prx-SO₃, P-Erk1/2 and ATP levels did not recover by 24hr post-exposure, which suggested that the -AO cultures were unable to maintain the stable phenotype maintained in +AO cultures following CS exposures. Consequently, in cultures -AO, increased levels of Prx-SO₃ would exhibit biochemical instability, for which Prx oxidation state would act as a consistent biomarker. In +AO

cultures, the biphasic ATP response further confirmed the use of the NHBE model in conjunction with the Prx system, with repair responses at the biochemical and morphological levels being observed. With regard to Prx as a biomarker of intracellular oxidative stress, its oxidation state has been shown to be sensitive enough to detect recovery responses; which will be further examined in Chapter 6.

CHAPTER 6:

***IN VIVO* CORRELATION OF PEROXIREDOXIN STATUS**

6.1 INTRODUCTION

In vivo correlation is integral to the validation and development of *in vitro* analysis (Emami, 2006), and as such, it was essential that Prx status within the NHBE model was comparable to that of the *in vivo* situation. To assess this IHC was performed, using 1° Prx ABs, on human lung tissue that contained a variety of epithelial phenotypes (i.e. re-epithelisation, basal cell hyperplasia, goblet cell hyperplasia and inflammation). These epithelial phenotypes (excluding inflammation) also represented the various stages of NHBE recapitulation from patient donors upon cell culturing (Prytherch, 2010). All samples were retrieved from very severe, i.e. GOLD4 (GOLD, 2006) COPD patients, that had undergone total lung transplants. Unfortunately, there was no healthy lung tissue available for direct comparison, therefore all Prx status comparisons were carried out between the tissues obtained from the three GOLD4 patients. The COPD lung tissue was prepared in the same manner, for histopathological and IHC assessments, as the NHBE cultures.

In conjunction with Prxs, the expression of cytokeratin 5/6 (CK 5/6) was also analysed. The cytokeratins are a family of intermediate filaments (Ordonez, 1998) that form three-dimensional filament arrays extending from the nucleus to the cell membrane. They are integral for the maintenance of cell shape and viability (Presland and Jurevic, 2002) and have been extensively used to differentiate between epithelial cell types (Kasper *et al.*, 1993). CK 5/6 is also a basal cell marker (Presland and Dale, 2000) used to evaluate the injury and repair capacity of the epithelium (Pierce *et al.*, 1994).

6.1.1 RESEARCH AIMS

The research aims for experimental work in Chapter 6 (Figure 6.1) were as follows:

- Obtain human bronchial tissue samples from COPD (GOLD4) patients that had undergone total lung transplants.

- Undertake pathological assessment of the human bronchial tissue samples through H+E staining.
- Utilise the IHC chromogenic detection system to analyse CK 5/6 expression and Prx status, including expression level and oxidation state, within the human bronchial tissue samples.

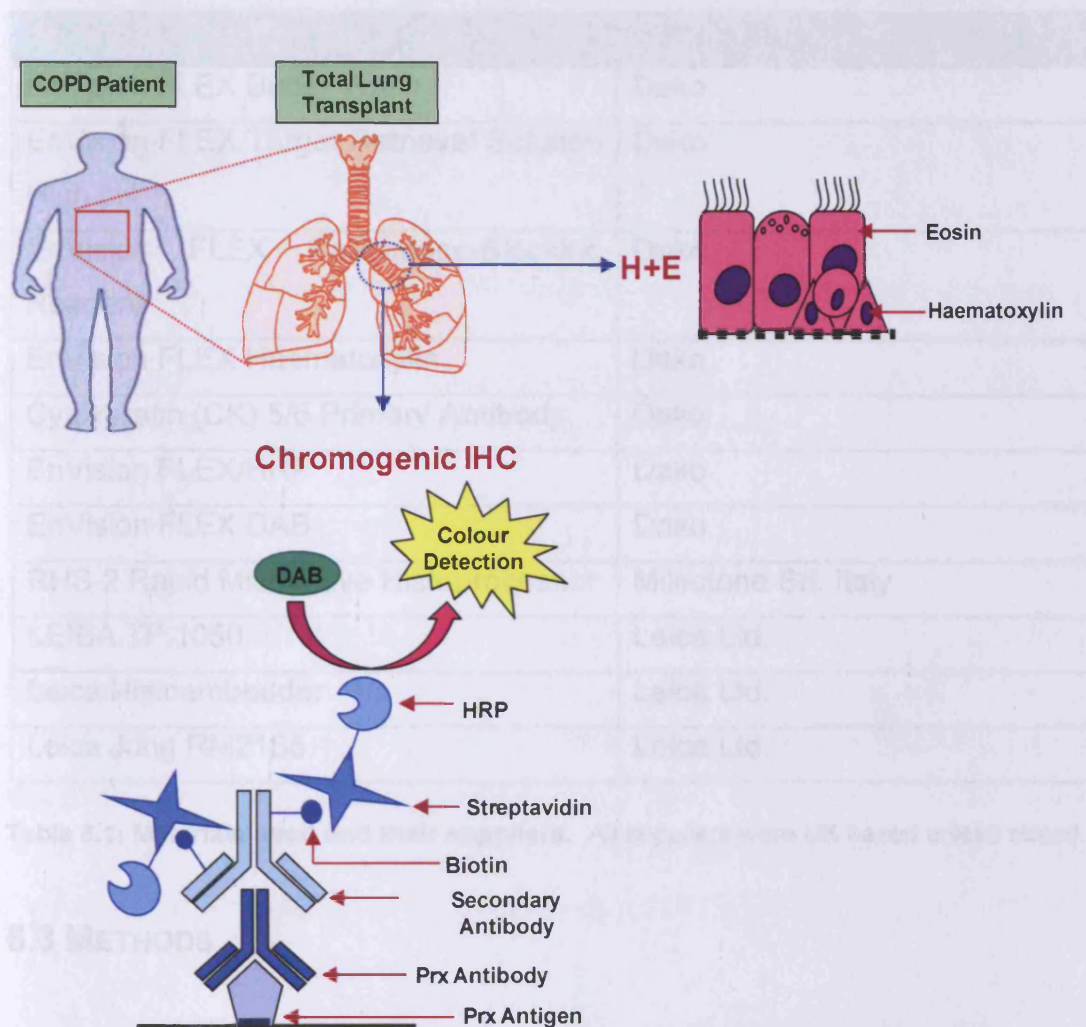


Figure 6.1: Flowchart of experimental work in Chapter 6.

Experimental aims included histological analysis utilising H+E staining, and immunological (IHC) analysis which utilised the Prx 1^o ABs along with the chromogenic DAB detection system. These methods were used to analyse the tissue pathology and Prx status within BE samples from COPD (GOLD4) patients.

6.2 MATERIALS AND STOCK SOLUTIONS

Materials and stock solutions from previous Chapters have not been included.

6.2.1 MATERIALS AND SUPPLIERS

MATERIALS:	SUPPLIER:
EnVision FLEX Buffer Wash	Dako
EnVision FLEX Target Retrieval Solution High pH	Dako
EnVision FLEX Peroxidase-Blocking Reagent	Dako
EnVision FLEX Haematoxylin	Dako
Cytokeratin (CK) 5/6 Primary Antibody	Dako
EnVision FLEX/HRP	Dako
EnVision FLEX DAB	Dako
RHS-2 Rapid Microwave Histoprocessor	Milestone Srl. Italy
LEICA TP 1050	Leica Ltd.
Leica Histoembedder	Leica Ltd.
Leica Jung RM2155	Leica Ltd.

Table 6.1: Materials used and their suppliers. All suppliers were UK based unless stated.

6.3 METHODS

6.3.1 HISTOLOGICAL ANALYSIS OF THE HUMAN TISSUE SAMPLES

Tissue processing, i.e. paraffin embedding, sectioning and haematoxylin and eosin (H+E) staining, was carried out in the AstraZeneca Histology Department, Loughborough, UK. Experiments were performed with the expert guidance of Dr. Kate Brown.

6.3.1.1 SAMPLE ACQUISITION

Lung lobes from COPD (GOLD4) patients whom underwent total lung transplants (Table 6.2) were provided by AstraZeneca, and originally obtained from the University Hospital of Leicester, with full ethical consent.

Patient (N°)	Age	Gender	Smoking Status	Lobe Data
3	46	Male	Ex-Smoker	Left Lower Lobe
4	55	Female	Ex-Smoker	Left Lower Lobe
9	52	Female	Ex-Smoker	Right Lower Lobe

Table 6.2: Demographics of Three COPD Patients undergoing total lung transplants.

Three COPD (GOLD4) patients underwent total lung transplants, all were ex-smokers. Patient 3 was deficient in α -1 antitrypsin, and therefore more emphysematous histopathology was expected. One lobe was taken from each patient for IHC analysis.

6.3.1.2 SAMPLE PREPARATION

The tissue samples were fixed in 10% NBF for 48hr at RT, and then dissected into 3mm slices for overnight embedding using a Leica Tissue Processor (LEICA TP 1050 fully enclosed vacuum tissue processor). Embedded tissues were then dehydrated using a series of increasing alcohol concentrations (i.e. 30%, 50%, 70%, 90% and 100%) prior to being placed into paraffin wax using the Leica Histoembedder. Final wax-tissue blocks were stored at RT until use.

6.3.1.3 SECTIONING, DE-WAXING AND HAEMATOXYLIN AND EOSIN STAINING

Sections were cut to 4 μ m thickness using a Leica Jung RM2155. The sections were floated on water at 37°C, and subsequently transferred to charged slides that were dried overnight at 45°C. De-waxing was performed as outlined in Section 3.3.1.4. H+E staining was performed as outlined in Section 3.3.1.5

6.3.2 CHROMOGENIC IMMUNOHISTOCHEMISTRY OF THE HUMAN TISSUE SAMPLES

Sample preparation and de-waxing procedures were carried out as described in Sections 6.3.1.1 to 6.3.1.3.

6.3.2.1 ANTIGEN RETRIEVAL

Pre-treatment allowed the target retrieval of antigens prior to IHC staining procedures. Following de-waxing, the slides were submerged in EnVision FLEX target retrieval solution high pH and heated to 98°C for 1min in the rapid microwave histoprocessor. Slides were then allowed to cool for 5min before being immersed in the EnVision FLEX wash buffer at RT.

6.3.2.2 ANTIBODY INCUBATION AND DETECTION

Following pre-treatment, slides were washed using the EnVision FLEX wash buffer for 2min (3x). To block endogenous peroxidase activity, the slides were immersed in EnVision FLEX peroxidase-blocking reagent (further blocking steps were unnecessary) for 5min. Slides were then incubated with Prx 1° AB (Table 6.2) or serum control (a negative control was performed for every dilution of primary antibodies used). ABs were diluted in 1% BSA/PBS + 0.05% Tween.

Following 1° AB incubation, the slides were submerged in EnVision FLEX wash buffer for 2min (3x); slides were then incubated with EnVision FLEX/HRP for 20min. Slides were again submerged EnVision FLEX wash buffer for 2min (3x). To allow AB visualisation, the slides were incubated with FLEX DAB chromogen solution (Table 6.3). The chromogen was removed by placing the slides under running tap water for 2min, followed by counter-staining by briefly immersing in EnVision FLEX haematoxylin. Any excess staining was removed by washing the slides in running tap water for 10min. Dehydration and mounting was carried out as described in Chapter 3, Section 3.3.1.6.

1° Antibody	Dilution	Final Concentration	Incubation Period	DAB Incubation Period
Prx I	1:500	2µg/ml	20min (RT)	5min
Prx III	1:5000	200ng/ml	20min (RT)	5min
Prx-SO ₃	1:2000	500ng/ml	20min (RT)	10min
CK 5/6	1:30	33.3µg/ml	20min (RT)	5min

Table 6.3: Optimisation of 1° AB concentrations and incubation periods.

The 1° AB concentrations and incubation times used for Prx I, III, -SO₃ and CK 5/6 detection within the BE of COPD patient samples. All 1° AB stock concentrations were 1mg/ml.

6.4 RESULTS

The featured sections were representative of all three COPD patients.

6.4.1 GROSS PATHOLOGY

Bronchial tissue samples were taken from three COPD (GOLD4) patients that had undergone total lung transplants. One lobe from each patient (Table 6.2) was used for histopathology and IHC analysis. The lobe from Patient 9 (Figure 6.2) was blackened in appearance and contained significant lesions and tar deposits on the external surface that pervaded throughout the lobe; this was consistent with observations from all three patient lobes. The lung pathology was caused by persistent and heavy smoking, restricting the patients' airflow, and eventually leading to loss of lung function, and hence, the need for a total lung transplant.

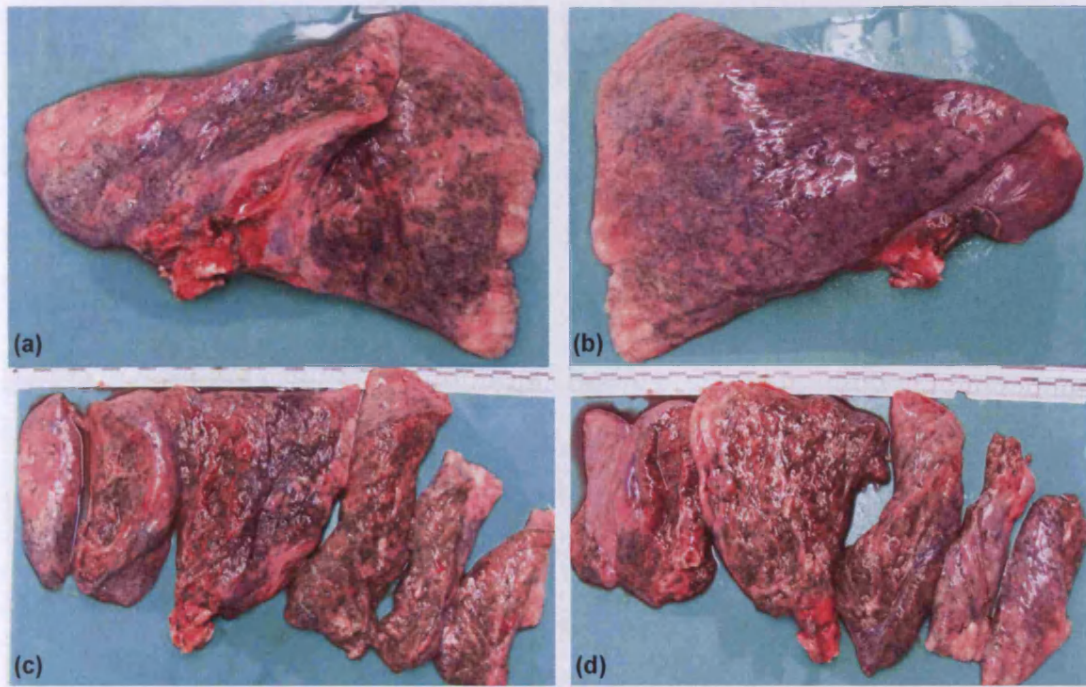


Figure 6.2: Right lower lobe from Patient 9.

AstraZeneca obtained one lobe from each COPD (GOLD4) patient undergoing a total lung transplant (Patients 3, 4 and 9). The right lower lobe of Patient 9 (a and b) revealed tar accumulation, as a result of heavy and persistent smoking, that was visible throughout the entire lobe (c and d). The appearances of the lobes from all three patients were consistent with that of Patient 9.

6.4.2 RE-EPITHELISATION (EARLY STAGE REPAIR)

Serial sections of the remodelling airway demonstrated a severely injured, and consequently, denuded epithelium with areas of goblet cell hyperplasia (GCH) (Figure 6.3). The denudation triggered a repair attempt whereby the remaining basal (progenitor) cells proliferated along the exposed airway in order to repopulate the area (i.e. re-epithelisation), resulting in a leading edge effect which could be seen via the CK 5/6 staining. Prx III expression was detected within the immature basal cells during early stage re-epithelisation and within the areas of GCH along with elevated Prx-SO₃. In regard to COPD pathologies, there was excess mucus throughout the lumen due to GCH.

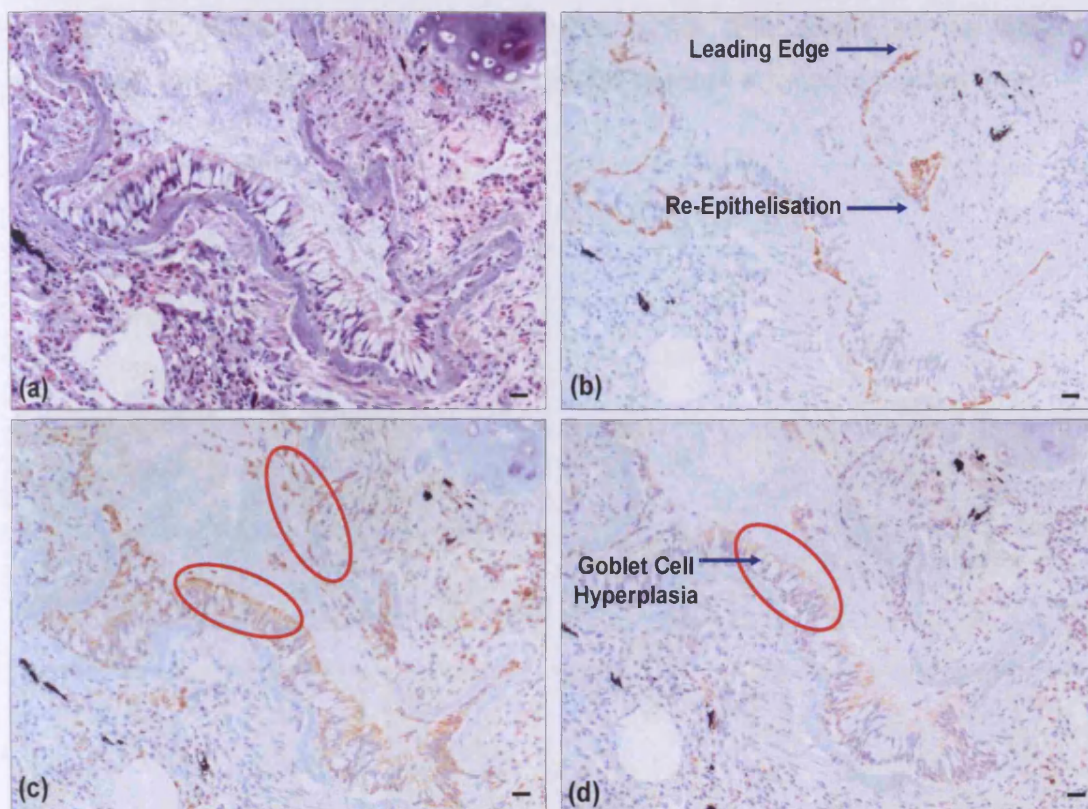


Figure 6.3: Early stage repair (Re-epithelisation).

Serial sections of a BE from the lower right lobe of Patient 9 contained re-epithelisation and GCH (prominent mucus granules), demonstrated by H+E staining (a). Basal cells, denoted by CK 5/6 expression (b), were proliferating in order to repopulate the denuded airway. Red denoted areas of interest, with Prx III expression (c) within the basal cells during re-epithelisation and in the apical regions of the columnar cells during hyperplasia. There was also Prx-SO₃ (d) detected within the regions of hyperplasia. Scale bars represented 20µm.

Following histological and immunohistological analysis of serial sections, an airway containing several different stages of remodelling was observed (Figure 6.4). Within the single airway there were regions of re-epithelisation and hyperplasia. The earliest stage of repair, re-epithelisation, was indicated by squamous epitheloid and basal (progenitor) cells, whereby the basal cells proliferated to protect the exposed airway; within this region there was no Prx I expression. The hyperplastic region contained a disorganised epithelium, characterised by excessive columnar cell numbers and basal cells admixed within columnar cell regions, associated with elevated Prx I expression. The areas of the epithelium that appeared morphologically 'normal' (i.e. organised pseudo-stratified epithelium) contained lower Prx I expression in comparison

to the hyperplastic region. It should be noted this albeit normal-looking epithelium may not be representative of that seen in a healthy human lung.

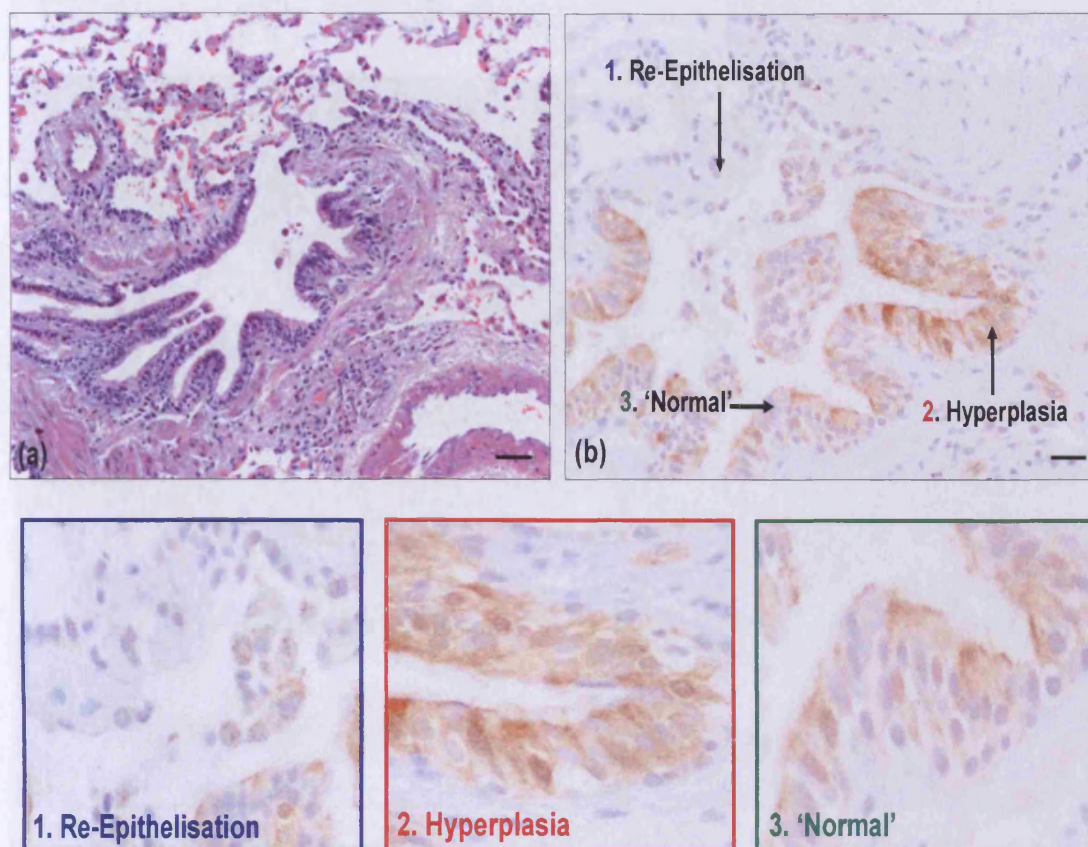


Figure 6.4: Repairing airway.

Serial sections of a BE from the lower left lobe of Patient 3 contained a repairing airway with several stages of remodelling, visualised via H+E staining (a). The three stages of remodelling included: (1) early stage repair and re-epithelisation, with no Prx I expression (b); (2) areas of hyperplasia, with elevated levels of Prx I expression (b); (3) areas of epithelia that appeared morphologically 'normal' (i.e. organised pseudo-stratified epithelium) contained moderate Prx I expression (b). Scale bars represented (a) 20µm and (b) 10µm.

6.4.3 HYPERPLASIA

The relatively small airway contained a thickened basement membrane, indicating a degree of remodelling following injury (Figure 6.5). The CK 5/6 expression was consistently present in the basal cells adjacent to the basement membrane, with some staining in the columnar cell region. Prx III was expressed mainly in the apical regions of the columnar cells, in particular in the regions of increased hyperplasia. The mucus within the numerous

goblet cells was highly visible, however no Prx III or -SO₃ was present in these regions. Prx-SO₃ expression followed a similar distribution pattern to Prx III.

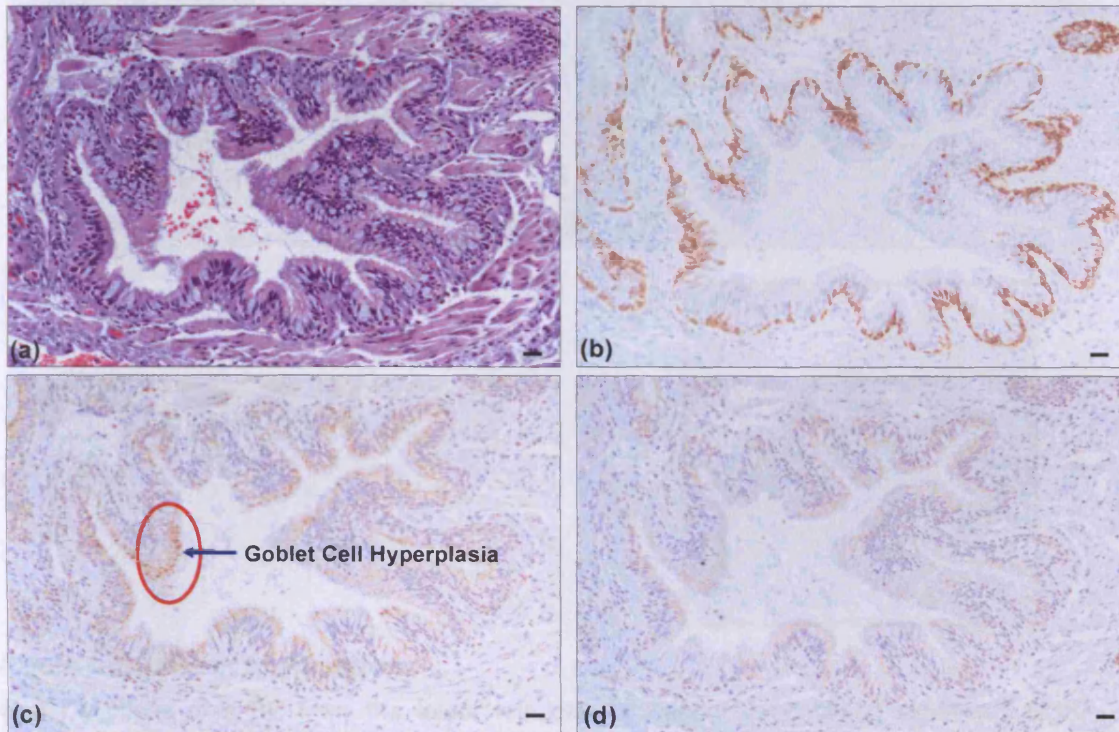


Figure 6.5: Goblet cell hyperplasia.

Serial sections of a BE from the lower left lobe of Patient 3 contained areas of GCH observed via H+E staining (a). Consistent CK 5/6 expression (b) indicated a healthy basal cell population. Red denoted areas of interest, with elevated Prx III (c) in regions of hyperplasia and Prx-SO₃ (d) following a similar distribution pattern to Prx III. Scale bars represented 20µm.

Histological assessment of the serial sections revealed basal cell hyperplasia (BCH) throughout the BE of the airway (Figure 6.6). Hyperproliferation of the progenitor (basal) cells was consistent with airway repair, as the re-epithelisation of the damaged BE exceeded the requirement, leading to hyperplasia. There was no Prx I expression within the basal cells including those in the areas of BCH. The columnar cells appeared to be expressing Prx I, with the stronger staining present in the more disorganised hyperplastic regions, adjacent to the region of BCH.

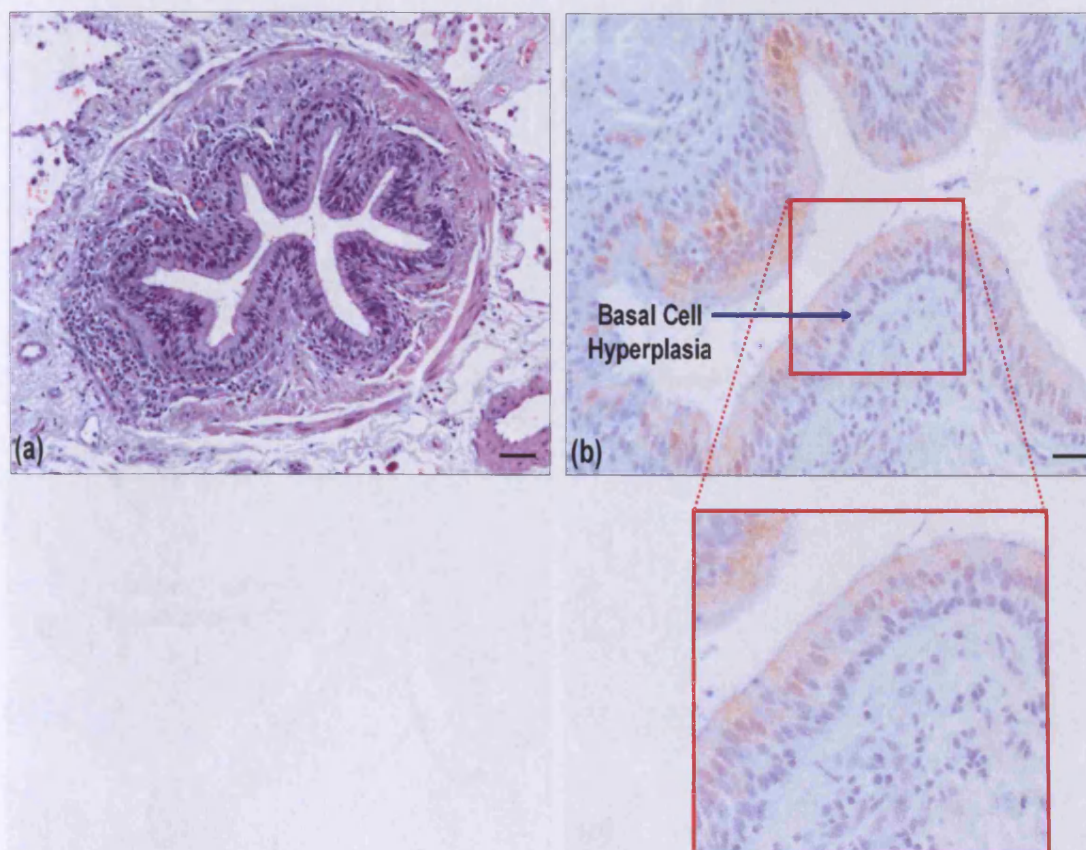


Figure 6.6: Basal cell hyperplasia.

Serial sections of a BE from the lower left lobe of Patient 4 contained significant BCH, demonstrated by the H+E staining (a). Red denoted areas of interest with no Prx I expression (b) within the basal cells, and moderate levels throughout the columnar cells. Scale bars represented (a) 20µm and (b) 10µm.

Histological and IHC assessment revealed regions of BCH and GCH, suggestive of airway remodelling (Figure 6.7). The CK 5/6 expression was elevated in areas of BCH. There was also CK 5/6 expression extending throughout some areas populated by columnar cells, indicating either regions of incomplete differentiation or regions with admixed basal and columnar cell populations. Prx III expression was elevated in regions of GCH, particularly toward the apical region of the columnar cells. Prx-SO₃ was highly elevated as a result of GCH, following a similar distribution pattern to Prx III. With regard to the COPD pathology, there was excessive mucus and inflammatory cells present in the lumen of the airway, which could result in increased the levels of oxidative stress.

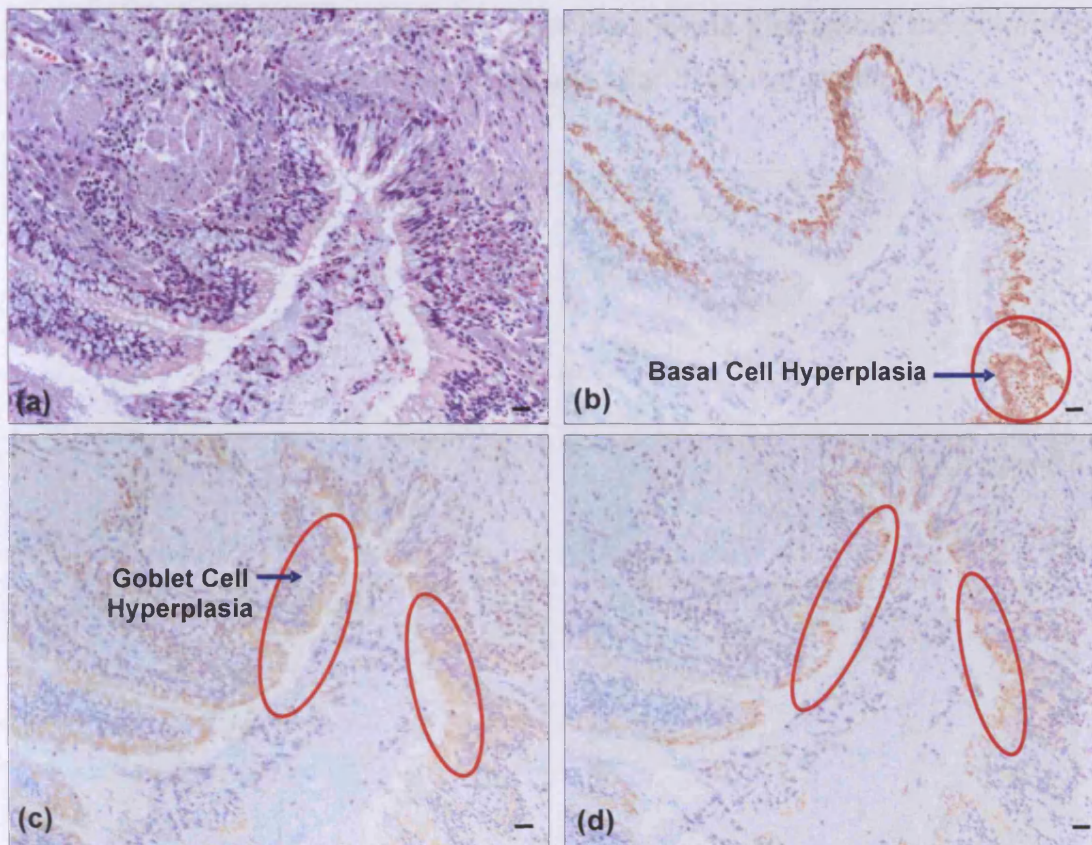


Figure 6.7: Goblet and basal cell hyperplasia.

Serial sections of a BE from the lower right lobe of Patient 9 underwent H+E staining (a), which revealed GCH indicative of late stage remodelling and elevated oxidative stress. Red denoted areas of interest with elevated CK 5/6 expression (b) in areas of BCH, with moderate Prx III and Prx-SO₃ in this region. There was elevated Prx III (c) and Prx-SO₃ (d) levels within the regions of GCH. Scale bars represented 20µm.

6.4.4 INFLAMMATION

Histological analysis, of BE serial sections, identified an acute inflammatory response within the airway, which was confirmed by the abundance of macrophages and mononuclear cells within the surrounding lamina propria (Figure 6.8). The macrophages stained highly positive for Prx III, and moderately for Prx-SO₃. This occurred for all sections analysed from each of the three COPD (GOLD4) patients. In comparison, the lymphocytes did not stain for Prx III or Prx-SO₃. Prx III levels were also elevated throughout the BE during inflammation, with the apical region of the columnar cells demonstrating particularly high expression. The staining for Prx-SO₃ followed

a similar pattern to that of Prx III, with high levels throughout the columnar cells; suggesting elevated levels of intracellular oxidative stress.

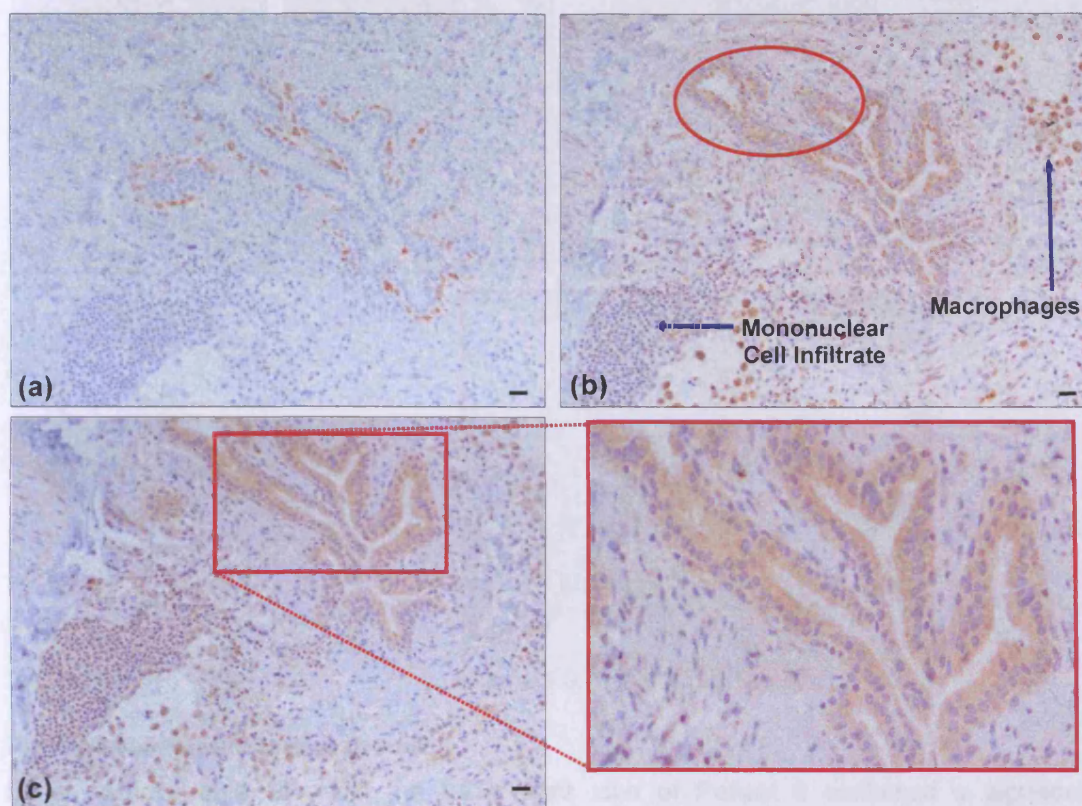


Figure 6.8: Inflammatory response.

Serial sections of a BE from the lower left lobe of Patient 4 contained severe inflammation, with an influx of mononuclear cells and macrophages, under these conditions there were increased levels of ROS. CK 5/6 expression (a), red denoted areas of interest with elevated Prx III (b) and Prx-SO₃ (c) within the airway as a result of the inflammatory response. Scale bars represented 20µm.

The inflammatory cell influx, elicited due to airway damage, was observed in the surrounding lamina propria of the entire airway (Figure 6.9). Consequently, the columnar cells of the BE responded through increasing Prx I expression within these regions. The regions of particularly high Prx I expression appeared hyperplastic in nature, in comparison to the regions with more moderate Prx I expression. Prx I was not expressed within the basal cells throughout all epithelial phenotypes.

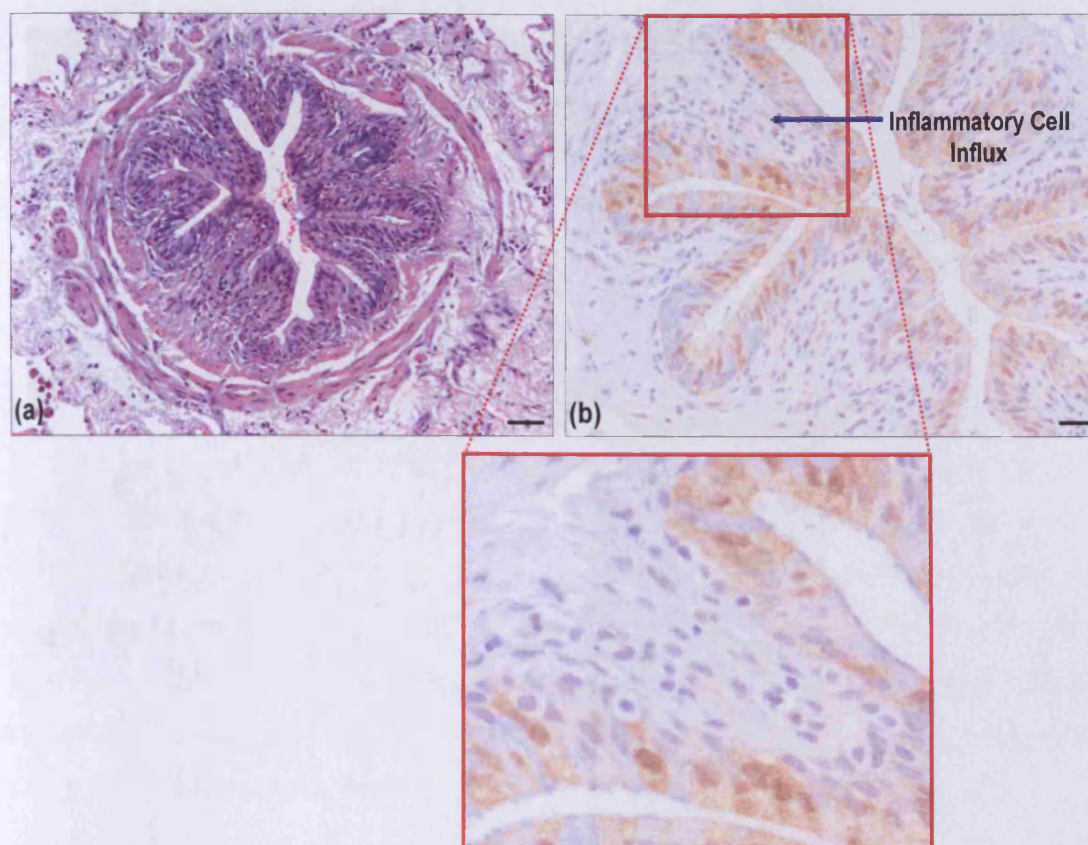


Figure 6.9: Inflammatory response.

Serial sections of a BE from the lower right lobe of Patient 9 contained a significant inflammatory cell influx, seen via the H+E stain (a). Red denoted areas of interest, with elevated Prx I expression (b) as a consequence of the inflammatory response. Scale bars represented (a) 20 μ m and (b) 10 μ m.

6.4.5 ENDOTHELIUM/ SMOOTH MUSCLE

The endothelium in samples from all three COPD (GOLD4) patients stained consistently positive for Prx III. However, the endothelial cells of the endothelium in close proximity to a damaged or repairing/remodelling airway had elevated levels of Prx III expression (Figure 6.10), which correlated with an inflammatory response triggered by the damaged airway. The staining extends beyond the endothelium to the smooth muscle surrounding the vessel, which could also be indicative of elevated oxidative stress within the tissue.

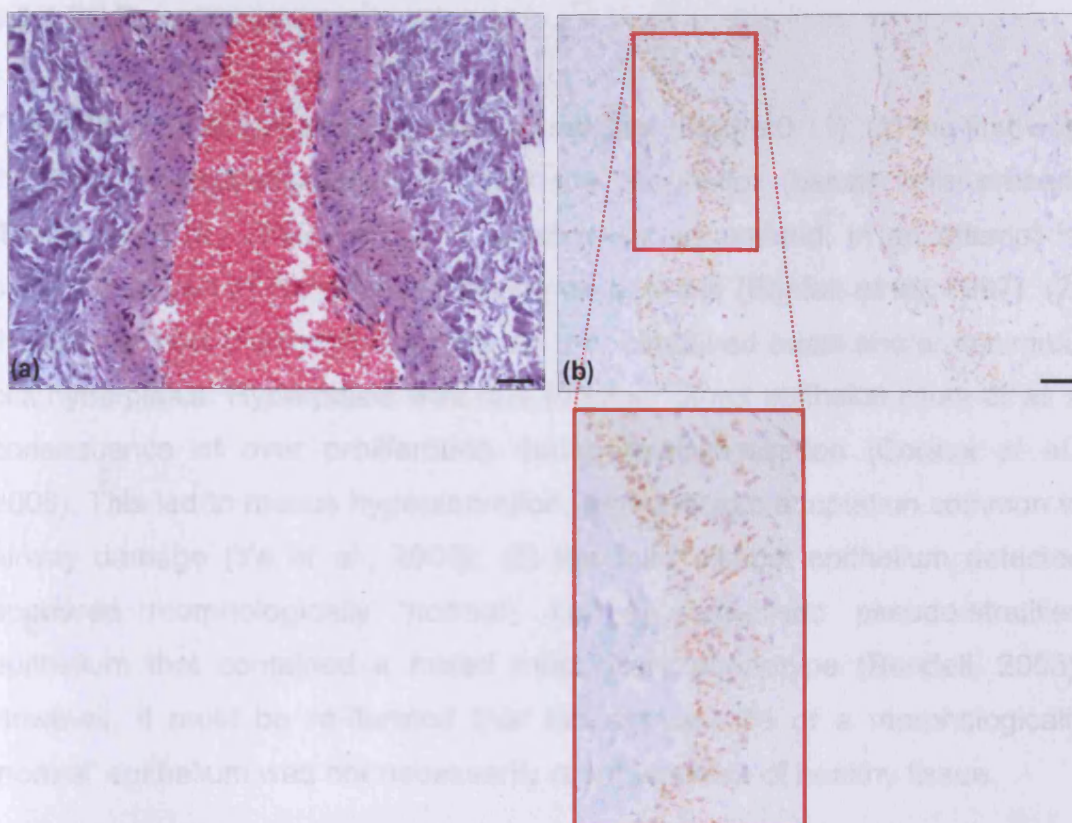


Figure 6.10: Endothelium/ Smooth muscle.

Serial sections of a BE from the lower left lobe of Patient 3 contained an endothelium adjacent to a repairing airway. The red blood cells and the surrounding endothelium were observed by H+E staining (a). Red denoted areas of interest, with elevated Prx III expression (b) within the endothelial cells of endothelium in close proximity to damaged/repairing airways. These levels, of Prx III, were elevated in comparison to the more moderate levels observed within endothelial cells not associated with an injured airway. Prx III expression also extended throughout the smooth muscle surrounding the endothelium. Scale bars represented 20µm.

6.5 DISCUSSION

Correlation with *in vivo* data was essential for validating the results obtained from the NHBE cell model. Human tissue often demonstrated several stages of injury and repair within the same airway (Puchelle *et al.*, 2006), which provided crucial information on the role of Prxs during BE remodelling; in concordance with the NHBE cell model morphogenesis. No healthy lung tissue was available for comparison therefore all Prx analysis was undertaken using comparative tissue from the three GOLD4 patients.

6.5.1 BE REMODELLING

There were three key stages in BE remodelling (Figure 6.11): (1) the first was the initial re-epithelisation, with only the progenitor (basal) cells present (Bucchieri *et al.*, 2009), some of which were squamated, in an attempt to protect as much of the exposed airway as possible (Erjefalt *et al.*, 1997): (2) the second was the hyperplasic region that contained basal and/or columnar cell hyperplasia. Hyperplasia was due to either direct epithelial injury or as a consequence of over proliferation during re-epithelisation (Coraux *et al.*, 2008). This led to mucus hypersecretion, a phenotypic adaptation common to airway damage (Ye *et al.*, 2009): (3) the third distinct epithelium detected appeared morphologically 'normal', i.e. an organised pseudo-stratified epithelium that contained a mixed mucociliary phenotype (Randell, 2006). However, it must be re-iterated that the appearance of a morphologically 'normal' epithelium was not necessarily representative of healthy tissue.

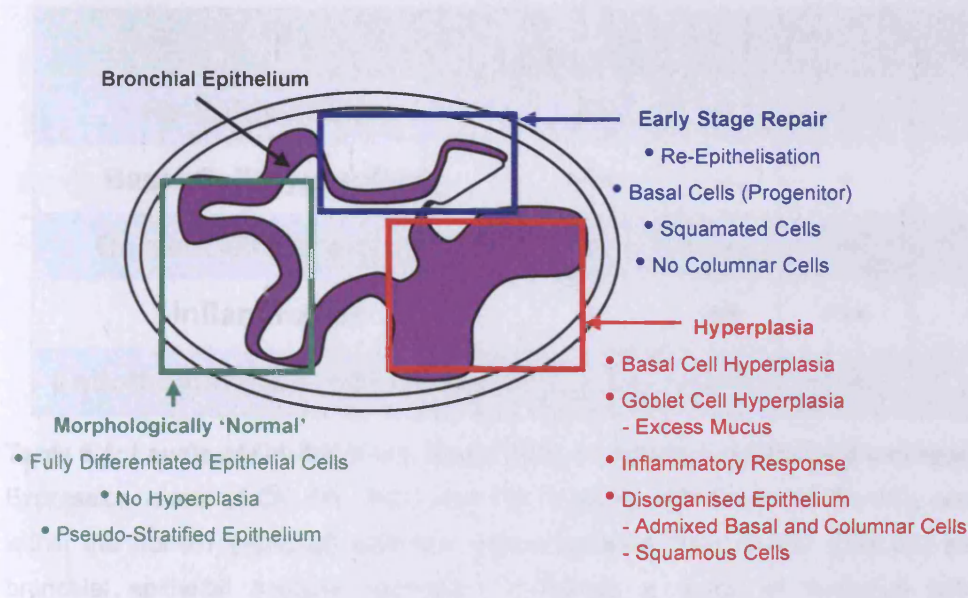


Figure 6.11: Three main stages of BE remodelling.

There were three main stages of remodelling evident in the human BE tissues analysed. The first was early stage repair (blue), whereby the epithelium had either been totally or partially denuded; in response to this the basal (progenitor) cells proliferated to re-populate the epithelium. The second stage contained a hyperplasic epithelial subtype (red), due to either direct epithelial injury or as a consequence of over proliferation during re-epithelisation. The third distinct epithelium detected was an epithelium that appeared morphologically 'normal' (i.e. organised pseudo-stratified epithelium) (green) containing fully differentiated bronchial epithelial cell types.

6.5.2 PRX AND CK 5/6 LEVELS IN THE BE OF THREE COPD PATIENTS

The samples from the three COPD patients demonstrated consistent Prx expression levels and oxidation states within the distinct epithelial phenotypes (Table 6.4). The expression levels of CK 5/6 were very high in areas of BCH, compared to moderate expression in areas of GCH. Prx I expression was not detectable within the basal cells, even within regions of BCH; however, there was increased expression in areas of GCH and inflammation. Prx III expression was elevated in regions of inflammation and hyperplasia, in addition to this Prx III was detected within the endothelial cells of endothelium in close proximity to damaged airways, which also extended throughout the surrounding smooth muscle of the vessels. The levels of Prx-SO₃ increased considerably in airways affected by oxidative stress i.e. inflammation and GCH.

Epithelial Phenotype	CK 5/6	Prx I	Prx III	Prx-SO ₃
Re-Epithelisation	++	–	+	+
Basal Cell Hyperplasia	+++	–	+	+
Goblet Cell Hyperplasia	+	++	++	++
Inflammation	+	++	+++	+++
Endothelium/ Smooth Muscle	–	–	++	±

Table 6.4: Levels of CK 5/6, Prx I, III and -SO₃ in different epithelial phenotypes.

Expression levels of CK 5/6, Prx I and Prx III along with levels of Prx-SO₃ were analysed within the human bronchial epithelial tissue samples from COPD (GOLD4) patients. The bronchial epithelial sections examined contained a range of epithelial subtypes. The endothelium/ smooth muscle of vessels in close proximity to damaged airways was also analysed. (-absent, ±minimal, +moderate, ++high and +++very high).

Basal cells have been identified as the progenitor cells of the BE (Bucchieri *et al.*, 2009) and lead the repair response through a process of dedifferentiation, migration and proliferation (Coraux *et al.*, 2008). CK 5/6 expression was used as a basal cell marker in the BE of human tissue samples, with considerable increases in areas of BCH and more modest increases during re-

epithelisation. Cytokeratin 5 was expressed baso-laterally in stratified tissue, i.e. the zone thought to replenish the more apical layer (Gomperts *et al.*, 2007). Cytokeratin 6 may be expressed supra-basally and associated with differentiation (Presland and Dale, 2000). CK 5/6 expression within the columnar cell population was suggestive of either difficulties with differentiation (incomplete differentiation) or basal cells admixed in this area.

The major region of Prx I expression was in disorganised and hyperplastic epithelia. Prx I has been identified as PAG1 (proliferation-associated gene 1) (Prosperi *et al.*, 1993), suggesting that the variances seen in Prx I expression may be due to the proliferative state of the cell, with elevated Prx I expression seen throughout areas of columnar cell hyperplasia and during cellular proliferation. In several morphologically identical columnar cells there were variances in Prx I expression, which could be indicative of cellular variations in intracellular oxidative stress; a biochemical variation that was undetectable by morphological analysis. There was no Prx I expression within the basal cells, even in tissue with BCH, suggesting an alternative antioxidant mechanism at work during re-epithelisation. The lack of Prx I expression within the basal cells was mirrored in the NHBE cultures, through the use of Western blotting and IHC techniques.

Prx III was highly expressed within the BE of all of the COPD samples analysed, which correlated to previous *in vivo* research (Kinnula *et al.*, 2002a), in addition to the expression patterns observed in the NHBE cell model throughout morphogenesis (i.e. Chapter 2 and 3). IHC analysis of the human tissue sections corroborated with IHC of the NHBE cell model, with strong Prx III expression at the apical region of the columnar cells (ciliated cells), conveying the considerable mitochondrial content in this region (Rhee *et al.*, 2001). With regard to epithelial damage and airway remodelling, the expression level of Prx III rose substantially in areas of GCH; a pathological adaptation often observed in COPD (Saetta *et al.*, 2000). The most common cause of GCH is elevated ROS levels, elicited by both endogenous inflammatory cells (Barnes, 2009) and CS (Baginski *et al.*, 2006). However, emerging evidence has suggested a role for the epidermal growth factor

(EGF) system in the initiation of GCH; with stimulation of the EGF receptor inducing the expression of MUC5AC within epithelial cells (Takeyama *et al.*, 1999; Takeyama *et al.*, 2000; Kim and Nadel, 2004). The inflamed epithelium also contained elevated levels of Prx III expression, which was a consequence of the inflammatory cells imparting further oxidant burden onto the injured epithelium, and hence, perpetuating the cycle of oxidative damage (Hansel and Barnes, 2004). There was also elevated Prx III expression within the endothelial cells of endothelium that was in close proximity to damaged airways. The immune cells within these vessels have been shown to respond to pro-inflammatory cytokines released by the epithelial cells, and migrate to the site of injury (Rennard, 1999; Becker *et al.*, 2005). This inflammatory cell exodus may have elicited an increase in endothelial cell Prx III expression. Prx III expression was also detected within the smooth muscle surrounding the endothelium, which may be an indicator of increased oxidative stress within the tissue. Additionally it may also represent the process of smooth muscle hypertrophy, which is one of the main clinical symptoms associated with COPD (Repine *et al.*, 1997).

Several studies have shown that increased oxidant burden elicited an increase in the levels of Prx hyperoxidation (Phalen *et al.*, 2006; Cox *et al.*, 2009b; Cox *et al.*, 2010b), and therefore, reversible inactivation (Woo *et al.*, 2003a; Woo *et al.*, 2003b). The level of Prx hyperoxidation was moderate in epithelium that appeared morphologically 'normal' (i.e. organised pseudo-stratified epithelium), which was encouraging as this corroborated with data from the NHBE cell cultures (+AO), whereby there was low to moderate basal levels of Prx-SO₃. There were high levels of Prx-SO₃ as a result of elevated levels of oxidative stress (Rabilloud *et al.*, 2002; Lehtonen *et al.*, 2005), i.e. within regions of GCH and inflammation (Barnes, 2009). There were particularly high Prx-SO₃ levels within the apical regions of the columnar cells that coincided with increases in Prx III expression. This may suggest that the elevated Prx-SO₃ levels were primarily that of Prx III-SO₃, as opposed to Prx I/II-SO₃. IHC of the human tissue samples confirmed previous data (i.e. Chapters 4 and 5), whereby increased oxidant burden elicited increased levels of Prx hyperoxidation. Further work should be carried out to ascertain

whether Prx expression and/or hyperoxidation co-localises with areas of oxidative stress, this could be achieved through utilising a stain for malondialdehyde, which is a product of polyunsaturated fatty acid peroxidation, widely used as a biomarker of oxidative stress in COPD research (Tug *et al.*, 2004; Rahman, 2008).

6.6 CONCLUSION

The IHC results derived from lung tissue of COPD patients (GOLD4), inferred that Prx I and III, in conjunction with Prx-SO₃, had the possibility of acting as an indicator of epithelial injury within the human bronchial epithelium. There were marked distinctions between Prx I and III expression levels throughout the various stages of airway remodelling (i.e. re-epithelisation, hyperplasia and inflammation), in conjunction with elevated levels of Prx-SO₃ in regions of increased oxidative stress (e.g. hyperplasia and inflammation). The levels of Prx III within the endothelium and surrounding smooth muscle were also a good indication of injury severity, with higher expression levels proportionate to damage within adjacent airways. Despite the lack of an *in vivo* corroboration of Prx status in healthy patient tissue (an imperative for future research), the collective results bode well for pursuing Prx as a detection method for lung research.

Prx I and Prx III, in conjunction with Prx-SO₃, could be used as an indicator of epithelial injury within the human bronchial epithelium. There were marked distinctions between Prx I and III expression levels detected in the three key stages of airway remodelling, i.e. healthy epithelia, re-epithelisation and hyperplasia. The levels of Prx III within the endothelium were also a good indication of injury severity, with higher expression levels proportionate to damage within adjacent airways. The levels of Prx-SO₃ remained low throughout the healthier epithelia, and increased within areas of hyperplasia and inflammation. This indicated that the Prxs in this area were stable, and that the oxidation status corroborated to findings within the *in vitro* NHBE cell model.

CHAPTER 7:

GENERAL DISCUSSION

7.1 RESEARCH OVERVIEW

The overall objective of this research was to determine whether the Prxs, in conjunction with the NHBE model, could be used as a reliable and sensitive *in vitro* system to resolve physiochemical events mediated by intracellular oxidative stress. To establish the biomarker potential of the Prxs, the NHBE model was analysed throughout morphogenesis and subsequently exposed to GOx and CS (i.e. oxidative stress mediators). Any detectable changes in Prx status, induced as a result of toxicological challenge, would be indicative of the capacity of the Prxs to respond to and inform on the surrounding environment (i.e. intelligent biomarkers of exposure and harm).

Disrupted redox signalling and cycling, or oxidative stress, is the primary cause of lung disease. Thus, highlighting the need for intelligent biomarkers, of exposure and harm, both during homeostasis and following injury (Therond *et al.*, 2000; Dalle-Donne *et al.*, 2005). In addition, there is a demand for high through-put *in vitro* systems that mimic the human *in vivo* lung environment. Previous studies have utilised cell lines to investigate Prx response to oxidant burden; however, the tumour-derived and immortalised cells lack many of the basic characteristics of the human BE (i.e. pseudo-stratified mucociliary phenotype; (BéruBé *et al.*, 2010b). Therefore, primary NHBE cultures would be a more prudent *in vitro* system, and would have provided more dependable insights into human Prx status *in vivo* (BéruBé *et al.*, 2010a). In addition, investigations have reported that *in vitro* cell culture conditions elicit elevated basal levels of oxidative stress within the *in vitro* cultures, rendering any such data as being unreliable (Halliwell, 2011). In light of this, AO supplementation was explored as a viable solution to ameliorate basal stress levels to enhance the NHBE models' ability to produce *in situ* like responses. Perturbations in redox cycling and signalling lead to cycles of injury and repair which precede morphological and phenotypic adaptations (Chapter 4, Figure 4.11). Accordingly, an important research aim was to determine the ability of the Prxs to respond to oxidative stress pre-phenotypic adaptation, informing on the earliest events of pulmonary injury.

7.1.1 RECAPITULATION OF HYPOTHESES

The first hypothesis was concerned with the premise that **“Prx status could be used in conjunction with the NHBE model as a biomarker of intracellular oxidative stress”**. This hypothesis was resolved to be correct in that distinct Prx I and III expression levels were detected, as observed *in vivo* (Kinnula *et al.*, 2002a), and furthermore, Prx oxidation state was an indicator of intracellular oxidative stress levels. For the Prxs to be judged as a reliable and sensitive biomarker, it was important that the expression levels and oxidation states remained stable under normal conditions; as a consequence, fluctuations in Prxs status could be fully attributed to oxidative burden. Elevated levels of hyperoxidation, and hence, oxidative stress (Lehtonen *et al.*, 2005), were detected by Western blotting and complementary IHC during the conventional dosing window (Prytherch, 2010), revealing biochemical instability. Consequently, there was a need to modify the dosing window, ensuring biochemical as well as morphological stability throughout toxicological analysis. Elevated basal levels of oxidative stress were detected throughout NHBE morphogenesis (Halliwell, 2003), conveying the need for AO supplementation. Preliminary AO work involved supplementing the cultures throughout morphogenesis; however, this inhibited culture proliferation and differentiation (data not shown). In light of this, a more conventional mode of supplementation, 24hr pre-exposure, was employed. The principal advantage of analysing the Prxs within the NHBE model was that the cells were genotypically and phenotypically more representative of normal epithelia in comparison to other more commonly used models e.g. A549 (Padar *et al.*, 2005) and BEAS-2B (Penn *et al.*, 2005). The *in vivo* comparable results obtained from the Prx analysis further strengthened the models credentials as a reliable *in vitro* alternative, avoiding the cross-species and ethical issues often encountered with other laboratory animal systems.

The second hypothesis was based upon the supposition that **“exposure of the NHBE cultures to H₂O₂ and CS will alter Prx status, providing a measurable parameter directly linked to the level of intracellular oxidative stress, injury severity and repair competency”**. This was indeed

the circumstance, whereby H₂O₂ and CS exposures elicited a significant increase in levels of Prxs hyperoxidation within the NHBE cultures (-/+AO). However, AO supplementation significantly alleviated the basal levels of oxidative stress and improved the repair competency of the cultures following insult, and subsequently, enhanced the *in vivo* like characteristics of the model. Post-toxicant exposures, junction integrity of cultures +AO were not compromised, confirming the resilience and *in vivo* like response of the BE multilayered cultures, in comparison to equivalent monolayers (Balharry *et al.*, 2008). The cell viability assay (ATP) revealed a dose-dependant hormetic response (Calabrese, 2004), typified by a decrease in viability at lower concentrations, often referred to as the 'initial stimulation', followed by a viability increase at higher concentrations. Reproducibility of this response was achieved post-exposure to both GOx and CS, which further strengthened the use of the NHBE model in toxicological screening. Bronchial epithelia within the *in vivo* environment demonstrate remodelling and repair following insult (Bucchieri *et al.*, 2009), and the ability of the NHBE model to achieve this was therefore essential. Accordingly, the cultures were analysed 3 and 24hr post-exposure to CS, with +AO cultures demonstrating recovery at the physiological level via improved cell viability and at the biochemical level via a reduction in levels of Prx hyperoxidation. Levels of hyperoxidation in +AO cultures were proportionate to toxicant concentration and decreased accordingly following a recovery period, denoting the ability of the Prx to act as a sensitive and consistent marker of intracellular oxidative stress. Furthermore, the significant increases in Prx hyperoxidation following exposure suggested a possible role for the Prxs as an 'early stage' biomarker, with disruptions in redox state occurring far in advance of phenotypic or morphological adaptations (Rahman *et al.*, 2006).

The third hypothesis postulated that **"*in vivo* correlation would substantiate the NHBE *in vitro* findings and confirm that Prx status was a sensitive biomarker of oxidative damage and epithelial remodelling"**. This was confirmed through IHC and complementary histopathology of COPD (GOLD4) bronchial samples. The samples were grouped by epithelial phenotype; healthy, early stage re-epithelisation, hyperplasia and inflammatory, with

distinct Prx expression patterns and oxidation states between subtypes. Prx I expression, which has also been identified as proliferation-associated gene 1 (PAG1), was elevated in areas of columnar cell hyperplasia, indicating a response to cellular proliferative state (Prosperi *et al.*, 1993) in addition to oxidative stress. The absence of Prx I expression within the basal cells corroborated with analysis of the NHBE model during morphogenesis (Chapter 2); these findings suggested that an alternate antioxidant defence was active within the basal cells. There was prevalent Prx III expression in regions of inflammation and hyperplasia; both subtypes were known to induce oxidative stress, with inflammatory cells in particular releasing ROS into the surrounding lamina propria (Hansel and Barnes, 2004). Prx hyperoxidation followed a similar distribution to Prx III, with elevated levels observed in inflammatory and hyperplastic airways. The elevated levels of hyperoxidation corroborated with exposures of the NHBE model to both GOx and CS, indicating a quantitative role for Prx oxidation state in the elucidation of intracellular oxidant burden *in vitro*. Each airway investigated contained several pathological modifications and various degrees of remodelling (Coraux *et al.*, 2008); all of which were represented by distinct Prx expression levels and oxidation states. Healthy epithelia were defined by moderate and regimented expression patterns, in contrast to the strong and diffuse patterns within hyperplastic regions.

7.2 CONCLUSIONS

The research objectives and hypotheses encompassed four fundamental areas of experimental focus for the deduction of Prx expression levels and oxidation state. These areas included NHBE cell model morphogenesis, *in vitro* toxicological exposures (H₂O₂ and CS) and *in vivo* correlations. The more salient features of these deductions may be summarised as follows.

Key deductions from NHBE model morphogenesis analysis:

- Prx I and III were detected throughout morphogenesis and in the fully differentiated NHBE model via Western blotting and IHC analysis

- IHC analysis revealed that Prx III was expressed predominantly in the apical region of the ciliated cells (LM), and more specifically in the mitochondria (EM)
- Western blotting in conjunction with IHC analysis revealed that Prx I was not expressed in the basal (progenitor) cells
- Prx II was not detected within the NHBE model via Western blotting or IHC analysis
- Basal levels of Prx hyperoxidation (Prx-SO₃) were elevated throughout morphogenesis (Days 1-39)
- Due to significantly elevated Prx-SO₃ levels at Day 33, the toxicological dosing window was modified from Days 27-33 to Days 25-30 (post-seeding into Millipore inserts). Prx I, III and SO₃ levels were stable throughout the modified dosing window

Key deductions from H₂O₂ exposures:

- Direct H₂O₂ exposure elicited an increase in Prx-SO₃ levels in proportion to H₂O₂ concentration at all exposure times
- TEER, ATP and Western blot analysis revealed that the optimum AO supplementation was 800µM glutathione; to be added basally to the cultures 24hr pre exposure
- AO supplementation minimised the basal levels of Prx-SO₃ within the NHBE model and enhanced the models *in vivo* like responses
- A biphasic response was observed when measuring cellular ATP levels, with an initial reduction in cell viability at low GOx concentrations, followed by an increase at a higher GOx concentration. The initial decrease in cell

viability occurred at a higher GOx concentration in cultures +AO in comparison to those -AO

- Levels of Prx-SO₃ increased in proportion to GOx concentration in cultures +AO, while in cultures -AO there was a peak following the 30min exposure and a subsequent decline in levels following the 1hr and 3hr exposures
- Levels of P-Erk1/2 significantly increased following all GOx exposures in cultures -AO, while in the corresponding +AO cultures there were no increases
- Levels of Prx III activity were higher in cultures +AO, in comparison to -AO, following all GOx exposures

Key deductions from CS exposures:

- Cultures +AO demonstrated recovery at the morphological and biochemical levels by 24hr post-exposure. Cell viability and Prx-SO₃ levels had improved in comparison with the corresponding cultures 3hr post-exposure, which further indicated the sensitivity of Prx oxidation state as a marker of oxidative stress
- Cultures -AO did not recover in the same manner as cultures +AO following CS exposure. Cell viability, Prx-SO₃ and P-Erk1/2 levels did not significantly improve by 24hr post-exposure in comparison to the corresponding cultures 3hr post-exposure. In contrast, the TEER values following the 1:30 and 1:50 CS exposures fell significantly at 3hr post-exposure and recovered significantly by 24hr post exposure
- Levels of active Prx III in cultures +AO were higher following 3hr post-exposure in comparison to 24hr post-exposure, indicating a delayed response

- Evidence of morphological damage, following the 1:30 CS exposure, was resolved by IHC analysis. Higher levels of Prx-SO₃ were observed in -AO control and CS exposed cultures in comparison to the corresponding +AO cultures
- IHC analysis revealed that there were no region specific increases in Prx III following CS exposures

Key deductions from IHC analysis of human tissue (*in vivo* correlation):

- Prx I and III expressions were ordered in regions of healthy epithelia, indicating a 'standard' expression pattern that could be utilised to comparatively grade damage in other BE
- Prx I expression was not expressed within the basal (progenitor) cells, and was therefore not a feature of 'early stage' repair
- Prx I and III expressions were elevated in regions of columnar cell hyperplasia, informing on the proliferative state in conjunction with levels of oxidative stress
- Prx-SO₃ levels were increased in airways demonstrating elevated levels of oxidative stress, i.e. inflammatory and hyperplastic airways
- Prx oxidation state could be used as a biomarker of COPD susceptibility, with only 15-20% of long-term smokers developing the disease

7.3 FUTURE WORK

7.3.1 *IN VITRO* NHBE MODEL

This study has advanced the development of the NHBE model via the addition of AO; however, there remains vast potential for further enhancements (Le

Visage *et al.*, 2004; Rothen-Rutishauser *et al.*, 2005). For example, the lungs represent a target for airborne detritus (e.g. particles and gases), that, upon gaining access, deposit in the conducting airways. The detritus may then go on to interact with macrophages, which, either result in its clearance or its entrance into the interstitium, making contact with fibroblasts, endothelial cells and cells of the immune system. Therefore, lung epithelial cells, macrophages and other immune cells represent key targets for observing toxicant effects with specific regard to inflammation, immuno-pathology, microbial defence and clearance (BéruBé, 2011). The creation of co-culture models with different combinations of these cell types, according to the potential target cell(s) of a given inhaled hazard, will offer more *in vivo* like systems (Wottrich *et al.*, 2004; Rothen-Rutishauser *et al.*, 2005; Diabate *et al.*, 2008; Lehmann *et al.*, 2011).

Another avenue for exploration would be to improve the biotransformation (BT) capabilities of the model. There is a low level of BT within the lung (Hukkanen *et al.*, 2000); therefore, there is a need to improve the limited xenobiotic-metabolising cytochrome P450 (CYPP450) enzyme activity within the NHBE cells (Prytherch, 2010). In order to achieve this, NHBE cells could be co-cultured with primary hepatocytes (Figure 7.1). Pilot studies within our lab have successfully co-cultured a NHBE-hepatocyte model (Metabo-Lung™, Patent pending), which provided Phase 1, 2 and P450 metabolic functions (W.A.G., 2010) data not published). The metabolising BE model now allows for the characterisation of toxic events following BT of parent compounds, yielding more *in vivo* like responsiveness.

Following on from the NHBE-Hepatocyte model, there could be further augmentation through the development of a full-thickness (FT) model. This would be achieved by the inclusion of primary human fibroblasts during sub-culturing of the NHBE cells (Figure 7.1). The fibroblasts would then establish hemidesmosomes (Andriani *et al.*, 2003) along the plasma membrane of the NHBE basal cells, while fine anchoring fibrils would connect to the underlying collagen matrix. This FT model would provide appropriate *in vivo* like

morphology and basement membrane development; attributes that will enable more realistic *in vitro* studies of airway epithelium.

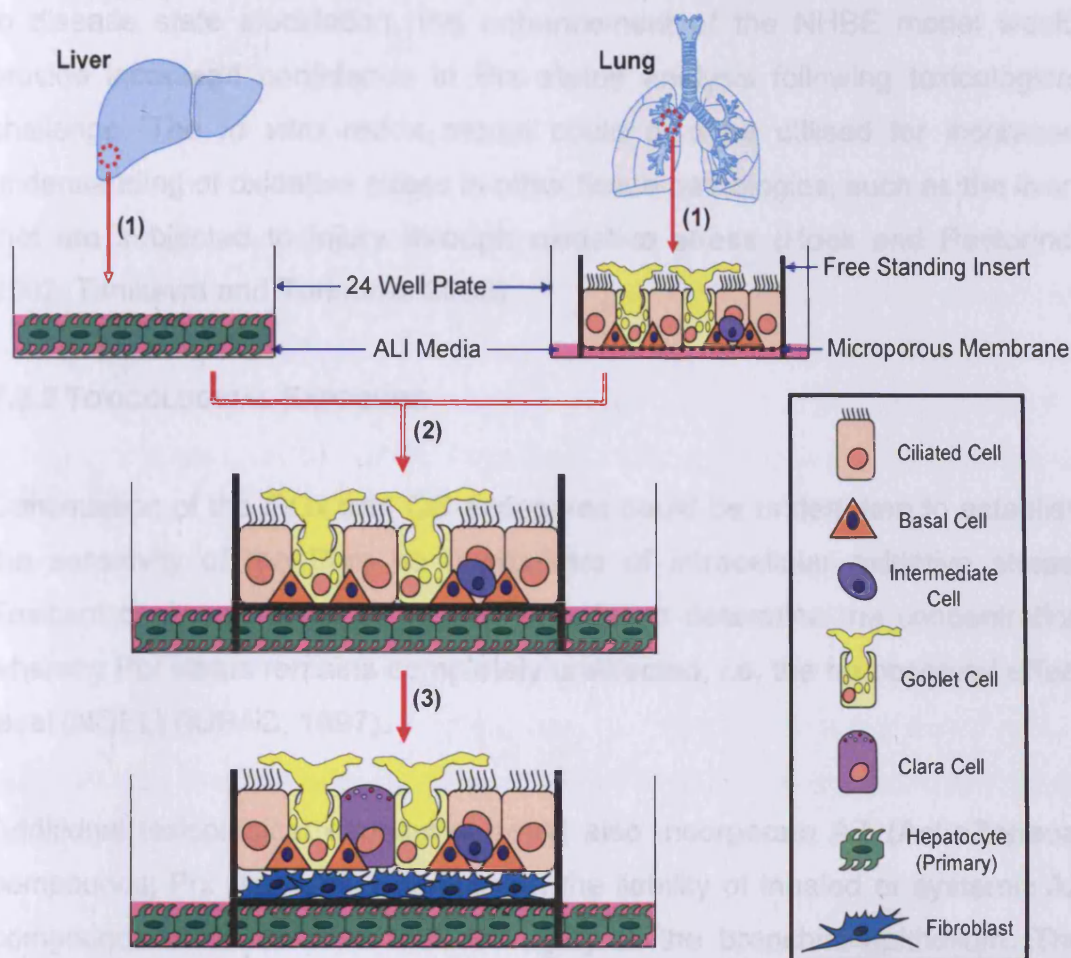


Figure 7.1 Metabolising full-thickness *in vitro* BE model.

In order to improve the existing NHBE cell culture model a xenobiotic metabolising full-thickness co-culture model could be developed. Initially the NHBE cells (ALI) and primary hepatocytes (submerged) would be cultured separately (1). The second phase would be to feed the NHBE cells with ALI culture media that contained primary hepatocytes (2). The hepatocytes would provide further BT capabilities to the model through the addition of metabolic activity including CYP450. The final stage would involve sub-culturing the fibroblasts and the NHBE cells (3); this would provide a metabolising full-thickness model that more closely resembled the *in vivo* human BE environment.

In addition to tissue-engineering morphological enhancements, the NHBE model could be further manipulated to incorporate disease phenotypes, i.e. GCH or inflammation. GCH can be induced by exposing the cells to IL-4 and IL-13 (e.g. EpiAirway-FTTM; (BéruBé *et al.*, 2010a). This would provide a more complex view of the unique signalling pathways active as a consequence of

phenotypic adaptation, and reveal the survival response and protective mechanisms employed by the bronchial epithelium following injury. In addition to disease state elucidation, the enhancement of the NHBE model would provide increased confidence in Prx status analysis following toxicological challenge. The *in vitro* redox model could also be utilised for increased understanding of oxidative stress in other tissue pathologies, such as the liver, that are subjected to injury through oxidative stress (Hoek and Pastorino, 2002; Tanikawa and Torimura, 2006).

7.3.2 TOXICOLOGICAL EXPOSURE

Continuation of the GOx and CS exposures could be undertaken to establish the sensitivity of the Prxs as biomarkers of intracellular oxidative stress. Toxicant challenge could be refined in order to determine the concentration whereby Prx status remains completely unaffected, i.e. the no observed effect level (NOEL) (IUPAC, 1997).

Additional toxicological exposures could also incorporate AZ (AstraZeneca) compounds; Prx status could inform on the liability of inhaled or systemic AZ compounds to cause ROS induced injury to the bronchial epithelium. The NHBE-Prx system could also have a role in the evaluation of candidate respiratory drugs and novel therapeutic formulations developed to treat lung injury and disease. Comparative *in vivo* investigations for corresponding AZ compounds would substantiate the NHBE-Prx *in vitro* data, enhancing the models credentials as a viable pre-screening toxicological tool, prior to animal testing.

7.3.3 EXPERIMENTAL DEVELOPMENT

In addition to the reducing and non-reducing gel electrophoresis conditions, non-denaturing or 'native' gel electrophoresis could be employed, which informs on the native state of a given protein (Westermeyer, 2005). The Prx undergo structural transitions in response to elevated levels of oxidative

stress (Phalen *et al.*, 2006), which would provide a further parameter linking levels of intracellular oxidative stress with Prx status.

In order to further develop the Prxs as biomarkers of oxidative stress, more detailed analysis of their regulatory mechanisms must be undertaken. Quantitative PCR (q-PCR) could be utilised through harvesting the mRNA of cultures post-exposure, this would inform on whether the changes in Prx status were at the translational and/or transcriptional level. The overriding advantage of using q-PCR is the relative sensitivity, detecting quantities as low as a few copy numbers (VanGuilder *et al.*, 2008); this would enhance the Western blot data, as sensitivity limitations were evident in detecting changes in expression post-toxicant exposure. Q-PCR could also be used to substantiate the stress response Western blot data, through providing a more detailed analysis of the pathways targeted by elevated oxidative stress, i.e. the p38 and JNK pathways (Torres and Forman, 2003). Knowledge of the signalling pathways that are critical to an injury and repair event would enlighten the biopharmaceutical industry on the novel therapeutic formulations required in the development of candidate respiratory drugs.

As an extension to the *in vivo* correlation analysis, Prx status within samples from healthy smokers could be investigated. Prx status within the bronchial epithelial of smokers with no COPD symptoms could be an indicator of the individuals' potential to develop COPD, and used as a further deterrent to smoking.

7.4 FUTURE BENEFITS

The NHBE-Prx system developed during this study encompasses a wide range of benefits for future *in vitro* biological and clinical research. These developments include:

- **A system for screening candidate respiratory drugs before entering animal testing.** The high cost involved in candidate drug selection has fuelled pharmaceutical companies to seek increasingly

accurate and cost-effective methods to screen pre-clinical drugs (Seethala, 2001). Fifty percent of new chemical entities fail (e.g. lack of efficacy/safety from use of poorly predictive cell lines and animal based assays) during Phase 3, and 25% fail during registration; all of which can take up to 10 years at an average cost of 800 million US dollars (BéruBé, 2011). An *in vitro* testing platform using primary, human derived cells to tissue-engineer *in vivo* like models, such as the NHBE-Prxs system would improve drug development to create more effective respiratory drugs with fewer side-effects and faster translational times.

- **Development of 3D *in vivo* like microenvironments.** It is well-established that cell culture monolayers, i.e. 2D cell systems, lack the complexity of whole-tissues and animal models themselves fail to capture important facets of human disease, thus limiting their potential to predict cellular responses of humans (Forbes, 2000). The use of human tissue equivalents (HTEs) can bridge the gap between cell culture monolayers and *in vivo* animal systems (BéruBé *et al.*, 2009). The NHBE-Prxs model can mimic to a certain degree the *in vivo* situation but also significantly reduces its complexity by the removal of confounding physiological factors to 'tease-out' finite and meaningful mechanistic information.
- **Delivery of drugs for non-pulmonary syndromes.** There could also be a role for the NHBE-Prxs system in the field of inhaled biopharmaceuticals and the delivery of drugs for non-pulmonary syndromes (Patton *et al.*, 2004). Drugs delivered by the respiratory system have improved pharmacokinetic profiles and offer an alternative delivery mode when conventional oral and intravenous routes are not suitable (Scheuch *et al.*, 2006; Shoyele and Cawthorne, 2006).

7.5 FINAL CONCLUSION

The Prxs were determined to be sensitive and reliable biomarkers of intracellular oxidative stress, injury severity and epithelial remodelling, thus indicating a role for the Prxs as an 'early stage' biomarker, with disruptions in redox state occurring far in advance of phenotypic or morphological adaptations. The *in vitro* NHBE cell model was developed further via the addition of AO, thereby reducing the basal levels of oxidative stress, and therefore, improving data viability and reproducibility. Furthermore, the NHBE model eliminated the issue of interspecies reactivity, indicating a potential role for the NHBE-Prx system as an *in vivo* pre-screening tool. It can therefore be concluded that the use of high content biology has developed the understanding of the association between morphological changes and biochemical pathways.

REFERENCES

Agusti, A. (2006). Thomas a. Neff lecture. Chronic obstructive pulmonary disease: a systemic disease. *Proc Am Thorac Soc* **3**: 478-481.

Akuthota, P., Wang, H.B., Spencer, L.A., and Weller, P.F. (2008). Immunoregulatory roles of eosinophils: a new look at a familiar cell. *Clin Exp Allergy* **38**: 1254-1263.

Alberts, B., Johnson, A., Lewis, J., Raff, M., Roberts, K., and Walter, P. (2002). *Molecular biology of the cell*. Garland Science.

Anderson, G.P. (2006). COPD, asthma and C-reactive protein. *Eur Respir J* **27**: 874-876.

Andriani, F., Margulis, A., Lin, N., Griffey, S., and Garlick, J.A. (2003). Analysis of microenvironmental factors contributing to basement membrane assembly and normalized epidermal phenotype. *J Invest Dermatol* **120**: 923-931.

Antonicelli, F., Parmentier, M., Drost, E.M., Hirani, N., Rahman, I., Donaldson, K., and MacNee, W. (2002). Nacystelyn inhibits oxidant-mediated interleukin-8 expression and NF-kappaB nuclear binding in alveolar epithelial cells. *Free Radic Biol Med* **32**: 492-502.

Ataullakhanov, F.I., and Vitvitsky, V.M. (2002). What determines the intracellular ATP concentration. *Biosci Rep* **22**: 501-511.

Ayers, M.M., and Jeffery, P.K. (1988). Proliferation and Differentiation in Mammalian Airway Epithelium. *European Respiratory Journal* **1**: 58-80.

Baginski, T.K., Dabbagh, K., Satjawatcharaphong, C., and Swinney, D.C. (2006). Cigarette smoke synergistically enhances respiratory mucin induction by proinflammatory stimuli. *American journal of respiratory cell and molecular biology* **35**: 165-174.

- Baldwin, F.** (1994). Basal cells in human bronchial epithelium. *Anat Rec* **238**: 360-367.
- Balharri, D., Sexton, K., and BeruBe, K.A.** (2008). An in vitro approach to assess the toxicity of inhaled tobacco smoke components: Nicotine, cadmium, formaldehyde and urethane. *Toxicology* **244**: 66-76.
- Barnes, P.J.** (2009). The cytokine network in chronic obstructive pulmonary disease. *American journal of respiratory cell and molecular biology* **41**: 631-638.
- Barnes, P.J., Chowdhury, B., Kharitonov, S.A., Magnussen, H., Page, C.P., Postma, D., and Saetta, M.** (2006). Pulmonary biomarkers in chronic obstructive pulmonary disease. *American Journal of Respiratory and Critical Care Medicine* **174**: 6-14.
- Barnes, P.J., Shapiro, S.D., and Pauwels, R.A.** (2003). Chronic obstructive pulmonary disease: molecular and cellular mechanisms. *Eur Respir J* **22**: 672-688.
- Barranco-Medina, S., Lazaro, J.J., and Dietz, K.J.** (2009). The oligomeric conformation of peroxiredoxins links redox state to function. *Febs Letters* **583**: 1809-1816.
- Bast, A., Haenen, G.R., and Doelman, C.J.** (1991). Oxidants and antioxidants: state of the art. *Am J Med* **91**: 2S-13S.
- BDWG.** (2001). Biomarkers and surrogate endpoints: preferred definitions and conceptual framework. *Clin Pharmacol Ther* **69**: 89-95.
- Becker, S., Mundandhara, S., Devlin, R.B., and Madden, M.** (2005). Regulation of cytokine production in human alveolar macrophages and airway epithelial cells in response to ambient air pollution particles: further mechanistic studies. *Toxicol Appl Pharm* **207**: 269-275.

Berne, R.M., Levy, M.N., Koeppen, B.M., and Stanton, B.A. (2004). Physiology. Mosby.

BéruBé, K.A. (2011). Alternatives for lung research: stuck between a rat and a hard place. *Altern Lab Anim* **39**: 121-130.

BéruBé, K.A., Aufderheide, M., Breheny, D., Clothier, R., Combes, R., Duffin, R., Forbes, B., Gaca, M., Gray, A., Hall, I., Kelly, M., Lethem, M., Liebsch, M., Merolla, L., Morin, J.P., Seagrave, J., Swartz, M.A., Tetley, T.D., and Umachandran, M. (2009). *In vitro* models of inhalation toxicity and disease. The report of a FRAME workshop. *Altern Lab Anim* **37**: 89-141.

BéruBé, K.A., Pitt, A., Hayden, P., Prytherch, Z., and Job, C. (2010a). Filter-well technology for advanced three-dimensional cell culture: perspectives for respiratory research. *Altern Lab Anim* **38 Suppl 1**: 49-65.

BéruBé, K.A., Prytherch, Z., Job, C., and Hughes, T. (2010b). Human primary bronchial lung cell constructs: The new respiratory models. *Toxicology* **278**: 311-318.

Bianchi, M.E. (2007). DAMPs, PAMPs and alarmins: all we need to know about danger. *J Leukoc Biol* **81**: 1-5.

Biteau, B., Labarre, J., and Toledano, M.B. (2003). ATP-dependent reduction of cysteine-sulphinic acid by *S. cerevisiae* sulphiredoxin. *Nature* **425**: 980-984.

Bittar, E.E. (2002). Pulmonary biology in health and disease. Springer.

Blenkinsopp, W.K. (1967). Proliferation of respiratory tract epithelium in the rat. *Exp Cell Res* **46**: 144-154.

- Boers, J.E., Ambergen, A.W., and Thunnissen, F.B. (1998).** Number and proliferation of basal and parabasal cells in normal human airway epithelium. *Am J Respir Crit Care Med* **157**: 2000-2006.
- Boers, J.E., Ambergen, A.W., and Thunnissen, F.B. (1999).** Number and proliferation of clara cells in normal human airway epithelium. *American Journal of Respiratory and Critical Care Medicine* **159**: 1585-1591.
- Boots, A.W., Haenen, G.R., and Bast, A. (2003).** Oxidant metabolism in chronic obstructive pulmonary disease. *Eur Respir J Suppl* **46**: 14s-27s.
- Boyton, R.J., and Openshaw, P.J. (2002).** Pulmonary defences to acute respiratory infection. *Br Med Bull* **61**: 1-12.
- Braiman, A., and Priel, Z. (2008).** Efficient mucociliary transport relies on efficient regulation of ciliary beating. *Respir Physiol Neurobiol* **163**: 202-207.
- Breeze, R.G., and Wheeldon, E.B. (1977).** The cells of the pulmonary airways. *Am Rev Respir Dis* **116**: 705-777.
- Brody, A.R. (1984).** Inhaled particles in human disease and animal models: use of electron beam instrumentation. *Environ Health Perspect* **56**: 149-162.
- Bucchieri, F., Fucarino, A., Rizzuto, L., Pitruzzella, A., Noto, A., Cappello, F., and Zummo, G. (2009).** Stem cell populations and regenerative potential in chronic inflammatory diseases. *The Open Tissue Eng Regen Med J* **2**: 34-39.
- Calabrese, E.J. (2004).** Hormesis: a revolution in toxicology, risk assessment and medicine. *EMBO Rep* **5 Spec No**: S37-40.
- Cantin, A.M. (2010).** Cellular response to cigarette smoke and oxidants: adapting to survive. *Proceedings of the American Thoracic Society* **7**: 368-375.

- Castell, J.V., Donato, M.T., and Gomez-Lechon, M.J.** (2005). Metabolism and bioactivation of toxicants in the lung. The in vitro cellular approach. *Exp Toxicol Pathol* **57 Suppl 1**: 189-204.
- Cerveri, I., and Brusasco, V.** (2010). Revisited role for mucus hypersecretion in the pathogenesis of COPD. *Eur Respir Rev* **19**: 109-112.
- Cha, M.K., Yun, C.H., and Kim, I.H.** (2000). Interaction of human thiol-specific antioxidant protein 1 with erythrocyte plasma membrane. *Biochemistry* **39**: 6944-6950.
- Chae, H.Z., Chung, S.J., and Rhee, S.G.** (1994a). Thioredoxin-dependent peroxide reductase from yeast. *J Biol Chem* **269**: 27670-27678.
- Chae, H.Z., Kim, H.J., Kang, S.W., and Rhee, S.G.** (1999). Characterization of three isoforms of mammalian peroxiredoxin that reduce peroxides in the presence of thioredoxin. *Diabetes Res Clin Pract* **45**: 101-112.
- Chae, H.Z., Robison, K., Poole, L.B., Church, G., Storz, G., and Rhee, S.G.** (1994b). Cloning and sequencing of thiol-specific antioxidant from mammalian brain: alkyl hydroperoxide reductase and thiol-specific antioxidant define a large family of antioxidant enzymes. *Proc Natl Acad Sci U S A* **91**: 7017-7021.
- Chae, H.Z., Uhm, T.B., and Rhee, S.G.** (1994c). Dimerization of thiol-specific antioxidant and the essential role of cysteine 47. *Proc Natl Acad Sci U S A* **91**: 7022-7026.
- Chang, J.W., Jeon, H.B., Lee, J.H., Yoo, J.S., Chun, J.S., Kim, J.H., and Yoo, Y.J.** (2001). Augmented expression of peroxiredoxin I in lung cancer. *Biochem Biophys Res Commun* **289**: 507-512.

Chang, T.S., Cho, C.S., Park, S., Yu, S., Kang, S.W., and Rhee, S.G. (2004). Peroxiredoxin III, a mitochondrion-specific peroxidase, regulates apoptotic signaling by mitochondria. *J Biol Chem* **279**: 41975-41984.

Chang, T.S., Jeong, W., Choi, S.Y., Yu, S., Kang, S.W., and Rhee, S.G. (2002). Regulation of peroxiredoxin I activity by Cdc2-mediated phosphorylation. *J Biol Chem* **277**: 25370-25376.

Chemuturi, N.V., Hayden, P., Klausner, M., and Donovan, M.D. (2005). Comparison of human tracheal/bronchial epithelial cell culture and bovine nasal respiratory explants for nasal drug transport studies. *J Pharm Sci* **94**: 1976-1985.

Chen, C., Arjomandi, M., Balmes, J., Tager, I., and Holland, N. (2007). Effects of chronic and acute ozone exposure on lipid peroxidation and antioxidant capacity in healthy young adults. *Environ Health Perspect* **115**: 1732-1737.

Chen, H., Wang, D., Bai, C., and Wang, X. (2010). Proteomics-based biomarkers in chronic obstructive pulmonary disease. *J Proteome Res* **9**: 2798-2808.

Chen, J.W., Dodia, C., Feinstein, S.I., Jain, M.K., and Fisher, A.B. (2000). 1-Cys peroxiredoxin, a bifunctional enzyme with glutathione peroxidase and phospholipase A2 activities. *J Biol Chem* **275**: 28421-28427.

Chen, Q., Zhang, S.M., Liu, H.Y., and Li, Y.Q. (2009). Protective effect of glutathione against oxidative injury in intestinal epithelial cells of piglet *in vitro*. *J Anim Biol* **59**: 263-272.

Chilvers, M.A., and O'Callaghan, C. (2000). Local mucociliary defence mechanisms. *Paediatr Respir Rev* **1**: 27-34.

- Choi, H.J., Kang, S.W., Yang, C.H., Rhee, S.G., and Ryu, S.E. (1998).** Crystal structure of a novel human peroxidase enzyme at 2.0 Å resolution. *Nat Struct Biol* **5**: 400-406.
- Churg, A., Wang, R.D., and Wright, J.L. (2006).** Cigarette smoke causes small airway remodeling by direct growth factor induction and release. *Proceedings of the American Thoracic Society* **3**: 493.
- Ciencewicki, J., Trivedi, S., and Kleeberger, S.R. (2008).** Oxidants and the pathogenesis of lung diseases. *J Allergy Clin Immunol* **122**: 456-468; quiz 469-470.
- Com, E., Bourgeon, F., Evrard, B., Ganz, T., Colleu, D., Jegou, B., and Pineau, C. (2003).** Expression of antimicrobial defensins in the male reproductive tract of rats, mice, and humans. *Biol Reprod* **68**: 95-104.
- Comhair, S.A., and Erzurum, S.C. (2002).** Antioxidant responses to oxidant-mediated lung diseases. *Am J Physiol Lung Cell Mol Physiol* **283**: L246-255.
- Coraux, C., Roux, J., Jolly, T., and Birembaut, P. (2008).** Epithelial cell-extracellular matrix interactions and stem cells in airway epithelial regeneration. *Proceedings of the American Thoracic Society* **5**: 689-694.
- Costello, M.L., Mathieu-Costello, O., and West, J.B. (1992).** Stress failure of alveolar epithelial cells studied by scanning electron microscopy. *The American review of respiratory disease* **145**: 1446-1455.
- Cox, A.G., Pearson, A.G., Pullar, J.M., Jonsson, T.J., Lowther, W.T., Winterbourn, C.C., and Hampton, M.B. (2009a).** Mitochondrial peroxiredoxin 3 is more resilient to hyperoxidation than cytoplasmic peroxiredoxins. *Biochem J* **421**: 51-58.

Cox, A.G., Peskin, A.V., Paton, L.N., Winterbourn, C.C., and Hampton, M.B. (2009b). Redox potential and peroxide reactivity of human peroxiredoxin 3. *Biochemistry* **48**: 6495-6501.

Cox, A.G., Winterbourn, C.C., and Hampton, M.B. (2010a). Measuring the redox state of cellular peroxiredoxins by immunoblotting. *Methods Enzymol* **474**: 51-66.

Cox, A.G., Winterbourn, C.C., and Hampton, M.B. (2010b). Mitochondrial peroxiredoxin involvement in antioxidant defence and redox signalling. *Biochem J* **425**: 313-325.

Cozens, A.L., Yezzi, M.J., Kunzelmann, K., Ohrui, T., Chin, L., Eng, K., Finkbeiner, W.E., Widdicombe, J.H., and Gruenert, D.C. (1994). CFTR expression and chloride secretion in polarized immortal human bronchial epithelial cells. *American journal of respiratory cell and molecular biology* **10**: 38-47.

D'Autreaux, B., and Toledano, M.B. (2007). ROS as signalling molecules: mechanisms that generate specificity in ROS homeostasis. *Nat Rev Mol Cell Biol* **8**: 813-824.

Dalle-Donne, I., Scaloni, A., Giustarini, D., Cavarra, E., Tell, G., Lungarella, G., Colombo, R., Rossi, R., and Milzani, A. (2005). Proteins as biomarkers of oxidative/nitrosative stress in diseases: the contribution of redox proteomics. *Mass Spectrom Rev* **24**: 55-99.

Davies, J.R., Herrmann, A., Russell, W., Svitacheva, N., Wickstrom, C., and Carlstedt, I. (2002). Respiratory tract mucins: structure and expression patterns. *Novartis Found Symp* **248**: 76-88; discussion 88-93, 277-282.

Davis, C.W., and Dickey, B.F. (2008). Regulated airway goblet cell mucin secretion. *Annu Rev Physiol* **70**: 487-512.

Declercq, J.P., Evrard, C., Clippe, A., Stricht, D.V., Bernard, A., and Knoops, B. (2001). Crystal structure of human peroxiredoxin 5, a novel type of mammalian peroxiredoxin at 1.5 Å resolution. *J Mol Biol* **311**: 751-759.

Decramer, M., De Benedetto, F., Del Ponte, A., and Marinari, S. (2005). Systemic effects of COPD. *Respiratory Medicine* **99 Suppl B**: S3-10.

Decramer, M., Sibille, Y., Bush, A., Carlsen, K.H., Rabe, K.F., Clancy, L., Turnbull, A., Nemery, B., Simonds, A., and Troosters, T. (2011). The European Union conference on chronic respiratory disease: purpose and conclusions. *The European respiratory journal : official journal of the European Society for Clinical Respiratory Physiology* **37**: 738-742.

Dekhuijzen, P.N., Aben, K.K., Dekker, I., Aarts, L.P., Wielders, P.L., van Herwaarden, C.L., and Bast, A. (1996). Increased exhalation of hydrogen peroxide in patients with stable and unstable chronic obstructive pulmonary disease. *American Journal of Respiratory and Critical Care Medicine* **154**: 813-816.

Diabate, S., Mulhopt, S., Paur, H.R., and Krug, H.F. (2008). The response of a co-culture lung model to fine and ultrafine particles of incinerator fly ash at the air-liquid interface. *Altern Lab Anim* **36**: 285-298.

Doelman, C.J., and Bast, A. (1990). Oxygen radicals in lung pathology. *Free Radic Biol Med* **9**: 381-400.

Drexler, H.G., Dirks, W.G., Matsuo, Y., and MacLeod, R.A. (2003). False leukemia-lymphoma cell lines: an update on over 500 cell lines. *Leukemia* **17**: 416-426.

Drost, E.M., Skwarski, K.M., Sauleda, J., Soler, N., Roca, J., Agusti, A., and MacNee, W. (2005). Oxidative stress and airway inflammation in severe exacerbations of COPD. *Thorax* **60**: 293-300.

- Dubuisson, M., Vander Stricht, D., Clippe, A., Etienne, F., Nauser, T., Kissner, R., Koppenol, W.H., Rees, J.F., and Knoop, B. (2004).** Human peroxiredoxin 5 is a peroxynitrite reductase. *FEBS Lett* **571**: 161-165.
- Dytham, C. (2003).** Choosing and using statistics: a biologist's guide. Blackwell Publishing.
- Ebert, R.V., and Hanks, P.B. (1981).** Mucus secretion by the epithelium of the bronchioles of cigarette smokers. *Br J Dis Chest* **75**: 277-282.
- Elbert, K.J., Schafer, U.F., Schafers, H.J., Kim, K.J., Lee, V.H., and Lehr, C.M. (1999).** Monolayers of human alveolar epithelial cells in primary culture for pulmonary absorption and transport studies. *Pharm Res* **16**: 601-608.
- Ellis, H.R., and Poole, L.B. (1997).** Roles for the two cysteine residues of AhpC in catalysis of peroxide reduction by alkyl hydroperoxide reductase from *Salmonella typhimurium*. *Biochemistry* **36**: 13349-13356.
- Emami, J. (2006).** In vitro - in vivo correlation: from theory to applications. *J Pharm Pharm Sci* **9**: 169-189.
- Engelhardt, J.F., Schlossberg, H., Yankaskas, J.R., and Dudus, L. (1995).** Progenitor cells of the adult human airway involved in submucosal gland development. *Development* **121**: 2031-2046.
- Erjefalt, J.S., Sundler, F., and Persson, C.G. (1997).** Epithelial barrier formation by airway basal cells. *Thorax* **52**: 213-217.
- Evans, M.D., Dizdaroglu, M., and Cooke, M.S. (2004).** Oxidative DNA damage and disease: induction, repair and significance. *Mutat Res* **567**: 1-61.
- EU Directive 76/68/EEC. (2003).** Directive 2003/15/EC of the European parliament and of the council of 27 February 2003. *Official Journal of the European Union*. **L66**: 26-35.

Finkel, T. (1998). Oxygen radicals and signaling. *Curr Opin Cell Biol* **10**: 248-253.

Finkelstein, R., Fraser, R.S., Ghezzi, H., and Cosio, M.G. (1995). Alveolar inflammation and its relation to emphysema in smokers. *American Journal of Respiratory and Critical Care Medicine* **152**: 1666-1672.

Fletcher, C., Peto, R., Tinker, C., and Speizer, F.E. (1976). The natural history of chronic bronchitis and emphysema. Oxford: Oxford University Press.

Fletcher, C.M., and Pride, N.B. (1984). Definitions of emphysema, chronic bronchitis, asthma, and air-flow obstruction - 25 years on from the CIBA symposium. *Thorax* **39**: 81-85.

Fliegauf, M., Benzing, T., and Omran, H. (2007). When cilia go bad: cilia defects and ciliopathies. *Nat Rev Mol Cell Biol* **8**: 880-893.

Folkerts, G., and Nijkamp, F.P. (1998). Airway epithelium: more than just a barrier! *Trends in pharmacological sciences* **19**: 334-341.

Forbes, I.I. (2000). Human airway epithelial cell lines for in vitro drug transport and metabolism studies. *Pharm Sci Technol Today* **3**: 18-27.

Forman, H.J., Fukuto, J.M., and Torres, M. (2004). Redox signaling: thiol chemistry defines which reactive oxygen and nitrogen species can act as second messengers. *Am J Physiol Cell Physiol* **287**: C246-256.

Foronjy, R.F., and D'Armiento, J.M. (2006). The effect of cigarette smoke-derived oxidants on the inflammatory response of the lung. *Clin Appl Immunol Rev* **6**: 53-72.

- Foster, K.A., Avery, M.L., Yazdanian, M., and Audus, K.L.** (2000). Characterization of the Calu-3 cell line as a tool to screen pulmonary drug delivery. *Int J Pharm* **208**: 1-11.
- Freshney, R.I.** (2005). *Culture of animal cells: a manual of basic techniques*. Wiley.
- Fridovich, I., and Freeman, B.** (1986). Antioxidant defenses in the lung. *Annu Rev Physiol* **48**: 693-702.
- Garban, Z., Avacivici, A., Garban, G., Ghibu, G.D., Velciov, A.B., and Pop, C.I.** (2005). Biomarkers: Theoretical aspects and applicative peculiarities. Note I. General characterisation of biomarkers. *J Agroalimentary Process Technol* **11**: 139-146.
- Gardner, D.E.** (2006). *Toxicology of the lung*.
- Genestra, M.** (2007). Oxyl radicals, redox-sensitive signalling cascades and antioxidants. *Cell Signal* **19**: 1807-1819.
- Germann, W., and Stanfield, C.** (2004). *Principles of human physiology*. Benjamin Cummings, New York.
- Gillard, J.** (2011). Performing the one-way ANOVA test when samples are not equally distributed. School of mathematics, Cardiff University **Personal communication**.
- GOLD.** (2006). Global initiative for chronic obstructive lung disease. Global strategy for diagnosis, management and prevention of COPD. National institute of health / World health organisation. www.goldcopd.org.
- Gomperts, B.N., Belperio, J.A., Fishbein, M.C., Keane, M.P., Burdick, M.D., and Strieter, R.M.** (2007). Keratinocyte growth factor improves repair in

the injured tracheal epithelium. *American journal of respiratory cell and molecular biology* **37**: 48-56.

Grainger, C.I., Greenwell, L.L., Lockley, D.J., Martin, G.P., and Forbes, B. (2006). Culture of Calu-3 cells at the air interface provides a representative model of the airway epithelial barrier. *Pharm Res* **23**: 1482-1490.

Greer, K.A., Pine, M., and Busbee, D.L. (2005). Development of an *in vitro* model of excess intracellular reactive oxygen species. *Age* **27**: 97-105.

Griffith, L.G., and Swartz, M.A. (2006). Capturing complex 3D tissue physiology in vitro. *Nat Rev Mol Cell Biol* **7**: 211-224.

Hackett, N.R., Heguy, A., Harvey, B.G., O'Connor, T.P., Luettich, K., Flieder, D.B., Kaplan, R., and Crystal, R.G. (2003). Variability of antioxidant-related gene expression in the airway epithelium of cigarette smokers. *Am J Respir Cell Mol Biol* **29**: 331-343.

Hall, A., Parsonage, D., Poole, L.B., and Karplus, P.A. (2010). Structural evidence that peroxiredoxin catalytic power is based on transition-state stabilization. *J Mol Biol* **402**: 194-209.

Halliwell, B. (1991). Reactive oxygen species in living systems: source, biochemistry, and role in human disease. *Am J Med* **91**: 14S-22S.

Halliwell, B. (2003). Oxidative stress in cell culture: an under-appreciated problem? *Febs Letters* **540**: 3-6.

Halliwell, B. (2006). Reactive species and antioxidants. Redox biology is a fundamental theme of aerobic life. *Plant Physiol* **141**: 312-322.

Halliwell, B. (2007a). Biochemistry of oxidative stress. *Biochem Soc Trans* **35**: 1147-1150.

- Halliwell, B.** (2007b). Oxidative stress and cancer: have we moved forward? *Biochem J* **401**: 1-11.
- Halliwell, B.** (2011). Free radicals and antioxidants - quo vadis? *Trends in pharmacological sciences* **32**: 125-130.
- Halliwell, B., and Gutteridge, M.C.** (1999). Free radicals in biology and medicine. Oxford University Press.
- Hansel, T.T., and Barnes, P.J.** (2004). An atlas of chronic obstructive pulmonary disease COPD. The Parthenon Publishing Group.
- Haridas, V., Ni, J., Meager, A., Su, J., Yu, G.L., Zhai, Y., Kyaw, H., Akama, K.T., Hu, J., Van Eldik, L.J., and Aggarwal, B.B.** (1998). TRANK, a novel cytokine that activates NF-kappa B and c-Jun N-terminal kinase. *J Immunol* **161**: 1-6.
- Harris, J.R.** (1968). Release of a macromolecular protein component from human erythrocyte ghosts. *Biochim Biophys Acta* **150**: 534-537.
- Harris, J.R.** (1969). Some negative contrast staining features of a protein from erythrocyte ghosts. *J Mol Biol* **46**: 329-335.
- Harris, J.R., Schroder, E., Isupov, M.N., Scheffler, D., Kristensen, P., Littlechild, J.A., Vagin, A.A., and Meissner, U.** (2001). Comparison of the decameric structure of peroxiredoxin-II by transmission electron microscopy and X-ray crystallography. *Biochim Biophys Acta* **1547**: 221-234.
- Hasleton, P.S.** (1996). Spencer's pathology of the lung. McGraw-Hill.
- Heintz, N.** (2008). A model for the role of ROS in the pathogenesis of disease
Personal communication.

Hill, E.M., Eling, T., and Nettesheim, P. (1998). Differentiation dependency of eicosanoid enzyme expression in human tracheobronchial cells. *Toxicol Lett* **96-97**: 239-244.

Hirotsu, S., Abe, Y., Okada, K., Nagahara, N., Hori, H., Nishino, T., and Hakoshima, T. (1999). Crystal structure of a multifunctional 2-Cys peroxiredoxin heme-binding protein 23 kDa/proliferation-associated gene product. *Proc Natl Acad Sci U S A* **96**: 12333-12338.

Hlastala, M.P., and Berger, A.J. (2001). *Physiology of respiration*. Oxford University Press.

Hoek, J.B., and Pastorino, J.G. (2002). Ethanol, oxidative stress, and cytokine-induced liver cell injury. *Alcohol* **27**: 63-68.

Hofmann, B., Hecht, H.J., and Flohe, L. (2002). Peroxiredoxins. *Biol Chem* **383**: 347-364.

Hong, K.U., Reynolds, S.D., Watkins, S., Fuchs, E., and Stripp, B.R. (2004). Basal cells are a multipotent progenitor capable of renewing the bronchial epithelium. *Am J Pathol* **164**: 577-588.

Hukkanen, J., Lassila, A., Paivarinta, K., Valanne, S., Sarpo, S., Hakkola, J., Pelkonen, O., and Raunio, H. (2000). Induction and regulation of xenobiotic-metabolizing cytochrome P450s in the human A549 lung adenocarcinoma cell line. *American journal of respiratory cell and molecular biology* **22**: 360-366.

IARC. (2004). Tobacco smoke and involuntary smoking. *IARC monographs on the evaluation of carcinogenic risks to humans* **83**.

Ilumets, H., Ryttilä, P.H., Sovijärvi, A.R., Tervahartiala, T., Myllärniemi, M., Sorsa, T.A., and Kinnula, V.L. (2008). Transient elevation of neutrophil

proteinases in induced sputum during COPD exacerbation. *Scand J Clin Lab Invest* **68**: 618-623.

Immenschuh, S., and Baumgart-Vogt, E. (2005). Peroxiredoxins, oxidative stress, and cell proliferation. *Antioxidants & redox signaling* **7**: 768-777.

Invitrogen. (2011). SeeBlue pre-stained standard.

Ishii, T., Yamada, M., Sato, H., Matsue, M., Taketani, S., Nakayama, K., Sugita, Y., and Bannai, S. (1993). Cloning and characterization of a 23-kDa stress-induced mouse peritoneal macrophage protein. *J Biol Chem* **268**: 18633-18636.

IUPAC. (1997). No observed effect level (NOEL). International union of pure applied chemistry.

Iwahara, S., Satoh, H., Song, D.X., Webb, J., Burlingame, A.L., Nagae, Y., and Muller-Eberhard, U. (1995). Purification, characterization, and cloning of a heme-binding protein (23 kDa) in rat liver cytosol. *Biochemistry* **34**: 13398-13406.

Janeway, C.A., Jr., and Medzhitov, R. (2002). Innate immune recognition. *Annu Rev Immunol* **20**: 197-216.

Janoff, A., Carp, H., Laurent, P., and Raju, L. (1983). The Role of Oxidative Processes in Emphysema. *American Review of Respiratory Disease* **127**: S31-S38.

Janssen-Heininger, Y.M.W., Mossman, B.T., Heintz, N.H., Forman, H.J., Kalyanaraman, B., Finkel, T., Stamler, J.S., Rhee, S.G., and van der Vliet, A. (2008). Redox-based regulation of signal transduction: Principles, pitfalls, and promises. *Free Radical Biology and Medicine* **45**: 1-17.

- Janssen, Y.M., Van Houten, B., Borm, P.J., and Mossman, B.T. (1993).** Cell and tissue responses to oxidative damage. *Lab Invest* **69**: 261-274.
- Jeffery, P.K. (2000).** Comparison of the structural and inflammatory features of COPD and asthma. Giles F. Filley Lecture. *Chest* **117**: 251S-260S.
- Jikimoto, T., Nishikubo, Y., Koshiba, M., Kanagawa, S., Morinobu, S., Morinobu, A., Saura, R., Mizuno, K., Kondo, S., Toyokuni, S., Nakamura, H., Yodoi, J., and Kumagai, S. (2002).** Thioredoxin as a biomarker for oxidative stress in patients with rheumatoid arthritis. *Mol Immunol* **38**: 765-772.
- Jin, D.Y., Chae, H.Z., Rhee, S.G., and Jeang, K.T. (1997).** Regulatory role for a novel human thioredoxin peroxidase in NF-kappaB activation. *J Biol Chem* **272**: 30952-30961.
- Jones, D.P. (2006).** Redefining oxidative stress. *Antioxid Redox Signal* **8**: 1865-1879.
- Jones, P.W., and Agusti, A.G. (2006).** Outcomes and markers in the assessment of chronic obstructive pulmonary disease. *Eur Respir J* **27**: 822-832.
- Kang, S.W., Baines, I.C., and Rhee, S.G. (1998a).** Characterization of a mammalian peroxiredoxin that contains one conserved cysteine. *J Biol Chem* **273**: 6303-6311.
- Kang, S.W., Chae, H.Z., Seo, M.S., Kim, K., Baines, I.C., and Rhee, S.G. (1998b).** Mammalian peroxiredoxin isoforms can reduce hydrogen peroxide generated in response to growth factors and tumor necrosis factor-alpha. *J Biol Chem* **273**: 6297-6302.
- Kasper, M., Rudolf, T., Verhofstad, A.A., Schuh, D., and Muller, M. (1993).** Heterogeneity in the immunolocalization of cytokeratin-specific monoclonal

antibodies in the rat lung: evaluation of three different alveolar epithelial cell types. *Histochemistry* **100**: 65-71.

Kawai, S., Takeshita, S., Okazaki, M., Kikuno, R., Kudo, A., and Amann, E. (1994). Cloning and characterization of OSF-3, a new member of the MER5 family, expressed in mouse osteoblastic cells. *J Biochem* **115**: 641-643.

Keatings, V.M., Collins, P.D., Scott, D.M., and Barnes, P.J. (1996). Differences in interleukin-8 and tumor necrosis factor-alpha in induced sputum from patients with chronic obstructive pulmonary disease or asthma. *Am J Respir Crit Care Med* **153**: 530-534.

Kelly, F.J. (1999). Gluthathione: in defence of the lung. *Food Chem Toxicol* **37**: 963-966.

Kelly, F.J., and Mudway, I.S. (2003). Protein oxidation at the air-lung interface. *Amino Acids* **25**: 375-396.

Kim, H.S., Manevich, Y., Feinstein, S.I., Pak, J.H., Ho, Y.S., and Fisher, A.B. (2003). Induction of 1-cys peroxiredoxin expression by oxidative stress in lung epithelial cells. *Am J Physiol Lung Cell Mol Physiol* **285**: L363-369.

Kim, K., Kim, I.H., Lee, K.Y., Rhee, S.G., and Stadtman, E.R. (1988). The isolation and purification of a specific "protector" protein which inhibits enzyme inactivation by a thiol/Fe(III)/O₂ mixed-function oxidation system. *J Biol Chem* **263**: 4704-4711.

Kim, K., Rhee, S.G., and Stadtman, E.R. (1985). Nonenzymatic cleavage of proteins by reactive oxygen species generated by dithiothreitol and iron. *J Biol Chem* **260**: 15394-15397.

Kim, S., and Nadel, J.A. (2004). Role of neutrophils in mucus hypersecretion in COPD and implications for therapy. *Treat Respir Med* **3**: 147-159.

Kim, S.K., Woodcroft, K.J., Oh, S.J., Abdelmegeed, M.A., and Novak, R.F. (2005). Role of mechanical and redox stress in activation of mitogen-activated protein kinases in primary cultured rat hepatocytes. *Biochem Pharmacol* **70**: 1785-1795.

Kim, S.Y., Jang, H.H., Lee, J.R., Sung, N.R., Lee, H.B., Lee, D.H., Park, D.J., Kang, C.H., Chung, W.S., Lim, C.O., Yun, D.J., Kim, W.Y., Lee, K.O., and Lee, S.Y. (2009). Oligomerization and chaperone activity of a plant 2-Cys peroxiredoxin in response to oxidative stress. *Plant Sci* **177**: 227-232.

Kim, S.Y., Kim, T.J., and Lee, K.Y. (2008). A novel function of peroxiredoxin 1 (Prx-1) in apoptosis signal-regulating kinase 1 (ASK1)-mediated signaling pathway. *FEBS Lett* **582**: 1913-1918.

Kim, W.D., Eidelman, D.H., Izquierdo, J.L., Ghezzi, H., Saetta, M.P., and Cosio, M.G. (1991). Centrilobular and panlobular emphysema in smokers. Two distinct morphologic and functional entities. *Am Rev Respir Dis* **144**: 1385-1390.

Kinnula, V.L. (2005). Focus on antioxidant enzymes and antioxidant strategies in smoking related airway diseases. *Thorax* **60**: 693-700.

Kinnula, V.L., Ilumets, H., Myllarniemi, M., Sovijarvi, A., and Ryttilä, P. (2007). 8-Isoprostane as a marker of oxidative stress in nonsymptomatic cigarette smokers and COPD. *The European respiratory journal : official journal of the European Society for Clinical Respiratory Physiology* **29**: 51-55.

Kinnula, V.L., Lehtonen, S., Kaarteenaho-Wiik, R., Lakari, E., Paakko, P., Kang, S.W., Rhee, S.G., and Soini, Y. (2002a). Cell specific expression of peroxiredoxins in human lung and pulmonary sarcoidosis. *Thorax* **57**: 157-164.

- Kinnula, V.L., Lehtonen, S., Sormunen, R., Kaarteenaho-Wiik, R., Kang, S.W., Rhee, S.G., and Soini, Y. (2002b).** Overexpression of peroxiredoxins I, II, III, V, and VI in malignant mesothelioma. *J Pathol* **196**: 316-323.
- Kirkham, P., and Rahman, I. (2006).** Oxidative stress in asthma and COPD: antioxidants as a therapeutic strategy. *Pharmacol Ther* **111**: 476-494.
- Kitano, K., Niimura, Y., Nishiyama, Y., and Miki, K. (1999).** Stimulation of peroxidase activity by decamerization related to ionic strength: AhpC protein from *Amphibacillus xylanus*. *J Biochem* **126**: 313-319.
- Knight, D.A., and Holgate, S.T. (2003).** The airway epithelium: structural and functional properties in health and disease. *Respirology* **8**: 432-446.
- Knoops, B., Clippe, A., Bogard, C., Aarsalane, K., Wattiez, R., Hermans, C., Duconseille, E., Falmagne, P., and Bernard, A. (1999).** Cloning and characterization of AOEB166, a novel mammalian antioxidant enzyme of the peroxiredoxin family. *J Biol Chem* **274**: 30451-30458.
- Koo, K.H., Lee, S., Jeong, S.Y., Kim, E.T., Kim, H.J., Kim, K., Song, K., and Chae, H.Z. (2002).** Regulation of thioredoxin peroxidase activity by C-terminal truncation. *Arch Biochem Biophys* **397**: 312-318.
- Korpas, J., and Honda, Y. (1996).** Aspects of airway defence mechanisms. *J. Pathophys* **3**: 81-86.
- Langen, R.C., Korn, S.H., and Wouters, E.F. (2003).** ROS in the local and systemic pathogenesis of COPD. *Free Radic Biol Med* **35**: 226-235.
- Le Visage, C., Dunham, B., Flint, P., and Leong, K.W. (2004).** Coculture of mesenchymal stem cells and respiratory epithelial cells to engineer a human composite respiratory mucosa. *Tissue Eng* **10**: 1426-1435.

- Lederer, J.A., Rodrick, M.L., and Mannick, J.A.** (1999). The effects of injury on the adaptive immune response. *Shock* **11**: 153-159.
- Lehmann, A.D., Daum, N., Bur, M., Lehr, C.M., Gehr, P., and Rothen-Rutishauser, B.M.** (2011). An in vitro triple cell co-culture model with primary cells mimicking the human alveolar epithelial barrier. *Eur J Pharm Biopharm* **77**: 398-406.
- Lehtonen, S.T., Markkanen, P.M., Peltoniemi, M., Kang, S.W., and Kinnula, V.L.** (2005). Variable overoxidation of peroxiredoxins in human lung cells in severe oxidative stress. *Am J Physiol Lung Cell Mol Physiol* **288**: L997-1001.
- Lehtonen, S.T., Ohlmeier, S., Kaarteenaho-Wiik, R., Harju, T., Paakko, P., Soini, Y., and Kinnula, V.L.** (2008). Does the oxidative stress in chronic obstructive pulmonary disease cause thioredoxin/peroxiredoxin oxidation? *Antioxid Redox Signal* **10**: 813-819.
- Lehtonen, S.T., Svensk, A.M., Soini, Y., Pääkkö, P., Hirvikoski, P., Kang, S.W., Säily, M., and Kinnula, V.L.** (2004). Peroxiredoxins, a novel protein family in lung cancer. *International Journal of Cancer* **111**: 514-521.
- Leist, M., Raab, B., Maurer, S., Rosick, U., and Brigelius-Flohe, R.** (1996). Conventional cell culture media do not adequately supply cells with antioxidants and thus facilitate peroxide-induced genotoxicity. *Free radical biology & medicine* **21**: 297-306.
- Levitsky, M.G.** (2003). *Pulmonary physiology*. McGraw-Hill.
- Leyens, G., Donnay, I., and Knoops, B.** (2003). Cloning of bovine peroxiredoxins-gene expression in bovine tissues and amino acid sequence comparison with rat, mouse and primate peroxiredoxins. *Comp Biochem Physiol B Biochem Mol Biol* **136**: 943-955.

- Lim, Y.S., Cha, M.K., Kim, H.K., Uhm, T.B., Park, J.W., Kim, K., and Kim, I.H. (1993).** Removals of hydrogen peroxide and hydroxyl radical by thiol-specific antioxidant protein as a possible role in vivo. *Biochem Biophys Res Commun* **192**: 273-280.
- Lin, H., Li, H., Cho, H.J., Bian, S., Roh, H.J., Lee, M.K., Kim, J.S., Chung, S.J., Shim, C.K., and Kim, D.D. (2007).** Air-liquid interface (ALI) culture of human bronchial epithelial cell monolayers as an in vitro model for airway drug transport studies. *J Pharm Sci* **96**: 341-350.
- Lin, J.H. (1998).** Applications and limitations of interspecies scaling and in vitro extrapolation in pharmacokinetics. *Drug Metab Dispos* **26**: 1202-1212.
- Lopez, A.D., Mathers, C.D., Ezzati, M., Jaimison, D.T., and Murray, C.J.L. (2006).** Global burden of disease and risk factors. Oxford University Press.
- MacNee, W. (2000).** Oxidants/antioxidants and COPD. *Chest* **117**: 303S-317S.
- MacNee, W. (2001).** Oxidative stress and lung inflammation in airways disease. *European Journal of Pharmacology* **429**: 195-207.
- MacNee, W., and Rahman, I. (2001).** Is oxidative stress central to the pathogenesis of chronic obstructive pulmonary disease? *Trends in Molecular Medicine* **7**: 55-62.
- Makris, D., Paraskakis, E., Korakas, P., Karagiannakis, E., Sourvinos, G., Siafakas, N.M., and Tzanakis, N. (2008).** Exhaled breath condensate 8-isoprostane, clinical parameters, radiological indices and airway inflammation in COPD. *Respiration* **72**: 138-144.
- Manevich, Y., Feinstein, S.I., and Fisher, A.B. (2004).** Activation of the antioxidant enzyme 1-CYS peroxiredoxin requires glutathionylation mediated by heterodimerization with pi GST. *Proc Natl Acad Sci U S A* **101**: 3780-3785.

- Manevich, Y., and Fisher, A.B.** (2005). Peroxiredoxin 6, a 1-Cys peroxiredoxin, functions in antioxidant defense and lung phospholipid metabolism. *Free Radic Biol Med* **38**: 1422-1432.
- Mannino, D.M., and Braman, S.** (2007). The epidemiology and economics of chronic obstructive pulmonary disease. *Proc Am Thorac Soc* **4**: 502-506.
- Mannino, D.M., and Buist, A.S.** (2007). Global burden of COPD: risk factors, prevalence, and future trends. *Lancet* **370**: 765-773.
- Martin, T.R., and Frevert, C.W.** (2005). Innate immunity in the lungs. *Proc Am Thorac Soc* **2**: 403-411.
- Matsumoto, A., Okado, A., Fujii, T., Fujii, J., Egashira, M., Niikawa, N., and Taniguchi, N.** (1999). Cloning of the peroxiredoxin gene family in rats and characterization of the fourth member. *FEBS Lett* **443**: 246-250.
- Matter, K., and Balda, M.S.** (2003). Functional analysis of tight junctions. *Methods* **30**: 228-234.
- McCay, P.B.** (1985). Vitamin E: interactions with free radicals and ascorbate. *Annu Rev Nutr* **5**: 323-340.
- McCord, J.M., and Fridovich, I.** (1969). Superoxide dismutase. An enzymic function for erythrocyte hemocuprein (hemocuprein). *J Biol Chem* **244**: 6049-6055.
- McDowell, E.M., Barrett, L.A., Glavin, F., Harris, C.C., and Trump, B.F.** (1978). The respiratory epithelium. I. Human bronchus. *J Natl Cancer Inst* **61**: 539-549.
- Medzhitov, R.** (2007). Recognition of microorganisms and activation of the immune response. *Nature* **449**: 819-826.

- Medzhitov, R., and Janeway, C.A., Jr.** (1997). Innate immunity: impact on the adaptive immune response. *Current opinion in immunology* **9**: 4-9.
- Mercer, B.A., Lemaitre, V., Powell, C.A., and D'Armiento, J.** (2006). The Epithelial Cell in Lung Health and Emphysema Pathogenesis. *Curr Respir Med Rev* **2**: 101-142.
- Meyrick, B., and Reid, L.** (1970). Ultrastructure of cells in the human bronchial submucosal glands. *J Anat* **107**: 281-299.
- Miller, F.J., Graham, J.A., and Gardner, D.E.** (1983). The changing role of animal toxicology in support of regulatory decisions. *Environ Health Perspect* **52**: 169-176.
- Mitsumoto, A., Takanezawa, Y., Okawa, K., Iwamatsu, A., and Nakagawa, Y.** (2001). Variants of peroxiredoxins expression in response to hydroperoxide stress. *Free Radic Biol Med* **30**: 625-635.
- Montuschi, P., Barnes, P.J., and Ciabattini, G.** (2010). Measurements of 8-isoprostane in exhaled breath. *Meth Mol Biol* **594**: 73-84.
- Moore, B.B., Moore, T.A., and Toews, G.B.** (2001). Role of T- and B-lymphocytes in pulmonary host defences. *Eur Respir J* **18**: 846-856.
- Morgan, D.O.** (1995). Principles of CDK regulation. *Nature* **374**: 131-134.
- Morrison, D., Rahman, I., Lannan, S., and MacNee, W.** (1999). Epithelial permeability, inflammation, and oxidant stress in the air spaces of smokers. *Am J Respir Crit Care Med* **159**: 473-479.
- Mossman, B.T., Lounsbury, K.M., and Reddy, S.P.** (2006). Oxidants and signaling by mitogen-activated protein kinases in lung epithelium. *Am J Respir Cell Mol Biol* **34**: 666-669.

MRC. (1965). Definition and classification of chronic bronchitis for clinical and epidemiological purposes. A report to the Medical Research Council by their Committee on the Aetiology of Chronic Bronchitis. *Lancet* **1**: 775-779.

Nagase, T., Miyajima, N., Tanaka, A., Sazuka, T., Seki, N., Sato, S., Tabata, S., Ishikawa, K., Kawarabayasi, Y., Kotani, H., and Nobuo, N. (1995). Prediction of the coding sequences of unidentified human genes. III. The coding sequences of 40 new genes (KIAA0081-KIAA0120) deduced by analysis of cDNA clones from human cell line KG-1. *DNA Res* **2**: 37-43.

Nakayama, T., Church, D.F., and Pryor, W.A. (1989). Quantitative analysis of the hydrogen peroxide formed in aqueous cigarette tar extracts. *Free Radic Biol Med* **7**: 9-15.

Newman, G.R., and Hobot, J.A. (2001). Resin microscopy and on-section immuno-cytochemistry. Springer.

Nicod, L.P. (1999). Pulmonary defence mechanisms. *Respiration* **66**: 2-11.

Noske, W., Stamm, C.C., and Hirsch, M. (1994). Tight junctions of the human ciliary epithelium: regional morphology and implications on transepithelial resistance. *Exp Eye Res* **59**: 141-149.

Nowak, D., Antczak, A., Krol, M., Pietras, T., Shariati, B., Bialasiewicz, P., Jeczowski, K., and Kula, P. (1996). Increased content of hydrogen peroxide in the expired breath of cigarette smokers. *European Respiratory Journal* **9**: 652-657.

Nowak, D., Kasielski, M., Antczak, A., Pietras, T., and Bialasiewicz, P. (1999). Increased content of thiobarbituric acid-reactive substances and hydrogen peroxide in the expired breath condensate of patients with stable chronic obstructive pulmonary disease: no significant effect of cigarette smoking. *Respiratory Medicine* **93**: 389-396.

- Nussbaumer-Ochsner, Y., and Rabe, K.F.** (2011). Systemic manifestations of COPD. *Chest* **139**: 165-173.
- Okada, S.F., Nicholas, R.A., Kreda, S.M., Lazarowski, E.R., and Boucher, R.C.** (2006). Physiological regulation of ATP release at the apical surface of human airway epithelia. *The Journal of biological chemistry* **281**: 22992-23002.
- Ordenez, N.G.** (1998). Value of cytokeratin 5/6 immunostaining in distinguishing epithelial mesothelioma of the pleura from lung adenocarcinoma. *Am J Surg Pathol* **22**: 1215-1221.
- Oudijk, E.J., Lammers, J.W., and Koenderman, L.** (2003). Systemic inflammation in chronic obstructive pulmonary disease. *Eur Respir J Suppl* **46**: 5s-13s.
- Owen, C.A.** (2005). Proteinases and oxidants as targets in the treatment of chronic obstructive pulmonary disease. *Proceedings of the American Thoracic Society* **2**: 373-385; discussion 394-375.
- Padar, S., Bose, D.D., Livesey, J.C., and Thomas, D.W.** (2005). 2-Aminoethoxydiphenyl borate perturbs hormone-sensitive calcium stores and blocks store-operated calcium influx pathways independent of cytoskeletal disruption in human A549 lung cancer cells. *Biochem Pharmacol* **69**: 1177-1186.
- Pampaloni, F., Reynaud, E.G., and Stelzer, E.H.** (2007). The third dimension bridges the gap between cell culture and live tissue. *Nat Rev Mol Cell Biol* **8**: 839-845.
- Papadakos, P.J., and Lachman, B.** (2008). Mechanical ventilation: clinical applications and pathophysiology.

Park, J.H., Kim, Y.S., Lee, H.L., Shim, J.Y., Lee, K.S., Oh, Y.J., Shin, S.S., Choi, Y.H., Park, K.J., Park, R.W., and Hwang, S.C. (2006a). Expression of peroxiredoxin and thioredoxin in human lung cancer and paired normal lung. *Respirology* **11**: 269-275.

Park, J.W., Piszczek, G., Rhee, S.G., and Chock, P.B. (2011). Glutathionylation of peroxiredoxin I induces decamer to dimers dissociation with concomitant loss of chaperone activity. *Biochemistry* **50**: 3204-3210.

Park, K.S., Wells, J.M., Zorn, A.M., Wert, S.E., Laubach, V.E., Fernandez, L.G., and Whitsett, J.A. (2006b). Transdifferentiation of ciliated cells during repair of the respiratory epithelium. *American journal of respiratory cell and molecular biology* **34**: 151-157.

Patton, J.S., Fishburn, C.S., and Weers, J.G. (2004). The lungs as a portal of entry for systemic drug delivery. *Proceedings of the American Thoracic Society* **1**: 338-344.

Penn, A., Murphy, G., Barker, S., Henk, W., and Penn, L. (2005). Combustion-derived ultrafine particles transport organic toxicants to target respiratory cells. *Environ Health Perspect* **113**: 956-963.

Peskin, A.V., Cox, A.G., Nagy, P., Morgan, P.E., Hampton, M.B., Davies, M.J., and Winterbourn, C.C. (2010). Removal of amino acid, peptide and protein hydroperoxides by reaction with peroxiredoxins 2 and 3. *Biochem J* **432**: 313-321.

Peskin, A.V., Low, F.M., Paton, L.N., Maghzal, G.J., Hampton, M.B., and Winterbourn, C.C. (2007). The high reactivity of peroxiredoxin 2 with H₂O₂ is not reflected in its reaction with other oxidants and thiol reagents. *J Biol Chem* **282**: 11885-11892.

Phalen, T.J., Weirather, K., Deming, P.B., Anathy, V., Howe, A.K., van der Vliet, A., Jonsson, T.J., Poole, L.B., and Heintz, N.H. (2006). Oxidation

state governs structural transitions in peroxiredoxin II that correlate with cell cycle arrest and recovery. *J Cell Biol* **175**: 779-789.

Pierce, G.F., Yanagihara, D., Klopchin, K., Danilenko, D.M., Hsu, E., Kenney, W.C., and Morris, C.F. (1994). Stimulation of all epithelial elements during skin regeneration by keratinocyte growth factor. *J Exp Med* **179**: 831-840.

Poli, G., Leonarduzzi, G., Biasi, F., and Chiarotto, E. (2004). Oxidative stress and cell signalling. *Curr Med Chem* **11**: 1163-1182.

Popp, J.A., and Martin, J.T. (1984). Surface topography and distribution of cell types in the rat nasal respiratory epithelium: scanning electron microscopic observations. *Am J Anat* **169**: 425-436.

Presland, R.B., and Dale, B.A. (2000). Epithelial structural proteins of the skin and oral cavity: function in health and disease. *Crit Rev Oral Biol Med* **11**: 383-408.

Presland, R.B., and Jurevic, R.J. (2002). Making sense of the epithelial barrier: what molecular biology and genetics tell us about the functions of oral mucosal and epidermal tissues. *J Dent Educ* **66**: 564-574.

Prosperi, M.T., Ferbus, D., Karczinski, I., and Goubin, G. (1993). A human cDNA corresponding to a gene overexpressed during cell proliferation encodes a product sharing homology with amoebic and bacterial proteins. *J Biol Chem* **268**: 11050-11056.

Proud, D. (2008). The pulmonary epithelium in health and disease. John Wiley and Sons Ltd.

Prussin, C., and Metcalfe, D.D. (2003). 4. IgE, mast cells, basophils, and eosinophils. *J Allergy Clin Immunol* **111**: S486-494.

- Pryor, W.A., and Stone, K.** (1993). Oxidants in cigarette smoke. Radicals, hydrogen peroxide, peroxyxynitrate, and peroxyxynitrite. *Annals of the New York Academy of Sciences* **686**: 12-27; discussion 27-18.
- Prytherch, Z.C.** (2010). An *in vitro* NHBE model of the human bronchial epithelium for toxicological testing **Thesis**.
- Puchelle, E., Zahm, J.M., Tournier, J.M., and Coraux, C.** (2006). Airway epithelial repair, regeneration, and remodeling after injury in chronic obstructive pulmonary disease. *Proceedings of the American Thoracic Society* **3**: 726-733.
- Puntmann, V.O.** (2009). How-to guide on biomarkers: biomarker definitions, validation and applications with examples from cardiovascular disease. *Postgrad Med J* **85**: 538-545.
- Rabilloud, T., Heller, M., Gasnier, F., Luche, S., Rey, C., Aebersold, R., Benahmed, M., Louisot, P., and Lunardi, J.** (2002). Proteomics analysis of cellular response to oxidative stress. Evidence for *in vivo* overoxidation of peroxiredoxins at their active site. *J Biol Chem* **277**: 19396-19401.
- Raherison, C., and Girodet, P.O.** (2009). Epidemiology of COPD. *Eur Respir Rev* **18**: 213-221.
- Rahman, I.** (2006). Antioxidant therapies in COPD. *Int J Chron Obstruct Pulmon Dis* **1**: 15-29.
- Rahman, I., and Adcock, I.M.** (2006). Oxidative stress and redox regulation of lung inflammation in COPD. *Eur Respir J* **28**: 219-242.
- Rahman, I., Biswas, S.K., and Kode, A.** (2006). Oxidant and antioxidant balance in the airways and airway diseases. *Eur J Pharmacol* **533**: 222-239.

Rahman, I., and MacNee, W. (1998). Role of transcription factors in inflammatory lung diseases. *Thorax* **53**: 601-612.

Randell, S.H. (2006). Airway epithelial stem cells and the pathophysiology of chronic obstructive pulmonary disease. *Proceedings of the American Thoracic Society* **3**: 718-725.

Rennard, S.I. (1999). Inflammation and repair processes in chronic obstructive pulmonary disease. *American Journal of Respiratory and Critical Care Medicine* **160**: S12-16.

Rennard, S.I. (2007). Inflammation in COPD: a link to systemic comorbidities. *Eur Respir Rev* **16**: 91-97.

Repine, J.E., Bast, A., and Lankhorst, I. (1997). Oxidative stress in chronic obstructive pulmonary disease. Oxidative Stress Study Group. *Am J Respir Crit Care Med* **156**: 341-357.

Reynolds, S.D., and Malkinson, A.M. (2010). Clara cell: progenitor for the bronchiolar epithelium. *The international journal of biochemistry & cell biology* **42**: 1-4.

Rhee, S.G. (2006). Cell signaling. H_2O_2 , a necessary evil for cell signaling. *Science* **312**: 1882-1883.

Rhee, S.G., Bae, Y.S., Lee, S.R., and Kwon, J. (2000). Hydrogen peroxide: a key messenger that modulates protein phosphorylation through cysteine oxidation. *Sci STKE* **2000**: PE1.

Rhee, S.G., Chae, H.Z., and Kim, K. (2005a). Peroxiredoxins: a historical overview and speculative preview of novel mechanisms and emerging concepts in cell signaling. *Free Radic Biol Med* **38**: 1543-1552.

- Rhee, S.G., Chang, T.S., Bae, Y.S., Lee, S.R., and Kang, S.W. (2003).** Cellular regulation by hydrogen peroxide. *J Am Soc Nephrol* **14**: S211-215.
- Rhee, S.G., Kang, S.W., Chang, T.S., Jeong, W., and Kim, K. (2001).** Peroxiredoxin, a novel family of peroxidases. *IUBMB Life* **52**: 35-41.
- Rhee, S.G., Kang, S.W., Jeong, W., Chang, T.S., Yang, K.S., and Woo, H.A. (2005b).** Intracellular messenger function of hydrogen peroxide and its regulation by peroxiredoxins. *Curr Opin Cell Biol* **17**: 183-189.
- Rhee, S.G., Yang, K.S., Kang, S.W., Woo, H.A., and Chang, T.S. (2005c).** Controlled elimination of intracellular H₂O₂: regulation of peroxiredoxin, catalase, and glutathione peroxidase via post-translational modification. *Antioxid Redox Signal* **7**: 619-626.
- Rhodin, J.A. (1966).** The ciliated cell. Ultrastructure and function of the human tracheal mucosa. *Am Rev Respir Dis* **93**: Suppl:1-15.
- Rinalducci, S., D'Amici, G.M., Blasi, B., and Zolla, L. (2011).** Oxidative stress-dependent oligomeric status of erythrocyte peroxiredoxin II (PrxII) during storage under standard blood banking conditions. *Biochimie* **93**: 845-853.
- Rogers, D.F. (2003).** The airway goblet cell. *Int J Biochem Cell Biol* **35**: 1-6.
- Rose, M.C., and Voynow, J.A. (2006).** Respiratory tract mucin genes and mucin glycoproteins in health and disease. *Physiol Rev* **86**: 245-278.
- Rothen-Rutishauser, B.M., Kiama, S.G., and Gehr, P. (2005).** A three-dimensional cellular model of the human respiratory tract to study the interaction with particles. *American journal of respiratory cell and molecular biology* **32**: 281-289.

Rozman, K.K., and Doull, J. (2003). Scientific foundations of hormesis. Part 2. Maturation, strengths, limitations, and possible applications in toxicology, pharmacology, and epidemiology. *Crit Rev Toxicol* **33**: 451-462.

Russell, W., and Burch, R. (1959). The principles of humane experimental technique.

Rytla, P., Plataki, M., Bucchieri, F., Uddin, M., Nong, G., Kinnula, V.L., and Djukanovic, R. (2006). Airway neutrophilia in COPD is not associated with increased neutrophil survival. *The European respiratory journal : official journal of the European Society for Clinical Respiratory Physiology* **28**: 1163-1169.

Saetta, M. (1999). Airway inflammation in chronic obstructive pulmonary disease. *Am J Respir Crit Care Med* **160**: S17-20.

Saetta, M., Turato, G., Baraldo, S., Zanin, A., Braccioni, F., Mapp, C.E., Maestrelli, P., Cavallero, G., Papi, A., and Fabbri, L.M. (2000). Goblet cell hyperplasia and epithelial inflammation in peripheral airways of smokers with both symptoms of chronic bronchitis and chronic airflow limitation. *American Journal of Respiratory and Critical Care Medicine* **161**: 1016-1021.

Scheuch, G., Kohlhaeufel, M.J., Brand, P., and Siekmeier, R. (2006). Clinical perspectives on pulmonary systemic and macromolecular delivery. *Adv Drug Deliv Rev* **58**: 996-1008.

Schneeberger, E.E., and Lynch, R.D. (1992). Structure, function, and regulation of cellular tight junctions. *Am J Physiol* **262**: L647-661.

Schroder, E., and Ponting, C.P. (1998). Evidence that peroxiredoxins are novel members of the thioredoxin fold superfamily. *Protein Sci* **7**: 2465-2468.

Scotton, C.J. (2011). A breath of fresh air for tissue engineering? *Materials Today* **14**: 212-216.

- Seethala, R.** (2001). Handbook of drug screening.
- Seo, M.S., Kang, S.W., Kim, K., Baines, I.C., Lee, T.H., and Rhee, S.G.** (2000). Identification of a new type of mammalian peroxiredoxin that forms an intramolecular disulfide as a reaction intermediate. *J Biol Chem* **275**: 20346-20354.
- Sexton, K.** (2009). Identification of intelligent biomarkers of exposure in the respiratory epithelia to tobacco smoke components **Thesis**.
- Sexton, K., Balharry, D., and BeruBe, K.A.** (2008). Genomic biomarkers of pulmonary exposure to tobacco smoke components. *Pharmacogenet Genom* **18**: 853-860.
- Shau, H., and Kim, A.** (1994). Identification of natural killer enhancing factor as a major antioxidant in human red blood cells. *Biochem Biophys Res Commun* **199**: 83-88.
- Shier, D., Butler, J., and Lewis, R.** (2004). Hole's human anatomy and physiology. McGraw-Hill.
- Shoyele, S.A., and Cawthorne, S.** (2006). Particle engineering techniques for inhaled biopharmaceuticals. *Adv Drug Deliv Rev* **58**: 1009-1029.
- Siafakas, N.M., and Tzortzaki, E.G.** (2002). Few smokers develop COPD. Why? *Respiratory Medicine* **96**: 615-624.
- Simet, S.M., Sisson, J.H., Pavlik, J.A., Devasure, J.M., Boyer, C., Liu, X., Kawasaki, S., Sharp, J.G., Rennard, S.I., and Wyatt, T.A.** (2010). Long-term cigarette smoke exposure in a mouse model of ciliated epithelial cell function. *American journal of respiratory cell and molecular biology* **43**: 635-640.

- Sin, D.D., Anthonisen, N.R., Soriano, J.B., and Agusti, A.G. (2006).** Mortality in COPD: Role of comorbidities. *Eur Respir J* **28**: 1245-1257.
- Singh, G., and Katyal, S.L. (2000).** Clara cell proteins. *Annals of the New York Academy of Sciences* **923**: 43-58.
- Sisson, J.H., Papi, A., Beckmann, J.D., Leise, K.L., Wisecarver, J., Brodersen, B.W., Kelling, C.L., Spurzem, J.R., and Rennard, S.I. (1994).** Smoke and viral infection cause cilia loss detectable by bronchoalveolar lavage cytology and dynein ELISA. *American Journal of Respiratory and Critical Care Medicine* **149**: 205-213.
- Sleigh, M.A. (1990).** Ciliary adaptations for the propulsion of mucus. *Biorheology* **27**: 527-532.
- Snider, G.L. (1989).** Chronic Obstructive Pulmonary-Disease - Risk-Factors, Patho-Physiology and Pathogenesis. *Annual Review of Medicine* **40**: 411-429.
- Snoeck-Stroband, J.B., Lapperre, T.S., Gosman, M.M., Boezen, H.M., Timens, W., ten Hacken, N.H., Sont, J.K., Sterk, P.J., and Hiemstra, P.S. (2008).** Chronic bronchitis sub-phenotype within COPD: inflammation in sputum and biopsies. *The European respiratory journal : official journal of the European Society for Clinical Respiratory Physiology* **31**: 70-77.
- Steimer, A., Haltner, E., and Lehr, C.M. (2005).** Cell culture models of the respiratory tract relevant to pulmonary drug delivery. *J Aerosol Med* **18**: 137-182.
- Stoller, J.K., and Aboussouan, L.S. (2005).** [alpha]1-antitrypsin deficiency. *The Lancet* **365**: 2225-2236.
- Szilasi, M., Dolinay, T., Nemes, Z., and Strausz, J. (2006).** Pathology of chronic obstructive pulmonary disease. *Pathol Oncol Res* **12**: 52-60.

Takeyama, K., Dabbagh, K., Jeong Shim, J., Dao-Pick, T., Ueki, I.F., and Nadel, J.A. (2000). Oxidative stress causes mucin synthesis via transactivation of epidermal growth factor receptor: role of neutrophils. *Journal of Immunology* **164**: 1546-1552.

Takeyama, K., Dabbagh, K., Lee, H.M., Agusti, C., Lausier, J.A., Ueki, I.F., Grattan, K.M., and Nadel, J.A. (1999). Epidermal growth factor system regulates mucin production in airways. *Proceedings of the National Academy of Sciences of the United States of America* **96**: 3081-3086.

Takeyama, K., Fahy, J.V., and Nadel, J.A. (2001). Relationship of epidermal growth factor receptors to goblet cell production in human bronchi. *American Journal of Respiratory and Critical Care Medicine* **163**: 511-516.

Takizawa, H., Tanaka, M., Takami, K., Ohtoshi, T., Ito, K., Satoh, M., Okada, Y., Yamasawa, F., and Umeda, A. (2000). Increased expression of inflammatory mediators in small-airway epithelium from tobacco smokers. *Am J Physiol Lung Cell Mol Physiol* **278**: L906-913.

Tanikawa, K., and Torimura, T. (2006). Studies on oxidative stress in liver diseases: important future trends in liver research. *Med Mol Morphol* **39**: 22-27.

Taylor, J.D. (2010). COPD and the response of the lung to tobacco smoke exposure. *Pulm Pharmacol Ther* **23**: 376-383.

Teramoto, S., Tomita, T., Matsui, H., Ohga, E., Matsuse, T., and Ouchi, Y. (1999). Hydrogen peroxide induced apoptosis and necrosis in human lung fibroblasts: protective roles of glutathione. *Jpn J Pharmacol* **73**: 33-40.

Tetley, T.D. (2002). Macrophages and the pathogenesis of COPD. *Chest* **121**: 156S-159S.

Thannickal, V.J., Day, R.M., Klinz, S.G., Bastien, M.C., Larios, J.M., and Fanburg, B.L. (2000). Ras-dependent and -independent regulation of reactive oxygen species by mitogenic growth factors and TGF-beta1. *Faseb J* **14**: 1741-1748.

Thannickal, V.J., and Fanburg, B.L. (1995). Activation of an H₂O₂-generating NADH oxidase in human lung fibroblasts by transforming growth factor beta 1. *J Biol Chem* **270**: 30334-30338.

Thannickal, V.J., and Fanburg, B.L. (2000). Reactive oxygen species in cell signaling. *Am J Physiol Lung Cell Mol Physiol* **279**: L1005-1028.

Therond, P., Bonnefont-Rousselot, D., Davit-Spraul, A., Conti, M., and Legrand, A. (2000). Biomarkers of oxidative stress: an analytical approach. *Curr Opin Clin Nutr Metab Care* **3**: 373-384.

Thomassen, D.G., and Nettesheim, P. (1990). Biology, toxicology and carcinogenesis of respiratory epithelium. Hemisphere Publishing Corporation.

Thornton, D.J., and Sheehan, J.K. (2004). From mucins to mucus: toward a more coherent understanding of this essential barrier. *Proceedings of the American Thoracic Society* **1**: 54-61.

Tonello, A., and Poli, G. (2011). Rethinking chronic obstructive pulmonary disease. *Med Hypotheses* **76**: 358-360.

Torres, M., and Forman, H.J. (2003). Redox signaling and the MAP kinase pathways. *Biofactors* **17**: 287-296.

Travis, C.C. (1991). Interspecies extrapolation in risk analysis. *Ann Ist Super Sanita* **27**: 581-593.

Travis, S.M., Singh, P.K., and Welsh, M.J. (2001). Antimicrobial peptides and proteins in the innate defense of the airway surface. *Curr Opin Immunol* **13**: 89-95.

Tsuji, K., Copeland, N.G., Jenkins, N.A., and Obinata, M. (1995). Mammalian antioxidant protein complements alkylhydroperoxide reductase (ahpC) mutation in *Escherichia coli*. *Biochem J* **307** (Pt 2): 377-381.

Turner, J., Roger, J., Fitau, J., Combe, D., Giddings, J., Heeke, G.V., and Jones, C.E. (2011). Goblet cells are derived from a FOXJ1-expressing progenitor in a human airway epithelium. *American journal of respiratory cell and molecular biology* **44**: 276-284.

Valko, M., Leibfritz, D., Moncol, J., Cronin, M.T., Mazur, M., and Telser, J. (2007). Free radicals and antioxidants in normal physiological functions and human disease. *The international journal of biochemistry & cell biology* **39**: 44-84.

Van der Vliet, A., Eiserich, J.P., Halliwell, B., and Cross, C.E. (1997). Formation of reactive nitrogen species during peroxidase-catalyzed oxidation of nitrite. A potential additional mechanism of nitric oxide-dependent toxicity. *The Journal of biological chemistry* **272**: 7617-7625.

VanGuilder, H.D., Vrana, K.E., and Freeman, W.M. (2008). Twenty-five years of quantitative PCR for gene expression analysis. *Biotechniques* **44**: 619-626.

Veranth, J.M., Kaser, E.G., Veranth, M.M., Koch, M., and Yost, G.S. (2007). Cytokine responses of human lung cells (BEAS-2B) treated with micron-sized and nanoparticles of metal oxides compared to soil dusts. *Part Fibre Toxicol* **4**: 2.

Veranth, J.M., Reilly, C.A., Veranth, M.M., Moss, T.A., Langelier, C.R., Lanza, D.L., and Yost, G.S. (2004). Inflammatory cytokines and cell death in

BEAS-2B lung cells treated with soil dust, lipopolysaccharide, and surface-modified particles. *Toxicol Sci* **82**: 88-96.

W.A.G. (2010). Early stage development fund for a small pilot study to realise the development of the 'Metabo-Lung'. Welsh Assembly Government: Pilot study.

Waris, G., and Ahsan, H. (2006). Reactive oxygen species: role in the development of cancer and various chronic conditions. *J Carcinog* **5**: 14.

Waskiewicz, A.J., and Cooper, J.A. (1995). Mitogen and stress response pathways: MAP kinase cascades and phosphatase regulation in mammals and yeast. *Curr Opin Cell Biol* **7**: 798-805.

Watabe, S., Kohno, H., Kouyama, H., Hiroi, T., Yago, N., and Nakazawa, T. (1994). Purification and characterization of a substrate protein for mitochondrial ATP-dependent protease in bovine adrenal cortex. *J Biochem* **115**: 648-654.

West, J.B. (1995). *Respiratory physiology*. Williams & Wilkins.

West, J.B., and Mathieu-Costello, O. (1999). Structure, strength, failure, and remodeling of the pulmonary blood-gas barrier. *Annu Rev Physiol* **61**: 543-572.

Westermeier, R. (2005). *Electrophoresis in practice*.

Westmoreland, C., Walker, T., Matthews, J., and Murdock, J. (1999). Preliminary Investigations into the use of a Human Bronchial Cell Line (16HBE14o-) to Screen for Respiratory Toxins In Vitro. *Toxicol In Vitro* **13**: 761-764.

White, S.H., Wimley, W.C., and Selsted, M.E. (1995). Structure, function, and membrane integration of defensins. *Curr Opin Struct Biol* **5**: 521-527.

- Widdicombe, J.H.** (2002). Regulation of the depth and composition of airway surface liquid. *J Anat* **201**: 313-318.
- Wilson, R., and Turner, A.P.F.** (1992). Glucose oxidase: An ideal enzyme. *Biosens Bioelect* **7**: 165-185.
- Winterbourn, C.C., and Hampton, M.B.** (2008). Thiol chemistry and specificity in redox signaling. *Free radical biology & medicine* **45**: 549-561.
- Woo, H.A., Chae, H.Z., Hwang, S.C., Yang, K.S., Kang, S.W., Kim, K., and Rhee, S.G.** (2003a). Reversing the inactivation of peroxiredoxins caused by cysteine sulfinic acid formation. *Science* **300**: 653-656.
- Woo, H.A., Kang, S.W., Kim, H.K., Yang, K.S., Chae, H.Z., and Rhee, S.G.** (2003b). Reversible oxidation of the active site cysteine of peroxiredoxins to cysteine sulfinic acid. Immunoblot detection with antibodies specific for the hyperoxidized cysteine-containing sequence. *J Biol Chem* **278**: 47361-47364.
- Wood, Z.A., Poole, L.B., Hantgan, R.R., and Karplus, P.A.** (2002). Dimers to doughnuts: redox-sensitive oligomerization of 2-cysteine peroxiredoxins. *Biochemistry* **41**: 5493-5504.
- Wood, Z.A., Poole, L.B., and Karplus, P.A.** (2003a). Peroxiredoxin evolution and the regulation of hydrogen peroxide signaling. *Science* **300**: 650-653.
- Wood, Z.A., Schroder, E., Robin Harris, J., and Poole, L.B.** (2003b). Structure, mechanism and regulation of peroxiredoxins. *Trends Biochem Sci* **28**: 32-40.
- Wottrich, R., Diabate, S., and Krug, H.F.** (2004). Biological effects of ultrafine model particles in human macrophages and epithelial cells in mono- and co-culture. *Int J Hyg Environ Health* **207**: 353-361.

Yamamoto, T., Matsui, Y., Natori, S., and Obinata, M. (1989). Cloning of a housekeeping-type gene (MER5) preferentially expressed in murine erythroleukemia cells. *Gene* **80**: 337-343.

Yang, K.S., Kang, S.W., Woo, H.A., Hwang, S.C., Chae, H.Z., Kim, K., and Rhee, S.G. (2002). Inactivation of human peroxiredoxin I during catalysis as the result of the oxidation of the catalytic site cysteine to cysteine-sulfinic acid. *J Biol Chem* **277**: 38029-38036.

Ye, L., Wang, X., and Jin, M. (2009). Role of airway epithelial cells in development of chronic obstructive pulmonary disease. *J Epithelial Biol Pharmacol* **2**: 44-50.

Yoshida, Y., Yoshikawa, A., Kinumi, T., Ogawa, Y., Saito, Y., Ohara, K., Yamamoto, H., Imai, Y., and Niki, E. (2009). Hydroxyoctadecadienoic acid and oxidatively modified peroxiredoxins in the blood of Alzheimer's disease patients and their potential as biomarkers. *Neurobiol Aging* **30**: 174-185.

Yoshisue, H., Puddicombe, S.M., Wilson, S.J., Haitchi, H.M., Powell, R.M., Wilson, D.I., Pandit, A., Berger, A.E., Davies, D.E., Holgate, S.T., and Holloway, J.W. (2004). Characterization of ciliated bronchial epithelium 1, a ciliated cell-associated gene induced during mucociliary differentiation. *American journal of respiratory cell and molecular biology* **31**: 491-500.

APPENDIX

APPENDIX I

Protocol provided by Lonza

Recipe for Bronchial Epithelial Growth Medium (BEGM)

For every 10ml of Bronchial Epithelial Basal Medium (BEBM) the following growth supplements were added in order to make 10ml BEGM:

VOLUME	SUPPLEMENT
40µl	Bovine Pituitary Extract
10 µl	Insulin
10 µl	Hydrocortisone
10 µl	Transferrin
10 µl	Triiodothyronine
10 µl	Epinephrine
10 µl	Epidermal Growth Factor
10 µl	Gentamicin/Amphotericin
10 µl	Retanoic Acid

APPENDIX II

Recipe for Air-Liquid Interface (ALI) growth medium

For every 20ml of ALI the following recipe was followed:

VOLUME	SUPPLEMENT
10ml	BEBM
10ml	DMEM
80µl	Bovine Pituitary Extract
20 µl	Insulin
20 µl	Hydrocortisone
20 µl	Transferrin
20 µl	Triodothronin
20 µl	Epinepherine
20 µl	Epidermal Growth Factor
20 µl	Gentamicin/Amphoteracin
20 µl	Retanoic Acid

